



**HAL**  
open science

# Contribution of random sampling in the context of rotating machinery diagnostic

Mayssaa Hajar

► **To cite this version:**

Mayssaa Hajar. Contribution of random sampling in the context of rotating machinery diagnostic. Signal and Image Processing. Université de Lyon; Université Libanaise, 2018. English. NNT : 2018LYSES001 . tel-02137521

**HAL Id: tel-02137521**

**<https://theses.hal.science/tel-02137521>**

Submitted on 23 May 2019

**HAL** is a multi-disciplinary open access archive for the deposit and dissemination of scientific research documents, whether they are published or not. The documents may come from teaching and research institutions in France or abroad, or from public or private research centers.

L'archive ouverte pluridisciplinaire **HAL**, est destinée au dépôt et à la diffusion de documents scientifiques de niveau recherche, publiés ou non, émanant des établissements d'enseignement et de recherche français ou étrangers, des laboratoires publics ou privés.



N°d'ordre NNT :  
2018LYSES001

**THESE de DOCTORAT DE L'UNIVERSITE DE LYON**  
**Université Jean-Monnet de Saint-Etienne, LASPI, France**

**Ecole Doctorale N° 484**  
**Université Jean-Monnet de Saint-Etienne**  
**Ingénierie**  
**Image Vision Santé**

Soutenue publiquement à huis clos le 26/01/2018, par :  
**Mayssaa Hajar**

---

**APPORT DE L'ECHANTILLONNAGE**  
**ALEATOIRE DANS LE CADRE DE**  
**DIAGNOSTIC DES MACHINES**  
**TOURNANTES**

---

Devant le jury composé de :

Moubayed Nazih	Professeur à l'Université Libanaise	Examineur
Antoni Jérôme	Professeur à l'Université de Lyon	Rapporteur
Diab Mohamad	Professeur à l'Université de Rafic Hariri	Rapporteur
Guillet François	Professeur à l'UJM, Saint-Etienne	Examineur
Al Badaoui Mohamad	Professeur à l'UJM, Saint-Etienne	Co-directeur
Raad Amani	Professeur à l'Université Libanaise	Co-encadrant
Khalil Mohamad	Professeur à l'Université Libanaise	Co-Directeur
Dib Rabih	Professeur à l'Université Libanaise	Invité

**CONTRIBUTION OF RANDOM SAMPLING IN THE  
CONTEXT OF ROTATING MACHINERY DIAGNOSTIC  
A THESIS**

Submitted in partial fulfillment of the requirements for the degree of

**Doctor of Philosophy in Engineering**

At

**UNIVERSITY OF LYON, JEAN MONNET SAINT-ETIENNE UNIVERSITY,  
LASPI, FRANCE**

Under a Codirecting Convention with

**LEBANESE UNIVERSITY- DOCTORAL SCHOOL OF SCIENCE AND  
TECHNOLOGY- AZM CENTER FOR RESEARCH IN BIOTECHNOLOGY AND  
ITS APPLICATIONS**

**BY**

**HAJAR Mayssa**

**Tripoli, 2018**

**HAJAR MAYSSA, 2018**

## *Acknowledgment*

*Though only my name appears on the cover of this dissertation, many people have contributed to its production. I owe my sincere gratitude to God then to all those who supported me to achieve this work.*

*First and foremost, I want to thank my advisors Dr.Amani Raad and Prof. Mohammed El Badaoui for their support and guidance all along this thesis. They had been actively interested in my work and always available to advise me.*

*Words are never capable to help me to thank Dr.Raad, though, I am so grateful for her patience, motivation, understanding, encouragement and knowledge. Prof.Badaoui didn't let distances and countries to impede the fruitful cooperation between us. I am immensely thankful for his support, his encouragement, his flexibility and all the opportunities he offered to me during this thesis.*

*I would also like to give a heartfelt special thanks to my directors Prof. Francois Guillet and Dr. Mohamad Khalil for giving me the opportunity to do this dissertation and supporting me from the beginning until the end.*

*I am also very thankful to Dr.Frederic Bonnardot for his support, his cooperation, his rich knowledge and for offering me all the help I needed during the experimentation in LASPI.*

*For this dissertation, I would like to thank my review committee members Prof. Jerome Antoni and Prof. Mohamad Diab for accepting to read my dissertation. I would also thank my examination committee members. Thank you in advance for your time and constructive comments and suggestions.*

*I am especially grateful for my brother Taha Hajar for his great company during my travels to France. In fact, it is not the only thing that makes you so exceptional...*

*I would love to thank also, Dr. Halil Ibrahim Çackar, my colleagues Dr. Firas Zakaria and Dr. Donald Rotimbo and Mr.Lucien Peris for their gentle support in accomplishing my acquisitions, Without your efforts and inspirational discussions I could not have been able to validate my work.*

*A special thanks to my family, especially my mom, who offered my kids a tender environment during my travel and all the work time I spent during the years of thesis. A special thanks to my sister Sarah Hajar, sister in law Mira Haddad, my special friends Dr. Lina Nachabe and Rim Haj Ali, you will never know how much your support has been priceless for me.*

*As I scramble, I still not find words that express my gratitude to all my family and my friends. For my family in law, thank you for all the sacrifices that you have made on my behalf. For my Mom and Dad thank you for giving me a solid foundation to conquer life challenges. It is from you and my siblings, especially my brother Dr. Nasser Hajar, that I have learned hard working, self-confidence, persistence and independency. It is due to these factors I am accomplishing my dissertation now even though all my critical situations.*

*For my two angels, Sana and Mohamad, you had been a twinkle in my eyes since you were born. You are the bright light of my life. Your presence motivated and inspired me. I love you so much.*

*Last but not least, my sincere and deep gratitude goes to my husband Rabie Messayke. You cannot imagine what your presence in my life meant to me. Thank you for supporting me and offering me all the facilities to accomplish this dissertation, without you I would never get here.*

*Thanks God for all you have given to me during these years.*

# TABLE OF CONTENTS

<b>LIST OF ABBREVIATIONS</b> .....	7
<b>LIST OF VARIABLES</b> .....	8
<b>ABSTRACT</b> .....	11
<b>INTRODUCTION</b> .....	12
<b>1 Chapter 1: Random Sampling Definition</b> .....	16
1.1 Introduction .....	16
1.2 Compressed Sensing Theory .....	19
1.2.1 CS Definition.....	19
1.2.2 Sparsity and Incoherence Definition .....	20
1.2.3 Reconstruction in CS.....	21
1.3 Random Sampling: Definition and Condition of Use .....	21
1.3.1 Random point process .....	22
1.3.2 Stationary point process .....	23
1.3.3 Temporal condition .....	25
1.4 Random Sampling Modes .....	27
1.4.1 Additive Random Sampling (ARS).....	27
1.4.2 Jittered Random Sampling .....	35
1.4.3 Random Skip Sampling (RSS).....	40
1.4.4 Time-quantized Random Sampling (TQRS) .....	41
1.5 Conclusion.....	46
<b>2 Chapter 2: Spectral Analysis of Random Sampling</b> .....	47
2.1 Introduction .....	47
2.2 Spectral Analysis in Uniform Sampling.....	47
2.2.1 Fourier Transform of Deterministic Signal .....	47
2.2.2 Spectral Analysis for Random Signals .....	50
2.3 Spectral Analysis for Random Sampling.....	53
2.3.1 FT of the Deterministic Signal .....	54
2.3.2 PSD of $x_s(t)$ .....	56
2.3.3 RS Impact .....	62
2.3.4 Time Quantization Effect on RS PSD .....	76
2.3.5 Spectral Analysis Techniques for Randomly Sampled Signals.....	79
2.1 Conclusion.....	83
<b>3 Chapter 3: Simulation and Hardware Implementation</b> .....	85

3.1	Introduction .....	85
3.2	Impact of Time Step Quantization $\Delta$ .....	86
3.3	Procedure of RS and Simulation of Simple Examples .....	87
3.4	Simulation Study of RS .....	90
3.4.1	Impact of R .....	91
3.4.2	Impact of N .....	94
3.5	Zero Insertion Impact .....	98
3.5.1	Selection of Welch Parameters .....	99
3.6	Hardware Implementation .....	101
3.6.1	Review .....	101
3.6.2	Acquisition of Signals from Function Generator .....	103
4	Chapter 4: Application on Vibration Signals .....	107
4.1	Introduction .....	107
4.2	Bearing .....	107
4.2.1	Definition .....	108
4.2.2	Possible Defections .....	108
4.2.3	Diagnostic Methods .....	110
4.3	Gear .....	112
4.3.1	Definition .....	113
4.3.2	Possible Defections .....	114
4.3.3	Diagnostic Methods .....	115
4.4	RS Application .....	116
4.4.1	Bearing .....	116
4.4.2	Gear .....	128
4.5	Conclusion .....	139
5	Conclusion & Perspective .....	141
	<b>BIBLIOGRAPHY</b> .....	145
	Appendix A: Compressed Sensing Review .....	153
A.1	Compressed Sensing Theory .....	153
A.2	CS Definition .....	153
A.3	Sparsity Definition .....	154
A.4	Incoherence .....	155
A.5	Restricted Isometry Property .....	155
A.6	Reconstruction in CS .....	156
	Appendix B: Calculation of $\sigma/T_{Sm}$ in TQRS .....	157

Appendix C: PSD calculation of Beutler and Leneman ..... 159

## LIST OF FIGURES

Figure 1.1 Simple Example of Each Type of Sampling .....	17
Figure 1.2 Level-Crossing Sampling .....	18
Figure 1.3 Vibration signal of a Gear in Time and Frequency Domain .....	20
Figure 1.4 Time Process for $n \geq 1$ .....	23
Figure 1.5 The PDF of the instants $t_n$ in the ARS mode with the Uniform distribution $[0,2]$ .....	30
Figure 1.6 The PDF of the instants $t_n$ in the ARS mode with a Gaussian distribution $(1,1)$ .....	30
Figure 1.7 $p_s(t)$ of ARS mode with Uniform distribution, where $T_{sm}=1$ , and $\sigma$ varying to have multiple values of $\sigma/T_{sm}$ and $N=30$ .....	32
Figure 1.8 $p(t)$ of ARS with Gaussian distribution, $T_{sm}=1$ , $N=30$ and $\sigma$ varying .....	33
Figure 1.9 HARS mode the sequence after $tN/2$ is symmetric to the sequence before .....	35
Figure 1.10 $p_n(t)$ of a JRS with uniform distribution ( $\sigma=0.2887$ ) at the instants 1 to 7 with 15 and 25 .....	39
Figure 1.11 $p_n(t)$ of a JRS mode with Gaussian distribution at the instants 1 to 7 with 15 and 25 .....	39
Figure 1.12 $p_n(t)$ of JRS with uniform distribution ( $\sigma=0.115$ ) at the instants 1 to 7 with 15 and 25 .....	39
Figure 1.13 $P_s(t)$ for the JRS with Gaussian distribution with $T_{sm}=1$ and different values of $\sigma$ ...	40
Figure 1.14 Explication of TQRS for $q_T=3$ .....	42
Figure 1.15 TQRSH for $q_T=3$ .....	43
Figure 1.16 Quantized standard deviation variation in term of $q_T$ .....	46
Figure 2.1 An example of a signal $x(t)$ with its FT before and after uniform sampling .....	48
Figure 2.2 Uniform sampling with a period $F_s < 2F_{max}$ .....	49
Figure 2.3 Methods of Spectral Analysis for Random Signals in Uniform Sampling .....	51
Figure 2.4 The application of Bartlett and Welch modifications .....	52
Figure 2.5 The noise term $N(f)$ in ARS with uniform distribution for different values of $r < 0.5$ and $T_{sm}=10s$ .....	63
Figure 2.6 The noise term $N(f)$ in ARS with uniform distribution for different values of $r > 0.5$ and $T_{sm}=10$ .....	63
Figure 2.7 The noise term $N(f)$ in ARS with uniform distribution for different values of $T_{sm}$ with $r=0.5$ (left) and $r=1$ (right) .....	64
Figure 2.8 The spectrum $\Phi_{xs}(f)$ in ARS with uniform distribution for different values of $T_{sm}$ with $r=0.5$ (left) and $r=1$ (right) .....	64
Figure 2.9 The Maximum of $N(f)$ in term of $T_{sm}$ for $r=0.5$ and $r=1$ .....	66
Figure 2.10 The Noise Term Convoluting $\Phi_x(f)$ for Different Values of $\sigma$ with $T_{sm}=1$ .....	67
Figure 2.11 The Spectrum $\Phi_{xs}(f)$ for Different Values of $T_{sm}$ with $\sigma=0.167T_{sm}$ (left) and $\sigma=0.333T_{sm}$ (right) .....	68
Figure 2.12 The Noise Term Convoluting $\Phi_x(f)$ for $T_{sm}=0.1$ with $\sigma=0.167$ , $T_{sm}$ (left) and $\sigma=0.333T_{sm}$ (right) .....	68
Figure 2.13 The Maximum of $N(f)$ in term of $T_{sm}$ for $\sigma=0.333$ and $\sigma=167$ .....	69
Figure 2.14 Noise term convoluting $\Phi_x(f)$ with a cutting frequency $1/T_{sm}$ .....	71
Figure 2.15 The Spectrum $\Phi_{xs}(f)$ of $x_{sin}(t)$ in case of JRS with uniform distribution for different $T_{sm}$ Values .....	72
Figure 2.16 Module of the CF of Gaussian distribution in JRS Mode with $T_{sm}=1$ for different $\sigma$ values .....	73
Figure 2.17 $N_q(f)$ in case of TQJRS with uniform distribution over the interval $[0; 10 \Delta]$ .....	78
Figure 2.18 $N_q(f)$ in Case of TQJRS with Uniform Distribution Over almost one Period $\Delta$ .....	79
Figure 3.1 Two Simulations of a Signal (100 Hz and 150Hz) with a Quantization Step = 0.006 at the Top and Step=0.003 at the Bottom .....	86
Figure 3.2 The PSD of the signal $x_{sin}(t)$ in ARS with Gaussian for $N=39$ $T_{sm}=0.1s$ and $R=1$ .....	89
Figure 3.3 The PSD of the signal $x_{sin}(t)$ in ARS with Gaussian for $N=39$ $T_{sm}=0.01s$ and $R=1$ ...	89

Figure 3.4 The PSD of the signal $X_{\sin}(t)$ in ARS with Gaussian for $N=100$ $T_{Sm}=0.001s$ and $R=1$	89
Figure 3.5 The PSD of the signal $x_{\sin}(t)$ with ARS mode and Gaussian distribution: $N=390$ $T_{Sm}=0.01s$ with $R=1$ (left) and $R=2$ (right)	90
Figure 3.6 Amplitude/Alias variation in term of $R$ in ARS+ Uniform	92
Figure 3.7 Amplitude/Alias variation in term of $R$ in ARS +Gaussian	93
Figure 3.8 Amplitude/Alias variation in term of $R$ variation in JRS+uniform	93
Figure 3.9 Amplitude/Alias variation in term of $R$ variation in JRS+Gaussian	94
Figure 3.10 Comparison of the smallest amplitude of the signal to the noise in ARS with uniform distribution	95
Figure 3.11 Comparison of the smallest amplitude of the signal to the noise in ARS with Gaussian distribution	96
Figure 3.12 Comparison of the Smallest Amplitude of the Signal to the Noise in JRS with Uniform Distribution	97
Figure 3.13 DFT of the RS signal before and after zero insertion	98
Figure 3.14 PSD of the signal before and after zero insertion and the correlation between both PSD	99
Figure 3.15 Apodization windows in time and frequency domains	100
Figure 3.16 FFT of the triangular waveform with uniform sampling	105
Figure 3.17 Comparison between two DFT of a triangular signal having a frequency of 1 kHz and sampled using a JRS (on the left) and an ARS (on the right)	105
Figure 4.1 Bearing Components	108
Figure 4.2 A Pair of Gears with a ratio $G_r$	113
Figure 4.3 The bench containing the rotating motor with bearing	116
Figure 4.4 The accelerometer acquiring vibration signals from the bearing	117
Figure 4.5 The uniformly sampled signal of the normal bearing in time domain	118
Figure 4.6 The FFT (a) and the Welch periodogram (b) of the envelop of the uniformly sampled signal of a normal bearing	118
Figure 4.7 Variation of amplitudes in term of $\Delta$ (sec)	119
Figure 4.8 The variation of amplitudes in term of $F_{Sm}$ (Hz) in Welch periodogram	120
Figure 4.9 The variation of amplitudes in term of $F_{Sm}$ (Hz) in LS periodogram	120
Figure 4.10 The Welch (a) and the LS (b) periodogram of the envelop of the randomly sampled signal in ARS with unifrom of the normal bearing	121
Figure 4.11 The randomly sampled signal of the normal bearing in time domain within 4 seconds (a) and 40 seconds (b)	121
Figure 4.12 The FFT (a) and the Welch periodogram (b) of the envelop of the uniformly sampled signal of defected bearing	122
Figure 4.13 The uniformly sampled signal of defected bearing time domain	122
Figure 4.14 The amplitudes of characteristic frequencies compared to noise amplitude in term of $R$ in case of JRS+Unif in Welch periodogram	123
Figure 4.15 The variation of the amplitudes in term of $F_{Sm}$ ( $1/T_{Sm}$ ) in ARS+Unif	125
Figure 4.16 The variation of amplitudes in term of $F_{Sm}$ ( $1/T_{Sm}$ ) in ARS+Gauss	125
Figure 4.17 The variation of amplitudes in term of $F_{Sm}$ ( $1/T_{Sm}$ ) in JRS+Unif	125
Figure 4.18 The variation of amplitudes in term of $N$ in ARS+Unif	126
Figure 4.19 The variation of amplitudes in term of $N$ in ARS+Gauss	126
Figure 4.20 The variation of amplitudes in term of $N$ in JRS+Unif	126
Figure 4.21 The randomly sampled signal of the defected bearing within ARS+Unif in time domain	127
Figure 4.22 The Welch (a) and the LS (b) periodograms of the randomly sampled signal envelop of the defected bearing in ARS+Unif	127

Figure 4.23 The Welch (a) and the LS (b) periodograms of the randomly sampled signal envelop of the defected bearing in JRS+Unif .....	128
Figure 4.24 Gear test bench with an accelerometer directly above the gear under test.....	129
Figure 4.25 Gear test bench kinematic scheme .....	129
Figure 4.26 The FFT of the uniformly sampled gear vibration around $F_{\text{mesh}}$ .....	130
Figure 4.27 The Welch periodogram of gear vibration with different apodization windows around $F_{\text{mesh}}$ .....	131
Figure 4.28 the Welch periodogram of gear vibration with Kaiser window for different L .....	131
Figure 4.29 the Welch periodogram of gear vibration with Hamming window for different L..	132
Figure 4.30 the Welch periodograms of the gear vibration and the structure transfer function..	132
Figure 4.31 Amplitudes and noise variation with $F_{\text{Sm}}$ in Welch and LS periodograms of the gear vibration in ARS+Unif .....	134
Figure 4.32 Amplitudes and noise variation with $F_{\text{Sm}}$ in Welch and LS periodograms of the gear vibration in ARS+Gauss.....	135
Figure 4.33 Amplitudes and noise variation with $F_{\text{Sm}}$ in Welch and LS periodograms of the gear vibration in JRS+Unif .....	135
Figure 4.34 Amplitudes and noise variation with N in LS periodogram of the gear vibration in ARS+Unif.....	136
Figure 4.35 Amplitudes and noise variation with N in LS periodogram of the gear vibration in ARS+Gauss .....	136
Figure 4.36 Amplitudes and noise variation with N in LS periodogram of the gear vibration in JRS+Unif .....	137
Figure 4.37 LS periodogram around $F_{\text{mesh}}$ of the gear vibration in ARS+Unif .....	137
Figure 4.38 LS periodogram around $F_{\text{mesh}}$ of the gear vibration in ARS+Gauss.....	138
Figure 4.39 LS periodogram around $F_{\text{mesh}}$ of the gear vibration in JRS+Unif .....	138
Figure C.1 Relationship between $N_s(t)$ and $s(t)$ .....	159

List of Tables

Table 1.1 the $T_{\text{sd}}$ for each case of the ARS with the Uniform distribution.....	32
Table 1.2 the Tsd for each case of the ARS with the Uniform distribution .....	33
Table 2.1 Summary on RS modes features and parameters selection .....	75
Table 3.1 Different simulated values of Tsm, N and R.....	91

## LIST OF ABBREVIATIONS

<b>ADC</b>	Analog to <b>D</b> igital <b>C</b> onverter
<b>AR</b>	Auto- <b>R</b> egressive
<b>ARMA</b>	Auto- <b>R</b> egressive <b>M</b> oving <b>A</b> verage
<b>ARS</b>	Additive <b>R</b> andom <b>S</b> ampling
<b>CDF</b>	<b>C</b> umulative <b>D</b> ensity <b>F</b> unction
<b>CF</b>	<b>C</b> haracteristic <b>F</b> unction
<b>CRS</b>	<b>C</b> orrelated <b>R</b> andom <b>S</b> ampling
<b>CS</b>	<b>C</b> ompressed <b>S</b> ensing
<b>DCT</b>	<b>D</b> iscrete <b>C</b> osine <b>T</b> ransform
<b>DFT</b>	<b>D</b> iscrete <b>F</b> ourier <b>T</b> ransform
<b>DASP</b>	<b>D</b> igital <b>A</b> lias-free <b>S</b> ignal <b>P</b> rocessing
<b>DTFT</b>	<b>D</b> iscrete <b>T</b> ime <b>F</b> ourier <b>T</b> ransform
<b>ESD</b>	<b>E</b> nergy <b>S</b> pectral <b>D</b> ensity
<b>FFT</b>	<b>F</b> ast <b>F</b> ourier <b>T</b> ransform
<b>FT</b>	<b>F</b> ourier <b>T</b> ransform
<b>HARS</b>	<b>H</b> ybrid <b>A</b> dditive <b>R</b> andom <b>S</b> ampling
<b>iid</b>	independent and identically distributed
<b>JRS</b>	<b>J</b> ittered <b>R</b> andom <b>S</b> ampling
<b>LS</b>	<b>L</b> omb and <b>S</b> cargle
<b>MA</b>	<b>M</b> oving <b>A</b> verage
<b>MRI</b>	<b>M</b> edical <b>R</b> esonance <b>I</b> maging
<b>MUSIC</b>	<b>M</b> ultiple <b>S</b> ignal <b>C</b> lassification
<b>NUS</b>	<b>N</b> on-Uniform <b>S</b> ampling
<b>PDF</b>	<b>P</b> robability <b>D</b> ensity <b>F</b> unction
<b>PSD</b>	<b>P</b> ower <b>S</b> pectral <b>D</b> ensity
<b>RIAA</b>	<b>R</b> eal-valued <b>I</b> terative <b>A</b> daptive <b>A</b> pproach
<b>RIP</b>	<b>R</b> estricted <b>I</b> sometry <b>P</b> roperty
<b>RS</b>	<b>R</b> andom <b>S</b> ampling
<b>RSS</b>	<b>R</b> andom <b>S</b> kip <b>S</b> ampling
<b>SPP</b>	<b>S</b> tationary <b>P</b> oint <b>P</b> rocess
<b>TQRS</b>	<b>T</b> ime-quantized <b>R</b> andom <b>S</b> ampling
<b>TQRSH</b>	<b>TQRS</b> in <b>H</b> ardware implementation
<b>WSN</b>	<b>W</b> ireless <b>S</b> ensor <b>N</b> etwork

## LIST OF VARIABLES

$a$	Sparse representation of the original signal
$T_s$	Sampling period
$T_{Sm}$	Mean Sampling period
$T_{Sa}$	Period for Periodic Arbitrary Sampling
$x(t)$	Original signal to be sampled
$y$	Observation of $x$ in CS
$\Phi$	Sensing matrix
$\Psi$	Sparsity matrix
$\varphi_k$	Sensing waveforms
$s$	Sparse solution
$n$	Index of the sample or the sampling instant
$P$	Number of measurements
$\delta(t)$	Dirac impulse function
$x_s(t)$	Sampled signal
$S(t)$	sampling signal
$t_n$	$n^{\text{th}}$ instant of sampling
$\{t_n\}$	Stationary random time process
$\{\alpha_n\}$	Stationary random impulse process
$\{\theta_n\}$	Random time point process
$\{y_n\}$	Discrete time random process
$\rho$	Correlation between two consecutive impulses
$p_n(t)$	PDF of the $n^{\text{th}}$ instant of sampling ( $t_n$ )
$p_s(t)$	Sampling point density function
$\theta_n$	Random time interval between two consecutive instants
$T_{sd}$	Stationarity delay time
$\sigma$	Standard deviation of random variable
$\mu$	Mean value of random variable
$X(f)$	Fourier Transform of the sampled signal $x(t)$
$X_s(f)$	Fourier Transform of the sampled signal $x_s(t)$
$p_{unif}(t)$	PDF of uniform distribution
$p_{gauss}(t)$	PDF of Gaussian distribution
$p_{exp}(t)$	PDF of exponential distribution
$f_{exp}(t)$	CDF of exponential distribution
$E[t_i]$	Expectation for $t_i$
$\lambda$	Rate parameter or mean of the exponential distribution

$r_g$	Ratio of the geometric series
$N$	Number of samples
$M$	Segment length
$L$	Number of segments
$u$	Random jitter
$\tau$	Random time interval
$u^+$	Positive jitter
$\partial$	Random skipping interval in RSS
$\Delta$	Time Quantization Step
$q_T$	Temporal quantization factor
$q(t)$	Probability of quantization
$P_i(t)$	Cumulative density function
$p_u(t)$	PDF of the random jitter
$D$	Deviation of the interval of support
$D_U$	Deviation in the uniform distribution
$D_G$	Deviation in the Gaussian distribution
$F_m$	Nyquist frequency
$\Delta f$	frequency resolution
$T$	total duration of the acquired signal $x(t)$
$\hat{x}_d(f)$	DTFT of $x(t_n)$
$ESD_{x(t_n)}$	Energy Spectral Density of $x(t_n)$
$R_{x_s}(k)$	Discrete autocorrelation of $x_s(t)$
$PSD_{x_s}(t)$	PSD of $x_s(t)$
$PSD_P(f)$	Periodogram of $x_s(t)$
$PSD_{P_m}(f)$	Modified periodogram of $x_s(t)$
$PSD_{C_{BT}}(f)$	Correlogram of $x_s(t)$
$\varphi_u(f)$	Characteristic function of the random jitter $u$
$\varphi_\tau(f)$	Characteristic function of the random interval $\tau$
$\hat{X}_{ARS}(f)$	FT of $x_s(t)$ in ARS
$\hat{X}_{JRS}(f)$	FT of $x_s(t)$ in JRS
$\Phi_x(f)$	PSD of $x(t)$
$\Phi_s(f)$	PSD of $S(t)$
$\Phi_{x_s}(f)$	PSD of $x_s(t)$
$\hat{n}(f)$	Apparition noise

$N_s(t)$	Primitive of $S(t)$
$N(t)$	Noise term in time domain
$N(f)$	Noise term in frequency domain
$X_{\sin}(t)$	Signal composed of sum of two sine waves

## ABSTRACT

Nowadays, machine monitoring and supervision became one of the most important domains of research. Many axes of exploration are involved in this domain: signal processing, machine learning and several others. Besides, industrial systems can now be remotely monitored because of the internet availability. In fact, as many other systems, machines can now be connected to any network by a specified address due to the Internet of Things (IOT) concept. However, this combination is challenging in data acquisition and storage. In 2004, the compressive sensing was introduced to provide data with low rate in order to save energy consumption within wireless sensor networks. This aspect can also be achieved using random sampling (RS). This approach is found to be advantageous in acquiring data randomly with low frequency (much lower than Nyquist rate) while guaranteeing an aliasing-free spectrum. However, this method of sampling is still not available by hardware means in markets. Thus, a comprehensive review on its concept, its impact on sampled signal and its implementation in hardware is conducted. In this thesis, a study of RS and its different modes is presented with their conditions and limitations in time domain. A detailed examination of the RS's spectral analysis is then explained. From there, the RS features are concluded. Also, recommendations regarding the choice of the adequate mode with the convenient parameters are proposed. In addition, some spectral analysis techniques are proposed for RS signals in order to provide an enhanced spectral representation. In order to validate the properties of such sampling, simulations and practical studies are shown. The research is then concluded with an application on vibration signals acquired from bearing and gear. The obtained results are satisfying, which proves that RS is quite promising and can be taken as a solution for reducing sampling frequencies and decreasing the amount of stored data. As a conclusion, the RS is an advantageous sampling process due to its anti-aliasing property. Further studies can be done in the scope of reducing its added noise that was proven to be cyclostationary of order 1 or 2 according to the chosen parameters.

# INTRODUCTION

Rotating machinery, as one of the most common types of mechanical equipment, plays an important role in industrial applications [1]. The field of the rotating machinery goes back to 5000 years ago when the human invented the wheel, and is being developed until this moment [2]. This shows that this type of solution is irreplaceable in the engineering areas. Hence, much effort was, and is still being spent in evolving rotating machinery.

Almost reaching the physical limitations, engineers are now pushing the complexity of the rotating machines to a different level. Not only the machines are getting more complicated, but also stricter constraints on the precision are demanded. This is making the fault at the same time, harder to analyze and more expensive. From this point, a strong demand for advanced fault diagnosis techniques has emerged and becomes more and more significant[3].

Most of the used machinery operates by means of bearings, gears and other rotating parts. The nature of these components and the harsh environment where they are installed produce frequent faults. Average faults may cause decrease in the machine's performance and on the long run a complete breakdown [4]. In order to keep the machine performing at its best and avoid personal casualties and economical loss, different methods of fault diagnosis have been developed and used effectively to detect and localize machine faults. These methods tend to detect defections as soon as possible in order to minimize the damage. One of the principal tools for diagnosing rotating machinery problems is the vibration analysis [5][6]. Through the use of some processing techniques of vibration signals, it is possible to obtain vital diagnosis information. These techniques are used to extract the fault features and then identify the fault patterns. In this context, many conventional methods such as spectral analysis and time-frequency analysis are studied in researches since their apparition and implemented in many applications [3]. On one hand, the most widely used tool in spectrum analysis is the power spectrum, yet some useful auxiliary tools for spectrum analysis are applied for condition monitoring as envelope analysis, side band structure analysis and spectral indicators like the spectral kurtosis. Despite the wide acceptance of power spectrum, other useful spectra for signal processing have been developed to offer advanced diagnosing, for instance, high-order spectrum, like bispectrum or trispectrum. Bispectrum analysis has been shown to have wide application in machinery diagnostics for components as bearings and gears in rotating machines. In addition, some deduced techniques out of the spectral domain are also used for monitoring such as the Cepstrum obtained by the inverse Fourier transform. On the other hand, the time-frequency

domain analysis is advantageous in its ability to deal with stationary and non-stationary signals. Its main feature remains in visualizing the distribution of the frequency components within the dimension of time. Examples of methods using such approach are: Short Time Fourier Transform, Wigner-Ville Distribution, Wavelet Transform and the Empirical Mode Decomposition and its variants.

Apart from the advanced diagnosis methods, a revolution is arising in the machine monitoring domain, as many others, due to the availability of the internet. The Internet of Things (IoT), wireless sensor networks (WSN) and many other concepts are being introduced to all types of industries. Consequently, the remote monitoring for machinery became available to respond to the needs of the diagnostic domain. In fact, distant surveillance is highly appreciated in industry for multiple reasons. One, it adds more flexibility in monitoring. Two, it provides safer environments for human resources. Three, it creates opportunities to profit from international expertise. Last but not least, it eases automating data collection and big data analysis. Hence, all these advantages participate intensely in increasing the productivity and decreasing the cost [7].

Nonetheless, the listed advantages come with some challenges. The data offered by remote monitoring must be taken, delivered and processed “on time”. Otherwise, most of the advantages of this added complication are lost. This fact has led to tie these remote applications to the field of real-time systems. By definition, in a real-time system being a network, a collection of sensors, a collection of processors or a combination of all the mentioned, the correctness of a task relies not only on the logical result of the task but also delivering before the deadline. In such systems, the more tasks are assigned to the system, the higher the risk to meet the deadline becomes. Therefore, in industrial applications, a critical state might be reached, when the assigned tasks are numerous and each one is of high frequency [8].

Besides, designs of such real-time embedded systems usually push the device capabilities to the bare minimum in terms of storage as well as processing in order to minimize the size, the power consumption and the latency [9]. To address the processing constraints, most of the effort in the researches was around optimizing the system architecture [10]. Some other researches tackled the issue using cloud computing services [11][12].

As for the storage constraint, most of the recent researches were conducted to find the best distributed storage solution, whereas only few kept trying to find compressed storage solutions [13][14].

But what if only a small subset of this data is really needed to fulfill the same goal?

In the context of machinery monitoring, a frequent probing task or a highly demanding processing job may overload the processor and the storage. This contradicts the basics of the real-time system designs. Though, in remote monitoring, many machines are to be surveyed to make a real profit from the installation of the remote system. Consequently, a critical issue appears in implementing remote monitoring within a real time management for a set of machinery where vibration signals are usually acquired at high rate frequencies within long period of time which demands large data storage. Although many researches are of subject to enhance the performance of real-time capabilities of embedded systems, only few has optimized the solution based on the type of data in the circumstances of remote monitoring for industrial machines specifically.

For instance, in many applications where WSN are used, sensors are required to capture data at high frequencies which creates a major problem due to the high energy consumption and the demand of large data storage knowing that such sensors are of limited capacity. Consequently, the Compressive Sensing (CS) was invented to reduce the data storage and decrease the frequency of sampling [15]. The distinction introduced by such process of sensing resides in finding a way to capture just the important information from the object of interest. Though, this recently invented sampling mode is based on two essential principles counting on the sparsity of the signal, and on the use of random sensing matrices.

Such invention was as a source of inspiration that lead to this thesis scope. In reality, RS, which presents common aspect of CS, is applied in many applications[16], [17] [18]. Due to its anti-aliasing property, it may be inferred that within such process, sampling might be accomplished with low frequencies. But, as in CS, the signal to be acquired must be sparse in certain domain to achieve the advantage of low frequencies and low amount of data. Indeed, industrial machines are not of very high rotational speed, though the condition required by the Nyquist frequency imposes on the acquisition of vibration signals to be at the minimum double the highest frequency present in the corresponding spectrum. And consequently, to have better resolution, long signal are required in such conditions. These details, in addition to the sparse aspect in the frequency domain [19], make the probability of success in applying the RS on vibration signals very high and thus , the reduction of sampling frequency and amount of data is possible which helps in resolving already listed issues in remote monitoring.

According to the literature, RS is a promising sampling process due to its anti-aliasing property within some defined conditions. Though, the question that must be answered is: are these conditions compatible with the circumstances of vibration analysis? In addition, according to same references, the eliminated aliases are replaced by an additive noise floor, which may affect the low peaks in

vibration signal spectrum. So, is the RS really efficient and worth to be used in machine monitoring? What are then its limitations and how it could be managed??

In the aim of responding on these questions and doubts this thesis is conceived, and the following contributions were accomplished during the thesis work:

1. A very first real application of RS on vibration signals acquired from a normal gear and a bearing in normal and defected states, in order to evaluate the potential of RS in machine monitoring.
2. Quantitative formulations that gives the user a clear guide to choose the number of samples, the mean sampling period and the standard deviation when applying RS within its different modes.
3. A specific determination of the RS noise cyclostationarity order.
4. An enhanced method for spectral analysis of RS signals based on the zero insertion and the periodogram of welch.

This thesis begins in chapter 1 with a summary on the different sampling processes found in the literature to continue with the state of art on the already accomplished studies on RS within time domain with defining its different modes and different used probability distributions, to finally conclude with the temporal condition and stationarity condition that is essential for anti-aliasing property. In chapter 2, spectral analysis is reviewed for uniform sampling to continue in a consistent way with the spectral analysis for RS. The spectrum of randomly sampled signal is studied to conclude with the aspect of the added noise and the quantitative recommendations on the selection of the mean sampling frequency, the number of points and the standard deviation. After a review on the variety of techniques for spectral analysis for RS already present in the literature, the most adequate techniques are chosen to be applied on RS signals in simulation and on real acquired signals. In chapter 3, a verification of the results obtained in chapter 1 and 2 are verified by a simulation study, followed by a hardware implementation of RS done to verify the results on simple signals. Then, in chapter 4, a clear vision is presented on the most important features of vibration signals acquired from the essential machinery components: bearings and gears. To continue with the experimentation results obtained by the application of RS on a bearing in normal and defected state and a gear in normal state. A brief recapitulation on the achieved results is presented in the conclusion to evaluate the RS as a solution for the real-time monitoring of industrial machinery with a perspective on possible works that could be driven after this thesis.

# 1 Chapter 1: Random Sampling Definition

## 1.1 Introduction

In signal processing, the sampling process is the main step to pass from the continuous to the discrete time domain, in order to deal with numerical instead of analogical signals. This process may be applied in different ways according to the nature of the signal and the conditions of its environment. In this introduction the different sampling processes are overviewed. The comparison focuses on RS, in order to reveal the edge it has over the other sampling methods from the perspective of this thesis.

The generalized form of sampling is the Non-Uniform Sampling (NUS) or irregular sampling, where the acquired samples may be chosen arbitrarily, randomly or whenever the signal is available [20]. Although the instants of sampling are not evenly spaced in NUS, the sequence of these instants may be periodic leading to a periodic form of NUS. In Uniform Sampling, one of the most common sampling techniques in data acquisition, the samples are chosen at a constant rate without interruption and with period  $T_s$ . Though, in cases where data is missed or unreached, the sampling is no longer uniform and is considered as NUS. In Figure 1.1, examples of the various sampling methods are shown. In Arbitrary Sampling, the instants of sampling are chosen without any previous assumption, while in RS the time inter-sample intervals follow a random distribution having a constant mean equal to  $T_{sm}$ . In fact, the examples shown in Figure 1.1 are all clock-based sampling. However, there exist some samplings that are event-based and are considered as Random or Arbitrary Sampling [21]. One of the most used processes is the Level-Crossing Sampling, which is considered as a RS based on events instead of clock signals. Figure 1.2 illustrates the concept of this process: the Analog to Digital Converter (ADC) acquires a sample from the signal every time the latter is equal to any level of the predetermined amplitude levels. The acquired amplitudes and their corresponding instants of acquisition are saved as the randomly sampled signal with its time vector [22]. The analysis of such type of sampling is considered to be difficult and less used than periodic and clock based sampling [21], [23], thus this thesis is focused on sampling based on time clock signal.

Hence, whether it is clock based or event-based, Non-Uniform Sampling is imposed in some cases due to inconvenient circumstances. One example is the unavailability of data at some instants like in astronomy, medicine, geophysical sciences and others [24]. Another example is the loss of some samples because of instrumentation malfunction or problems in communication [25], [26]. Besides,

in other cases, Non-Uniform Sampling is used on purpose in context of data compression, Digital Alias-free Signal Processing (DASP) and Compressed Sensing. In fact, when relating the sampling rate to the signal rate, the number of samples decreases when the signal varies slowly, which will lead to data compression [26], [27]. Moreover, RS, as a NUS process, is proposed in DASP in order to take advantage of its properties of anti-aliasing and sampling with low frequencies which are proven by Shapiro and Silverman in [27], [28]. Finally, a new way of sampling sparse signals is proposed to decrease the data storage and the sampling rate to minimize the energy consumption by sensors that are used in WSN [29]. This sampling process is known as the Compressed Sensing (CS), that is based on random sensing matrices [30] which is, somehow, equivalent to RS.

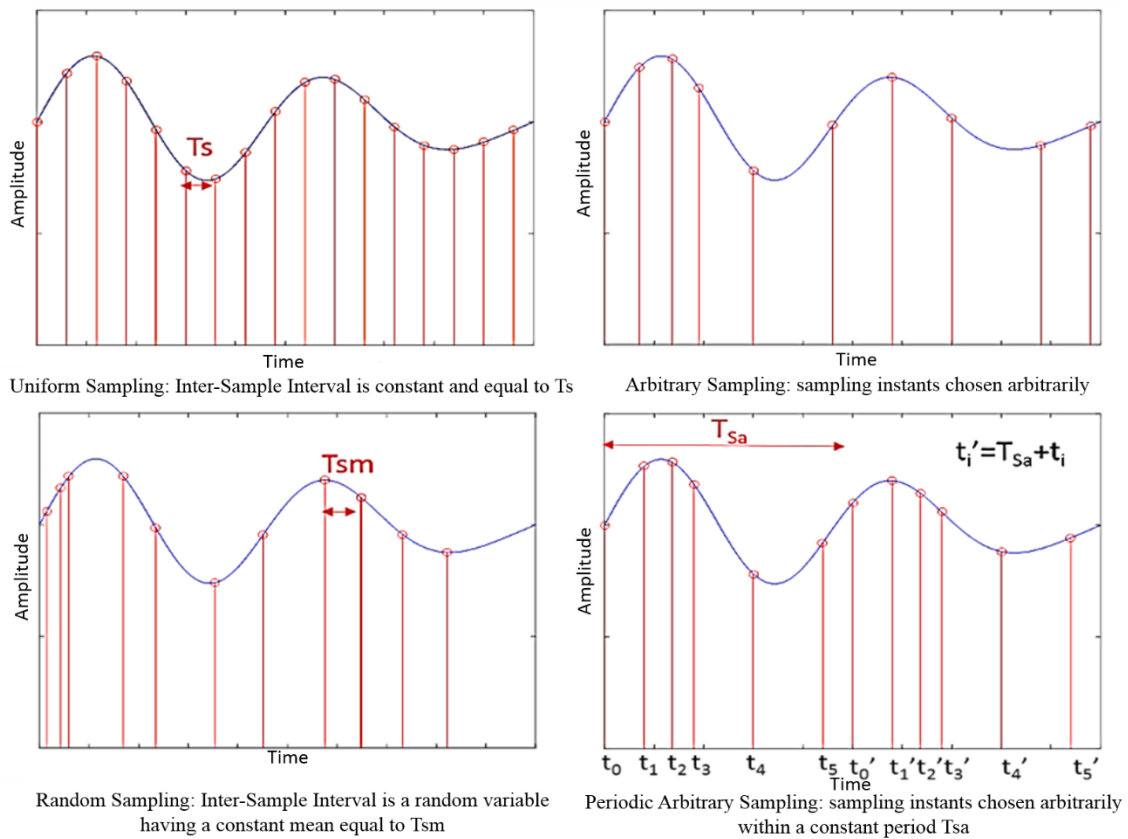


**Figure 1.1 Simple Example of Each Type of Sampling**

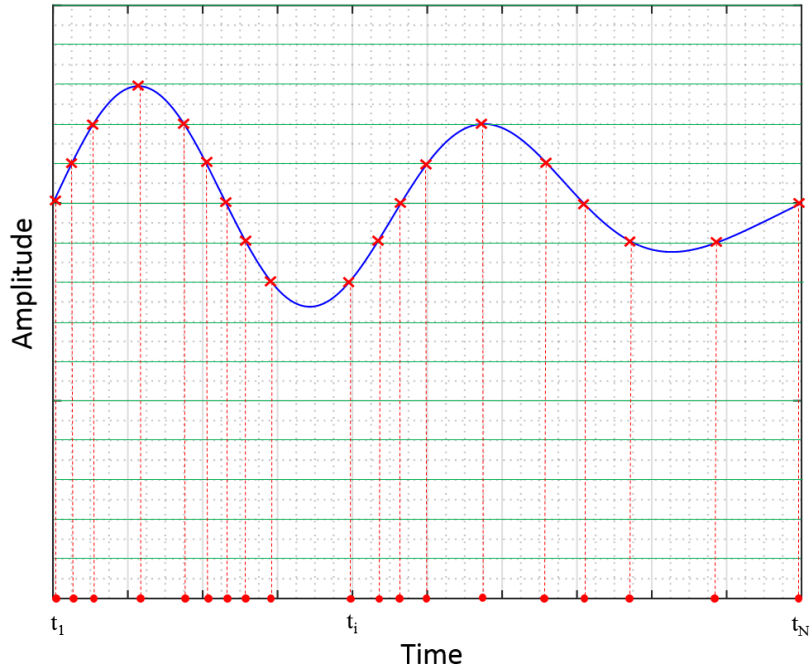


**Figure 1.2 Level-Crossing Sampling**

Consequently, CS and RS were applied in different domains and were the subject of many recent researches. On one hand, RS was first introduced as an intentionally used sampling by Shapiro and Silverman in [31] in 1960, and many publications were made then by Beutler and Leneman in the same period of time to study the spectral density of such process [32]–[34]. Later on, many theoretical studies were made, until 2000 when Wojtiuk explored the RS in simulation and suggested methods of practical implementation to use RS in radio communication [35]. This research was continued by Ben Romdhane in 2009 who gave more concise details of RS to be used in digitalization of multistandard signal[36]. Finally, Luo has elaborated a practical study of NUS, especially the RS with connecting it to the CS results, without determining the nature of signals to be sampled or their domain [37]. On the other hand, CS was first conceived in 2004. Since then, many applications of this process were studied in Computer Sciences, Astronomy, Medicine, Seismology, Radar and Telecommunication [38]. However, there was no application mentioned until the date of writing this thesis that indicates the use of RS or CS on vibration signals acquired from rotating machinery. Additionally, despite all these researches and studies, there are no sensors or devices manufactured to acquire samples at random instants in commercial markets.

In conclusion, having advantages in eliminating alias and in reducing the sampling frequency and the storage of data, the RS is found to be worth studying and exploring when applied on vibration signals. In addition, some important notions found in CS are used in RS application and merit to be mentioned. So, in this chapter, a brief summary on CS is presented in section 1.2 to reveal its

important advantages that can be exported to RS process application on vibration signals. Then the RS properties in time domain are studied in details. At the beginning, the definition of RS and its condition of use are presented in section 1.3 to clarify the methodology of selection of the sampling process parameters. In section 1.4, the different modes of RS with the probability distributions are explored and discussed. In Section 1.4.4, the notion of time quantization is introduced, as an RS mode, to complete the study of RS in the numerical time domain, as all the applications of RS are implemented in digital devices which deal with discontinuous time vectors. In the conclusion, a brief summary on the mode and parameter selection of the RS is given.

## 1.2 Compressed Sensing Theory

The intent of this section is to briefly overview the basic theory of CS, in order to highlight the fact that randomness can lead to a very effective sensing mechanism. More details are presented in Appendix A.

In fact, the CS was conceived for two major advantages: compressing data and managing the under-sampling situations. The main contribution in data compression in such sampling technique is in directly acquiring a compact amount of data instead of acquiring and then compressing. Therefore, the CS is used in many different domains where the data compression is needed or the number of measurements is limited. For instance, CS is mainly a research subject in Medical Resonance Imaging (MRI) [39][40], in astronomy imaging [41], Microarray sequencing in Biology [42], seismic imaging, and modal identification within civil engineering [38] and in many WSN based solutions [29].

### 1.2.1 CS Definition

CS is defined as a technique to acquire and represent compressible signals in a compressive way, at a rate significantly below the Nyquist rate. Foremost, the signal to be sampled or measured is  $x \in \mathbb{R}^P$ , the observation of  $x$  designated by  $y$  is defined by (1.1).

$$y = \Phi x \quad (1.1)$$

Where  $y \in \mathbb{R}^N$  and  $\Phi \in \mathbb{R}^{N \times P}$ .  $\Phi$  is defined as the sensing matrix, where  $\{\varphi_k\}_{k=1 \dots N}$  are the sensing waveforms. The problem of CS is expressed by how to choose  $\Phi$  in order to find an observation  $y$  of size  $N \ll P$  with the ability to reconstruct  $x$  from  $y$ . Hence, the CS is based on two main principles: the sparsity and incoherence, where the first is a condition concerning the original signal  $x$  and the second is related to the sensing matrix  $\Phi$ [43].

### 1.2.2 Sparsity and Incoherence Definition

The sparsity is a property equivalent to the compressibility of the signal, and it is verified when there exists a basis  $\Psi$  (known also as a dictionary) where the projection of the signal  $x$  is  $k$ -sparse. This means that the majority of the coefficients of  $x$  in the basis  $\Psi$  are zeros except  $k$  elements. Thus, when applying the CS on a compressible signal  $x$ , it is essential to find the basis  $\Psi$  where the coefficients of  $x$  in  $\Psi$ , are of majority of zero. A variant of transformations is used to find a sparse expansion of  $x$ , like the Fourier, the Wavelet, the Curvelet and the Discrete Cosine Transform (DCT) [15], [34], [38],[41]. Finally, due to the representation of  $x$  in the  $\Psi$  domain, the relation between  $x$  and its observation  $y$  becomes (1.2), where  $a$  is the vector representing  $x$  in  $\Psi$ .

$$y = \Phi x = \Phi \Psi a = A a \quad (1.2)$$

An example that clarifies this property is illustrated in Figure 1.3, where a signal acquired from a gear is compared to its Fourier transform (only single-sided amplitude spectrum), to show how the sparsity is increased in the frequency domain. The percentage of coefficients smaller than 10% of the highest amplitude is 23% in the time domain, while it is greater than 98% in the frequency domain. This example is considered as a simple evidence that vibration signals acquired from rotating machinery are sparse in the frequency domain.

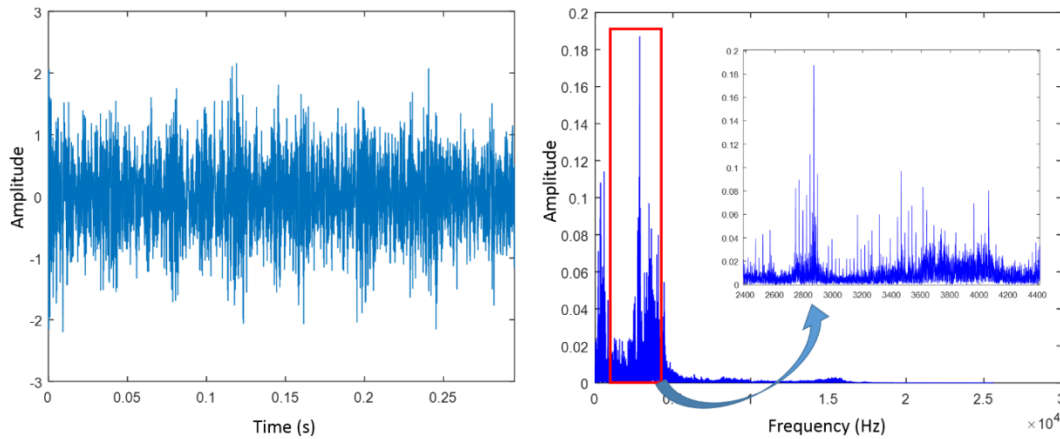


**Figure 1.3 Vibration signal of a Gear in Time and Frequency Domain**

As the purpose of CS is to conceive efficient sampling protocols that acquire the essential content of the sparse signal and condense it into a minor amount of data, these protocols must be non-adaptive and should capture the signal with a small number of fixed waveforms. Thus, these waveforms must be incoherent with the sparsifying basis  $\Psi$ . In other words, unlike the signal  $x$ , the sensing waveforms, that define the sensing matrix  $\Phi$ , must have a dense representation in the  $\Psi$  domain. In one of the pioneers references in CS, [43], it was concluded that the random matrices

are largely incoherent with any fixed basis  $\Psi$ . So, random sensing/sampling matrices are used within CS to guarantee incoherence condition. Therefore, the efficiency of RS is proven within the context of CS, where the data is acquired compressively with low rate sampling and can be reconstructed without loss.

### 1.2.3 Reconstruction in CS

The Restricted Isometry Property (RIP) is conceived to guarantee a robust signal reconstruction within CS [Appendix A]. According to [15],[45] and [46], it was proven that the random sensing matrices satisfy the RIP with an overwhelming probability when the number of measurements verifies the condition in (1.3).

$$N = O\left(k \log\left(\frac{p}{k}\right)\right) = \text{Cte.} \cdot k \quad (1.3)$$

The reconstruction in the CS context is to find the sparse solution 'a' that verifies the equation (1.2), the sparse solution s can be then expressed by (1.4).

$$s = \min_{a: Aa=y} \|a\|_{l_1} = A^T(AA^T)^{-1}y \quad (1.4)$$

Most of the reconstruction algorithms are based on this concept in finding the exact signal reconstructed, though, they differ in the criteria of minimization [Appendix A]. Greedy Iterative Algorithms are based on the  $l_2$  minimization like the Matching Pursuit, and the Convex optimization are based on the  $l_1$  minimization as the Basis Pursuit [43].

In conclusion, the CS captures the information contained in the signal within its sparsifying domain by the random sensing/sampling process with the ability of reconstructing the original signal when the number of measurements is a multiple of the k-sparse elements. As the vibration signals are considered sparse in the frequency domain, it can be deduced that RS is a promising sampling process when applied on such signals. Thus, this thesis is conceived to evaluate the potential of such sampling in vibration analysis context.

## 1.3 Random Sampling: Definition and Condition of Use

The sampling process is a way to convert continuous analogical signal  $x(t)$  into discrete time samples  $x_s(t)$ . These samples are chosen from the original signal at different instants. The time interval separating these instants is the fundamental criteria which determines the aspect of the sampling process is uniform or not. In time domain, the sampling process of the signal  $x(t)$  is modeled by a simple multiplication between  $x(t)$  and the sampling signal  $S(t)$ , where the model of

$S(t)$  varies according to the sampling process type. When the sampling is uniform,  $S(t)$  is defined as in (1.5).

$$S(t) = \sum_{n=-\infty}^{+\infty} \delta(t - t_n) \quad (1.5)$$

The  $n^{\text{th}}$  instant of sampling is  $t_n = nT_s$ , where the sampling period  $T_s$  is constant. The essential condition that must be respected in uniform sampling is the condition of Shannon or Nyquist: the sampling frequency  $F_s (=1/T_s)$  must be higher than twice the highest frequency within the signal  $x(t)$ , to assure a spectrum without distortion, though, aliases remain and should be filtered. While in RS, conditions are declared to guarantee compatibility with real implementations and to provide a spectrum free of aliases. In order to explain these conditions, the notion of the Random Point Process must be introduced first to present the model of the sampling signal in NUS and to clarify the concept of the Stationary Point Process and all the outcomes that may result from its validation. Afterward, the temporal condition that permits the implementation of RS in practice is explained.

### 1.3.1 Random point process

As the sampling instants  $\{t_n\}$  are considered points on the real timeline, they can be treated as a point process. As a statistical definition, a random point process is an ordered sequence of values along a time axis or a geographical space. In case of sampling signals, the random point process, which is used for samples' acquisition from real measured signals, must be a simple point process, i.e., all the points of the process  $\{t_n\}$  occur at distinct times [47].

Let  $\{\theta_n\}$ ,  $n=0, \pm 1, \pm 2, \dots$ , be the notation of the point process member :

$$t_n = \begin{cases} \theta_0 + \sum_{k=1}^n \theta_k & n \geq 1 \\ \theta_0 & n = 0 \\ \theta_0 - \sum_{k=n}^{-1} \theta_k & n \leq -1 \end{cases} \quad (1.6)$$

Where  $0 < \theta_n \leq \infty$  for all  $n$ .

For all values of  $n$  excluding zero each  $\theta_n$  represents the time interval between  $t_n$  and  $t_{n-1}$ . For  $n = 0$  the representation of  $\theta_0 = t_0$  is of an initial time value, or initial phase, of the sequence  $\{t_n\}$ .

Figure 1.4 represents a simple example of a time process for  $n \geq 1$ .

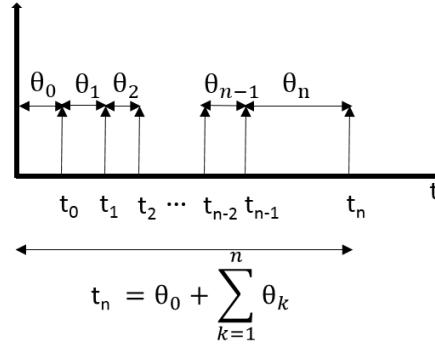


**Figure 1.4 Time Process for  $n \geq 1$**

Most of the recent studies on RS are based on the theory developed by Frederic Beutler and Oscar Leneman in the 1960's, where they concluded some important properties concerning the random point processes and their stationarity conditions [29]-[30]. Thus, they introduced the random impulse process as defined in (1.7).

$$S(t) = \sum_{n=-\infty}^{n=+\infty} \alpha_n \delta(t - t_n) \quad (1.7)$$

$S(t)$  is the sampling signal in case of NUS. It contains two random processes:  $\{t_n\}$  which is a stationary random time process, and  $\alpha_n$ , a stationary random process independent of  $\{t_n\}$ .  $\alpha_n$  is multiplying the Dirac Comb in order to include the concept of skipped (or missing) samples and amplitude errors' sampling. This process formula is conceived to model all the possible forms of NUS. To generalize the model of random impulse process,  $\rho$  is defined as the correlation between two consecutive impulses to take in consideration cases where pairwise independency is not confirmed (1.8).

$$\rho = E[\alpha_{n+m} \alpha_n] \quad (1.8)$$

### 1.3.2 Stationary point process

On one hand, according to [33], a random process is defined as stationary if the number of points in a set of fixed time intervals is invariant under any time shift which preserves the length and spacing of those intervals. Following this definition, three theorems were deduced concerning the stationary point process (SPP) and the autocorrelation function of  $S(t)$ , which will be discussed later in this chapter and in Chapter 2.

On the other hand, Bilinksis and Mikelson in [28] defined the SPP as the probability of a sample occurrence is the same everywhere on the time axis. To clarify this definition, some notations must be given.  $p_s(t)$ , the sampling point density function, is the sum of all the individual probability density functions (PDF)  $p_n(t)$ , where  $p_n(t)$  is the PDF of the  $n^{\text{th}}$  instant of sampling ( $t_n$ ). Also, if  $\theta_n$

is the random time interval between the sampling instants  $t_{n-1}$  and  $t_n$ ,  $T_{Sm}$  is the mean value of  $\theta_n$ . Thus, the condition of stationarity of a random point process is defined by (1.9).

$$p_s(t) = \sum_{n=1}^{\infty} p_n(t) = \frac{1}{T_{Sm}} \quad (1.9)$$

The convergence of the time sequence may be occurred after a certain time delay. So the authors also defined the stationarity time delay in (1.10).

$$T_{sd} = \frac{0.4 T_{Sm}^3}{\sigma^2} \quad (1.10)$$

$T_{Sm}$  and  $\sigma$  are the mean and the standard deviation of  $\theta_n$  [28]. This delay depends on the type of sampling, the probability distribution of sampling instants and the initial conditions of the sampling sequence. If the sampling point process is stationary, the sampling point density function  $p_s(t)$  is equal to  $1/T_{Sm}$  after a delay of time equal to  $T_{sd}$ . Consequently, when a sampling process is proven to be stationary, there are some properties that can be guaranteed. According to [35], once the sampling process is verified as stationary, with the assumption that the original signal is wide sense stationary, then it can be ensured that the sampled signal conserves the wide sense stationarity. Thus, in case the mechanical signals to be sampled have an aspect of cyclostationarity with a stationary random process, it can be assured that this aspect is conserved after sampling.

In [28], the authors define the SPP condition as the main origin of the anti-aliasing property of the RS. In fact, in the literature, many propositions were given to determine the circumstances that guarantee the alias-free aspect of RS. In [31], the authors explored the autocorrelation of the sampled signal and then deduced conditions on the autocorrelation of the sampling sequence, the latter autocorrelation function should be unique or belong to a limited family of functions to assure a unique spectrum for the sampled signal. In [48], these conditions were proved to be incomplete. The most sustaining condition is the one presented in [28], where the authors used the Fourier transform of periodic signals to prove that the RS applied by an SPP sequence leads to an alias free sampled signal. Moreover, in [36], the Fourier transform of aperiodic signals is used to prove the alias-free aspect of RS when verifying SPP condition. Due to the definition (1.9) where the sum of the PDF of  $n$  consecutive instants is equal to  $1/T_{Sm}$ , the calculation of the expectation of the Fourier transform  $X_s(f)$  of the sampled signal  $x_s(t)$  lead to a non-periodic result which is an alias-free spectrum.

And thus, according to the Alias-Free theorem, if the RS sequence verifies the SPP condition of Bilinskis and Mikelson, the spectrum of the analogic sampled signal is free of aliases. When the probability of acquiring a sample is the same on the whole time axis, there is a certainty in representing the signal in one realization without aliasing [28], [35].

### 1.3.3 Temporal condition

In [36], a study on the statistic parameters is introduced in order to measure the validity of the probability distribution to be used with RS within sampling real signals in practice. As mentioned before, the sampling instants  $\{t_n\}$  are considered as a random process, that should be simple. Thus, all  $t_n$  should be strictly increasing:  $0 \leq t_0 < t_1 < \dots < t_i < \dots < t_n$ , where  $\lim_{n \rightarrow \infty} t_n = +\infty$ . To fulfill such condition, limits in term of the mean sampling period are imposed on each instant  $t_i$ , to verify the relation in (1.11).

$$iT_{Sm} - \frac{T_{Sm}}{2} \leq t_i < iT_{Sm} + \frac{T_{Sm}}{2} \text{ for } 1 \leq i \leq n \quad (1.11)$$

However, the relation in (1.11) proposed by [36] is not general enough to take in consideration all possibilities of  $t_i$  that verify the increasing order condition. Thus, in this thesis, it is suggested that generally random instants  $t_i$  must validate the relation in (1.12) to guarantee a simple random process.

$$t_{i-1} < t_i \leq t_{i-1} + 2.T_{Sm} \text{ for } 1 \leq i \leq n \quad (1.12)$$

To determine this condition or limitation for each distribution, the PDF of the random instant of sampling ( $t_i$ ) and its corresponding interval must be clarified. In fact, in RS, the random instant is generated in terms of a random variable. The expression of the random instant varies according to the RS mode. In each mode, the random variable may follow any probability distribution. The most usable distributions with RS in the literature are: the uniform, Gaussian and exponential [35], some other distributions like Binomial and Bernoulli are used with RS to explore the missing data problem [37], which is not a studied case in this thesis. A brief summary on each distribution is presented in this section, in order to examine its validity with each mode of RS in the next section.

#### A) Uniform distribution

The uniform distribution is defined by the end limits of its interval  $[a,b]$  and its PDF by (1.13).

$$p_{unif}(t) = \frac{1}{b-a} \quad a < t < b \quad (1.13)$$

In this case of distribution, the mean  $\mu$  and the standard deviation  $\sigma$  are deduced from the end limits  $a$  and  $b$  as in (1.14) and (1.15).

$$\mu = \frac{a+b}{2} \quad (1.14)$$

$$\sigma = \frac{b - a}{\sqrt{12}} \quad (1.15)$$

Thus, according to (1.12) when the random variable follows a uniform distribution the probability  $p_i(t)$  of the instant ( $t_i$ ), having an interval  $[a_i, b_i]$  and a mean  $\mu_i$ , must verify (1.16).

$$\mu_i = \frac{a_i + b_i}{2} = t_{i-1} + T_{Sm} \text{ and } b_i - a_i = 2.T_{Sm} \quad (1.16)$$

### B) Gaussian Distribution

In case of Gaussian distribution, the PDF is defined by the variance  $\sigma^2$  and the mean  $\mu$ :

$$p_{gauss}(t) = \frac{1}{\sqrt{2\pi}\sigma} e^{-\frac{(t-\mu)^2}{2\sigma^2}} \quad (1.17)$$

The end points of the interval of the Gaussian distribution are not obvious as in the Uniform distribution. Considering a probability coverage of 99.7% is enough to represent the entire interval of distribution of a Gaussian random variable, the end points (minimum and maximum limits) of this interval can be deduced in term of  $\sigma$  and  $\mu$  as in (1.18) and (1.19).

$$min = \mu - 3\sigma \quad (1.18)$$

$$max = \mu + 3\sigma \quad (1.19)$$

Consequently, when the random variable in the random instant expression follows a Gaussian distribution, and having a mean  $\mu_i$  and a support interval  $[min_i, max_i]$ ,  $p_i(t)$  must verify (1.20).

$$\mu_i = t_{i-1} + T_{Sm} \text{ and } max_i - min_i = 6\sigma = 2.T_{Sm} \quad (1.20)$$

### C) Exponential Distribution

In case of Exponential distribution, the determination of the temporal condition in term of the distribution parameters get more complicated as the support of such distribution is  $[0, \infty)$ . The PDF of the Exponential distribution, known also as Poisson, is defined by (1.21), and its Cumulative Density Function (CDF) is defined by (1.22).

$$p_{exp}(t) = \lambda e^{-\lambda t} \quad (1.21)$$

$$f_{exp}(t) = 1 - e^{-\lambda t} \quad (1.22)$$

The mean value in such distribution is  $1/\lambda$ . To have an estimation of the interval of the random variable that follows an exponential distribution, the CDF is used to calculate the value of  $t$  at which the cumulative probability in (1.22) is equal to 0.999.

$$t_{0.999} = \frac{-\ln(0.001)}{\lambda} = \frac{6.9078}{\lambda} \quad (1.23)$$

Considering  $t_{0.999}$  is the end point of the interval of support of the exponential distribution, this interval is  $[0, \frac{6.9078}{\lambda}]$ .

So, when the random variable in the random instant expression follows an Exponential distribution,  $p_i(t)$ , having a mean  $\lambda_i$  and a support interval  $[\min_i, \max_i]$ , must verify the relations in (1.24).

$$\lambda_i = t_{i-1} + T_{Sm} \text{ and } \max_i - \min_i = \frac{6.9078}{\lambda_i} = 2 \cdot T_{Sm} \quad (1.24)$$

## 1.4 Random Sampling Modes

All the RS modes are based on the random impulse process defined in (1.7). The mode of RS is essentially declared by the definition of the process  $\{t_n\}$ . The modeling of skip sampling, which can be added to the main mode of RS defined by  $\{t_n\}$ , is an important effect contributed to the process  $\{\alpha_n\}$ . All the modes of RS mentioned in the literature are presented in this section, the most promising modes are explained and discussed to evaluate their potential to be used in real sampling and then be applied on mechanical vibration signals. In fact, to know how to choose the adequate mode of RS, and then how to choose the convenient distribution for random variables, the stationarity condition of RS (and thus the anti-aliasing property) and the time condition of the instants of sampling must be studied for each mode.

### 1.4.1 Additive Random Sampling (ARS)

The concept of the Additive Random Sampling (ARS) was first proposed by Shapiro and Silverman in [31] as a sampling method providing an alias-free processing for analogical signals. After defining the ARS process, discussing the validity of the temporal condition of this mode with the already mentioned probability distributions and verifying the stationarity condition in each case, an overview on its modified versions will be presented at the end of this section.

#### A) Definition

As the name indicates, the sampling instant in this mode is obtained by adding a random variable to its previous as declared in (1.25).

$$t_n = t_{n-1} + \tau_n \quad n = 0, 1, 2, \dots \quad (1.25)$$

$\tau_n$  are independent and identically distributed (iid) variables,  $p(\tau)$  is the probability distribution function (PDF) having a standard deviation  $\sigma$  and a mean  $\mu$ . As mentioned in paragraph 1.3.3, the

mode of RS is defined by the expression of  $(t_n)$  in term of a random variable. In this case, the inter-sample time interval  $\tau_n$  is the random variable to be generated. And, according to the random point process definition, the interval  $\theta_n$  is equal to the generated random variable  $\tau_n$ . Thus, the PDF  $p_n(t)$  of the instant  $t_n$  is deduced from the probability  $p(\tau)$  by respecting the expression in 1.25, where each instant of sampling is the cumulative sum of all its previous, and thus the randomness in such process is cumulated till the end of the sampling sequence, and the distribution of the last instant of sampling  $(t_N)$  is certainly dependent on the first instant of sampling  $(t_0)$ .

### B) Temporal Condition

According to paragraph 1.3.3, the instants  $t_i$  must be chosen in a strictly increasing order. As a consequence to relation (1.12), the mean and the interval length of  $p_i(t)$  are expressed in term of  $T_{Sm}$  in (1.16),(1.20) and (1.24), which will lead to the deduction of the mean and the interval of the random interval  $\tau$  in the ARS mode.

$$t_i = t_{i-1} + \tau_i = t_0 + \sum_{k=1}^i \tau_k \quad (1.26)$$

Ideally,  $t_0$  is a constant that must be equal to 0. And, the intervals  $\tau_k$  are iid variables. Then the expectations of these variables become:

$$E[t_i] = E \left[ \sum_{k=1}^i \tau_k \right] \Rightarrow E[t_{i-1}] + T_{Sm} = i \cdot E[\tau] \Rightarrow E[\tau] = T_{Sm} \quad (1.27)$$

As the interval of  $p_i(t)$  is equal to  $2T_{Sm}$  the interval of the random variable  $\tau$  in the ARS mode is  $[0; 2T_{Sm}]$ . This condition will be verified by comparing these intervals to the PDF's supports of different possible distributions.

#### B.1) Uniform Distribution Condition

In case of a uniform distribution, defined by its interval  $[a, b]$ , a ratio, based on definition (1.14) and (1.15), between  $\sigma$  and  $\mu$  ( $\sigma/\mu$ ) can be deduced for the ARS mode with the uniform distribution in term of the interval end points. As already deduced in the previous paragraph, the mean  $\mu$  is equal to  $T_{Sm}$ , for a simple representation the ratio  $\sigma/\mu$  is replaced by  $\sigma/T_{Sm}$ . In case of the interval  $[0; 2T_{Sm}]$ , the ratio  $\sigma/T_{Sm}$  verifies (1.28)

$$\sigma = \frac{b-a}{\sqrt{12}} \leq \frac{2T_{Sm}}{\sqrt{12}} \Rightarrow \frac{\sigma}{T_{Sm}} \leq \frac{2}{\sqrt{12}} = 0.577 \quad (1.28)$$

This ratio  $\sigma/T_{Sm}$  could be considered as an essential statistical parameter of the probability distribution used with RS mode, for the uniform distribution with ARS mode this parameter has a maximal value of 0.577 for the interval  $[0; 2T_{Sm}]$ .

### B.2) Gaussian Distribution Condition

The statistical parameter of the Gaussian distribution can be deduced for ARS mode from (1.18). As the interval of support is  $[0; 2T_{Sm}]$ , the ratio  $\sigma/T_{Sm}$  verifies (1.29).

$$\min = \mu - 3\sigma = T_{Sm} - 3\sigma \geq 0 \Rightarrow T_{Sm} \geq 3\sigma \Rightarrow \frac{\sigma}{T_{Sm}} \leq \frac{1}{3} = 0.333 \quad (1.29)$$

The same result can be verified by using the maximum limit formula (1.19).

$$\max = \mu + 3\sigma = T_{Sm} + 3\sigma \leq 2T_{Sm} \Rightarrow 3\sigma \leq T_{Sm} \Rightarrow \frac{\sigma}{T_{Sm}} \leq \frac{1}{3} = 0.333 \quad (1.30)$$

### B.3) Exponential Distribution Condition

When used with the ARS mode,  $\lambda$  of the Exponential distribution should be chosen to be equal to  $1/T_{Sm}$  and the random interval must be in  $[0; 2T_{Sm}]$ . As the first end point in both interval is 0, the condition must be verified within the second end point; because  $\lambda = 1/T_{Sm}$ , the interval of support became  $[0; 6.9078 T_{Sm}]$  which is not compatible with the Temporal condition. Thus the ARS mode can't be implemented in real applications with the exponential distribution.

In conclusion, the limitation imposed by the temporal condition creates a relation between the mean sampling period  $T_{Sm}$  and the standard deviation  $\sigma$  of the chosen distribution with the ARS mode. Due to this condition, the Exponential distribution cannot be used in practical implementation of ARS.

### C) ARS Stationarity Condition

In the aim of studying the stationarity of the ARS mode, the sampling point density function  $p_s(t)$  or its limit when  $t$  tend to the infinity must be defined. Referring to the relation (1.26), it can be deduced that the instant of sampling  $t_n$  is the sum of  $n$  independent random variables  $\tau_n$ . then the PDF of the instant  $t_n$  must verify the Central Limit Theorem, which is defined by: when independent random variables are added, their sum tends toward a normal distribution even if the original variables themselves are not normally distributed, but have the same mean  $\mu$  and the same variance  $\sigma^2$ . The mean of the sum is  $n\mu$  and the variance is  $n\sigma^2$ . As the random variables  $\tau_n$  follow the same distribution, then they must have the same mean ( $T_{Sm}$ ) and the same variance  $\sigma^2$ . Consequently, the PDF of the instant  $t_n$ ,  $p_n(t)$ , can be directly determined by (1.31).

$$p_n(t) = \frac{1}{\sqrt{2\pi n\sigma^2}} e^{-\frac{(t-nT_{sm})^2}{2n\sigma^2}} \quad (1.31)$$

In fact this result is verified by another probability theory, as by definition, the PDF of the sum of independent random variables is the convolution of the PDFs of these variables. So the PDF of the instant  $t_n$  can be deduced from the n-fold convolution of  $p(\tau)$  with itself [10].

$$p_n(t) = p_1(\tau) * p_2(\tau) * \dots * p_i(\tau) \dots * p_{n-1}(\tau) \quad (1.32)$$

For example, if the interval  $\tau$  follows a uniform distribution  $U[0,2]$ , then  $\mu=1$  and  $\sigma^2= 0.333$ . For  $N=25$ , the PDF of the instants  $t_1, t_2, t_3, t_7, t_{15}$  and  $t_{25}$  are shown in Figure 1.5.

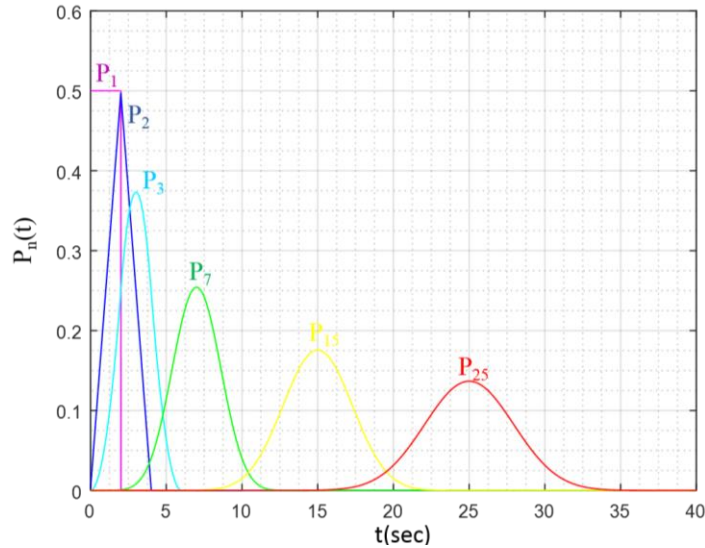


**Figure 1.5 The PDF of the instants  $t_n$  in the ARS mode with the Uniform distribution [0,2]**

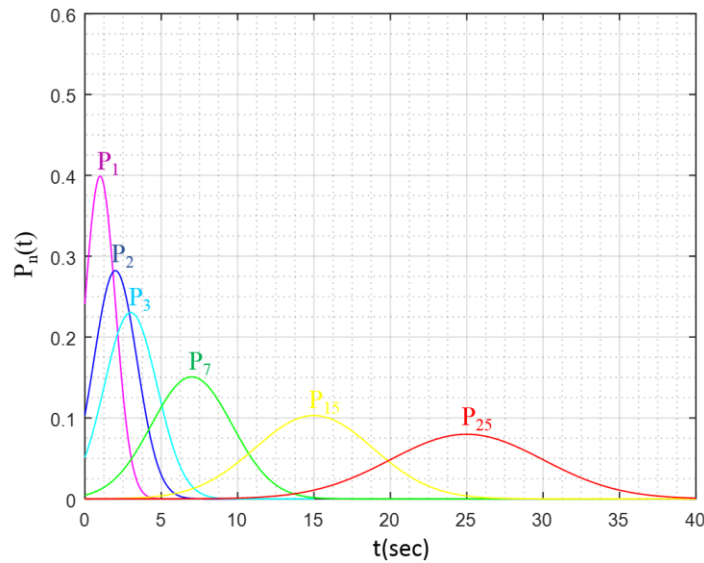


**Figure 1.6 The PDF of the instants  $t_n$  in the ARS mode with a Gaussian distribution (1,1)**

Another example of ARS mode with Gaussian distribution having  $\mu=1$  and  $\sigma^2=1$  is shown in Figure 1.6, also for  $N=25$ . It can be concluded from the PDF of the instants  $t_n$  presented in Figures 1.5 and

1.6 that the probability distribution in the ARS mode tends to be a Gaussian distribution with a mean equal to  $n\mu$  and a variance equal to  $n\sigma^2$ , which verifies the result in (1.31). So, in [36], the author used the characteristic function (CF) of  $p_n(t)$ , to transform CF of the point process probability  $p_s(t)$  to the sum of CF of the instants  $t_n$ , thus it becomes a sum of a geometric series of ratio  $r_g$  defined in (1.3)

$$r_g = e^{-j2\pi f T_{sm} - 2\pi^2 \sigma^2 f^2} \quad (1.33)$$

As  $f > 0$ , the ratio  $|r_g| < 1$ , consequently the sum will converge, and by using the final value theorem, it can be concluded that the probability point process is stationary according to (1.34).

$$\lim_{t \rightarrow \infty} p(t) = \frac{1}{T_{sm}} \quad (1.34)$$

As a result, the ARS mode is proven to be stationary without any specification or limitation concerning the probability distribution. According to section 1.4.1 part B, in order to verify the temporal condition, the ARS mode can be used with both: uniform and Gaussian distribution.

In Figures 1.7 and 1.8, a simple verification of the stationarity of the ARS mode with both distributions is presented. In addition, according to the  $T_{sd}$  definition, the delay is calculated in each case of ARS with uniform and Gaussian distributions and indicated for each plot. In some cases the  $T_{sd}$  can't be shown on the figure so the exact values are all given in the tables 1.1 and 1.2. In fact, the sum of individual probabilities  $p_s(t)$  already defined in (1.9) converges in all ARS cases, but the distribution and the standard deviation  $\sigma$  affect the delay of stationarity  $T_{sd}$  as declared in (1.10). So, in some cases when  $\sigma$  is small, the stationarity is reached after a longer delay of time and thus it requires a higher number of points. Actually, the best result can be achieved when the ratio  $\sigma / T_{sm}$  is equal to the maximum imposed by the temporal condition, as the stationarity delay is inversely proportional to  $\sigma$  when  $T_{sm}$  is fixed. So, whenever the sampling period is determined, the value of  $\sigma$  can be directly deduced from the temporal condition. Thus, the number of samples must be increased due to the temporal condition limitation. As the limitation with the Gaussian distribution is more selective than limitation with the uniform, the ARS with Gaussian distribution is more demanding in number of samples. Consequently, in combining the result of both limitations: the temporal and the stationarity conditions, a clear relation between the mean  $T_{sm}$  and the standard deviation  $\sigma$  is deduced.

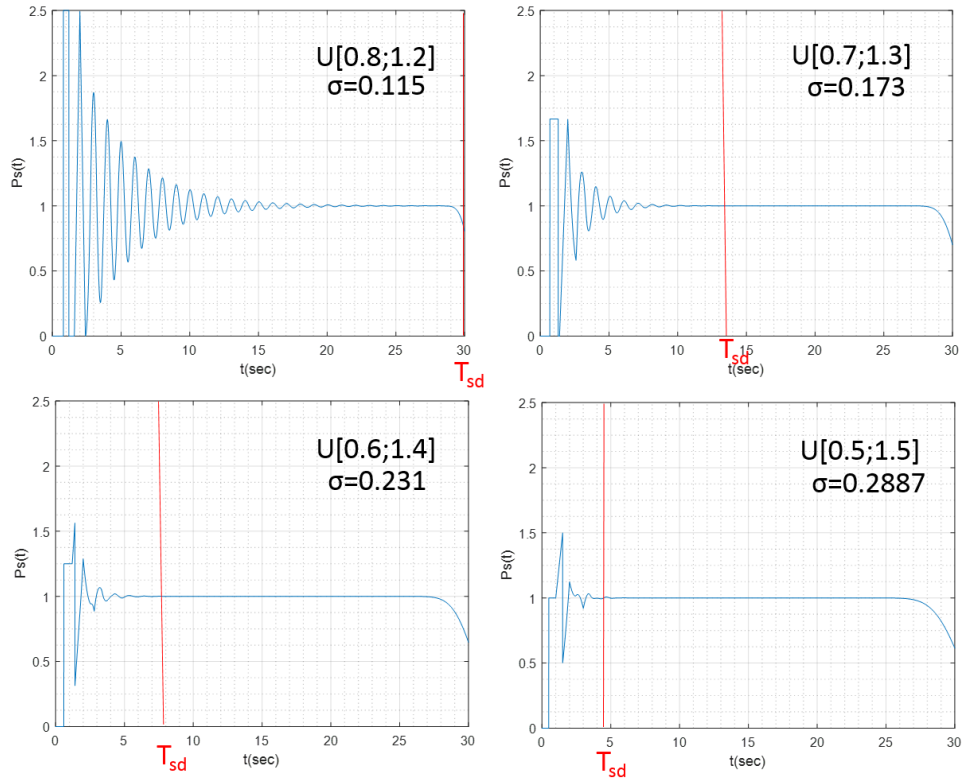


**Figure 1.7**  $p_s(t)$  of ARS mode with Uniform distribution, where  $T_{Sm}=1$ , and  $\sigma$  varying to have multiple values of  $\frac{\sigma}{T_{Sm}}$  and  $N=30$

Case	$T_{sd}(\text{sec})$
U[0.8;1.2]	30
U[0.7;1.3]	13.33
U[0.6;1.4]	7.5
U[0.5;1.5]	4.8

**Table 1.1** the  $T_{sd}$  for each case of the ARS with the Uniform distribution

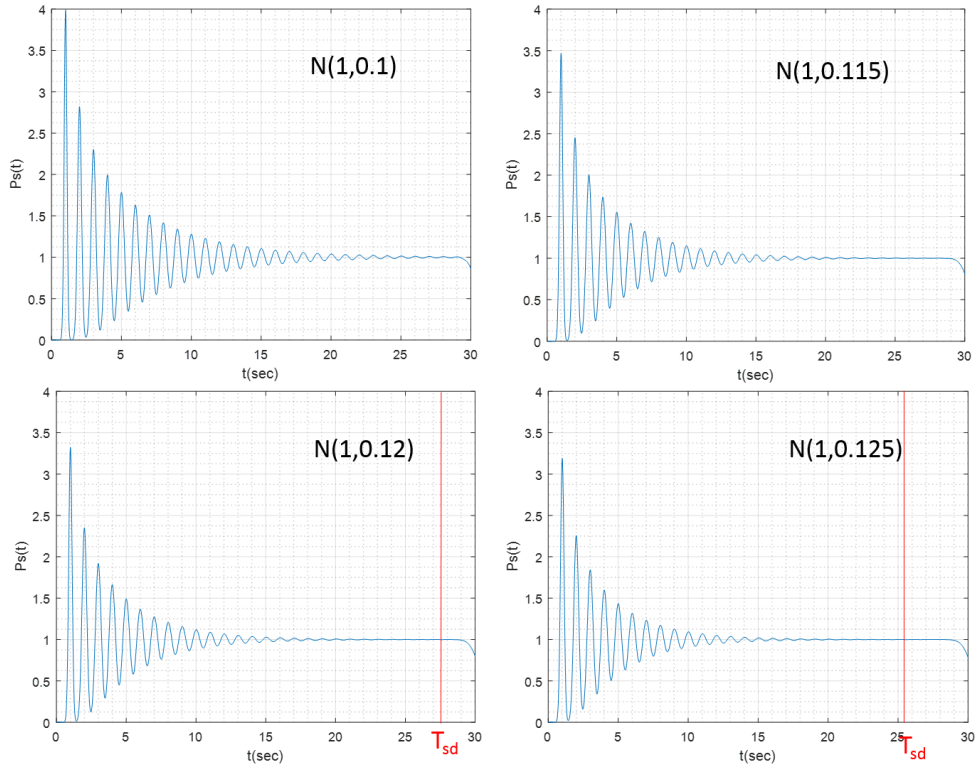


**Figure 1.8**  $p(t)$  of ARS with Gaussian distribution,  $T_{sm}=1$ ,  $N=30$  and  $\sigma$  varying

Case	$T_{sd}(\text{sec})$
N(1;0.1)	40
N(1;0.115)	30.2
N(1;0.12)	27.8
N(1;0.125)	25.6

**Table 1.2** the  $T_{sd}$  for each case of the ARS with the Uniform distribution

In conclusion, the ARS with uniform and Gaussian distribution is a RS mode guaranteeing an alias-free sampling due to its stationary aspect within the verification of the temporal condition which assures the ability of this mode to be implemented in hardware. To enhance this mode of sampling two variants were suggested by [49] to improve the alias suppression with the first one and reduce the number of calculation of the Discrete Fourier Transform (DFT) in the second. These two variants modes are briefly reviewed in the next two paragraphs.

## D) Variants of ARS

### D.1) Correlated ARS

A modified version of the ARS mode is proposed in [28], the Correlated Additive Random Sampling (CRS), to enhance the alias suppression. In fact, the condition of independency between the random intervals that separate samples, is not respected, and there exists a correlation between two adjacent sampling intervals. If it is positive, the RS sequence increases at a faster rate than the case of uncorrelated ARS, and thus reaches the stationarity more quickly. But, if the correlation is negative, the stationarity delay of the sampling sequence of CRS becomes longer [35]. A detailed study of the CRS spectrum is presented in [35] to explore all the effect of correlation on the ARS mode, where the main advantage remains in adding an “extra design parameter” that permits to shape the spectrum of the randomly sampled signal to fit particular applications. In conclusion, having a positive correlation between adjacent random intervals leads to stationarity and thus to an alias-free sampling, but the hardware implementation of such process is judged to be difficult [35] and not feasible [36].

### D.2) Hybrid ARS

Another modified version of ARS is introduced by Purvis in [49], it is called the Hybride Additive Random sampling (HARS). This mode has the same properties of the ARS, with the only modification of dividing the sampling sequence into an even number of sub-sequences, where each sequence is concatenated with its reverse, to simplify the calculation of the DFT of the randomly sampled signal. For a sampling of N points, and a number of sub-sequences equal 2, the instants of sampling are defined as in (1.35).

$$\begin{cases} t_n = t_{n-1} + \tau_n \\ t_{N-n} = 1 - t_n \end{cases} \quad (1.35)$$

Where  $t_0=0$ ,  $t_{N/2}=0.5$  and the total time of sampling is the unity in the normalized case. It is obvious in (1.35) that the first sub-sequence is exactly a sequence of an ARS mode. An example of a HARS sequence is shown in Figure 1.9 to clarify the concept of such mode. The property of Alias-Free sampling is conserved in this version. In addition, this reversed sub-sequence creates symmetrical terms in the DFT which simplifies the calculation and reduces the time of execution. Sufficient information on the HARS can be directly deduced by the exploration of the ARS mode as both have same properties. Thus, this thesis will be focused on the study of the ARS.

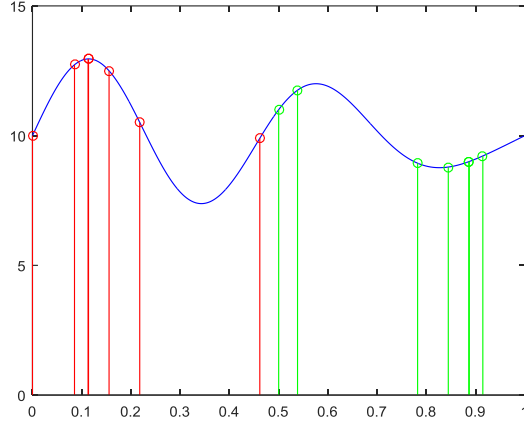


**Figure 1.9 HARS mode the sequence after  $tN/2$  is symmetric to the sequence before**

#### 1.4.2 Jittered Random Sampling

##### A) Definition

The Jittered Random Sampling (JRS) is a type of sampling where a jitter (error) is applied to a uniform sampling grid. This jitter appears frequently in practical sampling systems because of uncertainty of sampling clocks due to hardware imperfections [50]. Specifically this error is caused by the phase noise of the sampling clock, which leads to a fluctuation in the phase. In many cases the effect of the jitter can be ignored, but in some other cases, it may be of large level that can have a deliberate effect [51]. In fact, the notion of the jitter was first introduced as a problem and appears to be treated for the first time in [51]. Though, in RS this notion is imitated and modeled to be used as a mode of RS known as JRS. The sampling model in this case can be described by (1.36).

$$t_n = nT_{sm} + u_n \quad T_{sm} > 0 \quad n = 0, 1, 2, \dots \quad (1.36)$$

Where  $T_{sm}$  is the mean sampling period and  $u_n$  are iid variables with PDF  $p(u)$  having  $\sigma^2$  as a variance and a mean equal to zero. In case where the jitter is an error and should be ignored or eliminated depending on its level, the mean sampling period  $T_{sm}$  should be respecting the Shannon-Nyquist condition, because the sampling in this case is uniform before the apparition of the jitter. While in JRS, the  $T_{sm}$  is beyond the Shannon-Nyquist condition as the sampling is random and not uniform.

In comparing the model of JRS with that of ARS, it can be inferred that the randomness in the first model is not cumulated as in the second, at each instant of sampling a random number is added to the constant uniform interval or period of sampling. Which means that the distribution of each instant of sampling ( $t_n$ ) is independent of any other instant, it depends only on the distribution of

its added jitter ( $u_n$ ). This difference is confirmed by the modified model of ARS given by (1.37) that is based on the definition of ARS in (1.25), where  $\tau_n$  is a random variable following a distribution having a mean equal to  $T_{Sm}$  (as it is an ARS mode) and a standard deviation  $\sigma$ . When replacing  $\tau_n$  by a random variable  $\tau_{0n}$  following the same distribution with the same standard deviation but with a zero mean, the definition in (1.25) becomes as in (1.37).

$$t_n = t_{n-1} + \tau_n = t_{n-1} + \tau_{0n} + T_{Sm} = nT_{Sm} + \sum_{i=1}^n \tau_{0i} \quad (1.37)$$

The sum of  $\tau_{0i}$  is the sum of independent random variables having all the same PDF with the same mean ( $=0$ ) and the same standard deviation ( $\sigma$ ). Referring to the Central Limit Theorem, this sum can be considered as a random variable  $\gamma_n$  following a Normal distribution  $N(0, \sqrt{n}\sigma)$ . The formula in (1.37) becomes (1.38).

$$t_n = nT_{Sm} + \gamma_n \quad (1.38)$$

The reworded model of ARS in (1.38) is similar to the model of JRS in (1.36) with the only difference in the distribution of  $\gamma_n$  that is specified in the ARS mode, and the variance of this distribution that is proportional to  $n$ , which expresses the accumulation of randomness in the ARS case.

#### B) Temporal Condition

To evaluate the compatibility of the JRS mode with the different possible probability distributions for the real implementation, a study of the temporal condition is presented in this part. Due to condition (1.12) in paragraph 1.3.3, the mean and the interval length of  $p_i(t)$  are expressed in term of  $T_{Sm}$  in (1.16), (1.20) and (1.24) which will lead to the deduction of the mean and the interval of the random jitter  $u$  in the JRS. As mentioned in (1.36) for  $n=i$ , it can be deduced:

$$\begin{aligned} t_i = iT_{Sm} + u_i &\Rightarrow E[t_{i-1}] + T_{Sm} = E[iT_{Sm} + u_i] \Rightarrow i.T_{Sm} = i.T_{Sm} + E[u_i] \\ &\Rightarrow E[u_i] = 0 \end{aligned} \quad (1.39)$$

This relation confirms the definition of the JRS, where the jitter must be a zero mean random variable. In order to identify the interval of support of  $u_i$ , the relation (1.12) is applied on the JRS case in (1.40).

$$\begin{aligned} t_{i-1} < t_i &\leq t_{i-1} + 2.T_{Sm} \\ \Rightarrow (i-1)T_{Sm} + u_{i-1} &< iT_{Sm} + u_i \leq (i-1)T_{Sm} + u_{i-1} + 2.T_{Sm} \\ \Rightarrow -T_{Sm} + u_{i-1} &< u_i \leq u_{i-1} + T_{Sm} \end{aligned} \quad (1.40)$$

The best solution to respect the condition in (1.40) is to define the jitter  $u$  in  $[-0.5T_{Sm}; +0.5T_{Sm}]$  to keep the successive random variables iid. Thus the condition (1.11) already defined in [36] fits the JRS particularly while it limits many possibilities in ARS.

### B.1) Uniform Distribution

With the uniform distribution which is defined by its interval limit  $[a,b]$  the temporal condition in JRS mode is defined in (1.41).

$$\sigma = \frac{b - a}{\sqrt{12}} = \frac{(0.5T_{Sm} + 0.5T_{Sm})}{\sqrt{12}}$$

$$\frac{\sigma}{T_{Sm}} = 0.2887 \quad (1.41)$$

Similarly to the ARS mode, the ratio  $\sigma/T_{Sm}$  could be considered as an essential statistical parameter of the probability distribution used with RS mode, for the uniform distribution with JRS this parameter has a maximal value of 0.2887 for the interval  $[-0.5T_{Sm}; +0.5T_{Sm}]$  [36].

### B.2) Gaussian Distribution

The statistical parameter of the jitter  $u$  in the Gaussian distribution can be deduced from the interval  $[-0.5T_{Sm}; +0.5T_{Sm}]$  in (1.42).

$$min = \mu - 3\sigma = 0 - 3\sigma \geq -0.5T_{Sm} \Rightarrow 0.5T_{Sm} \geq 3\sigma \Rightarrow \frac{\sigma}{T_{Sm}} \leq \frac{1}{6} = 0.167 \quad (1.42)$$

The same result is obtained by using the maximum limit formula:

$$max = \mu + 3\sigma = 0 + 3\sigma \leq 0.5T_{Sm} \Rightarrow 3\sigma \leq 0.5T_{Sm} \Rightarrow \frac{\sigma}{T_{Sm}} \leq \frac{1}{6} = 0.167 \quad (1.43)$$

### B.3) Exponential Distribution

In case of the exponential distribution, the jitter  $u$  can't have negative values. In fact even if the interval of support within the JRS mode is defined only for a positive jitter  $u^+$  by  $[0; 2T_{Sm}]$ , when choosing a  $\lambda=1/T_{Sm}$ , the interval of the exponential distribution can't be limited by  $2T_{Sm}$  as declared in (1.24). So it can be concluded that like the ARS mode, the JRS can't be used with the exponential distribution. Although in theory and simulation it was proven that it guarantees an alias-free sampling [35], the exponential distribution can't be used with RS modes in practice, as its support is positive and the interval of the distribution is not centered at the mean value, so it couldn't verify the temporal condition and thus couldn't assure an increasing time process.

After determining the limitations of temporal condition on the use of JRS, it is important to explore the stationarity condition that is needed to guarantee a spectrum free of aliases for the randomly sampled signal.

### C) JRS Stationarity condition

As mentioned in paragraph 1.3.2, the definition of the stationarity condition in [33] introduced three theorems on stationary random processes, the second theorem concludes on the stationarity of the JRS process, this theorem can be summarized by: If  $\{t'_n\}$  is a periodic SPP with period  $T_{Sm}$ , and  $\{u_n\}$  is a discrete time stationary random process with  $-T/2 \leq u_n \leq T/2$ , then the new point process  $t''_n = t'_n + u_n$  is also an SPP, which is referred as jittered SPP [34]. An additional condition is declared in [28] about the delay of stationarity defined in (1.10), where the process reaches the stationarity after a delay determined by the probability distribution and its parameter. Thus, the stationarity of the JRS mode can't be proved without the identification of the probability distribution of the random jitter  $u_n$ . As in (1.9) the SPP is defined by the sampling point density function  $p_s(t)$ , in [36] the PDF of the instant  $t_n$  is conceived as in (1.44). In fact, from (1.36) it can be concluded that the PDF of instant  $t_n$  is of mean  $E[t_n]=nT_{Sm}$  and standard deviation  $\sigma$ , and the PDF of the instant  $t_n$  is the same of instant  $t_1$  translated by  $nT_{Sm}$ , as  $t_0$  is considered a constant with PDF equal to  $\delta(t)$ .

$$p_n(t) = p_1(t - nT_{Sm}) \quad 2 \leq n \leq N \quad (1.44)$$

$N$  is the total number of samples. Moreover,  $p_s(t)$ , the sum of all the PDF  $p_n(t)$  cannot be previewed without the determination of the probability distribution  $p_1(t)$ . In Figure 1.10  $p_n(t)$  ( $n=1$  to  $7$ ,  $n=15$  and  $25$ ) of a random instant in a JRS process with a uniform random jitter with  $T_{Sm}=1$  and  $\sigma=0.2887$ . In Figure 1.11,  $p_n(t)$  at the same instants of a JRS with a Gaussian distributed jitter following  $N(1,1)$ . It is shown how the selection of the distribution parameters affects the sampling point density function  $p_s(t)$ .

When a JRS is chosen with a uniform distribution, the sum of  $p_n(t)$  is dependent on the variance of the jitter, if  $\sigma$  is small and the interval of the jitter is less than  $[-0.5T_{Sm}; 0.5T_{Sm}]$  there will be a discontinuity in the sum of  $p_n(t)$  as in Figure 1.12, which will lead to a divergent sum and thus the SPP condition is not verified. But when the jitter is defined in  $[-0.5T_{Sm}; 0.5T_{Sm}]$  ( $\sigma=0.2887$ ), the sum of  $p_n(t)$  will be equal to  $1/T_{Sm}$ , like the example in Figure 1.13 of JRS with uniform distribution, as:

$$p_n(t) = \frac{1}{T_{Sm}} ; -\frac{nT_{Sm}}{2} \leq t_n \leq \frac{nT_{Sm}}{2} \quad (1.45)$$

Consequently, the JRS with the uniform distribution is a stationary random process when the standard deviation  $\sigma$  is equal 0.2887 where the interval of support of the jitter  $u$  is  $[-0.5T_{sm};0.5T_{sm}]$ .

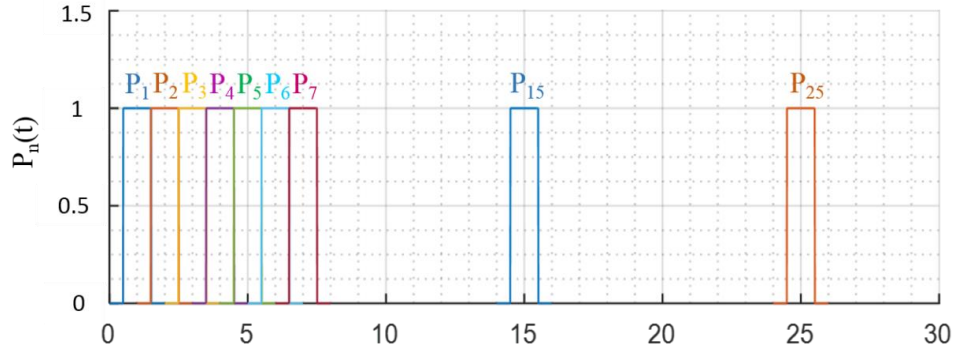


Figure 1.10  $p_n(t)$  of a JRS with uniform distribution ( $\sigma=0.2887$ ) at the instants 1 to 7 with 15 and 25

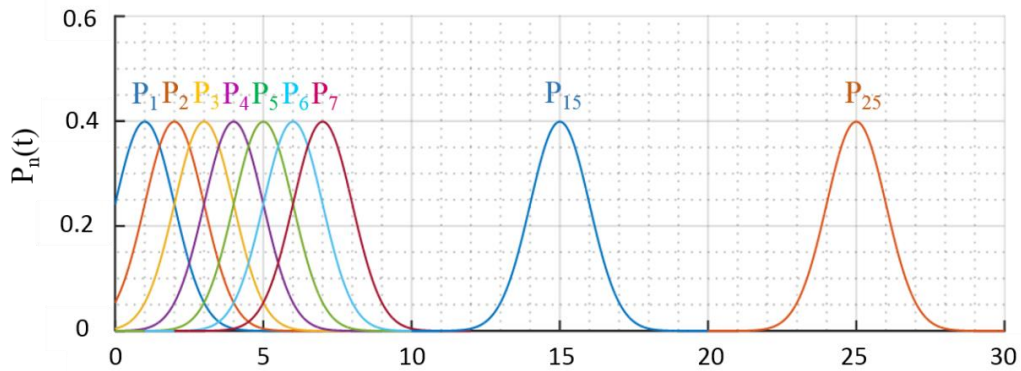


Figure 1.11  $p_n(t)$  of a JRS mode with Gaussian distribution at the instants 1 to 7 with 15 and 25

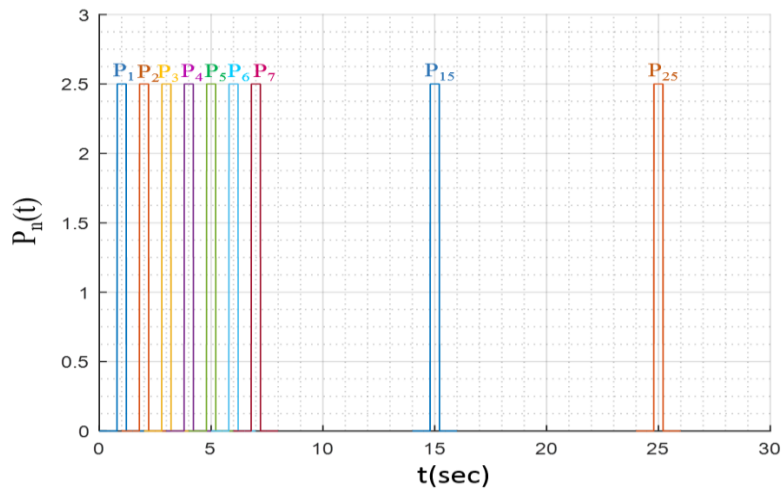
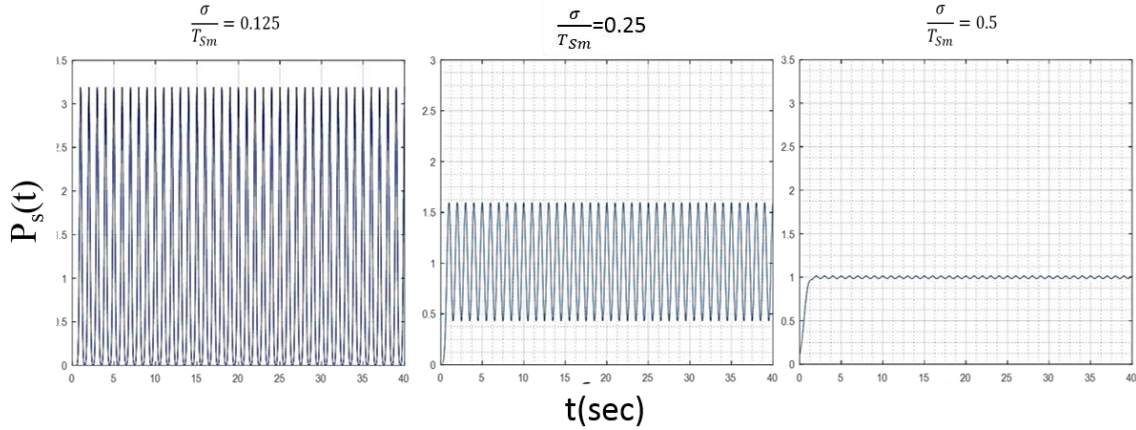


Figure 1.12  $p_n(t)$  of JRS with uniform distribution ( $\sigma=0.115$ ) at the instants 1 to 7 with 15 and 25

According to [35] and [36] the stationarity of a JRS mode with Gaussian distribution is not reached until  $\sigma/T_{Sm}$  is 0.5 due to the stationarity delay, in Figure 1.13 the sum of  $p_n(t)$  of the JRS mode with the Gaussian distribution having the same  $T_{Sm}$  and a varying  $\sigma$  is presented to evaluate the effect of  $\sigma/T_{Sm}$  on the SPP of this mode. This value is not within the temporal condition limitation when the jitter interval of definition is  $[-0.5 T_{Sm}; 0.5T_{Sm}]$ . Thus, the JRS mode with the Gaussian distribution cannot verify the stationarity property when implemented in real applications.



**Figure 1.13  $P_s(t)$  for the JRS with Gaussian distribution with  $T_{Sm}=1$  and different values of  $\sigma$**

In conclusion, the JRS mode must be used only with the uniform distribution to confirm both conditions: temporal and stationarity to be implemented in real hardware and assure anti-aliasing RS. As the ratio  $\sigma/T_{Sm}$  must be equal to the maximum determined by the temporal condition, the relation between these parameters is defined and whenever the value of the first is chosen, the value of the second is directly deduced.

#### 1.4.3 Random Skip Sampling (RSS)

According to the definition of the random impulse process in (1.7), the main random modes are determined by the process  $\{t_n\}$  which are the ARS and the JRS. While the process  $\{\alpha_n\}$  defines the existence of skip sampling that can be added to the main random modes, or to uniform sampling when  $\{t_n\}$  is a uniform process, as the fact of skipping samples may occur with any mode of acquisition. In [34], a theorem was deduced from the definition of the SPP which will define the RSS clearly: If  $\{t_n\}$  is an SPP,  $\{y_n\}$  is a discrete time stationary random process that takes the value of  $\{0,1\}$  and is independent of  $\{t_n\}$ , the new point process is formulated as follows: a new point process has a point at  $\{t_n\}$  if  $y_n = 1$ , but no point at  $\{t_n\}$  if  $y_n = 0$ , then the new point process  $\{t'_n\}$  is also an SPP, referred as random skip SPP. The process  $\{y_n\}$  is a particular form of  $\{\alpha_n\}$  that introduces the notion of skipping samples, while  $\{\alpha_n\}$  is a general process that represent also the

amplitude errors. Consequently, skipping samples conserves the stationary aspect of RS when imposed by discrete time stationary random process.

On the other hand, RSS with uniform sampling can be defined in other way proposed by [52] as a missing data problem:

$$t_k = t_{k-1} + \partial_k \quad (1.46)$$

Where the random variable  $\partial_k \in \{T_S, 2T_S, 3T_S, \dots\}$ . This definition expresses the RSS or the missing data problem as a special case of the ARS mode.

#### 1.4.4 Time-quantized Random Sampling (TQRS)

In general, the domain and the range of an analog signal  $x(t)$  are modeled as continuous, when transforming to digital signal with discrete domain and range, the process of digitizing the domain is called sampling and the process of digitizing the range is called quantization [53], [54]. Often, in uniform sampling, the quantization is restricted to the amplitude signal discretization, as it is not allowed to take on arbitrary values and it is limited to a finite number of levels. However, in RS the quantization is applied to both: the signal amplitude and the sampling instants, where the randomly chosen instants of sampling can't take on arbitrary values as hardware constraints impose limitations on these instants whose values are consequently digitized and defined at discrete and finite time steps. In fact, this quantization is the result of two procedures. First, the random interval or jitter, is generated and saved on registers in the digital sampling device, which will create the first restriction on the random value that will be obviously discrete and limited. Second, the task of sampling is assigned to the ADC which is available at the rising edge of a clock generated by the processor. The period of this clock is called time step, which is considered the minimum spacing on the time axis. Accordingly, the generated random instant should be a multiple of this time step. This notion of quantization was first introduced by [35] as a sampling scheme and was explored, by simulation, as a sampling process in time and frequency domain to reveal its effect on randomly sampled signals. A detailed study on the statistical parameters after quantization was done in [36] and a clarification on the effect of quantization on the spectrum of the randomly sampled signal is given in [37]. In this paragraph a brief summary on the TQRS aspect in time domain is presented.

According to [35], every interval  $\tau_k$  separating two adjacent samples ( $\tau_k = t_{k+1} - t_k$ ) when verifying the condition in (1.47) with the minimum time spacing  $\Delta$  known also as the time granulation or time step, it will be quantized and replaced by  $\tau_{kq}$ :

$$\text{if } \left(n - \frac{1}{2}\right)\Delta < \tau_k \leq \left(n + \frac{1}{2}\right)\Delta, \tau_{kq} = n\Delta \quad (1.47)$$

The mean sampling period  $T_{Sm}$  can also be expressed in term of  $\Delta$ :

$$\Delta = \frac{T_{Sm}}{q_T} \quad (1.48)$$

$q_T$  is the temporal quantization factor. To clarify the concept of time quantization, Figure 1.14 gives an example of TQRS for  $q_T=3$ .

In fact, the condition of quantification given in (1.47) is general and may be modified according to the hardware limitation imposed by the sampling device. In case where the RS is applied as a routine in a microcontroller where the order of sampling is executed by an interruption event, this order may occur at an instant where the ADC is not available, so the interruption will be held until the next period of ADC clock, so in such case, the condition of quantification is not exactly (1.47) it should be replaced by (1.49).

$$\text{if } (n-1)\Delta < \tau_k \leq n\Delta, \quad \tau_{k,q} = n\Delta \quad (1.49)$$

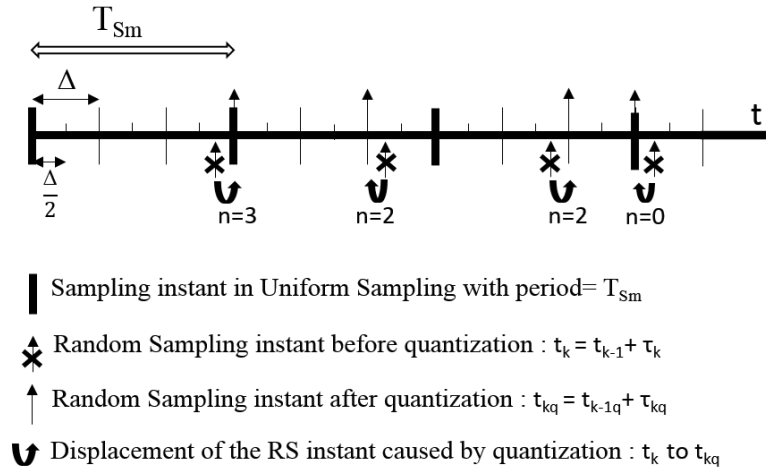


**Figure 1.14 Explication of TQRS for  $q_T=3$**

This condition represents the TQRS mode in Hardware implementation (TQRSH), this mode is applied with both mode of sampling: ARS and JRS. In fact, only in [35] the mode TQRS is mentioned as a mode of RS, while in [36] and [37] the TQRS is considered as an additional aspect added to the RS modes to be used (ARS or JRS). In Figure 1.15, an explanation on how the quantification is applied within the TQRSH is presented. In [35] to [37] the PDF of the TQRS mode is given by (1.50).

$$p_{1,q}(\tau_{kq}) = \sum_{n=0}^{m-1} q(n\Delta)\delta(\tau_{kq} - n\Delta) \quad (1.50)$$

$p_1(t)$  is the PDF of the RS mode as defined in 1.4.1 for ARS or 1.4.2 or JRS and  $P_1(t)$  is its cumulative function. Having the probability of quantization within the condition (1.47),  $q(t)$  is defined by (1.51).

$$q(t) = P_1\left(t + \frac{\Delta}{2}\right) - P_1\left(t - \frac{\Delta}{2}\right) \quad (1.51)$$

Within condition (1.49):

$$q(t) = P_1(t) - P_1(t - \Delta) \quad (1.52)$$

With  $t \in \{n\Delta, n \in [0, m - 1]\}$ ,  $m$  is the number of possible values for  $n$  within the interval of support of  $p_1(t)$  after quantization,  $P_1$  the cumulative density function is defined by:  $P_1 = \int_{-\infty}^t p_1(\tau) d\tau$ , and  $q(t)$  must verify the condition of discrete probability (1.53).

$$\sum_{n=0}^{m-1} q(n\Delta) = 1 \quad (1.53)$$

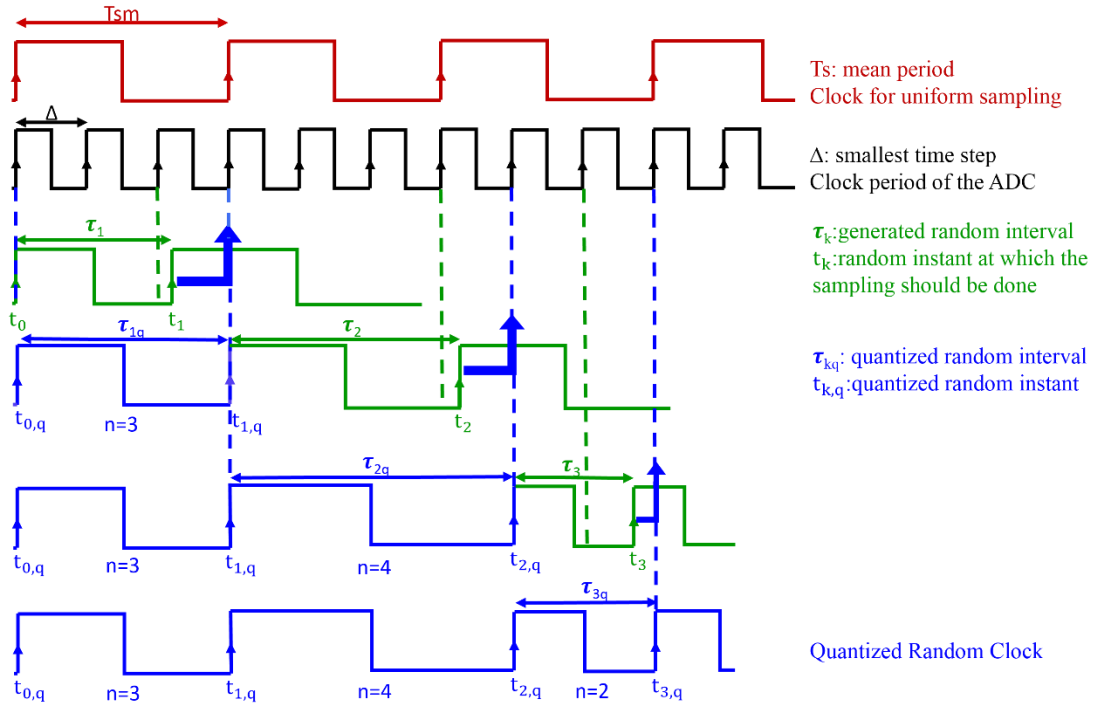


Figure 1.15 TQRSH for  $q_T=3$

From the formula of the PDF of the TQRS, the spectral density of a randomly sampled signal after time quantization can be deduced, in fact in the literature many studies were presented in [35] to [37] to figure out the effect of time quantization on RS, which will be discussed in chapter 2.

In [36] the definition of the standard deviation is used to conclude with the value of  $q_T$  that conserves the maximum of the statistical parameter  $\sigma/T_{Sm}$ .

$$\sigma = \sqrt{\frac{1}{m} \sum_{j=0}^{m-1} \left( j\Delta - \left( \frac{1}{m} \sum_{j=0}^{m-1} j\Delta \right) \right)^2} = \Delta \sqrt{\frac{m^2 - 1}{12}} \quad (1.54)$$

$$\Rightarrow \frac{\sigma}{T_{Sm}} = \frac{1}{q_T} \sqrt{\frac{q_T^2 - 1}{12}}$$

The formula deduced in (1.54) is conceived in order to express the maximal value of the ratio  $\sigma/T_{Sm}$  in term of  $q_T$  to deduce the best quantization factor to be used, thus the calculations in [36] was based on two conditions:

- 1) The random intervals are defined on an interval of support with length equal to  $T_{Sm}$ , so the number of possible quantized intervals  $m$  is equal to  $q_T$ .
- 2) The possible values of these random intervals are uniformly distributed and thus the probability of each is  $1/m$ .

These conditions are too particular which makes the formula in (1.54) specific for the uniform distribution cases with an interval of definition equal to  $[0.5T_{Sm}; 1.5T_{Sm}]$ . To generalize the formula of the ratio  $\sigma/T_{Sm}$  after quantization, the standard deviation  $\sigma$  is calculated according to its definition in (1.57) by applying the summation within the interval of support after quantization  $[a_q, b_q]$ , ( $a_q = a/\Delta$   $b_q = b/\Delta$ ). If  $D$  is the deviation of the interval of support defined by (1.55). Then the ratio  $R$  is defined by (1.56).

$$D = b - a \Rightarrow D_q = b_q - a_q = \frac{b - a}{\Delta} \quad (1.55)$$

$$R = \frac{D}{T_{Sm}} = \frac{D_q}{q_T} \quad (1.56)$$

The ratio  $\sigma/T_{Sm}$  (after quantization) of a sequence following a uniform distribution with any deviation is then concluded by (1.57), the details of calculation are presented in Appendix B.

$$\sigma = \sqrt{\frac{1}{D_q} \sum_{j=a_q}^{b_q} \left( j\Delta - \left( \frac{1}{D_q} \sum_{j=a_q}^{b_q} j\Delta \right) \right)^2} \Rightarrow \frac{\sigma}{T_{Sm}} = \frac{1}{q_T} \sqrt{\frac{R^2 q_T^2 - 1}{12}} \quad (1.57)$$

Consequently, the relation between the ratio  $\sigma/T_{Sm}$  and  $q_T$  is defined within the ratio  $R$  of the uniform continuous distribution interval determined before quantization. Figure (1.16) shows the variation of  $\sigma/T_{Sm}$  with  $q_T$  for different  $R$ . For example for  $R=1$ , the maximum value of  $\frac{\sigma}{T_{Sm}}$  is 0.2887, which can be reached for  $q_T=8$  with an error less than 1% [36], when the ratio is  $R=2$  the maximum is 0.577 which can be reached for  $q_T=7$  with same percentage of error. While in case of  $R=0.5$  the maximum is not reached until  $q_T$  is equal 16. Thus, the effect of quantization is higher on distributions with narrow intervals than on those with larger interval of support, which will impose on distributions with low  $R$  to use high frequency clocks having small time steps. In fact, the reason behind is that the quantization reduces the number of possible values within the interval of definition of the random instants, so when the interval of support is already restricted the quantization will affect the randomness more than for large interval of support.

Besides, for Gaussian distribution the same procedure of calculations cannot be followed, as its PDF is defined by  $\sigma$  and cannot be expressed in a discrete way. Therefore, a relation between the ratio  $\sigma/T_{Sm}$  of the Gaussian distribution in term of the same ratio in uniform distribution is conceived in order to define it in term of  $q_T$ . In RS, when the random jitter or interval is defined on a certain interval  $[a,b]$ , this interval remains the same whether it is a uniform or Gaussian distribution. Thus for the same  $T_{Sm}$  it can be concluded that:

$$\frac{D_U}{T_{Sm}} = \frac{D_G}{T_{Sm}} \quad (1.58)$$

Where  $D_U$  and  $D_G$  are the deviations in the uniform distribution and the Gaussian distribution respectively. Each deviation is expressed in term of  $\sigma$  of its own distribution:

$$D_U = \sigma_U \cdot \sqrt{12} \text{ and } D_G = 6 \cdot \sigma_G \quad (1.59)$$

Consequently the relation between  $\sigma_G$  and  $\sigma_U$  is deduced by:

$$\frac{\sigma_G}{T_{Sm}} = \frac{\sigma_U \cdot \sqrt{3}}{3 \cdot T_{Sm}} \quad (1.60)$$

In conclusion, the ratio  $\sigma/T_{Sm}$  in case of Gaussian distribution after quantization is defined by the same formula of the ratio in case of uniform distribution divided by  $\sqrt{3}$ . Hence, the effect of the

quantization on the Gaussian distribution support is the same of its effect on the uniform probability.

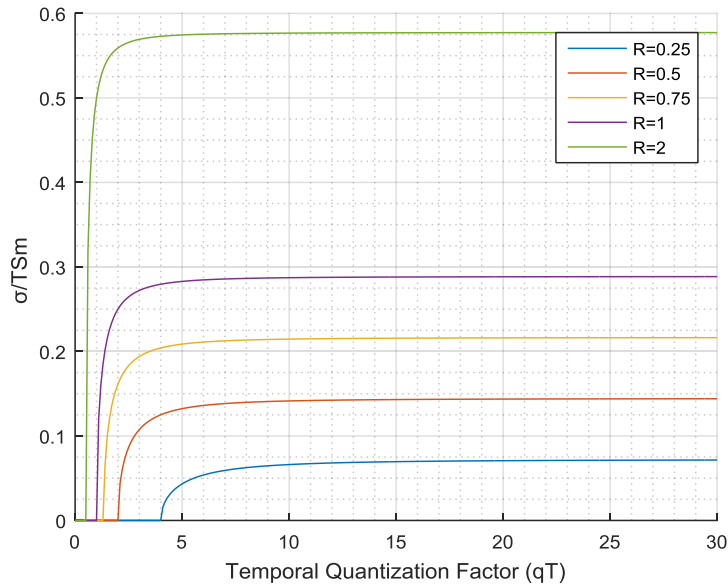


**Figure 1.16 Quantized standard deviation variation in term of qT**

## 1.5 Conclusion

Among multiple types of sampling, the RS was chosen to be studied in order to reveal its potential of use in real applications especially on mechanical vibration signals. First, a temporal condition is considered to be the main limitation to assure the possibility of implementation in real hardware. Then, the definition of the SPP condition is presented, as it is the essential condition for guaranteeing a sampling free of aliases which permits the use of low sampling frequency beyond the Shannon- Nyquist condition. After reviewing all the modes of RS with all possible random distributions to be used with, the most promising modes are the ARS and the JRS. The ARS with both distributions uniform and Gaussian verifies the SPP condition within respecting the temporal condition, while the JRS can verify both conditions with the uniform distribution only, it can be considered a stationary process with the Gaussian distribution disregarding the temporal limitation. As a conclusion, the ARS and the JRS with the uniform distribution and the ARS with Gaussian distribution are chosen to be studied in simulation and in practice to evaluate the possibility of their use in real applications. Before proceeding with the simulation, the study of the RS in spectral domain is a must to reveal all its properties. In addition, a revision on all the possible spectral analysis used with RS is presented to choose how to explore the randomly sampled signals in the frequency domain. Thus, the spectral analysis study is discussed in Chapter 2.

## 2 Chapter 2: Spectral Analysis of Random Sampling

### 2.1 Introduction

In general, the observation of signals in time domain is important, though, its content doesn't reveal all the needed information. Besides, electronic devices and automated systems are usually more responsive to the power and the frequency of signals, which makes the representation in the frequency domain more significant. Hence, the spectral analysis of the RS is essential to observe its impact on the sampled signal regardless the signification of this latter. In fact, the best way to evaluate such process is by comparing it to the classical method usually used: uniform sampling. As declared in Chapter 1 the sampled signal is the product of the analogical signal  $x(t)$  with the sampling signal  $S(t)$  which can be simply defined by the relation (2.1).

$$x_s(t) = x(t) \cdot S(t) \quad (2.1)$$

In signal processing, the spectral analysis approach varies according to the aspect of the signal to be sampled  $x(t)$ , and to the form of the sampling signal  $S(t)$  which is imposed by the process type of sampling whether it is uniform or random. In this chapter, a brief review on the spectral analysis of uniform sampling for deterministic and random analogical signal ( $x(t)$ ) is presented first. Second, a detailed study on different spectral analysis methodologies used for randomly sampled signals with both aspects deterministic or stochastic. A comparison between the analysis of both sampling processes is shown in order to explore the differences and reveal the effect of RS on the resulting signal.

### 2.2 Spectral Analysis in Uniform Sampling

#### 2.2.1 Fourier Transform of Deterministic Signal

According to the definitions already mentioned in chapter 1, in the time domain the sampled signal is defined by (2.2).

$$x_s(t) = \sum_{n=-\infty}^{n=+\infty} x(nTs) \delta(t - nTs) \quad (2.2)$$

Due to the Poisson summation formula applied on the Dirac comb function defined in (2.2), it can be confirmed that the Fourier transform (FT) of the Dirac comb in time domain is also a Dirac comb in the frequency domain, scaled with  $1/T_s$  as declared in (2.3).

$$\hat{S}(f) = \frac{1}{T_s} \sum_{n=-\infty}^{n=+\infty} \delta\left(f - \frac{n}{T_s}\right) \quad (2.3)$$

So the FT of the uniformly sampled signal deduced by the application of Plancherel theorem is defined by (2.4) [55].

$$\begin{aligned} \hat{x}_s(f) &= \hat{x}(f) * \hat{S}(f) = \frac{1}{T_s} \cdot \hat{x}(f) * \sum_{n=-\infty}^{n=+\infty} \delta\left(f - \frac{n}{T_s}\right) \\ \hat{x}_s(f) &= \frac{1}{T_s} \sum_{n=-\infty}^{n=+\infty} \hat{x}\left(f - \frac{n}{T_s}\right) \end{aligned} \quad (2.4)$$

Therefore, the FT of the uniformly sampled signal  $x_s(t)$  is a periodic function with period  $F_s$  equal to  $1/T_s$ . In Figure 2.1 a simple example is shown to illustrate the impact of uniform sampling on the sampled signal spectrum. In fact the spectrum of  $x(t)$  is limited between  $-F_m/2$  and  $+F_m/2$ , the other repetitions each  $F_s$  are the replicas of the spectrum of  $x(t)$  that appear due to the discretization of  $x(t)$  at a constant period  $T_s$ .

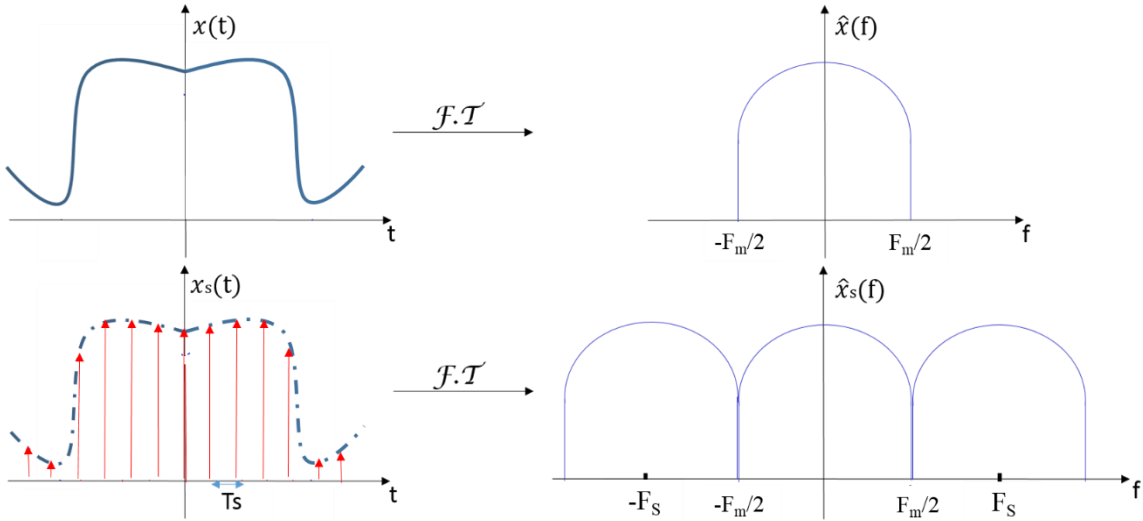


**Figure 2.1 An example of a signal  $x(t)$  with its FT before and after uniform sampling**

The example shown in Figure 2.1 clarifies the main condition set by the sampling theorem known by Shannon-Nyquist theorem (cited also by some references as Whittaker-Kotelnikov theorem), that imposes a limitation on the sampling period defined by (2.5).

$$F_s \geq F_m = 2 \cdot F_{max} \Leftrightarrow T_s \leq \frac{2}{F_{max}} \quad (2.5)$$

$F_m/2$  is the maximal frequency  $F_{\max}$  in the signal spectrum  $\hat{x}(f)$ . This condition is essential for preventing the spectrum of the sampled signal from distortion as shown in Figure 2.2 where the sampling frequency  $F_S$  is taken lower than  $2F_{\max}$ . And for eliminating the aliases, low-pass filters are used, but due to their low orders in real applications, it is recommended to choose  $F_S$  strictly or even highly greater than  $2F_{\max}$ . In addition, further condition on the frequency resolution is needed for a clear representation in the frequency domain [56].

$$\Delta f \leq \frac{1}{NT_s} = \frac{1}{T} \quad (2.6)$$

$\Delta f$  is the frequency resolution,  $N$  is the number of samples of  $x(t)$  taken in the time domain and  $T$  is the total duration of the acquired signal  $x(t)$ .

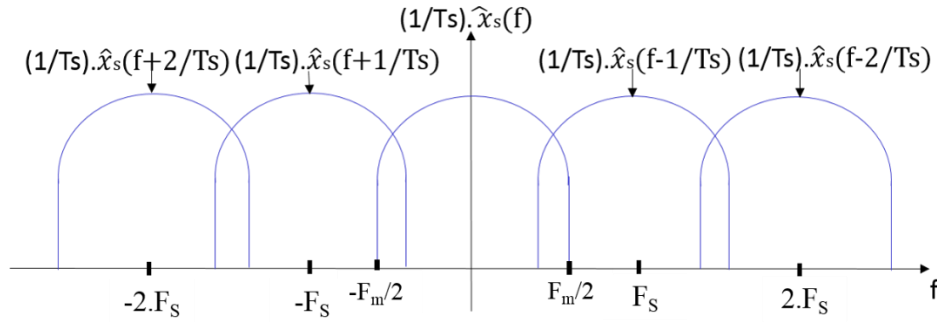


**Figure 2.2 Uniform sampling with a period  $F_S < 2F_{\max}$**

For a deterministic signal  $x(t_n)$ , the Discrete Time Fourier Transform (DTFT) is defined by:

$$\hat{x}_d(f) = \sum_{n=-\infty}^{+\infty} x(nT_s) e^{-i2\pi f n T_s} \quad (2.7)$$

And thus, the Energy Spectral Density of  $x(t_n)$  is defined by [57]

$$ESD_{x(t_n)} = |\hat{x}_d(f)|^2 \quad (2.8)$$

According to the Wiener-Kintchin theorem[58], the Power Spectral Density (PSD) of a signal is the FT of its autocorrelation function. The autocorrelation  $R_{xs}(\tau)$  of  $x_s(t)$  is defined by (2.9), thus from the relation (2.10), the relation between the ESD and the PSD of a deterministic signal can be deduced by (2.11) and then by (2.12).

$$R_{xs}(\tau) = \sum_{t=-\infty}^{\infty} x_s(t) x_s^*(t - \tau) \quad (2.9)$$

As  $x_s(t)$  is discretized and is composed of  $N$  samples, the discrete autocorrelation  $R_{x_s}(k)$  is defined in (2.10).

$$R_{x_s}(k) = \frac{1}{N} \sum_{n=0}^{N-1} x(nT_s)x^*(nT_s - k) \xrightarrow{F.T} PSD_{x_s(t)} \quad (2.10)$$

$$\begin{aligned} PSD_{x_s(t)} &= \frac{1}{N} \sum_{n=0}^{N-1} \sum_{n=0}^{N-1} x(nT_s)x^*(nT_s - k)e^{-j2\pi fnT_s}e^{-j2\pi f(nT_s-k)} \\ &= \frac{1}{N} \left[ \sum_{n=0}^{N-1} x(nT_s)e^{-j2\pi fnT_s} \right] \left[ \sum_{n=0}^{N-1} x(c)e^{-j2\pi fc} \right]^* \end{aligned} \quad (2.11)$$

$$PSD_{x_s(t)} = \frac{|\hat{x}_d(f)|^2}{N} = \frac{ESD_{x_s(t)}}{N} \quad (2.102)$$

### 2.2.2 Spectral Analysis for Random Signals

In fact, the importance of the spectral analysis resides in this part for determining or estimating the spectrum of random signals, as in most of the applications the sampled signal is not deterministic, it may have some known characteristics or some predictable features, but due to the noise and the wide variety of possible values, the acquired signal is considered as a random sequence of data. In order to treat this data and reveal its content, the spectral analysis techniques were conceived to estimate its spectrum and thus deduce the needed information. In Figure 2.3 the classification of the spectral analysis methods for random signals sampled uniformly is presented, including the most used techniques in the literature [22], [57]. As already mentioned, the spectral analysis is developed in purpose of estimating how the total power is distributed over frequency. On one hand, the Classical or Non-Parametric methods are based on the estimation of the spectrum after filtering the signal to extract the frequency band of interest. On the other hand, the parametric methods assume a model for the data which makes the spectrum parameterized, the fact that deviates the purpose of estimation to the parameters of the postulated model [22], [57].

#### A) Non-Parametric Methods

As presented in Figure 2.3, non-parametric methods are also divided into two major categories according to the way of estimating the spectrum: the Periodogram and the Correlogram [57]. In fact, these methods are conceived to calculate the spectrum according to the PSD definition. Thus, by referring to the relations (2.10) and (2.12), the PSD of the random signal is expressed by (2.13). From equation (2.13) both methods are defined: the periodogram-based methods conclude the

spectrum from the squared DTFT of the signal divided by the number of samples, while the Correlogram-based methods count on the FT of the autocorrelation of  $x_s(t)$  [22].

$$PSD_{x_s(t)} = \sum_{k=-\infty}^{+\infty} R_{x_s}(k) e^{-i2\pi f n T_s} = \lim_{N \rightarrow \infty} E \left[ \frac{1}{N} \left| \sum_{n=0}^{N-1} x(nT_s) e^{-i2\pi f n T_s} \right|^2 \right] \quad (2.13)$$

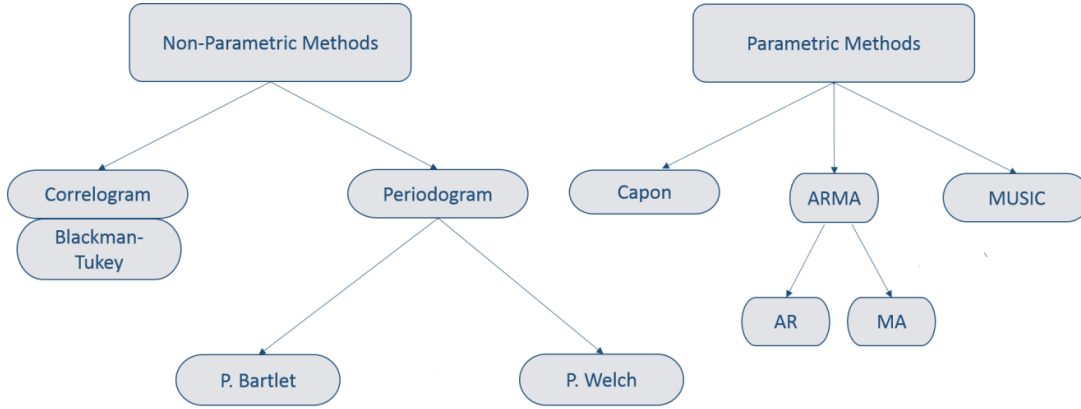


**Figure 2.3 Methods of Spectral Analysis for Random Signals in Uniform Sampling**

#### A.1) The Periodogram

The Periodogram is known also as the Schuster periodogram referring to its inventor [59]. This spectrum estimator is defined by (2.14) and has been used for determining the hidden periodicities in time series, which verifies its name.

$$PSD_P(f) = \frac{1}{N} \left[ \sum_{n=0}^{N-1} x(nT_s) e^{-i2\pi f n T_s} \right]^2 \quad (2.14)$$

Apparently, the periodogram can be directly deduced from the DTFT of the sampled signal. In order to reduce the computational complexity and thus the time of execution, the periodogram can be easily calculated by the mean of the Fast Fourier Transform algorithm (FFT) [57]. Many analysis were established on the periodogram estimator in order to qualify its performance. Therefore, statistical parameters as the variance and the bias were used [60]. In fact, the essential reason behind the difference between the estimator and the real spectrum is that the signal is acquired during a limited duration. This limitation can be seen as a truncation by a rectangular window that multiplies the signal in time domain. In the frequency domain, the estimator is convoluted with a sinc function. It was proven that the bias of the periodogram estimator is decreased when the number of sampled point is increased. Thus, it is considered as an asymptotically unbiased estimator, while it is

inconsistent due to its fluctuation around the real spectrum. Furthermore, problems like leakage and smearing appears in the periodogram when the spectrum to be estimated is peaky [57]. Thus, several modified periodograms were proposed, the modifications are based on the replacement of the signal truncation by a window apodization. Basically, these modified periodograms have the same concept but differ in the technique. The modified periodograms can be defined by (2.15).

$$PSD_{P_m}(f) = \frac{1}{NU} \left[ \sum_{n=0}^{N-1} w(n)x(nT_s) e^{-i2\pi f n T_s} \right]^2 \quad (2.15)$$

$$\text{with } U = \frac{1}{N} \sum_{n=0}^{N-1} |w(n)|^2$$

The first modified periodogram is proposed in [61] in the aim of reducing the variance of the periodogram. Thus, its concept is based on splitting up the signal (N samples) into multiple segments of M samples and averaging the resulting periodograms of all the segments to obtain the new estimated periodogram with less fluctuations. Although the variance is reduced by a factor equal to 1/L, where L=N/M, the resolution is also reduced by a factor of L compared to the original periodogram. This compromise is then resolved according to the application and the intentions of the user. On the same concept of the Bartlett periodogram, further modifications were added to conceive the Welch periodogram introduced in [62]. The segmentation is applied by window apodization with an overlapping between segments. Figure 2.4 illustrates the common and the different points between Bartlett and Welch periodograms.

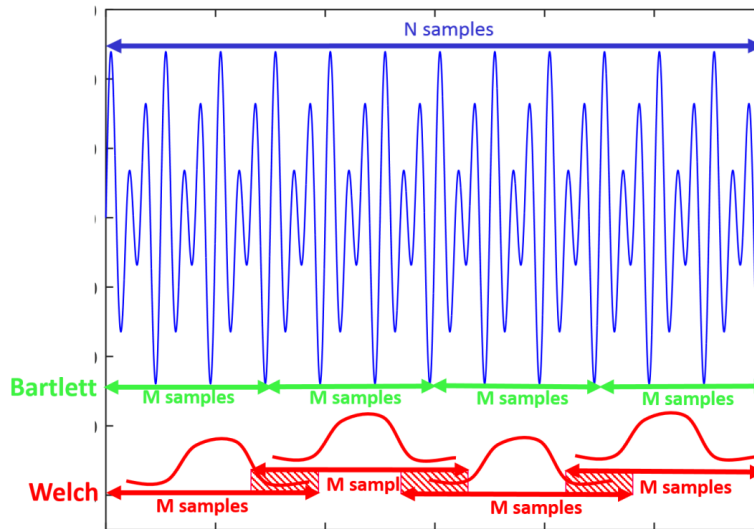


**Figure 2.4 The application of Bartlett and Welch modifications**

### A.2) The Correlogram

According to the equation in (2.13) the correlogram estimator is considered as an alternative to the periodogram, though, it is based on the FT of the autocorrelation  $R_{xx}(k)$  of the signal  $x(n)$ . Similarly to the periodogram, the correlogram is considered of high variance even in case of large signals. Thus, for same reasons, the Blackman-Tukey spectral estimate was proposed [63], based on weighted averaging in order to make the correlogram smoother and reduce the variability. The definition of such estimator can be expressed by (2.16).

$$PSD_{C_{BT}}(f) = \sum_{k=-(M-1)}^{M-1} w(k)R_{xx}(k) e^{-i2\pi f k T_s} \quad (2.16)$$

### B) Parametric Methods

As its name indicates, parametric methods are based on estimating parameters of the signal spectrum model instead of its whole spectrum. The difference between these methods resides essentially in the model assumed. Multiple Signal Classification (MUSIC) introduced by [64] is based on considering the signal a sum of exponential terms. When the signal  $x(n)$  is predictable and can be concluded from anterior samples, its model is the Auto-Regressive (AR), and when it is a linear combination of uncorrelated samples it is considered as Moving Average (MA). A combination of both models AR and MA can be also used, it is the generalized ARMA model [22]. Another variant of parametric methods can be found in Capon method introduced by [65], which is based on narrow band filters applied on multiple frequencies, where the aspect of the filters is data-dependent [57].

## 2.3 Spectral Analysis for Random Sampling

In order to apply the RS on vibration signals in machine monitoring context, the spectral analysis of this type of sampling must be studied to observe its impact on the spectrum of acquired signals as the vibration analysis of rotating machinery is usually conducted in the frequency domain [3]. Thus, the spectral analysis of the RS is essential for exploring this process in order to qualify its performance according to the mode of sampling and the probability distribution and in terms of the parameters of the sequence such as the mean sampling period ( $T_{sm}$ ), the standard deviation  $\sigma$  and the number of points  $N$ . By following the same procedure of the spectral analysis for uniform sampling, the direct application of the FT on the deterministic sampled signal in case of RS is presented in (2.17).

$$\sum_{n=-\infty}^{\infty} \delta(t - t_n) \xrightarrow{F.T} \sum_{n=-\infty}^{\infty} e^{i2\pi f t_n} = G(f) \quad (2.17)$$

According to [55] the value of  $G(f)$  is not known in general, which makes the interpretation of the FT of the randomly sampled signal ( $x_s(t)$ ) ambiguous and depends on the point process  $\{t_n\}$ . In fact, in [28] and later on in [36], some calculations were made in the aim of estimating the FT of  $x_s(t)$  only in case where the used sampling point process is stationary and they obtained (2.18) for both, periodic and aperiodic signals ( $x(t)$ ).

$$\hat{X}_s(f) = E \left[ \sum_{n=-\infty}^{+\infty} x(t_n) e^{-i2\pi f t_n} \right] = \frac{1}{T_{sm}} X(f) \quad (2.18)$$

As a result, the deduced form in (2.18) confirms the anti-aliasing property of the stationary random process but the exactitude is not guaranteed due to the use of the expectation of the signal, and it can't give further information on the spectrum of  $x_s(t)$ . Consequently, the direct application of the FT on  $x_s(t)$  is not much profitable. In reality, the spectral analysis of the randomly sampled signal has been the subject of many researches since this process of sampling appeared. In addition, the focus of these researches was on the calculation of the PSD of  $x_s(t)$  rather than its FT, until the research in [36] conceived the FT inspired from the work in [35] where the final forms of the PSD of  $x_s(t)$  sampled by different modes of RS were conceived and verified. Hence, the FT of the signal  $x_s(t)$  within both modes of RS is presented to deduce the basic properties of RS, then a brief review is shown on the researches done for developing the PSD formula of the randomly sampled signal within the different mode of RS. The link between the FT and the PSD is verified at the end to guarantee the equivalence between both representations. A detailed analysis is then done for the PSD of both RS modes with the different possible distributions.

### 2.3.1 FT of the Deterministic Signal

Inspired by the results of [32] and [35], the author of [36] deduced the FT of the deterministic randomly sampled signal in order to deduce the ESD of  $x_s(t)$ . The procedure of calculations is presented in both cases ARS and JRS.

#### A) FT of Deterministic Signal Sampled by ARS

In [36], the calculations were started by (2.19), where the sampling signal is defined by the Dirac distribution for the instant  $t_0$  whose value is deterministic, in addition to the sum of PDF of the random instants  $\{t_n\}$ . As declared in (1.26) in chapter 1, the instant  $t_n$  is the sum of all the previous random intervals  $\tau_i$ , thus according to (1.32) the PDF of  $t_n$  is the  $n$ -fold convolution which. So, by applying the FT as in (2.20), the result is obtained by (2.21).

$$x_s(t) = x(t) \left[ \delta(t) + \sum_{n=1}^{+\infty} p_n(t) \right] \quad (2.119)$$

Thus the FT of the PDF of the random instants becomes:

$$TF[p_n(t)] = TF[\otimes_{i=1}^n p(\tau_i)] = \prod_{i=1}^n \varphi_\tau(-f) \quad (2.20)$$

$$\hat{X}_{ARS}(f) = \frac{1}{T_{Sm}} X(f) + X(f) \otimes \frac{1}{[1 - \varphi_\tau(-f)]} \quad (2.12)$$

In the formula (2.21), the elimination of the aliases is obvious which verifies the results declared in chapter 1, where it was concluded that in case of an ARS the random point process is stationary independently from the probability distribution of the random interval  $\tau$ , so, the anti-aliasing property is always verified. Consequently, the low-pass filtering for anti-aliasing is not needed and the mean sampling period is not restricted by a maximum value as in the uniform sampling case due to the absence of aliasing. The second term in the addition of (2.21) is the additive noise resulting from the application of the RS. Finally, the ESD of  $x_s(t)$  is defined by:

$$ESD_{x_s} = |\hat{X}_{ARS}(f)|^2 \quad (2.13)$$

#### B) FT of Deterministic Signal Sampled by JRS

In the same methodology, the calculation begins with (2.23) a similar expression to (2.19), where the PDF  $p_n(t)$  of the random instant  $t_n$  is expressed by the PDF of the random jitter with a translation of  $nT_{Sm}$  as already declared in (1.44) of chapter 1. By applying the FT as in (2.24), the FT of the JRS sampled signal is deduced in (2.25), where  $X(f)$  is the FT of  $x(t)$  and  $\varphi_u(f)$  is the CF of the jitter  $u$  whose PDF is  $p_u(t)$ .

$$x_s(t) = x(t) \left[ \delta(t) + \sum_{\substack{n=-\infty \\ n \neq 0}}^{+\infty} p_n(t) \right] = x(t) \left[ \delta(t) + \sum_{\substack{n=-\infty \\ n \neq 0}}^{+\infty} p_u(t - nT_{Sm}) \right] \quad (2.14)$$

$$\hat{X}_{JRS}(f) = X(f) * TF \left[ \delta(t) + \sum_{\substack{n=-\infty \\ n \neq 0}}^{+\infty} p_u(t - nT_{Sm}) \right] \quad (2.154)$$

$$\hat{X}_{JRS}(f) = \frac{1}{T_{Sm}} \left\{ X(f) * [1 - \varphi_u(-f)] + \sum_{n=-\infty}^{+\infty} X\left(f - \frac{n}{T_{Sm}}\right) \varphi_u\left(-\frac{n}{T_{Sm}}\right) \right\} \quad (2.165)$$

As the CF of the jitter  $u$  is either for uniform distribution or Gaussian distribution, its shape is similar to a low pass filter, thus, it can be deduced from the FT of  $x_s(t)$  in (2.25), that the periodic

repetitions of  $X(f)$  within the second term of the summation in (2.25) are eliminated by the CF of the jitter [50]. The elimination of these replicas is dependent on the shape of CF which is determined by the parameters of the random jitter distribution. Hence, the results of chapter 1 are confirmed concerning the anti-alias property for the JRS which is dependent on the chosen distribution of the jitter  $u$ . The first term of (2.25) indicates the presence of an additive noise caused by the RS process. Similarly to the ARS case, the ESD of  $x_s(t)$  is defined by (2.26).

$$ESD_{x_s} = |\hat{X}_{JRS}(f)|^2 \quad (2.26)$$

### 2.3.2 PSD of $x_s(t)$

In order to define the PSD of  $x_s(t)$ , the start must be with its definition in term of  $x(t)$  and  $S(t)$ . As the sampling process is modeled in time domain by the relation (2.1) declared at the beginning of this chapter and as the analogic signal  $x(t)$  and the sampling signal  $S(t)$  are independent, the autocorrelation of  $x_s(t)$  ( $R_{x_s}(\tau)$ ) is equal to the product of the autocorrelation of  $x(t)$  ( $R_x(\tau)$ ) with the autocorrelation of  $S(t)$  ( $R_S(\tau)$ ). According to the Wiener-Kintchin theorem [58], the PSD of a signal is the FT of its autocorrelation function. Thus, the relation between the corresponding PSD in the frequency domain can be expressed by (2.27).

$$\Phi_{x_s}(f) = \Phi_x(f) \otimes \Phi_S(f) \quad (2.27)$$

Where  $\Phi_{x_s}(f)$ ,  $\Phi_x(f)$  and  $\Phi_S(f)$  are the PSD of the sampled signal, the analogic signal and the sampling signal respectively [32], [35], [37]. Thus, to explore the effect of RS on the sampled signal, it is crucial to determine the spectrum of the sampling sequence and deduce the spectrum of sampled signal by applying the convolution of the spectrum of the analogic signal with the spectrum of the sampling sequence.

The most reliable spectral analysis of RS was originally introduced by Beutler and Leneman, as they were the first authors to conceive the definition of the random impulse process in [34], they continued their study by determining the condition of stationarity in [33], and then by establishing the definition of the autocorrelation function and the PSD of the RS signal  $S(t)$  in [32].

In fact, many analyses were proposed in this concern by many different authors, since 1960. When introducing the ARS mode for the first time, Shapiro and Silverman proceeded in determining the power spectrum of this process in their early study in [31] to verify its free-aliasing aspect, especially when used with the exponential distribution whose statistical parameters doesn't verify the temporal condition as proved in Chapter 1. The power spectrum of an ARS sampled signal proposed in [31] is defined by (2.28).

$$\Phi_{xs}(f) = \int_{-\infty}^{+\infty} \Phi_x(f) \operatorname{Re} \left\{ \frac{1 + e^{i2\pi f} \varphi(z)}{1 - e^{i2\pi f} \varphi(z)} \right\} dz \quad (2.28)$$

With the condition of having an iid random interval with a PDF  $p(t)$  and a CF  $\varphi(f)$ . In their study of NUS as an advanced topic in sampling theory, Marvasti in [55] discussed the RS as a part of NUS and continued in determining the power spectrum of the randomly sampled signal in different RS modes. For ARS with exponential or uniform distribution the spectrum is defined by (2.29).

$$\Phi_{xs}(f) = \lambda^2 \Phi_x(f) + \lambda \eta_x(0) \quad (2.29)$$

$\eta_x(0)$  is the total power of  $x(t)$  and  $\lambda$  is the mean of the random interval.

For RSS the power spectrum is defined by (2.30).

$$\Phi_{xs}(f) = \Phi_x(f) + \sum_{n \neq 0} \Phi_x \left( f - \frac{n}{T_{Sm}} \right) + \frac{T_{Sm}(1-p)}{p} \eta_x(0) \quad (2.30)$$

$p$  is the probability of having a sampling pulse (the complement of the skipping probability).

For JRS the sampled signal has a power spectrum expressed in (2.31).

$$\begin{aligned} \Phi_{xs}(f) = & \Phi_x(f) + \sum_{n \neq 0} \Phi_x \left( f - \frac{n}{T_{Sm}} \right) \varphi \left( \frac{n\vartheta}{T_{Sm}} \right) + T_{Sm} \left\{ \varphi \left( \frac{n\vartheta}{T_{Sm}} \right) - \left| \varphi \left( \frac{n\vartheta}{T_{Sm}} \right) \right|^2 \right. \\ & \left. \otimes \Phi_x(f) \right\} \end{aligned} \quad (2.31)$$

$\varphi(f)$  is the CF of the jitter and  $\vartheta$  is the pulse width.

In addition, Martin in his thesis [66] on the theory and techniques of analyzing irregularly sampled signals developed the power spectrum of randomly sampled signals by starting with the results of Shapiro and Silverman in [31] to conclude for the ARS by (2.32).

$$\begin{aligned} \Phi_{xs}(f) = & \Phi_x(f) \otimes \left\{ \frac{1}{T_{Sm}} \delta(f) + \operatorname{Cont} \operatorname{Re} \left\{ \frac{1 + \varphi_\tau(f)}{1 - \varphi_\tau(f)} \right\} \right. \\ & \left. + \sum_{f_\delta \neq f} h_\delta \delta(f - f_\delta) \right\} \end{aligned} \quad (2.32)$$

$h_\delta$  is the strength of the impulse. The term ‘‘Cont’’ is used to emphasize the continuity of  $\operatorname{Re}\{.\}$  in the limit as  $f$  tend to  $f_\delta$ . And for the JRS, the spectrum is expressed by:

$$\Phi_{xs}(f) = \Phi_x(f) \otimes \left\{ 1 - |\varphi_u(f)|^2 + |\varphi_u(f)|^2 \sum_{n \in \mathbb{Z}} \delta \left( f - \frac{n}{T_{Sm}} \right) \right\} \quad (2.33)$$

However, the suggested definitions were judged to be contradicting or incompatible. Due to the absence of simulations or real measurements in these studies, it was hard to identify which model to consider. In his study of applying the RS in radio design, Wojtiuk developed in first place the power spectrum of random process in the JRS mode and then deduced the spectrum of the ARS. After verifying with simulations in [35], it was found out that the power spectrum definition originally proposed by Beutler and Leneman in [32] is the most accurate to be used. Thus, a brief review on the calculation method of the PSD in [32] is presented with the verification of the link between the FT and the PSD of the randomly sampled signal.

The sampling process  $S(t)$  is already declared in chapter 1 by (2.34).

$$S(t) = \sum_{n=-\infty}^{n=+\infty} \alpha_n \delta(t - t_n) \quad (2.34)$$

Which is the definition of the random impulse process defined by Beutler and Leneman. For  $S(t)$ , the autocorrelation  $R_S(\tau)$  is defined by (2.35).

$$R_S(\tau) = E[S(t)S(t + \tau)] = \lim_{T \rightarrow \infty} \frac{1}{2T} \int_{-T}^T S(t)S(t + \tau) dt \quad (2.35)$$

And thus, the PSD of  $S(t)$  is the FT of  $R_S(\tau)$  and is defined by (2.36).

$$\Phi_S(f) = \int_{-\infty}^{\infty} R_S(\tau) e^{-j2\pi f \tau} dt \quad (2.36)$$

In [32] the autocorrelation function of  $S(t)$  was deduced from the autocorrelation of its primitive  $N_S(t)$ , which is a stationary increment stochastic process, the calculations made in [32] are resumed in the Appendix C. The autocorrelation of  $S(t)$  is expressed by (2.37) within the third theorem deduced from the SPP condition already mentioned in Chapter 1.

$$R_S(\tau) = E[s(t)s(t + \tau)] = \frac{1}{T_{Sm}} \rho(0)\delta(\tau) + \frac{1}{T_{Sm}} \sum_{n=1}^{\infty} \rho(n)p_{\partial_n}(|\tau|) \quad (2.37)$$

Where  $1/T_{Sm}$  is considered as the average number of points per unit time interval, and  $\rho(n)$  is the correlation function for the process  $\{\alpha_n\}$ ,  $\rho(n)$  is defined by (2.38).

$$\rho(n) = E[\alpha_{u+n}\alpha_u] \quad \forall u \quad (2.38)$$

$p_{\partial_n}(t)$  is the PDF of  $\partial_n$  which is the sum of  $n$  consecutive time intervals. By referring to the definition of the time process  $\{t_n\}$  in Chapter 1, it can be deduced that  $t_n = \partial_n$ , which means that  $p_{\partial_n}(t) = p_n(t)$  in case when the  $n$  consecutive intervals are taken from the beginning of the sequence.

The expression of  $R_s(\tau)$  in (2.37) is considered as the essential definition upon which is based all the theory of RS conceived and developed in successive studies. In this thesis the correlation between random instants is not taken in consideration which simplifies the definition of  $R_s(\tau)$  to be replaced by (2.39).

$$R_s(\tau) = E[s(t)s(t + \tau)] = \frac{1}{T_{Sm}} \delta(\tau) + \frac{1}{T_{Sm}} \sum_{n=1}^{\infty} p_{\partial n}(|\tau|) \quad (2.39)$$

The definition of (2.39) is the autocorrelation of any sequence of RS, the selection of the mode and the distribution gives further details and thus makes the function more specific. In next paragraphs, the PSD of each mode is deduced with the verification of the link between the FT and the PSD.

#### A) ARS Case

To find the PSD of the ARS mode, the expression of  $p_{\partial n}(t)$  can be simply defined in term of the PDF of the random interval  $\tau$  by the n-fold convolution of the PDF the n consecutive intervals. As in the term (2.39) the summation of  $p_{\partial n}$  is from  $n=1$ , it can be confirmed that  $p_{\partial n}(t) = p_n(t)$ . Thus, the autocorrelation of the sampling signal is then deduced by (2.40).

$$\begin{aligned} R_s(\tau) &= \frac{1}{T_{Sm}} \left\{ \delta(\tau) + \sum_{n=1}^{+\infty} R_p(\tau) + \sum_{n=1}^{+\infty} R_p(-\tau) \right\} = \frac{1}{T_{Sm}} \left\{ \delta(\tau) + \sum_{n=1}^{+\infty} p_n(\tau) + \sum_{n=1}^{+\infty} p_n(\tau) \right\} \\ &= \frac{1}{T_{Sm}} \left\{ \delta(\tau) + \sum_{n=1}^{+\infty} \textcircled{*}_{i=1}^n p(\tau_i) + \sum_{n=1}^{+\infty} \textcircled{*}_{i=1}^n p(-\tau_i) \right\} \end{aligned} \quad (2.40)$$

The expression in (2.40) is the continuation of (2.39), where the term of  $R_p(\tau)$  can be directly assumed by (2.41).

$$R_p(\tau) = \int_{-\infty}^{\infty} p_0(-t)p_n(-t - \tau)dt = \int_{-\infty}^{\infty} \delta(-t)p_n(t + \tau)dt = p_n(\tau) \quad (2.41)$$

In fact, the second term of summation in (2.40) is added to complete the summation from  $-\infty$  to  $+\infty$ , by considering the ARS sequence is composed of two sequences, the first goes in the positive time direction, the second goes in the negative time direction and both meet at the common origin  $t_0$ . As already declared in (1.32) the PDF function  $p_n(\tau_n)$  is equal to n-fold convolution of all the random intervals  $\tau_n$ , so by applying the FT on  $R_s(\tau)$ , the PSD of  $S(t)$  is expressed by (2.42).

$$\Phi_s(f) = \frac{1}{T_{Sm}} \left\{ 1 + \sum_{n=1}^{\infty} \varphi_{\tau}^n(f) + \sum_{n=1}^{\infty} \varphi_{\tau}^n(-f) \right\}$$

$$= \frac{1}{T_{Sm}} \left\{ 1 + \sum_{n=1}^{\infty} \varphi_{\tau}^n(f) + \sum_{n=1}^{\infty} \varphi_{\tau}^{*n}(f) \right\} \quad (2.42)$$

The sum of  $\varphi_{\tau}^n(f)$  is considered as the sum of a geometric series with reason equal to  $\varphi_{\tau}(f)$ , which can be expressed as a Poisson kernel which will lead to the expression in (2.43) with resolving the singularity for  $f=0$ , by adding the  $\delta(f)$  function that recovers the spectrum of  $x(t)$  [35]. In fact, by proceeding with the autocorrelation of the expression of (2.19), and deducing  $R_p(\tau)$  by (2.41) and continuing with applying the FT to obtain the PSD in (2.43), the direct link between the FT of ARS with its PSD is confirmed.

$$\Phi_{xs}(f) = \frac{1}{T_{Sm}^2} \Phi_x(f) + \frac{1}{T_{Sm}} \Phi_x(f) \odot Re \left\{ \frac{1 + \varphi_{\tau}(f)}{1 - \varphi_{\tau}(f)} \right\} \quad (2.43)$$

Thus same conclusions deduced from the FT can be revealed from the PSD according the aliasing, more properties can be observed by defining the CF of possible distributions which will be presented in the next section after deducing the JRS PSD.

#### B) JRS Case

As already mentioned, the autocorrelation definition is expressed in term of the PDF of  $\partial_n$ , in case of the JRS this probability can be deduced from the PDF of the jitter by using its definition.

$$t_n = nT_{Sm} + u_n \quad (2.44)$$

The interval between two consecutive samples in JRS is then:

$$\tau_n = t_n - t_{n-1} = nT_{Sm} + u_n - (n-1)T_{Sm} - u_{n-1} = T_{Sm} + u_n - u_{n-1} \quad (2.45)$$

So the sum  $\partial_n$  can be expressed by (2.46).

$$\partial_n = \sum_{m=l}^{n+l-1} \tau_m = nT_{Sm} + u_{n+l-1} - u_{l-1} \quad \forall l \quad (2.46)$$

The term  $nT_{Sm}$  is deterministic. The variables  $u_{n+l-1}$  and  $u_{l-1}$  are random jitters that follow the same distribution having  $p_u(t)$  as PDF, thus the PDF of  $\partial_n$  is deduced by (2.47) as the PDF of the sum of variables is the convolution of their PDF:

$$p_{\partial n}(t) = \delta(t - nT_{Sm}) \odot p_u(t) \odot p_u(-t) \quad (2.47)$$

In fact, by definition, the autocorrelation  $R_y(t)$  of any signal  $y(t)$  is expressed by the convolution of  $y(-t)$  with  $y(t)$ , then:

$$R_{pu}(\tau) = p_u(-t) * p_u(t) \Rightarrow p_{\partial n}(t) = R_{pu}(t - nT_{Sm}) \quad (2.48)$$

Where  $R_{pu}(\tau)$  is the autocorrelation of the PDF of the jitter  $u$ . Which means that the PDF  $p_{\partial n}(t)$  is in reality the autocorrelation of the JRS sampling sequence by comparing it to the expression of  $x_s(t)$  in (2.23), thus the autocorrelation of the sampling signal in JRS is expressed by (2.49).

$$R_s(\tau) = \frac{1}{T_{Sm}} \delta(\tau) + \frac{1}{T_{Sm}} \sum_{n \neq 0} R_{pu}(\tau - nT_{Sm}) \quad (2.49)$$

This autocorrelation, as it can be directly deduced from (2.23) confirms the relation between the FT of RS and its PSD that can be concluded from it.

The FT of  $R_{pu}(\tau)$  gives the PSD of the PDF:

$$\Phi_p(f) = \varphi_u(-f) \times \varphi_u(f) = \varphi_u^*(f) \times \varphi_u(f) = |\varphi_u(f)|^2 \quad (2.50)$$

$\varphi_u(f)$  is the characteristic function of the PDF of the jitter which is a real function, so  $\varphi_u(f)$  is an Hermitian function.

Consequently the FT of  $R_s(\tau)$  is concluded by (2.51).

$$\Phi_s(f) = \frac{1}{T_{Sm}} \left(1 - \Phi_p(f)\right) + \frac{1}{T_{Sm}} \sum_{n=-\infty}^{\infty} \Phi_p(f) e^{-i2\pi f n T} \quad (2.51)$$

By replacing  $\Phi_p(f)$  by its value, and by using the Poisson summation to replace the exponential in the second term by a dirac comb, the PSD of  $s(t)$  becomes (2.52).

$$\Phi_s(f) = \frac{1}{T_{Sm}} (1 - |\varphi_u(f)|^2) + \frac{1}{T_{Sm}} \sum_{n=-\infty}^{\infty} |\varphi_u(f)|^2 \delta\left(f - \frac{n}{T_{Sm}}\right) \quad (2.52)$$

The PSD of  $x_s(t)$  is then deduced in (2.53).

$$\begin{aligned} \Phi_{x_s}(f) &= \Phi_x(f) \otimes \Phi_s(f) \\ &= \frac{1}{T_{Sm}} \left\{ \Phi_x \otimes [1 - |\varphi_u(f)|^2] + \frac{1}{T_{Sm}} \sum_{n=-\infty}^{\infty} \left| \varphi_u\left(\frac{n}{T_{Sm}}\right) \right|^2 \Phi_x\left(f - \frac{n}{T_{Sm}}\right) \right\} \quad (2.53) \end{aligned}$$

The PSD of the JRS sequence in (2.53) elucidates the impact of JRS on the sampled signal. The impact remains in the first continuous part considered as an added noise floor and in the second discrete part defined by a pulse train modulated with the characteristic function of the random jitter. After the convolution with the analogical signal  $x(t)$ , these pulses turn into aliases. The shape of the characteristic function may contribute in eliminating these aliases, which gives the JRS a potential to be an alias-free sampling.

After the verification of the link between the FT and the PSD of the randomly sampled signal  $x_s(t)$ , further analysis can be done by exploring the PSD in both modes of RS using different distributions, with the ability to identify the origin of each term in the PSD. Hence, a detailed study of the RS impact within its multiple versions is presented in next section.

### 2.3.3 RS Impact

#### A) ARS

##### A.1) PSD of ARS with Uniform Distribution

When considering the random interval  $\tau$  varying in the interval  $[T_{sm}(1-r); T_{sm}(1+r)]$ , the CF of the uniform distribution becomes (2.54)

$$\varphi_{unif}(f) = \frac{e^{i2\pi fb} - e^{i2\pi fa}}{i2\pi f(b-a)} = e^{i2\pi f T_{sm}} \text{sinc}(2\pi f r T_{sm}) \quad (2.54)$$

After replacing the CF of the uniform distribution in (2.53), and by using the notion of the Poisson Kernel the PSD of the ARS with the Uniform distribution becomes:

$$\begin{aligned} \Phi_{x_s}(f) = \Phi_x(f) \\ \otimes \left\{ \frac{1}{T_{sm}^2} \delta(f) \right. \\ \left. + \frac{1}{T_{sm}} \frac{1 - (\text{sinc}(2\pi f r T_{sm}))^2}{1 - 2\text{sinc}(2\pi f r T_{sm}) \cos(2\pi f T_{sm}) + (\text{sinc}(2\pi f r T_{sm}))^2} \right\} \end{aligned} \quad (2.55)$$

As the ARS is an aliasing-free sampling, the PSD in case of ARS with the uniform distribution is free of impulses causing replicas, though, the noise floor is not flat and it will affect the signal. In order to explore the effect of this noise and find the conditions to reduce it, the second term convoluting  $\Phi_x(f)$  in the PSD,  $N(f)$ , is plotted in Figures (2.5) to (2.7) by varying  $r$  and  $T_{sm}$ . According to the temporal condition discussed in Chapter 1 the value of  $r$  must not be greater than 1, and according to the stationarity condition, the best value of  $r$  is the maximum 1 ( which correspond to the ratio  $\sigma/T_{sm} = 0.577$ ) as the maximum limit imposed by the temporal condition tends to have the minimum stationarity delay  $T_{sd}$ . This choice is confirmed in Figures 2.5 and 2.6, where for a fixed  $T_{sm}=10s$ ,  $N(f)$  is figured for different values of  $r$ . In Figure (2.5) the best value to choose is  $r=0.5$  having the smallest variance, while in Figure (2.6) the function maxima at the aliasing frequencies ( $1/T_{sm}$  and its multiple) are the most reduced in case of  $r=1$ . In comparing both

cases,  $r=0.5$  is found to be better to choose, though, the effect of  $T_{sm}$  may enhance the shape of the function in  $r=1$  to make it convenient.

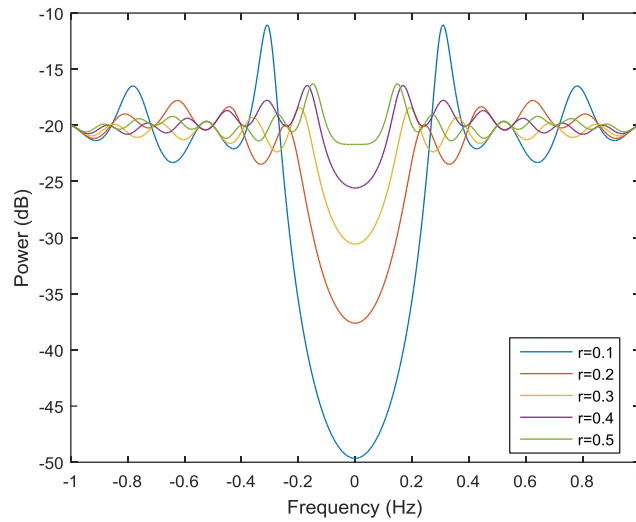


**Figure 2.5** The noise term  $N(f)$  in ARS with uniform distribution for different values of  $r < 0.5$  and  $T_{sm}=10s$

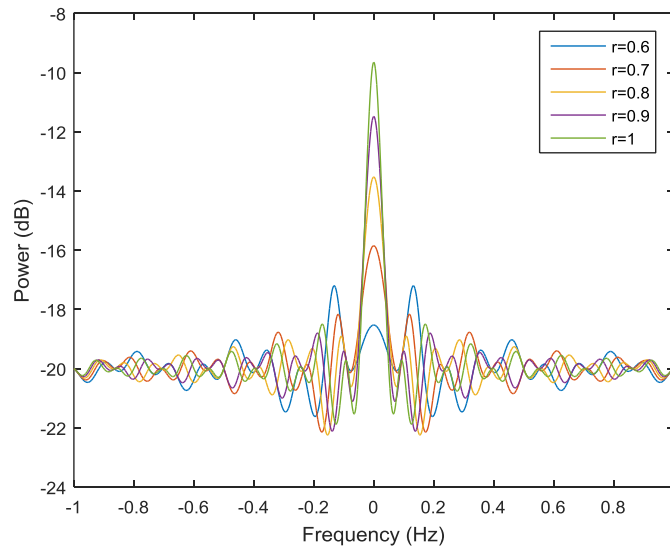


**Figure 2.6** The noise term  $N(f)$  in ARS with uniform distribution for different values of  $r > 0.5$  and  $T_{sm}=10$

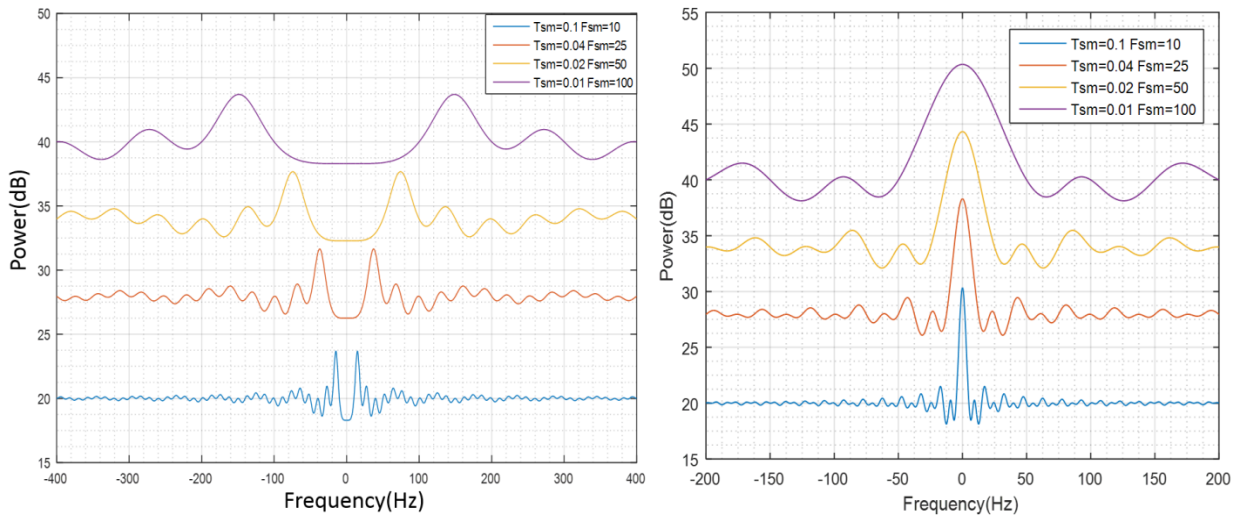


**Figure 2.7** The noise term  $N(f)$  in ARS with uniform distribution for different values of  $T_{Sm}$  with  $r=0.5$  (left) and  $r=1$  (right)

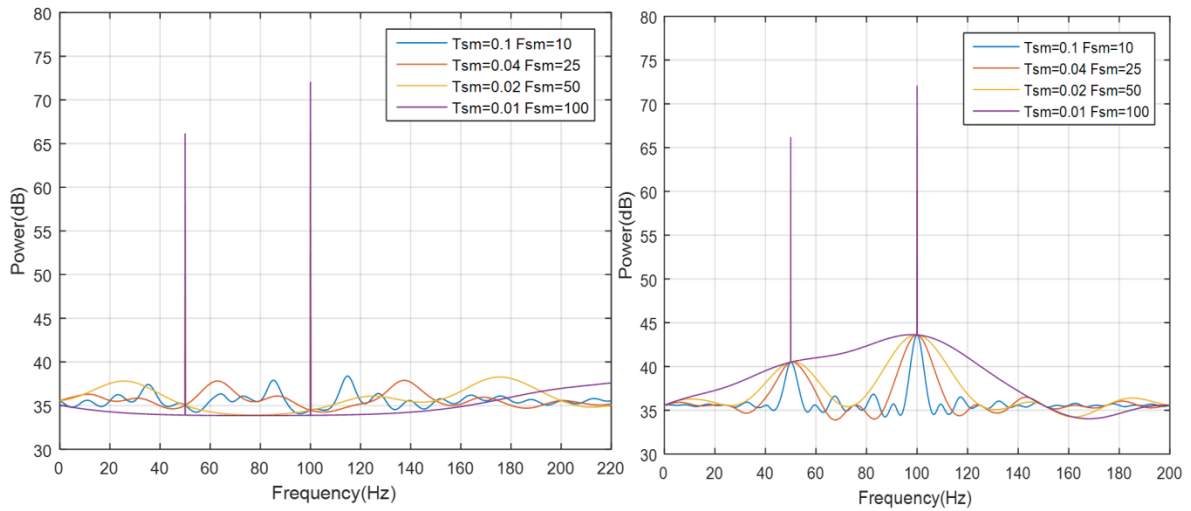


**Figure 2.8** The spectrum  $\Phi_{x_s}(f)$  in ARS with uniform distribution for different values of  $T_{Sm}$  with  $r=0.5$  (left) and  $r=1$  (right)

#### A.1.1) Recommendation for $T_{Sm}$

In case of  $r=0.5$ , the maximum of  $N(f)$  is reached at  $f=3/(2T_{Sm})$ , the variation of  $T_{Sm}$  affect then the location of this maximum and the width of the side lobe. While in case of  $r=1$ , the maximum is reached at  $f \rightarrow 0$  (as there exists a singularity in  $N(f)$  for  $f=0$ ) and when  $T_{Sm}$  is decreased the width of the main lobe increases. In fact, in this case the  $N(f)$  function has the form of a low pass filter with a cutting frequency proportional to  $1/T_{Sm}$ . To view the effect of this term on the whole spectrum an example of  $x_{sin}(t)$  composed of the sum of two sines at  $F_1=50\text{Hz}$  and  $F_2=100\text{Hz}$  with

amplitudes  $A_1=20$  and  $A_2=40$  is taken, the spectrum  $\Phi_{x_s}(f)$  is shown in figure 2.8 for both values of  $r$  (0.5 and 1) and for different values of  $T_{Sm}$ . The noise in this case is eventually the sum of  $N(f)$  repetitions located at the frequencies  $F_1$  and  $F_2$  of the signal  $x(t)$ . In case of  $r=0.5$  the noise is reduced between the two impulses while for  $r=1$  the noise reach its maximum. In the aim of reducing the noise added by the RS,  $r$  is preferred to be 0.5 ( which correspond to the ratio  $\sigma/T_{Sm}= 0.2887$ ) and  $T_{Sm}$  is chosen to be decreased to enlarge the distance between the two side lobes as in figure of  $N(f)$  and thus minimize the noise around the signal impulses. In fact the distance between the borders of the two side lobes is approximately  $2F_{Sm}$ , so  $F_{Sm}$  must be equal or greater than the distance between two peaks which is the difference  $(F_2-F_1)$ . This can be generalized for any spectrum having the highest frequency  $F_m$ , for the best noise reduction  $F_{Sm}$  must be equal or greater than  $F_{max}$ , which means  $T_{Sm}<T_m$ . In fact this condition is not crucial, it is just a recommendation to reduce the noise resulting from RS.

#### A.1.2) Recommendations for N

According to [35], [37] in order to examine the effect of the number of points in practical implementations, the noise term in the spectrum of  $x_s(t)$  is normalized by  $1/NT_{Sm}$ . Considering  $x_a(t)$  is an analytical signal defined by, with  $A_{min}$  is the minimal amplitude in  $x_a(t)$ . In worst cases where  $T_{Sm}$  is chosen higher than  $T_m$  and the function  $N(f)$  is convoluted with the spectrum  $\Phi_x(f)$  and thus located at the frequencies  $f_k$  and multiplied at each frequency by its corresponding amplitude  $A_k$ , so the maximum value in the noise term after normalization is (2.57) the term  $g$  multiplying the amplitudes is the maximum of the function  $N(f)$  before convolution. The maximum of the whole noise term must be lower than the minimum amplitude  $|A_{min}|^2/T_{Sm}^2$  of the signal  $x_a(t)$  by a certain ratio  $C$  determined within the constraint of the application using the ARS in sampling. This condition is expressed by (2.58) to simplify the notation and to find a minimal limitation of  $N$ , all the amplitudes  $A_k$  are considered to be equal to the minimum  $A_{min}$ , which will leads to the final form of the condition of  $N$  in (2.59). This relation between the number of samples  $N$  taken randomly with an ARS process and the number of peaks  $K$  of the original signal  $x_a(t)$  in the frequency domain where it is considered as  $K$ -sparse is very similar to the result of CS concerning the number of points captured in term of the sparse elements of the original signal as already mentioned in Chapter 1.

$$x_a(t) = \sum_{k=1}^K A_k e^{j2\pi f_k t} \quad (2.56)$$

$$\max(N(f) \otimes \Phi_x(f)) = \frac{\sum_{k=1}^K |g \cdot A_k|^2}{NT_{Sm}^2} \quad (2.57)$$

$$C \cdot \frac{\sum_{k=1}^K |A_k|^2}{N \cdot T_{Sm}^2} = \frac{|A_{min}|^2}{T_{Sm}^2} \Rightarrow N = C \cdot \frac{\sum_{k=1}^K |A_k|^2}{|A_{min}|^2} \quad (2.58)$$

$$N \geq g \cdot C \cdot K \quad (2.59)$$

According to Figure 2.9, for a fixed value of  $r$  the maximum of  $N(f)$  is nearly constant, in case of  $r=0.5$  it is perfectly constant for all the values of  $T_{Sm}$  as shown in Figure 2.9,  $g$  is then equal to 1.53 (3.7 in dB). By continuing with the same way, it can be deduced that  $N$  must verify (2.59) to minimize the noise added by the RS effect. In case of  $r=1$ ,  $g=3.289$  (10.34 in dB) which makes this case less advantageous and more requiring than  $r=0.5$ , which makes the ratio  $\sigma / T_{Sm} = 0.2887$  is the better choice.

In conclusion, in the aim of reducing the noise added by the RS two limitation values for the mean sampling period and for the number of randomly sampled point are proposed as recommendations for ARS with an anti-aliasing property guaranteed and a reduced additive noise.

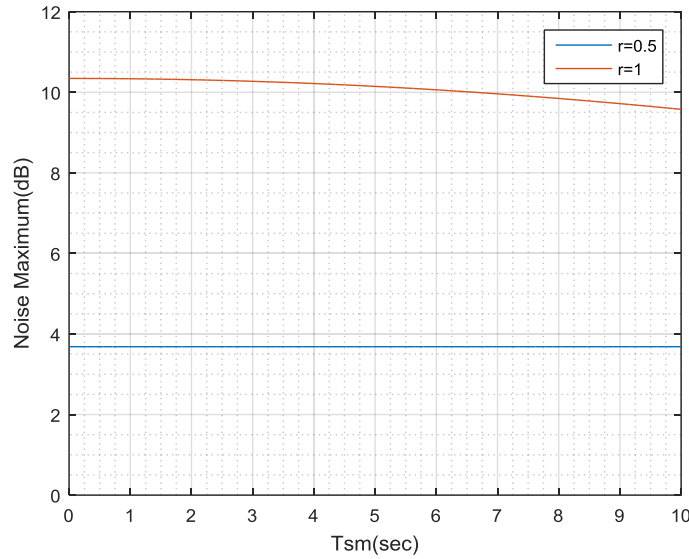


**Figure 2.9 The Maximum of  $N(f)$  in term of  $T_{Sm}$  for  $r=0.5$  and  $r=1$**

#### A.2) PSD of ARS with Gaussian Distribution

With ARS mode, the mean of the random interval is  $T_{Sm}$  and the standard deviation is  $\sigma$  so the CF of Gaussian distribution in this case is expressed by (2.60).

$$\varphi_{gauss}(f) = e^{i2\pi f T_{Sm}} e^{-2\pi^2 f^2 \sigma^2} \quad (2.60)$$

By applying the notion of Poisson kernel  $P(\rho, \theta)$  on the CF:  $\rho = e^{-2\pi^2 f^2 \sigma^2}$  and  $\theta = 2\pi f T_{Sm}$  the spectrum of the randomly sampled signal becomes (2.61).

$$\Phi_{x_s}(f) = \frac{1}{T_{Sm}^2} \Phi_x(f) + \frac{1}{T_{Sm}} \Phi_x(f) \otimes \left[ \frac{1 - (e^{-2\pi^2 f^2 \sigma^2})^2}{1 - 2(e^{-2\pi^2 f^2 \sigma^2}) \cos(2\pi f T_{Sm}) + (e^{-2\pi^2 f^2 \sigma^2})^2} \right] \quad (2.61)$$

It can be deduced from (2.61) that the PSD in case of ARS with the Gaussian distribution is free of aliases, but the noise floor is not flat and it will disturb the signal. The term causing this noise is the function  $N(f)$  convoluting the the spectrum  $\Phi_x(f)$  in the second element of addition of the spectrum  $\Phi_{x_s}(f)$ . As in previous cases, this function is presented in figures 2.10 and 2.11 with the variation of the parameters  $T_{Sm}$  and  $\sigma$  to view their impacts and conclude with the best values to obtain a resulting spectrum with minimum of noise. According to the discussions in chapter 1, the temporal condition imposed on the ratio  $\sigma/T_{Sm}$  a maximum value equal to 0.333, and according to the condition of stationarity and the definition of the delay of stationarity, it was deduced that this maximum value is the best to choose. In figure 2.10, it can be apparently verified that with  $\sigma/T_{Sm}$  equal to 0.167 and 0.33,  $N(f)$  has the minimum variance and its maxima at the aliasing frequencies are the most reduced. Thus, for these ratios,  $N(f)$  is shown for different values of  $T_{Sm}$  to view its effect and conclude with the best value to choose.

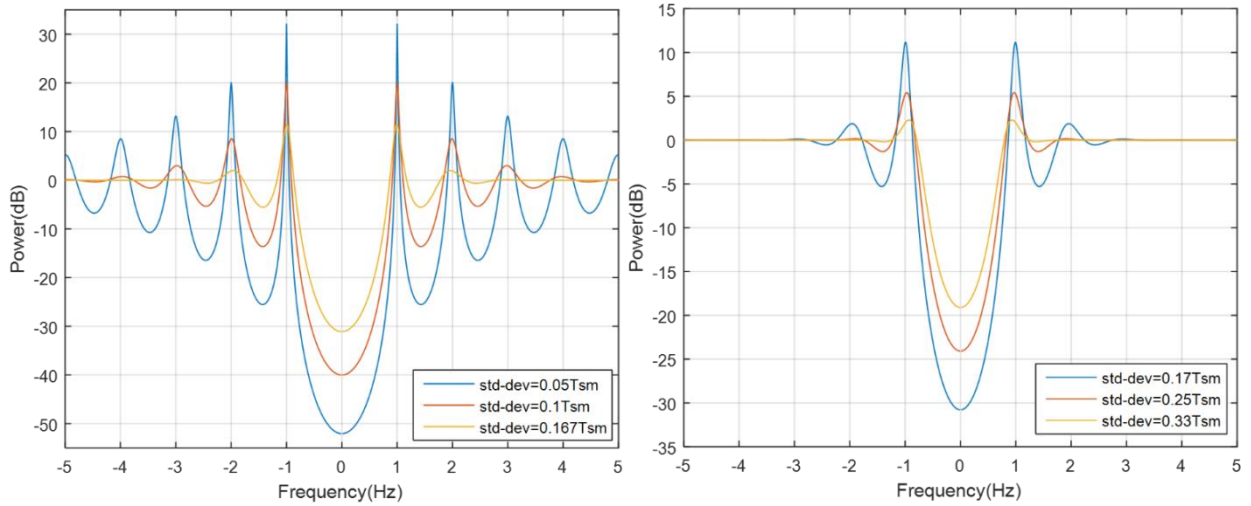


**Figure 2.10 The Noise Term Convoluting  $\Phi_x(f)$  for Different Values of  $\sigma$  with  $T_{Sm}=1$**

#### A.2.1) Recommendation for $T_{Sm}$

In both cases presented in figure (2.12) the maximum of side lobes is reached at  $1/T_{Sm}$ , so the value of  $T_{Sm}$  directly affects the width of the gap at  $f=0$ , the distance between side lobes maxima is  $2/T_{Sm}$ . The same example of  $x_{sin}(t)$  taken in the ARS with uniform distribution case ( $F_1=50\text{Hz}$  and  $F_2=100\text{Hz}$ ;  $A_1=20$  and  $A_2=40$ ) is used the case of Gaussian distribution. Similarly, the noise is the sum of  $N(f)$  repetitions located at the frequencies  $F_1$  and  $F_2$  of the signal  $x_{sin}(t)$ . But, in this case, the wider is the gap of  $N(f)$  at  $f=0$ , the more is the noise reduced around the signal impulses. Thus

the decreased values of  $T_{Sm}$  are appreciated. It can be deduced from this figure, that if  $F_{Sm}$  is equal or greater than the difference  $(F_2-F_1)$ , both gaps of the repeated  $N(f)$  will be joined in one wider gap, which will reduce the noise to the minimum between both impulses. This can be generalized for any spectrum having the highest frequency  $F_m$ , for the best noise reduction  $F_{Sm}$  must be equal or greater than  $F_{max}$ , which means  $T_{Sm} < T_m$ .

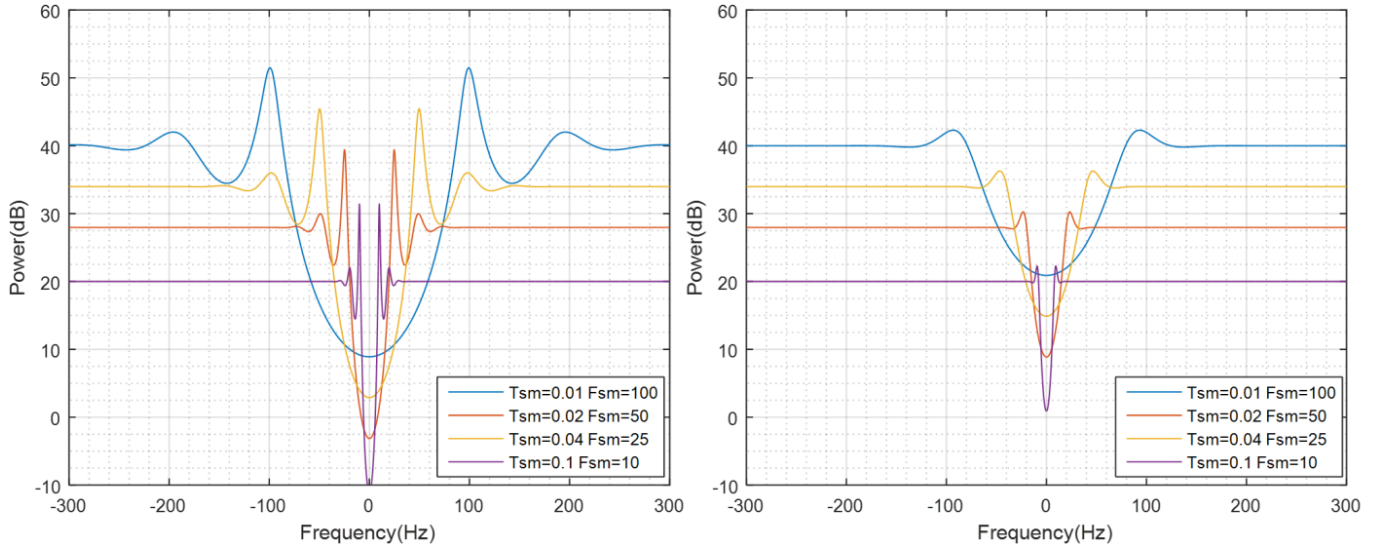


**Figure 2.11 The Spectrum  $\Phi_{xs}(f)$  for Different Values of  $T_{Sm}$  with  $\sigma=0.167T_{Sm}$ (left) and  $\sigma=0.333T_{Sm}$ (right)**

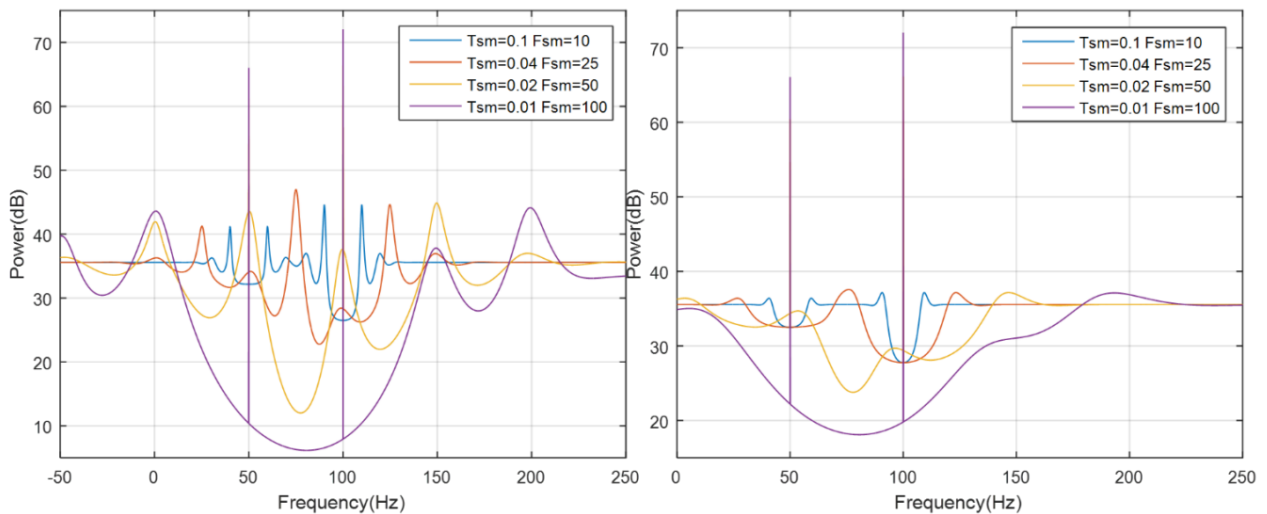


**Figure 2.12 The Noise Term Convoluting  $\Phi_x(f)$  for  $T_{Sm}=0.1$  with  $\sigma=0.167$ ,  $T_{Sm}$ (left) and  $\sigma=0.333T_{Sm}$ (right)**

### A.2.2) Recommendations for N

By applying the same example with the same methodology followed in the ARS with uniform distribution case, and referring to figure (2.13) the recommendation for N is expressed in (2.62).

$$N > g'.C.K \quad (2.62)$$

Where g' is 1.3 (2.3 in dB) in case of  $\sigma=0.333T_{Sm}$  and 3.7(11.4 in dB) in case of  $\sigma=0.167T_{Sm}$ , which make the latter case more demanding in number of points to be sampled.

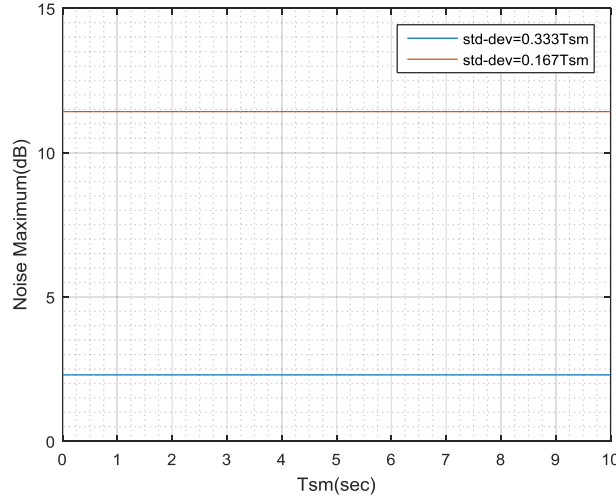


**Figure 2.13 The Maximum of N(f) in term of T<sub>Sm</sub> for  $\sigma=0.333$  and  $\sigma=167$**

### A.3) The Nature of Noise in ARS

After the study of each mode's PSD, it can be concluded that in both cases of ARS, with uniform and Gaussian distribution, the noise term origin is the function N(f) which is convoluting the spectrum  $\Phi_x$  in the second element of addition in  $\Phi_{xs}(f)$ . In order to identify the cause of the noise in the ARS mode, the origin of this term must be identified in the time domain by following the link between the PSD and the FT of the ARs mode. The main term responsible of the apparition of the noise is expressed in (2.63).

$$\hat{n}(f) = Re \left\{ \frac{1 + \varphi_\tau(f)}{1 - \varphi_\tau(f)} \right\} \quad (2.63)$$

In fact, this term is resulting from the FT of  $p_n(t)$  in the autocorrelation function in (2.40), which is equivalent to  $p_s(t)$  as defined in (2.64).

$$n(t) = \sum_{n=1}^{+\infty} p_n(t) = p_s(t) \quad (2.64)$$

As the second summation added for negative t is suggested for continuing the ARS sequence in time domain with the same distribution. As already mentioned in Chapter 1, that ARS sequences are always stationary without specifying the distribution having the sum  $p_s(t)$  tending towards  $1/T_{Sm}$ , thus:

$$\sum_{n=-\infty}^{-1} p_n(t) = \frac{1}{T_{Sm}} \quad (2.65)$$

So, the noise term in the time domain is expressed by (2.66).

$$N(t) = x(t) \left[ \delta(t) + \sum_{\substack{n=-\infty \\ n \neq 0}}^{+\infty} p_n(t) \right] \quad (2.66)$$

As the signal  $x(t)$  is independent from the sampling sequence distribution then the expectation of their product is equal to the product of expectations defined in (2.67).

$$E[N(t)] = E[x(0)] + E[x(t)] \times E \left[ \sum_{\substack{n=-\infty \\ n \neq 0}}^{+\infty} p_n(t) \right] = cte + E[x(t)] \times \frac{2}{T_{Sm}} \quad (2.67)$$

Thus, if  $x(t)$  is a periodic,  $N(t)$  within the ARS sampling process is cyclostationary of order 1.

## B) JRS mode

### B.1) PSD of JRS with Uniform Distribution

The CF of the uniform distribution in term of the interval limits  $[a,b]$  is defined by (2.68).

$$\varphi_{unif}(f) = \frac{e^{i2\pi fb} - e^{i2\pi fa}}{i2\pi f(b-a)} \quad (2.68)$$

In case of a zero mean random jitter ( $u_n$ ) the interval is  $[-a;a]$  so the CF becomes:

$$\varphi_{unif}(f) = \frac{e^{i2\pi fa} - e^{i2\pi f(-a)}}{i2\pi f(2a)} = \frac{\sin 2\pi fa}{2\pi fa} = \text{sinc}(2\pi fa) \quad (2.69)$$

By replacing the CF of the uniform distribution in the expression of the JRS PSD (2.53), the PSD of JRS with the uniform distribution becomes (2.70).

$$\Phi_{xs}(f) = \frac{1}{T_{Sm}} \left\{ \Phi_x(f) \otimes [1 - |\text{sinc}(2\pi fa)|^2] + \frac{1}{T_{Sm}} \sum_{n=-\infty}^{\infty} \left| \text{sinc} \left( \frac{2\pi an}{T_{Sm}} \right) \right|^2 \Phi_x \left( f - \frac{n}{T_{Sm}} \right) \right\} \quad (2.70)$$

The parameter  $a$  is usually chosen as a ratio of  $T_{Sm}$ :  $a=rT_{Sm}$ . Then, the module of the function sinc, which is modulating the impulse train that is causing aliases, can be expressed by (2.71).

$$\left| \text{sinc} \left( \frac{2\pi r T_{Sm} n}{T_{Sm}} \right) \right| = |\text{sinc}(2\pi r n)| \quad (2.71)$$

Knowing that the sinc function is null at all the multiple of  $\pi$ , in the expression of  $\Phi_{xs}(f)$ , the aliases are eliminated whenever  $r$  is equal to 1 or 1/2. But according to the temporal condition discussed in Chapter 1,  $r$  can't be greater than 1/2 (because  $\sigma/T_{Sm} < 0.2887$ ). Thus in JRS with the uniform distribution the random jitter should be defined in the interval  $[-T_{Sm}/2; +T_{Sm}/2]$  to guarantee an alias-free sampling.

Thus, the spectrum  $\Phi_{xs}(f)$  in case of the zero mean jitter can be expressed by (2.72).

$$\Phi_{xs}(f) = \frac{1}{T_{Sm}} \left\{ \Phi_x(f) \otimes \left[ 1 - \left| \text{sinc} \left( \frac{\pi f T_{Sm}}{2} \right) \right|^2 \right] + \frac{1}{T_{Sm}} \Phi_x(f) \right\} \quad (2.72)$$

Eventually, the spectrum of  $x(t)$  is recovered by the second term of the addition, while the first is considered as the added noise caused by the effect of RS. In fact, due to the elimination of aliases in this RS mode the Shannon-Nyquist condition on the sampling frequency can be ignored, though, the intention of eliminating the added noise will impose some restrictions on the mean sampling period and on the number of points to sample from the signal.

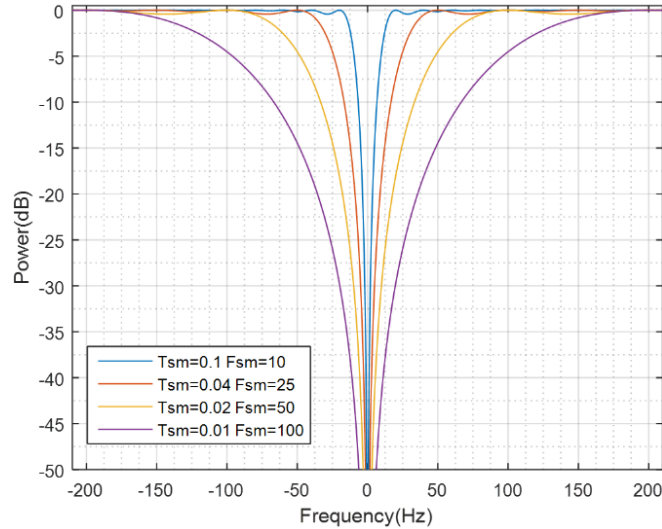
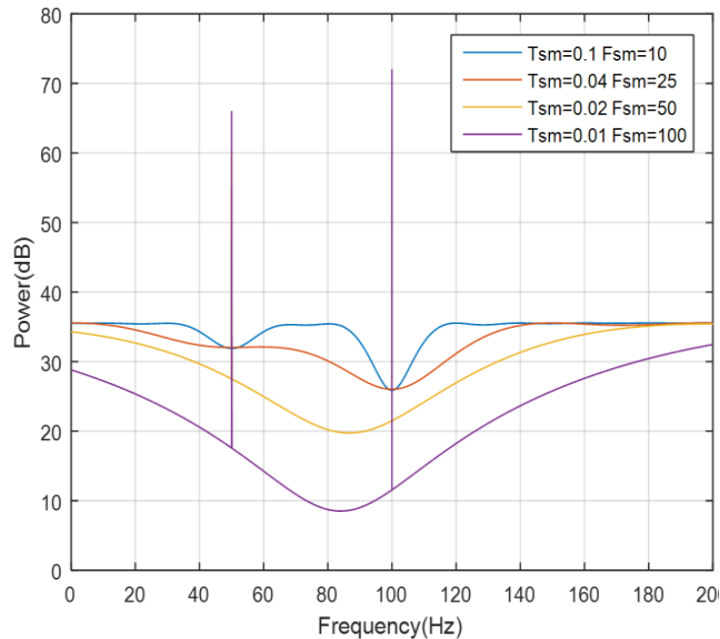


Figure 2.14 Noise term convoluting  $\Phi_x(f)$  with a cutting frequency  $1/T_{Sm}$

### B.1.1) Recommendations for $T_{Sm}$

The noise term  $N(f)$  is just the spectrum of  $x(t)$  convoluted with a function having a high pass filter form [50] with a cutting frequency equal to  $1/T_{Sm}$ . In Figure 2.14, the term  $N(f)$  is presented for different values of  $T_{Sm}$  to view its effect. The value of  $T_{Sm}$  imposes the cutting frequency of  $N(f)$  the high pass filter form function, and thus it determines the width of the gap created by this function at the frequency 0. To view the effect of this term on the whole spectrum the same example of  $x_{sin}(t)$  is taken ( $F_1=50\text{Hz}$  and  $F_2=100\text{Hz}$ ;  $A_1=20$  and  $A_2=40$ ). The spectrum  $\Phi_{xs}(f)$  is shown in Figure 2.16 for different values of  $T_{Sm}$ . Similarly, the noise in this case is the sum of  $N(f)$  repetitions located at the frequencies  $F_1$  and  $F_2$  of the signal  $x_{sin}(t)$ . In fact, the wider is the gap of  $N(f)$  at  $f=0$ , the more is the noise reduced around the signal impulses. Thus, the decreased values of  $T_{Sm}$  are appreciated. It can be deduced from this figure, that if  $F_{Sm}$  is equal or greater than the difference  $(F_2-F_1)$ , both gaps of the repeated  $N(f)$  will be joined in one wider gap, which will reduce the noise to the minimum between both impulses. This can be generalized for any spectrum having the highest frequency  $F_m$ , for the best noise reduction  $F_{Sm}$  must be equal or greater than  $F_{max}$ , which means  $T_{Sm} < T_m$ . In fact, as in previous cases, it is just a recommendation to reduce the noise resulting from JRS.



**Figure 2.15 The Spectrum  $\Phi_{xs}(f)$  of  $x_{sin}(t)$  in case of JRS with uniform distribution for different  $T_{Sm}$  Values**

### B.1.2) Recommendations for N

Proceeding with same methodology followed in the ARS case with both distribution, and taking the sampled signal is the analytical signal  $x_{sin}(t)$ , the maximum of the noise term after normalization

is deduced by (2.73) which is similar to the maximum of the noise in the ARS case with the only difference of replacing  $g$  by 1, as here in the JRS case,  $N(f)$  is with a maximum equal to unity.

$$\max(N(f) \otimes \Phi_x(f)) = \frac{\sum_{k=1}^K |A_k|^2}{NT_{Sm}^2} \quad (2.73)$$

$$N \geq C.K \quad (2.74)$$

In comparing the JRS with uniform distribution to the ARS case, both modes have the same recommendation for  $T_{Sm}$ , but for the number of points, ARS is more demanding due to the added noise.

### B.2) PSD of JRS with Gaussian Distribution

The CF of the Gaussian distribution with a mean  $\mu$  and variance  $\sigma^2$  is defined by (2.75).

$$\varphi_{gauss}(f) = e^{i2\pi f\mu} e^{-2\pi^2 f^2 \sigma^2} \quad (2.75)$$

In case of a random jitter, the mean  $\mu$  is equal to 0 so the CF becomes (2.76).

$$\varphi_{gauss}(f) = e^{-2\pi^2 f^2 \sigma^2} \quad (2.76)$$

Consequently the PSD of  $x_s(t)$  in JRS with the Gaussian distribution becomes (2.77).

$$\Phi_{xs}(f) = \frac{1}{T_{Sm}} \left\{ \Phi_x(f) \otimes [1 - |e^{-2\pi^2 f^2 \sigma^2}|^2] + \frac{1}{T_{Sm}} \sum_{n=-\infty}^{\infty} \left| e^{-2\pi^2 \frac{n^2}{T_{Sm}^2} \sigma^2} \right|^2 \Phi_x\left(f - \frac{n}{T_{Sm}}\right) \right\} \quad (2.77)$$

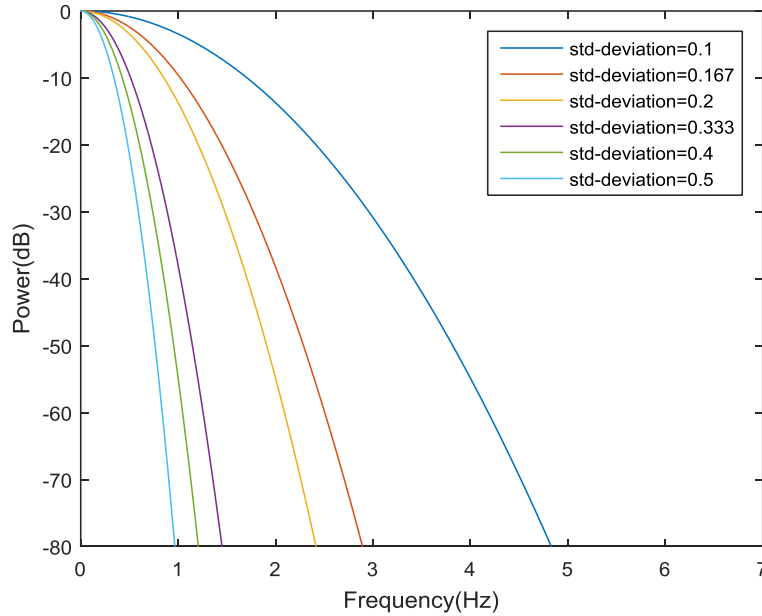


**Figure 2.16** Module of the CF of Gaussian distribution in JRS Mode with  $T_{Sm}=1$  for different  $\sigma$  values

According to the temporal condition for the zero mean jitter, the ratio  $\sigma/T_{Sm}$  can be at maximum equal to 0.167. Though, in Figure 2.16 the CF of the Gaussian distribution multiplying the periodic repetitions of  $\Phi_x(f)$  is plotted in term of the ratio  $\sigma/T_{Sm}$  varying from 0.1 to 0.5, where  $T_{Sm}$  is equal to 1. In fact, this function can reduce the aliases located at the multiple of  $1/T_{Sm}$  but for  $\sigma/T_{Sm} \geq 0.5$  the elimination is complete, this ratio value is nothing else than the minimum for having a stationary process in the sampling sequence. Though, this value is beyond the temporal condition in case of JRS with Gaussian distribution, which is a verification to the results already obtained in Chapter 1. In conclusion, the JRS with Gaussian distribution is not recommended for sampling with an anti-aliasing property as compared to JRS with uniform distribution which within predetermined conditions can radically delete the aliases.

### C) The Nature of Noise in JRS

After examining the spectrum of the randomly sampled signal by the JRS with both distributions, it can be deduced that the CF of the distribution is the responsible term of eliminating the aliases in the spectrum. Thus the alias-free property is related to the jitter distribution and its parameters. In fact, when the jitter does not verify the conditions needed for this property the CF function multiplying the repetitions of the spectrum  $\Phi_x$ , although it is not zero, but decreases their amplitudes similarly to the low-pass filtering effect. Hence, the essential term in the spectrum  $\Phi_{xs}(f)$  is the element of  $n=0$  in the second term of the summation in (2.53) which is the recovery of  $\Phi_x$ , all the remaining terms are considered as the added noise caused by the RS. In order to identify the origin of this noise, it is suggested to go back to the time domain definitions using the link between the PSD and the FT. The spectrum of  $S(t)$  expressed in (2.52) can be rewritten in (2.78).

$$\Phi_s(f) = \frac{1}{T_{Sm}} \left(1 - \Phi_p(f)\right) + \frac{1}{T_{Sm}} \sum_{n \neq 0}^{\infty} \Phi_p(f) e^{-i2\pi f n T} + \frac{1}{T_{Sm}} \Phi_p(f) \quad (2.78)$$

Where the last term is the term of recovering  $\Phi_x$ , then the autocorrelation function in (2.49) is rewritten in (2.79).

$$R_s(\tau) = \frac{1}{T_{Sm}} (\delta(\tau) - R_p(\tau)) + \frac{1}{T_{Sm}} \sum_{n \neq 0} R_p(\tau - nT_{Sm}) + \frac{1}{T_{Sm}} R_p(\tau) \quad (2.79)$$

Consequently, the noise in time domain is obtained by the multiplication of  $x(t)$  with the expression of  $S_n(t)$  deduced from  $R_s(\tau)$  without the term of recovering the spectrum of  $x(t)$ :

$$N(t) = x(t) \left[ \delta(t) - p_u(t) + \sum_{\substack{n=-\infty \\ n \neq 0}}^{+\infty} p_n(t - nT_{Sm}) \right] \quad (2.80)$$

As the signal  $x(t)$  is independent from the sampling sequence distribution then the expectation of their product is equal to the product of expectations as in (2.81).

$$E[N(t)] = E[x(0)] - E[x(t)] \times E[p_u(t)] + E[x(t)] \times E \left[ \sum_{\substack{n=-\infty \\ n \neq 0}}^{+\infty} p_n(t - nT_{Sm}) \right] \quad (2.81)$$

The expectations of  $x(0)$  and  $p_u(t)$  are constants, and the expectation of the last term in (2.80) is the sum  $p_s(t)$  of the PDF of the random instants  $\{t_n\}$  already defined in Chapter 1 in (1.9) which determines the SPP condition of the sampling sequence. Thus, if  $x(t)$  is a periodic signal, the aspect of  $N(t)$  is related to the stationarity of the JRS sampling process:

- If the process is stationary then the sum is constant and equal to  $1/T_{Sm}$ , the noise is then cyclostationary of order 1.
- If the process is not stationary, in the JRS case the sum will be periodic as figured in paragraph of Chapter 1, the noise is then cyclostationary of order 2. Which is verified by the Taylor expansion applied to the transfer function of the JRS sampling in [50].

In conclusion after reviewing the PSD of both modes with the different possible distributions the table 2.1 is concluded to be the guide in applying the RS and choosing the parameters ultimately.

Mode	Distribution	Anti-Aliasing?	Noise Aspect	Best Interval ( $\sigma/T_{Sm}$ )	$F_{Sm}$	N
JRS	Uniform	conditionally	CS.1/CS.2	$[-0.5 T_{Sm}; 0.5 T_{Sm}]$ (0.2887)	$>F_m$	$>C.K$
	Gaussian	no	CS.2	---	----	----
ARS	Uniform	yes	CS.1	$[0.5 T_{Sm}; 1.5 T_{Sm}]$ (0.2887)	$>F_m$	$>g.C.K$
	Gaussian	yes	CS.1	$[0; 2 T_{Sm}]$ (0.333)	$>F_m$	$>g'.C.K$

**Table 2.1 Summary on RS modes features and parameters selection**

Where  $g=1.5$  and  $g'=1.3$ .

In comparing the conditions of the different modes, it can be deduced that the JRS with uniform distribution is the less requiring mode in number of points. However, all the RS modes are able to apply sampling with low frequency rate and a considerably reduced number of points. Although  $F_{Sm}$  must be greater than  $F_m$  (which is half the condition of Nyquist), this condition is not considered to be crucial, it is a recommendation in order to reduce the noise that could be reduced by the mean of increasing the number of data, which is the classical compromise that is resolved according to the application constraints.

#### 2.3.4 Time Quantization Effect on RS PSD

The RS PSD already discussed and studied are expressed in continuous time domain. However, in practical applications the time is quantized and the PSD of the different modes of RS should be observed in discrete time domain to preview its performance in real implementations. Based on the PDF of the TQRS defined in (1.50) in Chapter 1, its corresponding CF is deduced by (2.82).

$$\varphi_q(f) = \sum_{k=0}^{m-1} \varphi\left(f - \frac{k}{\Delta}\right) \text{sinc}(\pi(f\Delta - k)) \quad (2.82)$$

Where  $\varphi(f)$  is the CF of the distribution of random variables (jitter or interval according to the mode on which the TQRS is applied). It is clear that discretization has introduced a periodicity to the sampling sequence, which will affect the spectrum of the sampled signal. The CF of the quantized interval  $\tau_q$  becomes periodic of  $1/\Delta$ , so is the PSD. In the interval  $[-1/(2\Delta); +1/(2\Delta)]$  no alias caused by the time quantization will occur[37]. For clarification, the impact of TQRS is examined by using its CF within the JRS and the ARS spectrums in next paragraphs.

##### A) PSD of TQARS

In order to simplify the representation of the TQARS, the PSD expression to be used is (2.53). By replacing the CF by the quantized CF the PSD of TQARS is deduced by (2.83).

$$\Phi_{xSARS}(f) = \frac{1}{T_{Sm}^2} \Phi_x(f) + \frac{1}{T_{Sm}} \Phi_x(f) \odot \text{Re} \left\{ \frac{1 + \sum_{k=0}^{q_T} \varphi_\tau\left(f - \frac{k}{\Delta}\right) \text{sinc}(\pi(f\Delta - k))}{1 - \sum_{k=0}^{q_T} \varphi_\tau\left(f - \frac{k}{\Delta}\right) \text{sinc}(\pi(f\Delta - k))} \right\} \quad (2.83)$$

In case of ARS with Uniform distribution  $\varphi_\tau\left(f - \frac{k}{\Delta}\right)$  is replaced by (2.84).

$$\varphi_{unif,q}(f) = e^{i2\pi T_{Sm}\left(f - \frac{k}{\Delta}\right)} \text{sinc}(2\pi r T_{Sm}\left(f - \frac{k}{\Delta}\right)) \quad (2.84)$$

As  $T_{Sm}=q_T\Delta$ , the spectrum of the TQARS with uniform distribution is defined by (2.85).

$$\begin{aligned}\Phi_{xSARS}(f) &= \frac{1}{T_{Sm}^2} \Phi_x(f) + \frac{1}{T_{Sm}} \Phi_x(f) \\ &\quad \circledast Re \left\{ \frac{1 + \sum_{k=0}^{q_T} e^{i2\pi(f\Delta-k)} \text{sinc}(2\pi r(f\Delta - k)) \text{sinc}(\pi(f\Delta - k))}{1 - \sum_{k=0}^{q_T} e^{i2\pi(f\Delta-k)} \text{sinc}(2\pi r(f\Delta - k)) \text{sinc}(\pi(f\Delta - k))} \right\}\end{aligned}\quad (2.85)$$

With the same methodology the spectrum of TQARS with Gaussian distribution is expressed by (2.86).

$$\begin{aligned}\Phi_{xSARS}(f) &= \frac{1}{T_{Sm}^2} \Phi_x(f) + \frac{1}{T_{Sm}} \Phi_x(f) \\ &\quad \circledast Re \left\{ \frac{1 + \sum_{k=0}^{q_T} e^{i2\pi(f\Delta-k)} e^{-2\pi^2\sigma^2(f-\frac{k}{\Delta})^2} \text{sinc}(\pi(f\Delta - k))}{1 - \sum_{k=0}^{q_T} e^{i2\pi(f\Delta-k)} e^{-2\pi^2\sigma^2(f-\frac{k}{\Delta})^2} \text{sinc}(\pi(f\Delta - k))} \right\}\end{aligned}\quad (2.86)$$

Although the impact of quantization affects only the noise term  $N(f)$ , the aliasing at the step of  $1/\Delta$  is applied on  $\Phi_x(f)$ , as  $N(f)$  is convoluted with the spectrum of the sampled signal. When  $\Delta$  is decreased the aliases are repeated at high frequencies and the terms multiplying the CF of the distributions tend towards 1 which will eliminate the effect of quantization. Further illustrations are given in next paragraph while examining the TQJRS case.

#### B) PSD of TQJRS

In the PSD of the JRS, the CF of the jitter  $\varphi_u$  is replaced by the CF of the TQRS  $\varphi_{u,q}$  to obtain (2.87).

$$\begin{aligned}\Phi_{x_sQJRS}(f) &= \frac{1}{T_{Sm}} \left\{ \Phi_x(f) \circledast \left[ 1 - |\varphi_{u,q}(f)|^2 \right] \right. \\ &\quad \left. + \frac{1}{T_{Sm}} \sum_{n=-\infty}^{\infty} \left| \varphi_{u,q}\left(\frac{n}{T_{Sm}}\right) \right|^2 \Phi_x\left(f - \frac{n}{T_{Sm}}\right) \right\} \\ &= \frac{1}{T_{Sm}} \left\{ \Phi_x(f) \circledast \left[ 1 - \left| \sum_{k=0}^{m-1} \varphi_u\left(f - \frac{k}{\Delta}\right) \text{sinc}(\pi(f\Delta - k)) \right|^2 \right] \right. \\ &\quad \left. + \frac{1}{T_{Sm}} \sum_{n=-\infty}^{\infty} \left| \sum_{k=0}^{m-1} \varphi_u\left(\frac{n}{q_T\Delta} - \frac{k}{\Delta}\right) \text{sinc}\left(\pi\left(\frac{n}{q_T} - k\right)\right) \right|^2 \Phi_x\left(f - \frac{n}{T_{Sm}}\right) \right\}\end{aligned}\quad (2.87)$$

In the term of sinc,  $T_{Sm}$  is replaced by  $q_T\Delta$ . It can be deduced that in the TQJRS mode the aliases are repeated at the multiples of two frequencies  $1/T_{Sm}$  and  $1/\Delta$ . Hence, the JRS with uniform distribution with the anti-aliasing property is the most recommended within TQJRS. The PSD of the JRS with a uniformly distributed jitter within the interval  $[-T_{Sm}/2; +T_{Sm}/2]$  after the quantization becomes (2.88).

$$\Phi_{xsQJRS}(f) = \frac{1}{T_{Sm}} \left\{ \Phi_x(f) \odot \left[ 1 - \left| \sum_{k=0}^{m-1} \text{sinc} \left( \frac{\pi T_{Sm}}{2} \left( f - \frac{k}{\Delta} \right) \right) \text{sinc}(\pi(f\Delta - k)) \right|^2 \right] + \frac{1}{T_{Sm}} \Phi_x(f) \right\} \quad (2.88)$$

$$\Phi_{xsQJRS}(f) = \frac{1}{T_{Sm}} \left\{ \Phi_x(f) \odot \left[ 1 - \left| \sum_{k=0}^{m-1} \text{sinc} \left( \frac{\pi q_T}{2} (f\Delta - k) \right) \text{sinc}(\pi(f\Delta - k)) \right|^2 \right] + \frac{1}{T_{Sm}} \Phi_x(f) \right\} \quad (2.89)$$

Obviously the term recovering the spectrum of  $x(t)$  is not affected, thus the study of the impact of TQRS is limited to the term of noise  $N(f)$  convoluting  $\Phi_x(f)$ . In figure (2.17) the function  $N(f)$  after quantization ( $N_q(f)$ ) is shown for  $T_{Sm}=10$  and  $q_T=10$  ( $\Delta=1$ ).

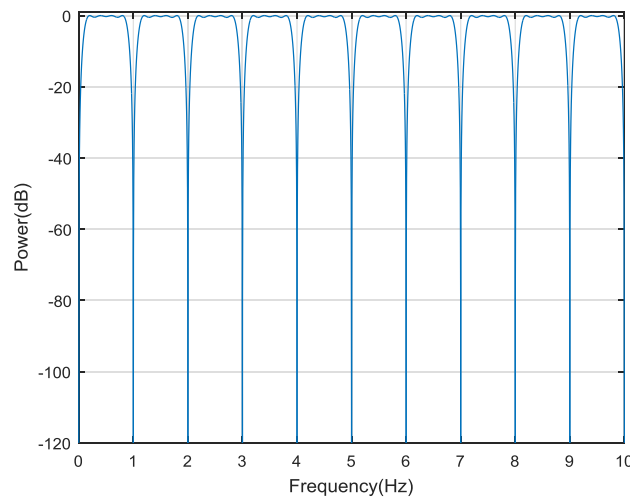


**Figure 2.17**  $N_q(f)$  in case of TQJRS with uniform distribution over the interval  $[0; 10 \Delta]$

Figure 2.17 shows the effect of aliasing produced by the quantization at the frequency  $1/\Delta$ , figure 2.18 presents the effect of the value of  $q_T$  on the shape of the term  $N(f)$ . It can be obviously seen how the increasing value of  $q_T$  decreases the modification of  $N(f)$ . Conforming the result of chapter 1, for  $q_T$  equal or higher than 8 the effect of quantization is easily neglected.

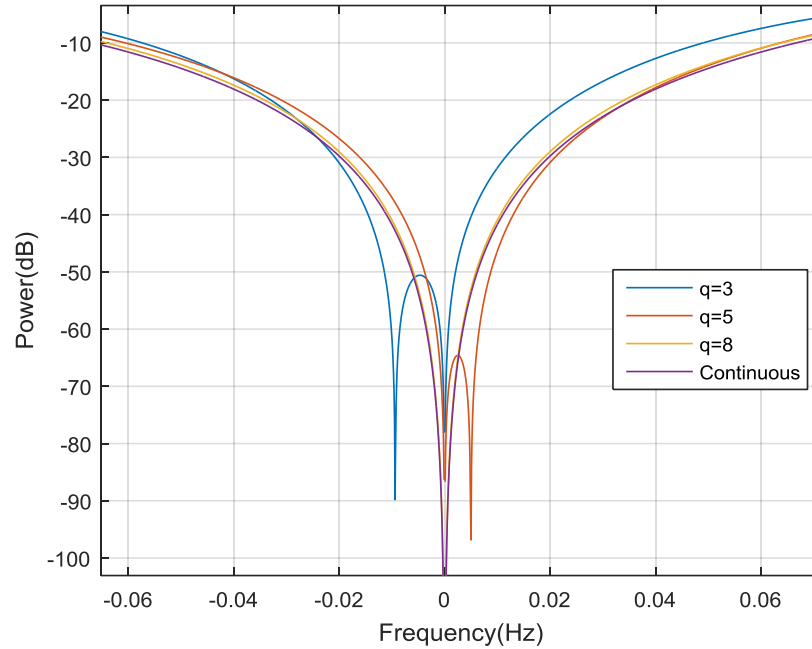


**Figure 2.18  $N_q(f)$  in Case of TQJRS with Uniform Distribution Over almost one Period  $\Delta$**

After exploring the PSD of RS within its different modes with different probability distributions, and revealing the impact of all the parameters included in such process, an overview on the variety of techniques used in the literature to analyze the randomly sampled data in the frequency domain is presented to conclude with the means that are compatible with the study in this thesis.

### 2.3.5 Spectral Analysis Techniques for Randomly Sampled Signals

#### A) Review

Spectral analysis methods are highly developed and frequently abound with new innovated techniques, though non-uniformly sampled data can't profit from this evolution due to the variable time step between successive samples. Thus, spectral analysis for NUS signals became the subject of many researches. In fact, a wide variety of techniques is found in the literature originally conceived from different domain of application. Some methods are directly deduced from the analysis used in uniform sampling, while others are introduced within the signal reconstruction phase as in CS and DASP.

In first place, Non-Parametric and Parametric methods, the main two categories of uniform sampling spectral analysis already defined in paragraph (2.2.2) of this chapter, are studied to be applied on NU sampled signals [20]. The major difference in calculating the DTFT and the Schuster periodogram is replacing the constant time-period  $nT_s$  by the random instants chosen for the sampling acquisition  $t_n$ .

The definitions in (2.14) and (2.15) are then modified to meet the NUS conditions by:

$$\hat{X}_{dr}(f) = \sum_{n=-\infty}^{+\infty} x_n e^{-i2\pi f t_n} \quad (2.90)$$

$$P_{rs}(f) = \frac{1}{N} \left[ \sum_{n=0}^{N-1} x_n e^{-i2\pi f t_n} \right]^2 \quad (2.91)$$

Dealing with numerical signals, obviously, the DTFT is replaced by the DFT. In non-uniform sampling, calculating the DFT at random instants is known as Point Rule NUT-DFT [67]. This method is enhanced by relying on linear interpolation between samples as in Trapezoidal method or on second order interpolation as in the Simpson method [68]. Similarly, the Lomb and Scargle (LS) periodogram and its modified version the Real-valued Iterative Adaptive Approach (RIAA) were introduced to improve the periodogram of Schutser [20]. Actually, between the two Non-parametric methods, only the periodogram was found to be applied in NUS, while the correlogram had never been proposed in such context. Besides, parametric methods conserve their concept as in uniform sampling, as they are applied in NUS after an exact signal reconstruction by using interpolation, slotted resampling or continuous time models [20].

In second place, as seen in Chapter 1, the CS was proposed in order to capture the signal in a compressed way by profiting of its sparse representation in, usually, the frequency domain. Hence, the reconstruction of the signal is accomplished by recovering its spectrum and then returning to time domain by the inverse FT. The spectrum recovery is done by either the Basis Pursuit or the Matching pursuit that rely respectively on  $l_1$  and  $l_2$  minimizations. In other application, as the DASP techniques, after the zero insertion, an iterative algorithm is executed in order to estimate all the signal components within a thresholding criteria [69] which is a similar approach of the CLEAN method based on deducing the signal spectrum from its ‘dirty’ version directly calculated by neglecting its non-uniform aspect [70].

Obviously, the majority of already cited methods counts on the signal reconstruction due to two essential reasons. According to the introduction of Chapter 1, NU sampled data results from loss or unavailability in many applications, thus the spectral analysis techniques were conceived as a

way for resolving such issue, which makes the signal reconstruction a crucial phase. In addition, in domains where the RS or CS are not imposed, the final acquired or compressed signal must meet human perceptions such as images, videos and sounds. Consequently, the spectral representation cannot be the final result, the signal exact recovery is vital. However, these conditions are not confronted in this thesis, as the RS is intentionally proposed and the spectral estimation is a contenting result to be processed for machinery diagnostic. Therefore, non-parametric methods are the best matching techniques for spectral analysis within the scope of this thesis.

#### A) Lomb and Scargle

According to the literature one of the most promising spectral analysis is the LS periodogram and its variants. In fact, this method was first introduced by Lomb and Scargle [71][72], where the technique is to detect the presence of periods in unequally sampled time series data and their significance is measured to level of significance calculated by the False Alarm Probability and the error is minimized by the least square fitting [73]. This method was enhanced and optimized to be easily developed within MATLAB [74] and then it becomes a built in function named “Plomb” in MATLAB 2015. Briefly, the LS method is based on finding an estimation of the signal periodogram in term of the periodic functions sinus and cosine, the first step is then to find a time delay  $\tau_{LS}$  at which the pair of sinusoids would be mutually orthogonal at samples times  $t_u$  [75]:

$$\tan 2\pi f \tau_{LS} = \frac{\sum_u \sin 2\pi f t_u}{\sum_u \cos 2\pi f t_u} \quad (2.92)$$

And thus the periodogram at the frequency  $f$  is estimated by (2.93).

$$P_{LS}(f) = \frac{1}{2} \left( \frac{[\sum_u x_u \cos 2\pi f (t_u - \tau_{LS})]^2}{\sum_u \cos^2 2\pi f (t_u - \tau_{LS})} + \frac{[\sum_u x_u \sin 2\pi f (t_u - \tau_{LS})]^2}{\sum_u \sin^2 2\pi f (t_u - \tau_{LS})} \right) \quad (2.93)$$

Similarly to periodograms in uniform sampling, the LS periodogram suffers from both local and global leakage problems or as already called smearing and leakage. Local leakage is due to the width of the main lobe of the spectral window, and it is what limits the resolution capability of the periodogram. Global leakage is due to the side lobes of the spectral window, and is what causes spurious peaks to occur (which leads to “false alarms”) and small peaks to drown in the leakage from large peaks (which leads to “misses”). Thus it is recommended to increase the number of samples and choose the frequencies, at which the periodogram is calculated, with high resolution. Besides, the authors of [20] went on to introduce a new enhanced method for spectral analysis of non-uniformly sampled data sequences called RIAA. The new method can be interpreted as an iteratively weighted LS that makes use of a data-dependent weighting matrix built from the most recent spectral estimate. Actually, this method was used and successfully applied on simulated

signals, but when applied on real signals acquired randomly, the results were not satisfying, because of the initial weights given at the first iteration must be suggested by the user, and should be adapted to the signal of interest. Thus in the majority of cases, the algorithm diverged and couldn't reach the best estimation. For more details regarding RIAA, the original paper and some applications are found in [76], [77].

#### B) Zero Insertion & Peridogram of Welch

In fact, as considered the basic method to transform the signal from time to frequency domain, the DFT in shape of the Schuster periodogram is used in the simulation phase to evaluate the RS effect on sampled signals as a first step of study. But, as the number of samples must be increased to enhance the quality of acquisition, the calculation cost becomes a real matter as the complexity of the algorithm is  $O(N^2)$ . Hence, in practical acquisitions the LS periodogram is preferred on the Schuster as its algorithm developed within MATLAB (Plomb) is of lower computational cost  $O(N \log N)$  [78]. However, the existence of noise in real signals rises the probability of occurrence of leakage problem in LS and increasing the number of samples may not be a sufficient solution. In [36], [37] fast practical ways are proposed to calculate the spectrum of randomly sampled signals based on the use of the FFT, where in signal, skipped samples are replaced by zeros (zero insertion) at the smallest time step  $\Delta$  and calculate then the FFT is calculated with taking the sampling frequency equal to  $1/\Delta$ . In [36] the noise introduced by the zero insertion is minimized by averaging, while in [37] the spectrum is enhanced by the least square fitting. Before adopting such methodology, it was a must to explore the effect of the zero insertion on the randomly sampled signal by proposing an expression that demonstrates the apparition of noise when inserting zeros to the signal. In (2.94) the signal  $x(t)$  is expressed after applying TQRS and the zero insertion.

$$x_{sqz}(t) = x(t) \sum_{n_r} \delta(t - n_r \Delta) + \sum_m \delta(t - m\Delta) \times \left[ 1 - \sum_m \delta(t - m\Delta) \right] \quad (2.94)$$

The first term of the addition is simply the randomly sampled signal after quantization,  $n_r$  represents the random number multiplying  $\Delta$  to obtain a random instant of sampling, while the second term is the model of inserting zeros at the constant time step  $\Delta$  in the resulting signal [79]. The expression in (2.94) is general, in real applications, the signal is sampled during a limited period of time  $T$  which will lead to a limited number of samples  $N$ , (2.95) is then deduced, it should be mentioned that  $M=T/\Delta$  the number of samples as if the sampling was uniform with a constant period=  $\Delta$ .

$$x_{sqz}(t) = x(t) \sum_{n_r=0}^{N-1} \delta(t - n_r \Delta) + \sum_{m=0}^{M-1} \delta(t - m\Delta) \times \left[ \text{Rect}(t) - \sum_{m=0}^{M-1} \delta(t - m\Delta) \right] \quad (2.95)$$

Where  $\text{Rect}(t)$  is defined by (2.96).

$$Rect(t) = \begin{cases} 1 & 0 \leq t \leq T \\ 0 & otherwise \end{cases} \quad (2.96)$$

To explore the effect on the spectrum of the sampled signal, the FT is applied on (2.95) to obtain (2.97). The FT of the TQRS signal is not detailed in this part in the aim of exploring the added part caused by the insertion of zeros.

$$\begin{aligned} \hat{X}_{sqz}(f) = & \hat{X}_{RSq}(f) \\ & + \frac{1}{\Delta} \sum_{m=0}^{M-1} \delta\left(f - \frac{m}{\Delta}\right) \otimes \left[ T \text{sinc}(\pi f T) - \frac{1}{\Delta} \sum_{m=0}^{M-1} \delta\left(f - \frac{m}{\Delta}\right) \right] \end{aligned} \quad (2.97)$$

According to section 1.4.4 in chapter 1 because of the effect of quantization, the observation of the spectrum is usually limited to the interval  $[0; 1/\Delta]$ ; Hence within this interval the expression of  $\hat{X}_{sqz}(f)$  is limited to  $m=0$  which is expressed by (2.98).

$$\hat{X}_{sqz}(f) = \hat{X}_{RSq}(f) + \frac{T}{\Delta} \text{sinc}(\pi f T) - \frac{1}{\Delta^2} \delta(f) \quad (2.98)$$

Therefore, to reduce the effect of the function sinc resulting from the rectangular interval where the insertion of zero is applied, a proposition is suggested of adding zeros at the end of the signal known as zero-padding, in order to increase  $T$  (which becomes  $T_z$  after zero padding) and thus decrease  $1/T$  to  $1/T_z$  which makes the function reduced to a narrow peak at  $f=0$ . Finally, it can be deduced that the noise added by the zero-insertion operation is additive and can be reduced by the zero padding extension.

By consequence, the application of zero insertion provides the possibility of profiting from the spectral analysis techniques of uniform sampling, as the time step between the resulting signal points becomes constant. Thus, in the aim of enhancing the spectrum by reducing its variance, the leakage problem and the effect of noise added by the quantization and the zero insertion, the chosen method to estimate the spectrum of the randomly sampled signal is the Periodogram of Welch.

As a result, inspired by the method performed by [36], [37], an enhanced method is conceived within this thesis by applying the zero insertion on the randomly sampled signal and then the spectrum estimation is accomplished by the Welch method.

## 2.1 Conclusion

In this chapter, after reviewing the basic parts of US study, with a similar methodology, a detailed review on the RS is presented in order to clarify all the important details that should be known on this distinct sampling process. After presenting the FT of the different mode of RS, the PSD is deduced and studied in details to conclude with some recommended limitations that help the user

to obtain the best results of RS. Recommendations on the selection of the sampling frequency and the number of points are offered to reduce the noise added by the RS to the minimum. This noise is proved to be cyclostationary of order 1 or 2 according to the mode of sampling. Although the JRS with Gaussian distribution was proven to be not recommended due to the unverified SPP, in this chapter the PSD of this mode confirmed this fact. As in the practical application the time is quantized, the effect of quantization is shown to explain how the quantization step must be chosen without defecting the results. At the end, a brief review on the spectral analysis methods used within NUS to explore the unevenly sampled signals in the frequency domain, and thus deducing the most convenient procedure to reveal the spectrum of RS signals within the context of this thesis. In first place, the DFT is used for analyzing simulation data as it is considered the basic spectral study, then due to high complexity, it is replaced by the LS and the Welch periodogram which is preceded by a step of zero insertion in order to fill gaps between random samples.

## 3 Chapter 3: Simulation and Hardware Implementation

### 3.1 Introduction

The main purpose of this Chapter is to verify, by simulation, the results already obtained in previous chapters in order to have a clear procedure to follow when any user attempts to apply RS in his application. Then, a brief study on the possibilities of RS hardware implementations is presented in order to introduce the simple application done on signals acquired from function generator. Many questions can be asked on the methodology of choosing parameters that define the RS process: the mode, the distribution, the mean sampling period, the standard deviation and the number of points. Although their significance is simple to understand, their value selection is not obvious as they have direct impact on the resulting signal as already seen. Hence, few examples will be shown to observe the direct influence of different parameters on the signal spectrum. To have more generalized conclusions, a simulation on the modes of RS is driven on a simulated signal with multiple frequencies with varying parameters values and figuring the results in few curves to have more clarified illustration. The outcomes are then verified in a simple practical study on signals from a function generator before applying RS on vibration signals within its different modes.

As this section is the transitional phase from theoretical studies to application and real implementation, the first issue to clarify is the impact of quantization introduced by  $\Delta$ . Second, after defining the procedure of conceiving the RS process, some examples of simple sinusoidal signals that are randomly sampled with particular modes of RS are shown. This is used to prove that the apparition of noise is caused only by the application of RS, and to evaluate the impact of  $T_{sm}$  and  $N$  on the shape of the spectrum. Third, an explanation of the simulation driven is presented, to deduce the most important criteria in the RS modes: ARS and JRS with different distributions: uniform and Gaussian. The results are calculated by the DFT as already mentioned in Chapter 2. However, in real applications, the DFT is replaced by the LS periodogram and the Welch periodogram which is applied on the randomly sampled signal after the zero insertion step. Thus, a simple evidence is shown to prove the zero insertion reduced effect on the spectrum of the sampled signal with a brief review on the selection of parameters used in the Welch periodogram. After the recapitulation on all the results obtained by the simulation study, the transition to the hardware implementation is summarized by, first, a review on the already applied methods of RS in the literature, second, an explanation of the chosen technique to perform RS in practice and third, the results of the first application of RS on simple signals acquired from function generator.

### 3.2 Impact of Time Step Quantization $\Delta$

As already discussed in Chapter 2, the time quantization affects the randomly sampled signals in two ways: the shape of the noise term  $N(f)$  and the aliasing at the frequency  $1/\Delta$ . Though, according to the relations (1.54) and (1.57) in Chapter 1 and to figure 2.18 in Chapter 2, it was concluded that for a value of  $q_T=8$ , the ratio  $\sigma/T_{Sm}$  reaches its maximum and the shape of  $N(f)$  is totally recovered. Hence, a simple example is done by simulation of a sine wave having two frequencies: 100 and 150 Hz to prove the limitation introduced by  $\Delta$  in having alias in randomly sampled signals. Similarly to uniform sampling, where the spectrum is repeated at each multiple of the sampling frequency, the spectrum of the signal in quantized or discrete RS is repeated every  $1/\Delta$ . In the bottom of Figure 3.1, as the frequencies of the signal are 100 and 150 Hz, and the quantization step is 0.003 ( $1/\Delta=333.3\text{Hz}$ ), the repetitions of 100Hz are at 433.3Hz ( $333.3+100$ ) and at 766.7 Hz ( $2*333.3+100$ ) and the repetitions of 150Hz are at 483.3Hz ( $333.3+150$ ) and at 816.7 Hz ( $2*333.3+150$ ). The other aliases are the opposite frequency (negative frequencies of the sine) of the replicas relative to the reference, for example, 233.3Hz is the opposite of 433.3Hz relative to 333.3 ( $=1/\Delta$ ):  $233.3=-100+333.3$ . Thus, the whole replied spectrum is found within the interval  $[-1/(2\Delta);+1/(2\Delta)]$  that is centered at  $1/\Delta$ , which means  $[1/(2\Delta);3/(2\Delta)]=[166.7;500]$ . The same concept is shown for  $\Delta=0.006$  with the only difference that distance between replicas is shorter.

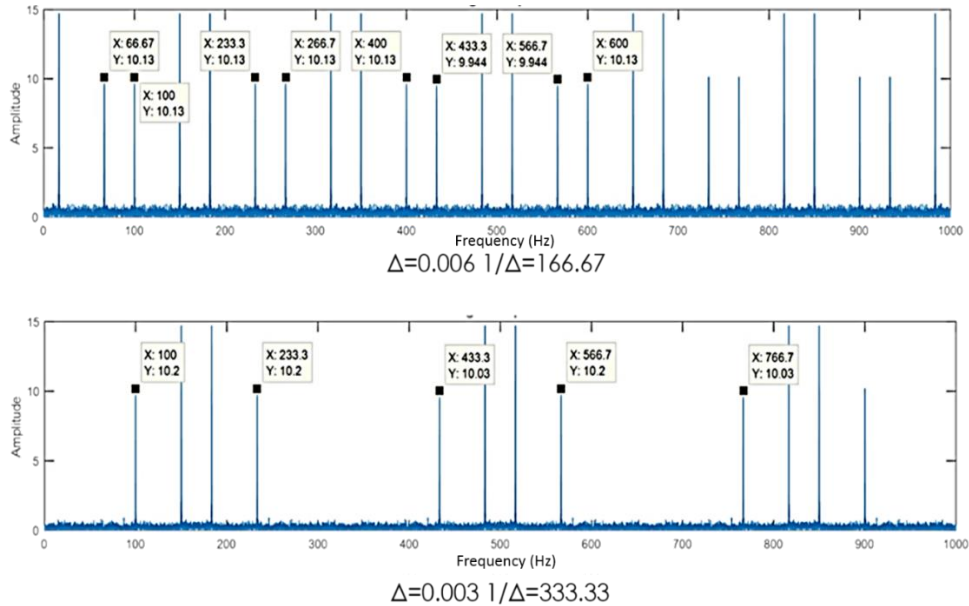


**Figure 3.1 Two Simulations of a Signal (100 Hz and 150 Hz) with a Quantization Step = 0.006 at the Top and Step=0.003 at the Bottom**

According to Figure 3.1 and the previous discussions on the value of  $q_T$ , small values of  $\Delta$  compared to  $T_{Sm}$  are recommended in order to eliminate the replicas from the signal spectrum. For instance,

when  $T_{sm}$  is equal to 0.1s,  $\Delta$  is recommended to be 12.5ms. In the following sections, a very low value of  $\Delta$  is picked to reduce the effect of quantization and focus on the impact of RS on the resulting signals.

### 3.3 Procedure of RS and Simulation of Simple Examples

The process of choosing the parameters of the RS is based on the mode, the distribution and its parameters and the number of points. In case of the uniform distribution, the limits of the interval of support [a;b] must be defined; whereas in case of the Gaussian distribution, the mean and the standard deviation must be declared. Thus, according to the mode chosen, the parameters of the distributions are deduced according to the relations (1.28) to (1.30) for the ARS mode and (1.41) to (1.43) for the JRS mode. In fact, these conditions are essential to verify the temporal limitation that is crucial for real implementations. Also, the stationarity condition is recalled for both modes ARS and JRS in paragraphs 1.4.1 and 1.4.2. For ARS, it was recommended to choose the highest ratio  $\sigma/T_{sm}$  allowed by the temporal condition to have a small delay of stationarity. As for JRS with uniform distribution, it was imposed to choose the highest ratio  $\sigma/T_{sm}$  to have the stationarity verified, while with Gaussian distribution the stationarity is reached beyond the temporal condition. In Chapter 2, these conditions are verified in the study of RS impact by analyzing the PSD of each mode in section 2.3.3. From these conditions and analysis, concise relations between the parameters of the probability distribution and limitations of RS can be concluded. To simplify and unify the notations for both distributions and modes, the relations are expressed in terms of the Deviation D and the ratio R already defined in (1.56) in Chapter 1.

In ARS with Uniform distribution the best conditions are proven for:

$$R = \frac{D}{T_{sm}} = \frac{b - a}{T_{sm}} = 1 \quad (3.1)$$

In ARS with Gaussian distribution, the best conditions are met for  $\sigma/T_{sm}=0.333$  and 0.167 which corresponds to  $R=2$  and 1. In JRS with Uniform distribution, the best performance is reached for  $R=1$ , and for Gaussian distribution the elimination of aliases may be reached for  $R=2$ . Consequently, in order to validate these conditions, it is easier for the user to configure the parameters of the distribution in terms of R and  $T_{sm}$ . For the ARS with uniform distribution:

$$a = T_{sm} \left(1 - \frac{R}{2}\right) \text{ and } b = T_{sm} \left(1 + \frac{R}{2}\right) \quad (3.2)$$

With Gaussian distribution: the mean  $\mu = T_{sm}$  and  $\sigma = R \cdot T_{sm}/6$ . In the JRS case with uniform distribution:

$$b = -a = R \cdot \frac{T_{Sm}}{2} \quad (3.3)$$

And for Gaussian distribution: mean  $\mu=0$  and  $\sigma=R \cdot T_{Sm}/6$ .

Therefore, due to these relations, the parameters of the probability distribution can be directly deduced whenever the features of the RS process are conceived. Besides, the generation of the time vector is determined according to the RS mode. The time vector in ARS mode is produced by adding the random variables generated within the selected distribution. While in the JRS mode, the generated random jitter is added to the constant clock of period  $T_{Sm}$ .

In order to verify the conclusions conducted from the discussion on the RS impact in section 2.3.3 of chapter 2, a simple sinusoidal signal, composed of two sines at the frequencies  $F_1=1000$  Hz and  $F_2=1100$ Hz, with respective amplitudes  $A_1=10$  and  $A_2=5$ , is used. The signal is taken without any noise addition to view the impact on RS clearly. In Figure 3.2, the PSD of the sampled signal by the ARS mode with the Gaussian distribution is presented. The number of samples  $N$  is 39, the sampling period is 0.1s and the standard deviation is taken equal to  $T_{Sm}/6$ . As the original signal is simulated without any noise addition, it can be obviously seen that the additive noise floor was added by RS. However, as the used sampling process is the ARS with Gaussian distribution, which verifies the anti-aliasing property, it can be directly confirmed that the spectrum of the resulting signal is empty of aliases. Thus, it can be also deduced that this added noise is cyclo-stationary of order 1. According to the recommendations delivered in section (2.3.3), the value of  $T_{Sm}$  should be, in this example, lower than 0.0009s ( $=1/1100$ Hz). The example in Figure 3.3 for  $T_{Sm}=0.01$ s is shown to verify the shape around the impulses similar the PSD shown in Figure 2.13 of Chapter 2. The peaks that appear around the signal's impulse result from shape of the noise term of the PSD the sampled signal. While in Figure 3.4, the reduction of noise reaches its maximum due to the mean sampling period value that is greater than the difference between the signal impulses and near to the lowest period of the signal  $T_m=1/F_m$ .

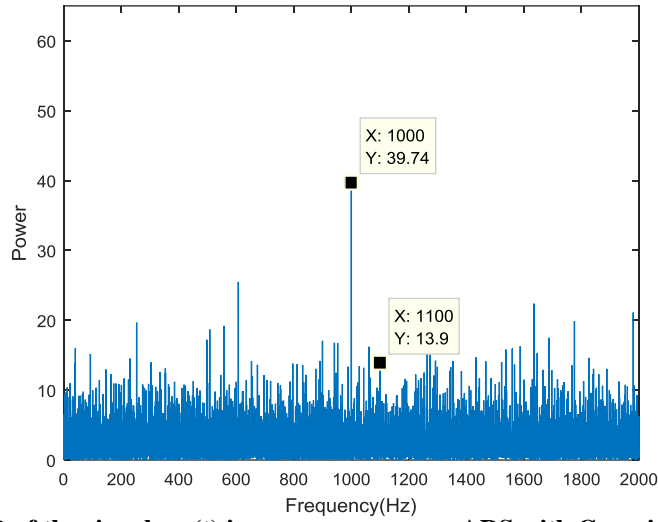


**Figure 3.2 The PSD of the signal  $x_{sin}(t)$  in ARS with Gaussian for  $N=39$   $T_{Sm}=0.1s$  and  $R=1$**

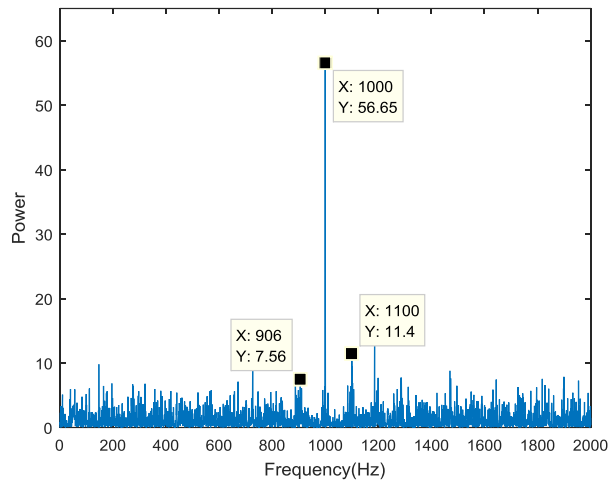


**Figure 3.3 The PSD of the signal  $x_{sin}(t)$  in ARS with Gaussian for  $N=39$   $T_{Sm}=0.01s$  and  $R=1$**

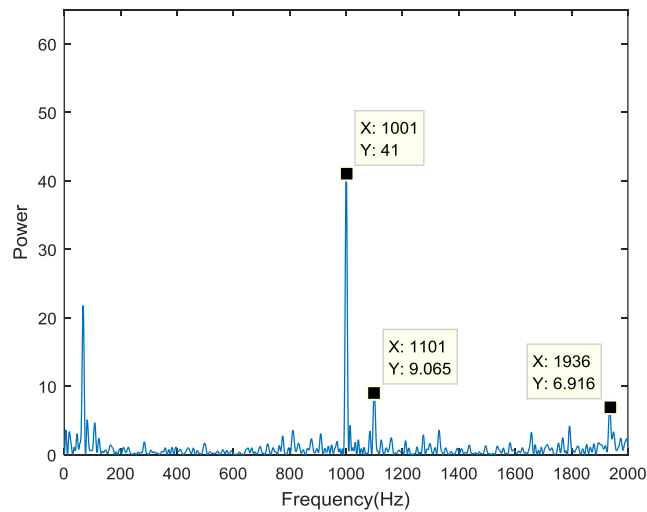


**Figure 3.4 The PSD of the signal  $X_{sin}(t)$  in ARS with Gaussian for  $N=100$   $T_{Sm}=0.001s$  and  $R=1$**

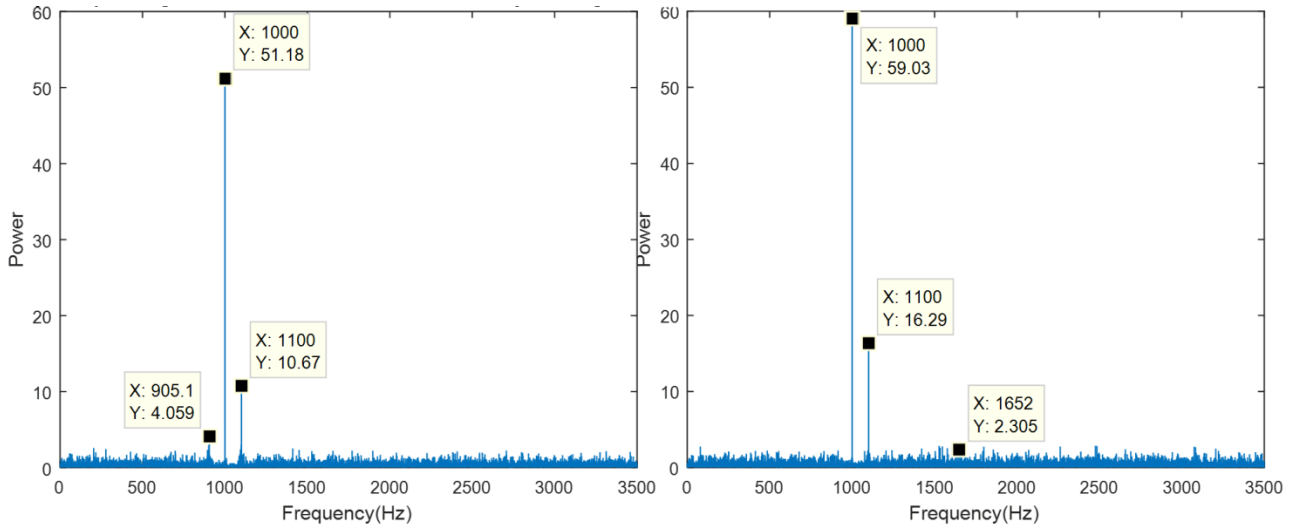


**Figure 3.5 The PSD of the signal  $x_{\sin}(t)$  with ARS mode and Gaussian distribution:  $N=390$   $T_{Sm}=0.01s$  with  $R=1$  (left) and  $R=2$ (right)**

In Figure 3.5, the number of samples is increased to 390. According to paragraph 2.3.3, when the mode of RS is ARS with Gaussian distribution with  $R=2$ , the constant  $g'$  is equal to 1.3. As the amplitudes are 10 and 5, their sum is considered as  $3 \cdot A_{\min}$ ; thus, to have the ratio between the maximum of noise and the minimum amplitude in the signal equal to 10, the number of points must be greater than 390. A comparison between cases of  $R=1$  and  $R=2$  verifies that the case of  $R=1$  requires a higher number of samples as  $g'$  in this case is equal to 3.7.

### 3.4 Simulation Study of RS

The purpose of this study is to evaluate the RS and explore its impact on a sampled noisy signal to consequently learn how to choose the sampling parameters in real applications. As the main objective of this thesis is to apply the RS on vibration signals, which is usually represented in the frequency domain by multiple peaks and their harmonics, the proposed signal model to be simulated is a sine wave having 4 frequencies with different amplitude for each. A zero mean Gaussian noise, or white noise, 'wn' is added to the signal having a variance equal to 5, the resulting expression is (3.4).

$$S = 10 \cdot \sin(2\pi \cdot 1000 \cdot t) + 3 \cdot \sin(2\pi \cdot 1100 \cdot t) + 5 \cdot \sin(2\pi \cdot 1500 \cdot t) + 7 \cdot \sin(2\pi \cdot 1510 \cdot t) + w_n \quad (3.4)$$

The time vector for sampling is generated by two methods: ARS and JRS. The intervals in ARS are random variables that follow a uniform distribution in the first case, and a Gaussian distribution in the second case. JRS is studied mainly with the uniform distribution. It is as well briefly studied with the Gaussian distribution to prove the presence of aliasing in such RS process. After determining the mode and the distribution with its parameters, the number of samples N or the length of the sampled signal must be determined. Multiple signal lengths are tested to analyze the effect of the samples' number on the resulted randomly sampled signal. In Table 3.1 all the tested values of  $T_{Sm}$ , R and N are shown. To have a clear view of the impact of each parameter, for every value of  $T_{Sm}$ , the ratio R and the number of samples are changed from their minimum to their maximum.

$T_{Sm}(\text{sec})$	0.002		0.005			0.0067			0.01		0.02		0.05		0.1		0.01			
N(pts)	25		50			80			100		150		200		400		800			
R	0.1	0.2	0.3	0.4	0.5	0.6	0.7	0.8	0.9	1	1.1	1.2	1.3	1.4	1.5	1.6	1.7	1.8	1.9	2

**Table 3.1 Different simulated values of  $T_{Sm}$ , N and R**

To have the ability of comparing the different modes and different distributions, the same values of these parameters are repeated in every case: ARS with uniform, ARS with Gaussian and JRS with Uniform. The JRS with Gaussian distribution is evaluated for identifying the possibility of having an anti-aliasing property. In fact, in the ARS mode the interval of support for all distributions may be taken with  $R=2$  and less due to the corresponding temporal condition. While the JRS is limited for  $R=1$  because of the same condition. However, in this part of study the ratio R is taken from 0.1 to 2 to all modes of RS with all distributions, as it is just a simulation without real implementation, to prove the anti-aliasing property and to choose the best value of R to be used in practice. The time quantization step is taken equal to 5 microseconds to focus on the influence of RS. To evaluate the sampled signals, each case of RS (same mode, same distribution and same parameters) is generated 50 times. Each time, the DFT of the signal is calculated and squared to obtain the periodogram of the generated signal, and then, the average of all the periodograms of the 50 signals is taken to represent the case studied (the mode, the distribution and the chosen parameters) and thus analyzed to explore the results.

### 3.4.1 Impact of R

First, to observe the anti-aliasing property of RS, the Amplitude/Alias (A/A) ratio is examined with the variation of the ratio R. This A/A ratio observation is proposed in all the researches that discuss the RS process [35][36]. In fact, R measures the “randomness” of the sampling process; so, this

analysis is done to study the effect of randomness on the anti-aliasing property. For both ARS and JRS with Uniform Distribution, the interval of support is changed to have a different R. The test is repeated for all frequencies, and in each case, same results are obtained. The case of mean frequency of 10Hz is presented. Since the number of points can have an influence on the results, the most significant cases of N are shown. In Figures 3.6 to 3.9, the variation of A/A ratio in term of R is shown for all tested N in all RS modes: ARS and JRS with uniform and Gaussian distribution.

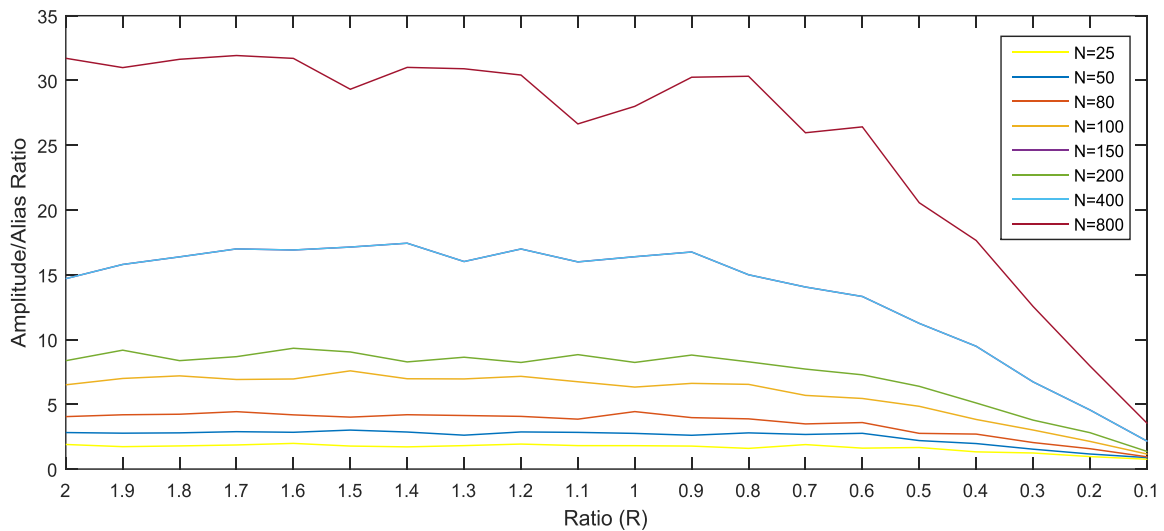


**Figure 3.6 Amplitude/Alias variation in term of R in ARS+ Uniform**

To have a satisfying anti-aliasing property, the A/A ratio must be higher enough than 1. In Figure 3.6, it can be seen how the A/A ratio decreases when R is decreased and how the number of points increases the A/A ratio but cannot avoid the impact of R diminution. However, in this mode (ARS with Uniform distribution), a value of R that is greater than 0.4 can provide a satisfying anti-aliasing property. This means that the length of the interval of the random variable must be higher than 40% the mean sampling period.

Same conclusions concerning the impact of R and number of points on the A/A ratio can be said on the ARS with Gaussian distribution according to figure 3.7. However in this case, to have a good anti-aliasing, the ratio R must be greater than 0.7, which is a limitation for such sampling mode concerning the anti-aliasing property. In fact the most suitable value of R in this case is 1 as it is already deduced in chapter 2 that ARS with Gaussian distribution is less requiring in number of samples.

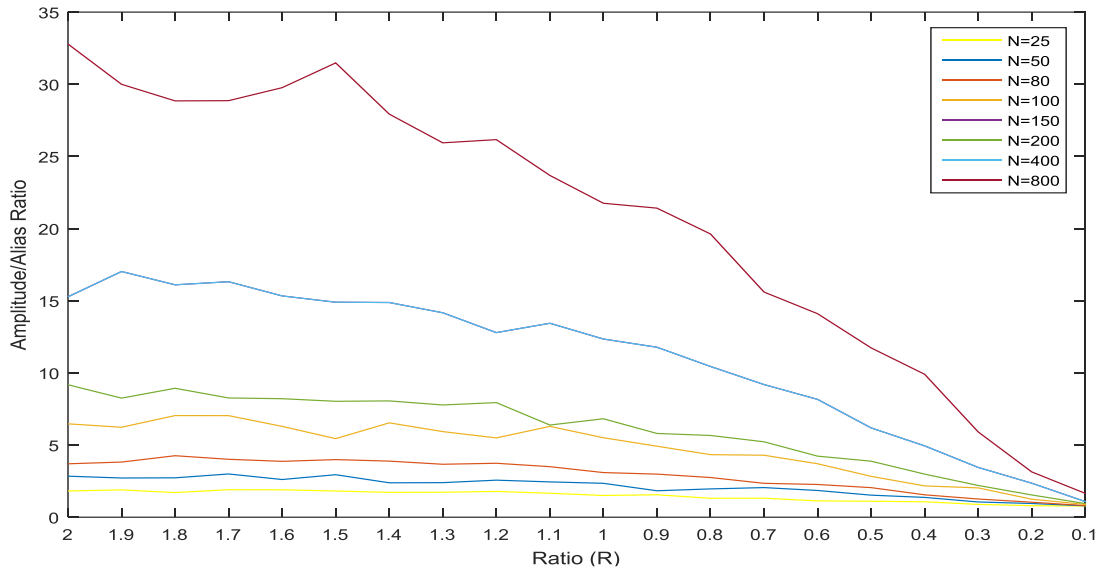


**Figure 3.7 Amplitude/Alias variation in term of R in ARS +Gaussian**

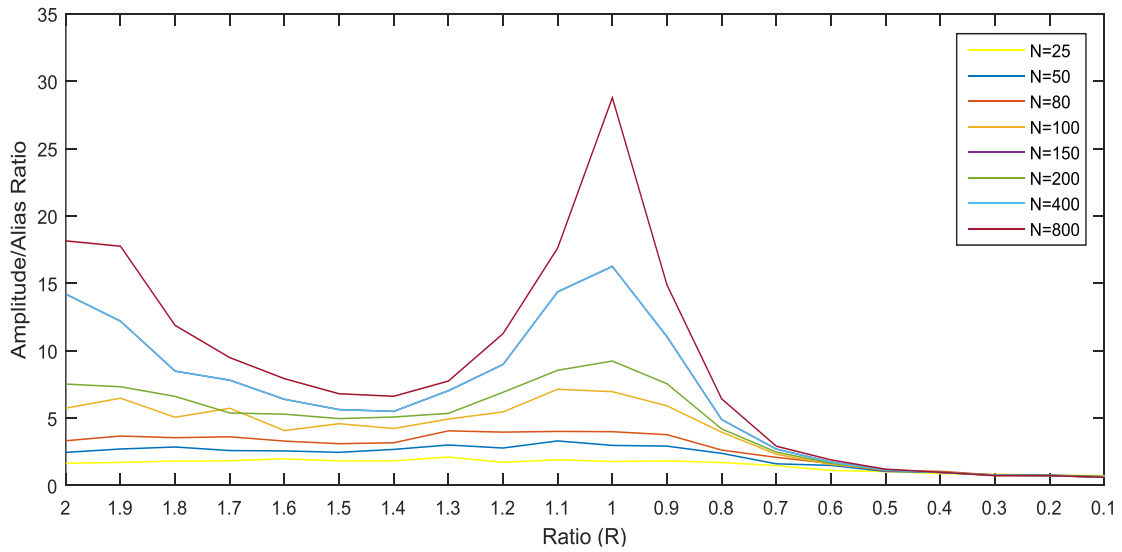


**Figure 3.8 Amplitude/Alias variation in term of R variation in JRS+uniform**

In case of JRS with uniform distribution, it is quite obvious how this mode is verifying the anti-aliasing property exactly at the ratio  $R=1$ , which is so compatible with the SPP condition verified for  $R=1$  and with the PSD of this mode which is free of aliasing in the same case. Other values of  $R$  as 0.9 and 1.1 are somehow acceptable, though only 0.9 can be implemented in real applications.

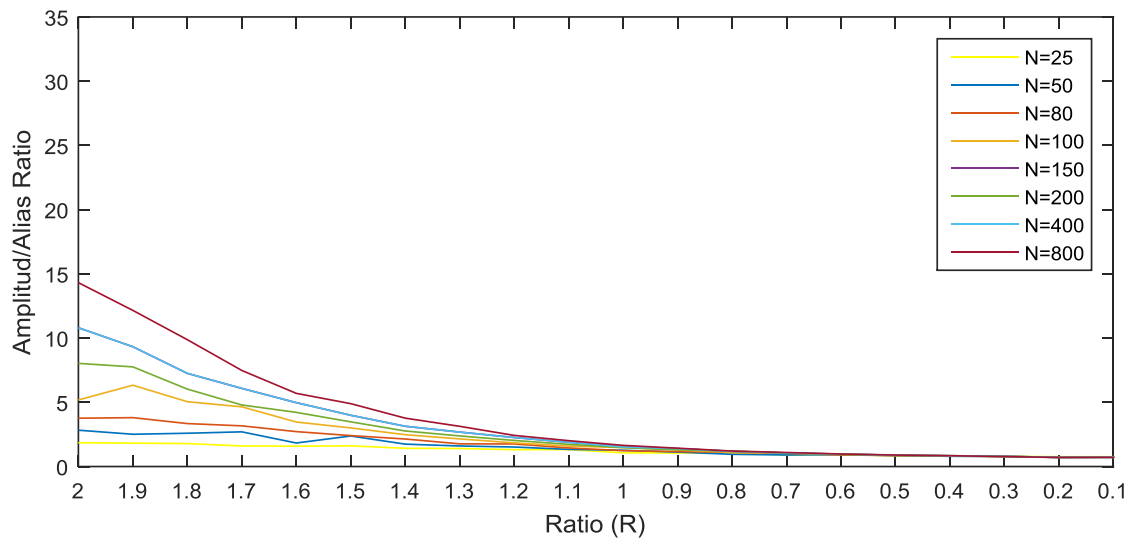


**Figure 3.9 Amplitude/Alias variation in term of R variation in JRS+Gaussian**

Finally, compared to other modes, the JRS with Gaussian distribution is the most prone to aliasing the best cases in anti-aliasing are far beyond the temporal condition, which is considered the clearest evidence to eliminate this mode from considerations of using RS for anti-aliasing feature.

In conclusion, the ARS with uniform distribution is approved to be the most competent mode of RS for its ability of anti-aliasing within multiple values of R. However ARS with Gaussian and JRS with uniform verify also this feature with less possibilities. In fact, although the ARS mode validates the temporal condition for  $R=2$ , the real implementation of random time interval with such ratio is not trivial, as some generated values may be too small ( $\sim 0$ ) and the acquisition at such small time steps is too demanding and difficult to apply in real-time processing which is highly contradicting with the final goal of this thesis. Thus, in the remaining part of this study, R is mostly taken near to 1 as it is the most convenient value for all modes of RS.

### 3.4.2 Impact of N

After the examination of the anti-aliasing property in term of the variation of R, the objective of this section is to observe the impact of RS on the ability to separate the sampled signal from the noise. In fact, the noise in the randomly sampled signal is not only the additive part 'wn' that is added in (3.4). Another part is introduced by the RS process, as discussed in Chapter 2, with a cyclo-stationary aspect as the sampled signal is periodic.

In Figures 3.10 to 3.12, the value of the smallest amplitude is compared to the highest value of the noise in order to examine how much the noise is eliminable in each case of anti-aliasing RS: ARS

with Uniform distribution, ARS with Gaussian distribution and JRS with Uniform distribution, and explore the impact of varying the mean sampling frequency (or period) and the number of samples taken. This comparison between the amplitudes is deduced from the definition of the Spurious Free Dynamic Range (SFDR) that measures the difference between the amplitude of the original signal and the noise caused by the mode of sampling [80]. In each figure, the color of the plot represents the result for a specified frequency. For the same frequency, two lines are drawn: the continuous line represents the value of the smallest amplitude of the signal and the dashed line represents the highest value of noise.

These curves (continuous and dashed) show the variation of corresponding amplitudes with the variation of the number of samples in the signal. In fact, the simulation is done for all of the already mentioned mean sampling periods (or frequencies) but only the most significant results are shown, for mean frequency equal to 500 Hz, 200Hz, 150 Hz and 50 Hz. The ratio R in these tests is fixed and is equal to 1.

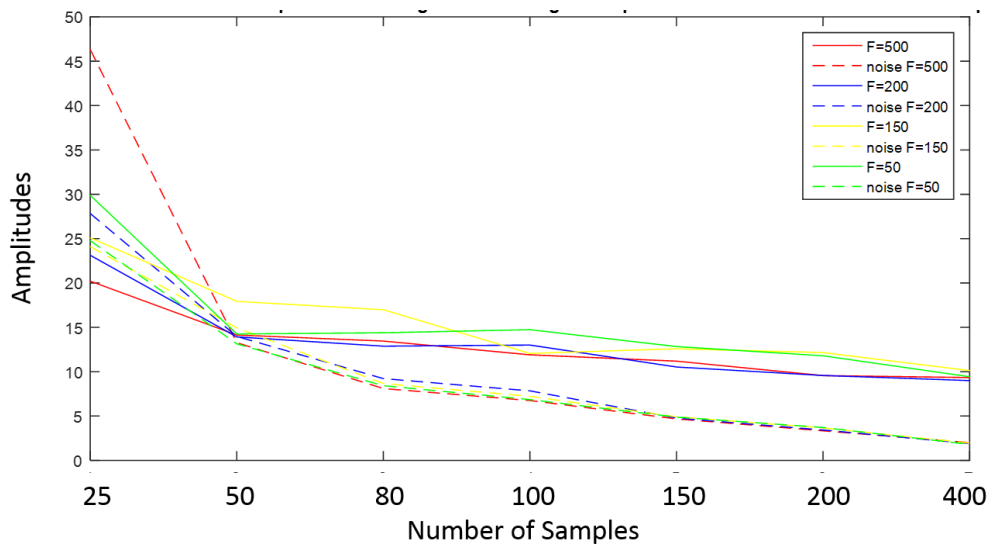


**Figure 3.10 Comparison of the smallest amplitude of the signal to the noise in ARS with uniform distribution**

It can be obviously seen that, in ARS with Uniform, the signal is easily distinguished from noise for a number of samples greater than 50 for all the mean frequencies. The smallest amplitude of the signal is perfectly reconstructed and way greater than the noise for a mean frequency of sampling that equals 50 Hz, a value that is much smaller than the Nyquist frequency. In fact, when going back to the recommendation given for N in the PSD analysis of this mode with the same distribution, it can be concluded that N must be greater than  $1.3 \cdot C \cdot K$ . Considering that the highest amplitude in the noise must be 10 times lower than the minimal amplitude of the signal, and by expressing the amplitudes of the peaks of the signal in term of the smallest amplitude, K is assumed

to be equal to 8, and the number of samples  $N$  must be greater than  $1.3 \cdot 10^8 = 104$ . By observing the curves in Figure 3.10, this relation is clearly satisfied.

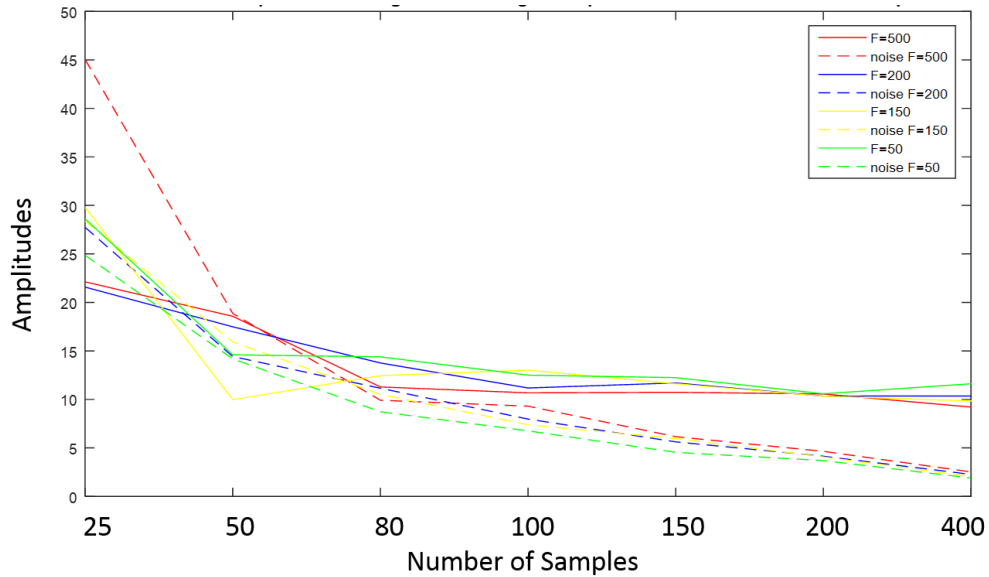


**Figure 3.11 Comparison of the smallest amplitude of the signal to the noise in ARS with Gaussian distribution**

In ARS with Gaussian distribution, the signal can be easily separated from noise for a number of points greater than 100. Also in this mode, the mean sampling frequency can be way smaller than Nyquist rate but with a limitation on number of samples that should be greater than 100. As the comparison is done between the different modes of RS for  $R=1$ , this limitation on the number of points is caused by the constant  $g'$  which is equal to 3.7 for  $R=1$  in ARS with Gaussian. Similarly to the ARS with uniform case, the limitation on the number of points in this mode with this distribution is given by:  $g' \cdot C \cdot K = 3.7 \cdot 10^8 = 296$ . Thus for  $N$  greater than 296, the ratio between the smallest amplitude of the signal and the highest amplitude of noise must be 10, which is obviously verified in Figure 3.11.

In JRS with the uniform distribution, in Figure 3.12, if each signal amplitude (continuous line) is examined with its corresponding noise maximum (dashed line having same color), it can be deduced that for a number of points equal or greater than 50, the signal is easily separated from the noise. As for other cases, the number of samples, when increased, enhances the signal and reduces the noise to its minimum, for low and high mean sampling frequencies. The recommendation for  $N$  already mentioned in Chapter 2 is easily verified in Figure 3.12 as  $N$  must be greater than  $C \cdot K = 10^8$  for the same considerations taken in previous cases.

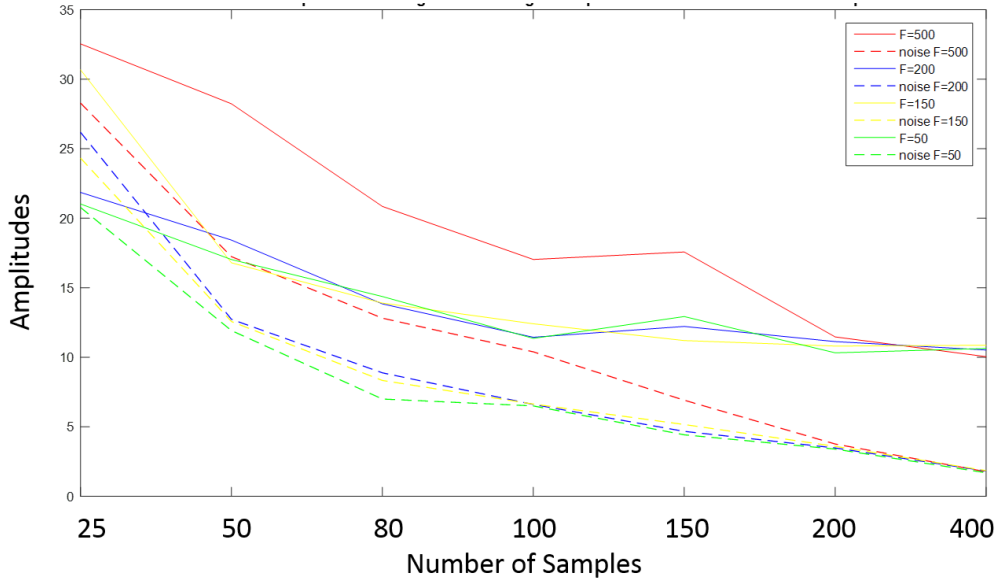


**Figure 3.12 Comparison of the Smallest Amplitude of the Signal to the Noise in JRS with Uniform Distribution**

Finally, it can be concluded from the comparison of these three ways of RS that the number of samples increases the performance and the low frequency can be easily used. However, for  $R=1$ , the ARS with Gaussian distribution is advantageous for a number of points greater than in ARS and JRS with uniform distribution which is verified by the higher value of  $g'$  ( $=3.7$ ) in this case. So, for cases where there is no limitation on data storage, the ARS with Gaussian distribution can be used for  $R=1$ . In addition, the results of JRS and ARS with uniform distribution confirms the recommendations already declared in Chapter 2, which can give a clear guide for the user on choosing the length of the signal when applying the RS on sparse signals with a good estimation of the number of sparse components.

After the verification of all the results already obtained in Chapter 1 and 2 concerning the different aspect of RS affected by the selection of its different parameters, hardware implementations can be conducted to validate and verify these conclusions in real applications. As the DFT used in the spectral analysis of RS signals in simulation, is of high complexity and consumes long durations in execution, the LS and Welch periodograms were proposed as convenient solutions for the spectral study of real signals acquired with RS, as they perform with reduced complexity and run within short period of time. The LS can be applied directly on raw RS signals, it simply requires the sampled data, the time vector containing the instants of sampling and the high limit frequency for the resulting spectrum. While the Welch periodogram must be preceded with a stage of zero insertion between random samples at each time step  $\Delta$ . A simple proof on the impact of zero

insertion on the signal spectrum is presented, then a brief explanation on choosing the Welch periodogram parameters to enhance its performance and reduce noise.

### 3.5 Zero Insertion Impact

According to the last section of Chapter 2, the effect of zero insertion in the randomly sampled signal adds some noise that can be reduced by extending the signal with Zero Padding, and by averaging the signal to reduce the noise variance. In order to verify the reduced impact of zero insertion with zero padding, a simple example is taken by randomly sampling the same signal used in the previous simulation by an ARS with uniform distribution process. At first, the DFT is calculated for both cases: randomly sampled signal with and without zero insertion. The resulting spectral representation is presented in figure 3.13. Both DFT are very similar, though the amplitude of the DFT is reduced due to the added zeros to the signal. In order to verify the similarities of both spectrums, the correlation is calculated for the PSD of both signals which are presented in figure 3.14. The high correlation between both PSD indicates that the impact of zero insertion can be handled and reduced by the application of zero padding and the averaging by the periodogram of Welch. Thus, the selection of the corresponding parameters is of high importance in increasing its performance by reducing noise and remediating leakage problems that may occurs in LS.

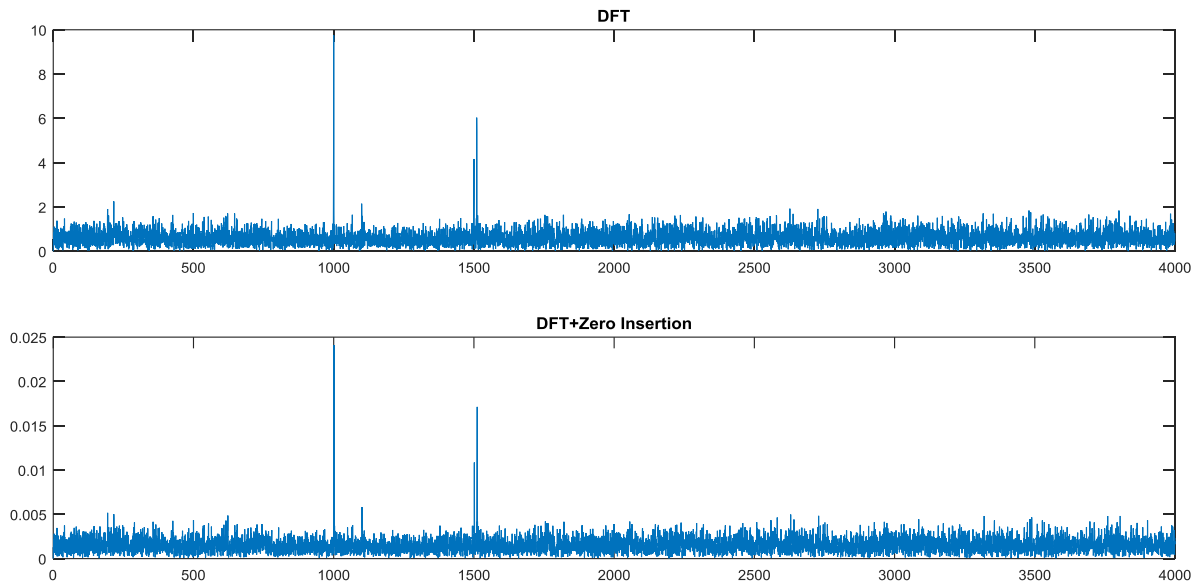


**Figure 3.13 DFT of the RS signal before and after zero insertion**

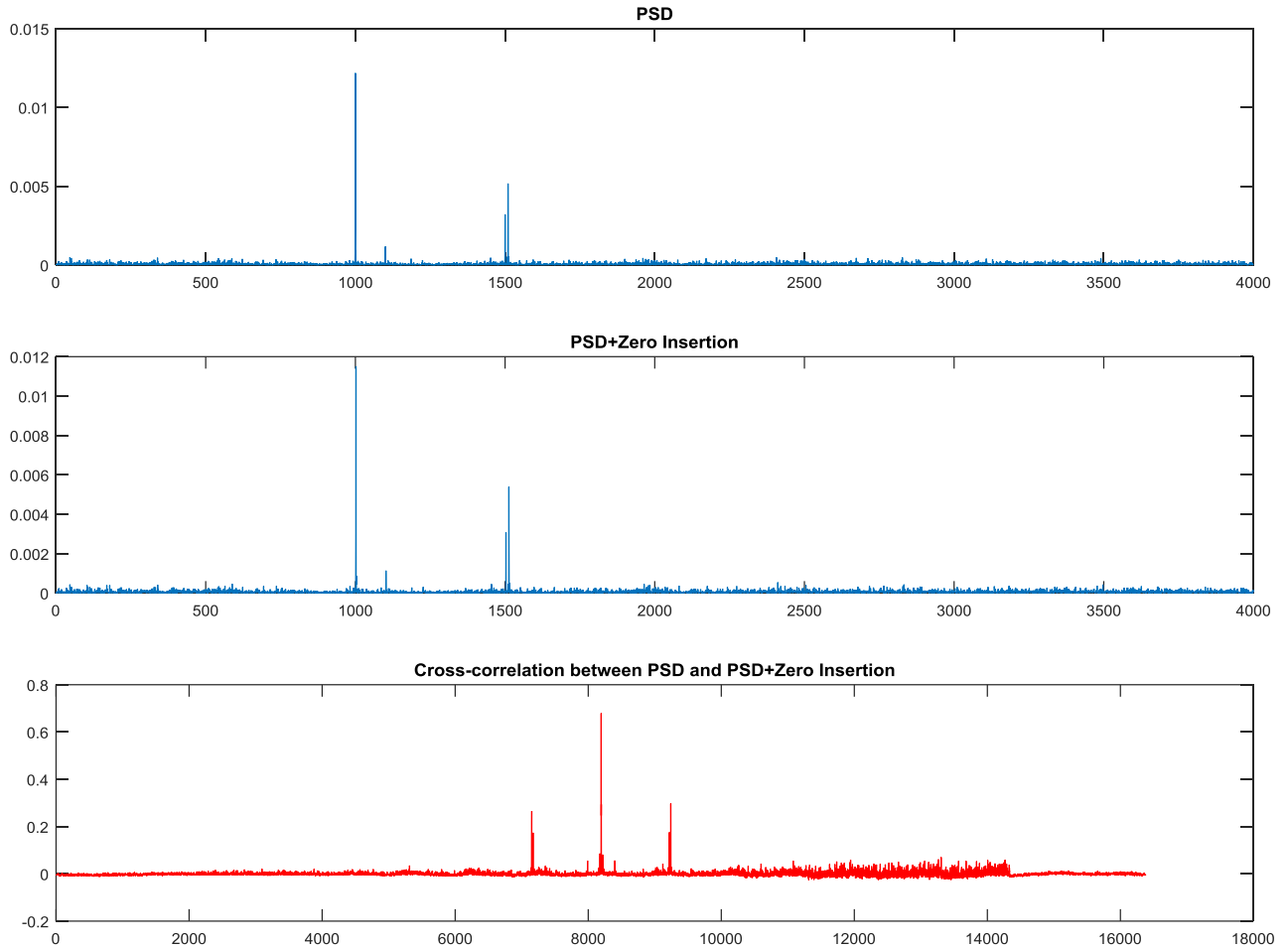


**Figure 3.14 PSD of the signal before and after zero insertion and the correlation between both PSD**

### 3.5.1 Selection of Welch Parameters

As already mentioned in chapter 2, the enhancement of the spectrum estimation by Welch is done by averaging, where finer resolution requires longer data segments and thus fewer number of segments. In addition, the percentage of overlapping determines the final number of segments obtained from the original signal, where a higher percentage of overlapping increases the number of segments and, after averaging, it reduces the error variance of the PSD final resolution. Thus the selection of the length of segments, the overlapping percentage and the type of apodization window is of high impact on the resulting periodogram. As the aim of using the Welch method is to reduce the noise added by the Zero insertion to the spectrum of the randomly sampled signal, in this section, the methodology in choosing the parameters in this estimation to accomplish such role is clarified.

Examples of used windows for apodization within Welch periodogram estimation are shown in Figure 3.15. More than a dozen of windows are proposed in the literature to be used for the signal segmentation within Welch periodogram estimation. The width of the main lobe, the height of sides lobes and the maximum amplitude error are the main criteria on which the selection of the window is based [57], [81]. The main lobe bandwidth is generally chosen according to the spectrum aspect of the signal of interest. Due to the width of the window in the frequency domain, each frequency bin collects its corresponding noise with adjacent bin noise, though, the effective noise bandwidth is corrected by dividing the result within averaging. Thus, for applications where the spectrum analysis is based on peaks detection and avoiding smeared peaks is required, selective windows are recommended for their narrow main lobes. The height of side lobes is obviously preferred to be reduced, according to [81] the reduction of side lobes level increases the bandwidth for a specific chosen window. Therefore, a compromise must be found between both criteria in the selection of the window and its parameters.

The maximum amplitude error  $e_{\max}$ , which is the maximal amplitude of the window function reached at  $f=0$ , expresses the maximal error in the amplitude estimation of a sinusoidal signal. Flat-Top windows are thus proposed for having low  $e_{\max}$ , but at the expense of wider bandwidth. Such windows are preferable if the amplitude of the signal must be estimated from the results. In [64] a study was made on the different types of windows by exploring their bandwidths and side lobes level,  $e_{\max}$  and other criteria as the Side Lobe Drop Rate and the Normalized Equivalent Noise Bandwidth to conclude with Kaiser and Flat-Top windows as good compromising choices. From figure 2.5 it can be deduced that Kaiser and Flat-top windows are preferred for having the low side lobes levels, however, the Flat-top is advantageous in having the lowest level and a minimum  $e_{\max}$  while the Kaiser is chosen for its narrow bandwidth.

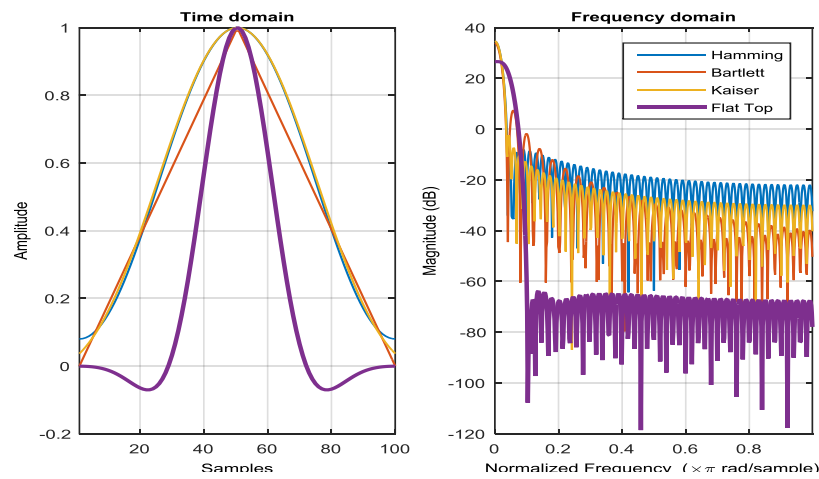


**Figure 3.15 Apodization windows in time and frequency domains**

The maximum of chosen overlapping is usually less than 75% due to two main reasons: the first one is the calculation cost, since more overlap means more calculation, the second is the fact that averaging reduces the error variance when averaged samples are considered uncorrelated, when the overlapping is higher than 75% the samples are essentially the same and thus averaging cannot reduce error variance anymore[82].

Due to the simulation study, all the features of the RS are examined and tested by the variation of all of its parameters. After the effect of  $\Delta$  is shown, a guide on the procedure to choose the different parameters of RS then, simple examples are driven to show the direct impact of the RS on the PSD of the randomly sampled signal. These examples verified the recommendations on  $T_{Sm}$  and  $N$  already given in Chapter 2 within the discussion on the RS impact. Further results are obtained by an extended simulation of RS on signals composed of multiple sines. The main conclusions of this simulation are perfectly compatible with the results of first and second chapters concerning the anti-aliasing properties of each mode, the reduced sampling frequency and the limitations on the number of points  $N$ . More verification and validations are to be shown in the next Chapter where a hardware implementation is developed on Arduino with experimentation on vibration signals.

In this chapter, the study of the hardware implementation of RS began with the review of some already applied methods for acquiring data at a non-constant rate used in CS architectures. Thus, a deduced technique is implemented on Arduino to evaluate the RS on simple signals at first place, then on vibration signal in second step.

## 3.6 Hardware Implementation

After reviewing the different features of RS in theory and simulation, an experimentation is conceived to apply the RS on real signals. In first place, a brief review on the already tested RS implementations is presented. Then, the proposed system to execute a random acquisition within this thesis is presented. Simple acquisitions are tested at the beginning in order to explore the process and enhance the performance. In the aim of conducting an experimentation on the random acquisition of vibration signals, a brief summary on the aspect of such signals is presented. A description of the practical application is presented followed by the results with a detailed analysis and study.

### 3.6.1 Review

Although, CS and RS had witnessed an increased interest recently with a high demand for fast, efficient and in-expensive signal processing algorithms, applications and devices, hardware implementation of both sampling process remains a subject of research and doesn't exist in the

market yet [15]. Thus one of the goals of this thesis is to find an adequate way for implementing the RS and apply it on vibration signal of rotating machines in a context of monitoring and fault detection. As a first step of research, few ways of CS implementation were overviewed in order to deduce the most convenient method that meets with the intention of this thesis. As the CS is used in different domains, multiple techniques of implementation were proposed in the literature: Random Demodulator and its variants, Random Sampling Slope ADC and the Non-Uniform Sampler. A brief summary on the concepts of these methods is presented to conclude with the method used in the application accomplished within this work.

#### A) Random Demodulator and Its Variants

One of the first random acquisitions applied within CS architectures, the Random Demodulator was first introduced in 2006 to test the new sampling design in communication application. The concept is based on a first stage demodulator whose input signal  $x(t)$  is multiplied by a continuous time sequence of pseudo-random numbers  $P_c(t)$  to obtain a continuous time demodulated signal  $z(t)$ . Starting with a sequence of pseudo random numbers that take values of +1 and -1 with an equal probability, it is used to create a continuous chipping sequence. This (ideal) demodulation signal takes values of +1 and -1 over each time frame and switches between the levels randomly at or faster than the Nyquist rate of the input signal  $x(t)$ . The final stage is a standard ADC to sample the signal at a low rate. A low-pass filter is used prior to ADC to prevent aliasing. In fact, the purpose of the demodulation is to spread the frequency content of the signal so that it is not destroyed by the second stage of the system. And, the chipping sequence must alternate between values at or faster than the Nyquist frequency of the input signal. In order to decrease the coherence in the sensing matrix within the CS implementation, many variants were proposed as the Random Demodulator Pre-Integrator and the Spread Spectrum Random Modulator Pre-Integrator to decrease the coherence and the sampling rate of the sampling ADC by acquiring data via multiple parallel channels [80][83]. However, this architecture is complex and not easily implemented and requires high rate frequencies for the generation of random sequences which is controversy with the intentions of this thesis.

#### B) Random Sampling Slope ADC

In [7] a new approach to acquire signals that are sparse in the frequency domain using RS. This solution comprises a very simple sampling hardware and a slightly adapted CS reconstruction to be applied in cognitive radio design. In particular, the ADC is based on a small modification of the well-known slope ADC and achieves a 100% hardware utilization to maximize the number of unequally-spaced samples that can be acquired without adding complexity to the sampling process.

The principle of a slope ADC is very simple: A linear voltage slope is generated as a reference signal and is compared to the input voltage. A counter measures the time until the reference slope reaches the level of the signal. The reference slope is periodically reset to its baseline [84]. The advantage of this architecture is its simplicity in hardware. Basic building blocks are only a current source, a capacitor, a comparator, and a counter. The Disadvantages are its slow speed, especially for high resolutions, and its concept is only compatible with event-based sampling, as the clock-based sampling can't be produced by such device.

### C) Non-Uniform Sampler

A Non-Uniform Sampler is suggested in [40] for wideband spectrally sparse environment where it is used as a receiver for a GSM channel. It is basically formed by a time generator (TG) that controls the Sample and Hold (SH) units. An external pattern generator is used to provide a NUS pattern based on a repeating Pseudo-Random Bit Sequence (PRBS), the NUS pattern is then re-clocked by the TG with a high frequency clock, called in the corresponding reference as Nyquist clock, to synchronously activate the SH unit that capture the sample from the analogical signal. The restriction in such process is the compatibility of the generated clock with the ADC rhythm. Thus, the resulting pulse width spacing must not be smaller than the clock period of the ADC. In a similar methodology, the RS is practically implemented on an Arduino microcontroller in the aim of examining its performance on simple signals in a first step, then on a variety of vibration signals in a second step to evaluate the worth of applying RS in machine monitoring. In next section, the hardware implementation of different mode of RS is explained followed by the results on simple signals.

#### 3.6.2 Acquisition of Signals from Function Generator

In order to apply RS on real signals, a program was developed on Arduino microcontroller<sup>1</sup>.

The main idea of the program is to generate random instants at which the samples are acquired by the ADC, both modes are applied: ARS with both distributions and JRS with the uniform distribution.

The algorithm is based on generating a random variable by using the concept of PRBS, when the probability distribution chosen is the Uniform, while in case of Gaussian distribution, the random variables are previously generated and saved on a file that is charged on an SD memory card so the microcontroller can access the random values by reading them from the memory card. According to the chosen mode this variable is either considered a time interval in case of ARS or a jitter in

---

<sup>1</sup> Arduino & Genuino Products, <https://www.arduino.cc/en/main/arduinoBoardUno>

case of JRS. In fact the generated time is saved in a timer register that when this time is up, an interruption is generated to enable the ADC to capture a sample. Thus, this value is considered as the time interval between two consecutive samples. So, in case of ARS the generated random variable is directly transmitted to the timer register, while in JRS case, the value sent to the timer is composed of the random jitter value added to  $T_{Sm}$  with the subtraction of the previous generated jitter, which is conform with the formula (2.45) in Chapter 2 where the interval is expressed in term of jitter in the JRS case. When the interruption occurs, the ADC is enabled, but the acquisition doesn't take place until the clock of the ADC is at a rising edge, which causes the time quantization creation. In addition, the ADC has a time for processing the current sample, so if the interruption of the successive sample capture occurs an error is generated and the current sample is lost. The ADC acquires inputs between 0 and 5V and saves the value of the sample on 10 bits, the microcontroller clock is 16 MHz, with a possibility to be divided by a Prescaler, so the time step  $\Delta$  could be increased and the clock rate of the ADC is decreased. This Prescaler is used in purpose of reducing the speed of the clock and thus makes the ADC slower, so the  $T_{Sm}$  may be tested for high values. Thus, in case of uniform distribution, the user must define the mean sampling period in term of clock period which is:  $q_T = T_{Sm}/\Delta$ . The deviation  $D_q$  also must be declared to limit the values generated by the PRBS, so the random variable is limited to the interval  $[q_T - D_q/2; q_T + D_q/2]$ , thus the random variable can't take negative values. Thus, for the JRS case, the results are figured for the positive jitter. Before proceeding with the code execution, the user must declare the value of  $q_T$ ,  $\Delta$ ,  $D_q$  and  $N$  according to the features of sampling that he attempts to use.

At the beginning, multiple tests were applied on a triangular waveform with a frequency of 1kHz and an amplitude of 2.5 V with an offset of 2.5V to be compatible with the ADC input, to reveal the impact of RS in practice. So, the time quantization step  $\Delta$  is determined by the ADC and by the clock of the microcontroller, when the clock has a low rate, large time granulation, the second and third harmonics were difficult to be detected due to the increased noise floor. Thus, small values of  $\Delta$  are used to focus on RS influence. Many tests were done for different values of  $q_T$ ,  $D_q$  and  $N$ . Due to hardware limitations the ratio  $R$  couldn't have an exact value of 1, it is slightly greater than 0.8. The samples of the signal with their instants of sampling are saved, so the DTFT is calculated for the randomly sampled signal within Matlab, similarly to the simulation study. The offset of the signal is eliminated before calculating the transformation to the frequency domain.

A uniformly sampled triangular waveform, with a frequency of 1 kHz, an amplitude equal to 2.5 and an offset of 2.5, is simulated on Matlab without noise. It has a spectrum with peaks on 1 kHz and its odd multiples as in Figure 4.1, and the fundamental has the highest amplitude while the

other harmonics have reduced amplitudes (the offset is eliminated before calculating the FFT). To observe the two harmonics at 3 kHz and 5 kHz, the uniform sampling frequency is taken 10.2 kHz, the length of the signal is 2040 points. The acquisition of the already mentioned triangular signal was done with different values of  $T_{sm}(q_T\Delta)$ ,  $D_q$  and number of points, one of the most important results is shown in Figure 4.2, the DFT of the triangular signal sampled with ARS and JRS with the uniform distribution having same parameters are compared. The mean frequency is approximately 200Hz, where the period is 4.99 ms and the ratio R is 0.8 (couldn't be greater due to hardware limitation). The number of samples taken is 4000 points.

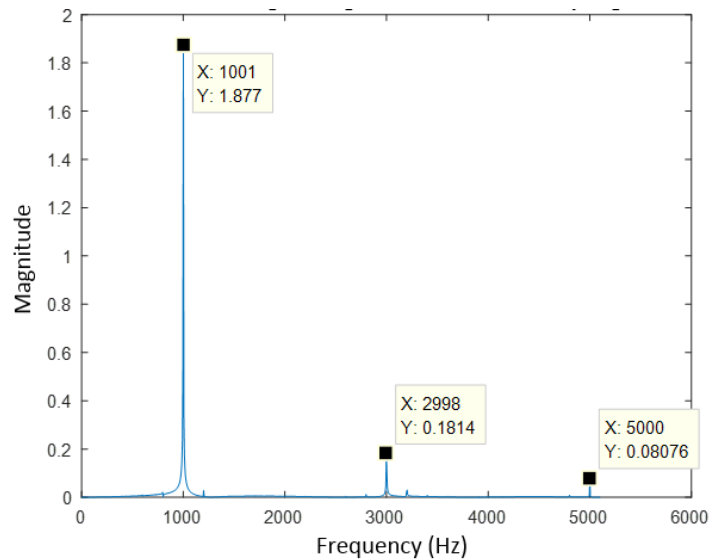


**Figure 3.16** FFT of the triangular waveform with uniform sampling

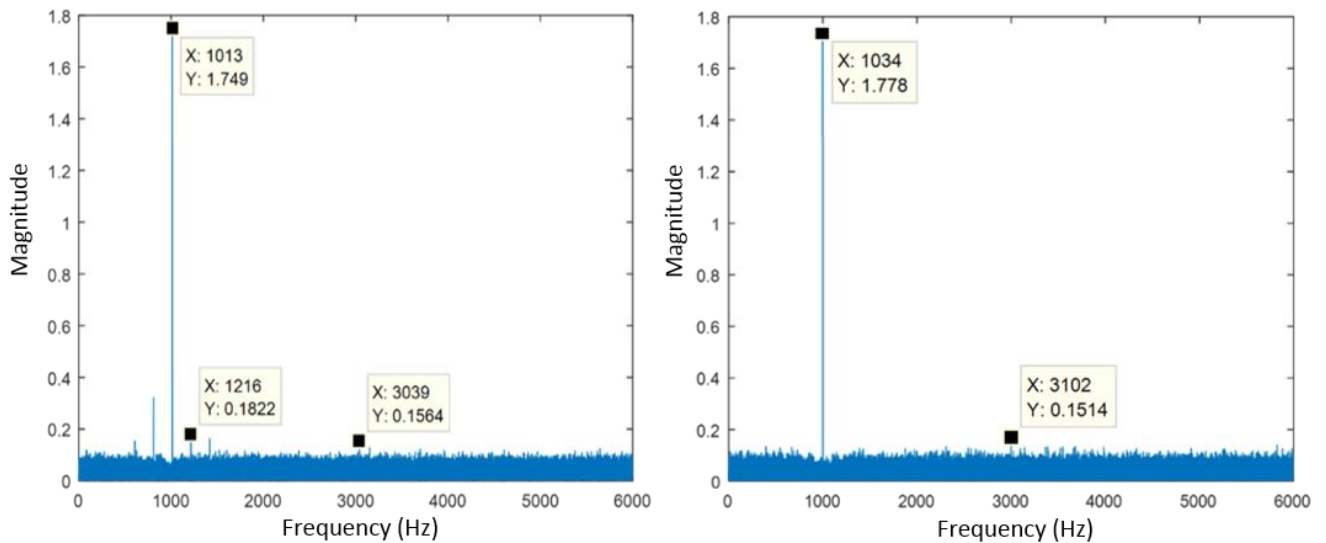


**Figure 3.17** Comparison between two DFT of a triangular signal having a frequency of 1 kHz and sampled using a JRS (on the left) and an ARS (on the right)

On one hand, when comparing both results, it can be seen that the aliases appears in the JRS mode, as the mean frequency of sampling is 200Hz , aliases appears around the fundamental with a distance of 200 Hz and its multiple, while in ARS no aliases appears.

This aliasing is due to two reasons: the uniform distribution of the jitter is not perfect enough so the condition of stationarity is not satisfied as in 1.4.2 and the ratio  $R$  (deviation/ $T_s$ ) is not greater than 80% as deduced from simulation. On the other hand, the main fundamental and its first harmonic appears in both cases, the second harmonic has a very low amplitude that can be easily covered by the noise due to hardware conditions and RS noise. Consequently, the ARS mode with uniform distribution is able to detect the peaks of the signals with a low frequency without aliasing with no limitations as in the JRS with Uniform distribution which requires a random sequence with a ratio higher than 0.8.

The whole research on RS and its different modes was done to study the possibility of its application on vibration signals in order to reduce the frequency of sampling and decrease the amount of data to be captured. After the test of RS in simulation and on simple signals (triangular waveform), it was concluded that the ARS mode with the uniform distribution is the combination with less limitations to be applied on real signals, plus, the time granulation should be the smallest possible value, and the ratio  $R$  should be higher than 0.5. In case of ARS with Gaussian distribution, for  $R=1$ ,  $N$  must be higher than the number acquired by the ARS with uniform, while for  $R=2$ ,  $N$  shouldn't be higher, but the generation of such random sequence is more challenging. And in case of JRS, the generated sequence must be accurate with a ratio  $R=1$  or 0.9. Though, in all these cases, the frequency can be smaller enough than the Nyquist frequency but around the maximal frequency of the signal and the number of points is recommended to be increased to have better result with less noise, in fact, these parameters are determined by the context of each application. These conclusions clarify the manner of choosing the RS mode, the corresponding distributions, the parameters of distributions including the sampling period and the number of points according to the aspect of the signal of interest. Thus, a brief review on the aspect and the techniques of analysis of vibration signals for both elements: Bearing and Gear is presented to choose the convenient mode of RS with adequate parameters in order to profit from RS and enhance its performance in such context.

## 4 Chapter 4: Application on Vibration Signals

### 4.1 Introduction

After exploring RS in simulation and practical implementation, deducing the most promising modes and concluding the best ranges for selecting its different parameters, this sampling process is applied on machinery vibration signals to evaluate its potential in conserving these vibrations aspect in the aim of monitoring and diagnosing rotating machines. In fact, Gears and bearings are important components of almost every machinery used in the industry. Hence, they were the subject of many recent researches to provide the needed tools for keeping them monitored and detect their deflection whenever it appears or even before. Most of these techniques are based on the vibration analysis [85], thus the RS was chosen to be applied on the vibration signals acquired from these two elements. In this chapter, a brief study on the bearings and gears is presented first in order to have a clear view on their functionality and the impact of deflections on their vibration signature. Then, an application of RS in its different modes and within the range of multiple parameters values is performed on each component in two separated experimentations. Actually, the RS application on bearing elements was done within a simple test bench where the bearing vibration signature appeared clearly, while the gears couple under test was part of a more complicated structure. Thus, multiple spectral analysis were used for the signal processing in each case according to its complexity, whether by the mean of the Welch or the LS periodogram. Both modes of RS are applied: the ARS with uniform and Gaussian distribution and the JRS with the uniform distribution. In each combination many sampling periods and numbers of samples were tested in order to enhance the result of RS to deduce the best values and compare them to those proposed in the theory.

### 4.2 Bearing

In this section, the bearing is described by defining its constituents, then the different possible deflections are cited, to end with an overview on the most used techniques for diagnosing such element. In fact, this review is presented to justify the choice of the bearing deflection and the method of monitoring in the application of RS on bearing vibrations.

#### 4.2.1 Definition

A bearing is a component used to enable rotational or linear movement, while reducing friction and handling stress, it is composed basically from an outer and inner race with rolling elements in between like balls or rollers contained in a cage set as shown in figure 4.3. Whether in rotating or sliding, the continuous interaction between these different components generates a complex vibration signature even in normal conditions. However, the apparition of faults significantly increases the vibration levels. Fatigue, corrosion, poor lubrication and faulty installation or design are all possible factors to cause premature bearing failures. The identification of the deflection is at the same level of importance of its detection in monitoring and repairing such component. Thus, many techniques were developed for detecting and localizing bearing faults.

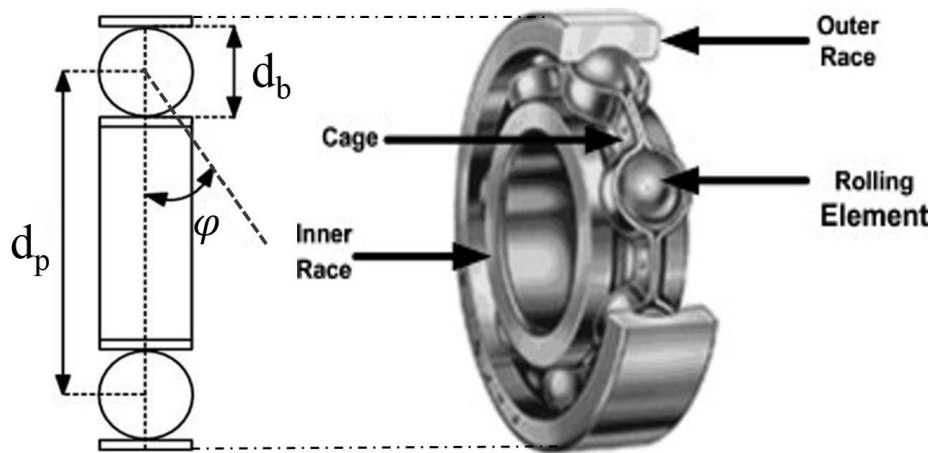


**Figure 4.1 Bearing Components**

#### 4.2.2 Possible Defections

To simplify the task of monitoring, bearing defects are divided in two categories according to their causes [85]:

##### a) Distributed Defections

They are mainly caused by imperfections or errors in manufacturing or installation. So, the contact force between the bearing elements varies the vibration aspect. Thus, the vibration analysis in such cases is used for quality inspection and condition monitoring for the enhancement of bearing reliability.

## b) Localized Defections

The dominant type of such defection is Spalls that may appear and develop over rolling surfaces when fatigue crack begins and propagates until the material fails and leave localized defection. According to [86] 90% of faults in bearings occur in the inner or outer race due to such type of imperfections. In these cases, the direct contact between the faulty element and the surface of its mating produces pulses of short duration [85]. These pulses produce vibration which can be monitored. The vibration signal generated by the faulty bearing can be analyzed in time and frequency domain [87]. Hence, in the rest of this study the scope of work is focused on faults localized on inner races.

In fact, whether the local fault appears on one of the rolling elements or on one of the two races (inner or outer), the fault is stroke by the mating rolling surface in contact which will introduce a shock that excites high frequency resonances of the whole structure between the bearing and the response transducer. These shocks excite series of broadband bursts that are featured by an amplitude modulation caused by two factors:

1. The strength of the bursts founds on the load endured by the rolling element(s), and this is normally modulated by the rate at which the fault is driven through the load zone.
2. Where the defection is moving, the transfer function of the transmission path changes with respect to the static placement of response transducers [88].

Hence, due to the existence of multiple components in the bearing, multiple faults may occur and the resulting signal contains then an impulse frequency that corresponds to the faulty component. These fundamental frequencies depend on the bearing characteristics as its geometry and its rotational speed, thus they are defined for each component by an expression in term of these characteristics [89]. For instance the Ball-pass Frequency of the Inner Race (BFIR) is defined by (4.1), so in case of defected inner race, in the spectrum, the frequency of rotation appears and the BFIR with their harmonics. The Ball-pass Frequency of the Outer Race (BFOR), the cage speed or the Fundamental Train Frequency (FTF) and the Rolling element Spin Frequency (RSF) are given in (4.2) to (4.4) [88].

$$BFIR = \frac{n_b}{2} f_r \left( 1 + \frac{d_b}{d_p} \cos \varphi \right) \quad (4.1)$$

$$BFOR = \frac{n_b}{2} f_r \left( 1 - \frac{d_b}{d_p} \cos \varphi \right) \quad (4.2)$$

$$FTF = \frac{f_r}{2} \left( 1 - \frac{d_b}{d_p} \cos \varphi \right) \quad (4.3)$$

$$RSF = \frac{d_p}{2d_b} \left\{ 1 - \left( \frac{d_b}{d_p} \cos \varphi \right)^2 \right\} \quad (4.4)$$

Where  $n_b$ =number of balls or rolling element,  $d_b$ = ball diameter,  $d_p$ =bearing pitch diameter,  $\varphi$ =bearing contact angle,  $f_r$ =rotor frequency.

The expressions in (4.1) to (4.4) are defining the kinematic frequencies of different possible errors within the assumption of absence of slip. In fact, each rolling element has particular effective properties, as the diameter  $d_b$  and the contact angle  $\varphi$ , which will make each element rolling at a different speed. Although the presence of the cage decreases the deviation of these rolling elements from their mean position, slip appears in random aspects and the bearing frequencies change of 1-2% [88].

#### 4.2.3 Diagnostic Methods

In the literature, many tools were proposed for monitoring machines components like bearings and gears, on one hand some applications were based on the acoustic emission for diagnosing or pattern recognition using artificial intelligence. On the other hand, many researches focused on vibration analysis and considered it the most efficient method for diagnosing such components in rotating machinery [5][6]. However, the vibration analysis may be applied in different ways within different possible domains, they are divided into three main categories [85] [90]:

- 1) Time Domain: where the analysis is based on many indicators calculated from the time signal as the root mean square (RMS), the Kurtosis, the Crest factor and many others. These time-domain features can be used alone or in combination with others. A popular time-domain analysis approach is time synchronous average (TSA), used to enhance the signal components of interest by using the ensemble average of the raw signal over a number of evolutions in an attempt to reduce noise and effects from other sources. More advanced approaches of time-domain analysis apply time series models to waveform data. The main idea of time series modelling is to fit the waveform data to a parametric time series model and extract features based on this parametric model (like ARMA, AR or MA).

- 2) **Frequency Domain:** the advantage of frequency-domain analysis is the ability to easily identify and isolate certain frequency components of interest. The most widely used spectrum analysis is processed by means of FFT. While the most commonly used tool in this analysis is the power spectrum. Some useful auxiliary tools for spectrum analysis are frequency filters, envelope analysis (EA) and side band structure analysis. Hilbert transform, which is a useful tool in EA, has also been used for machine fault detection and diagnostics. Despite the wide acceptance of power spectrum, other useful spectra for signal processing have been developed and have been shown to have their own advantages over FFT spectrum in certain cases. For instance, high-order spectrum, i.e., bispectrum or trispectrum, can provide more diagnostic information than power spectrum for non-Gaussian signals. Bispectrum analysis has been shown to have wide application in machinery diagnostics for components as gears in rotating machines.
- 3) **Time-Frequency Domain:** this analysis is advantageous in its ability to deal with stationary and non-stationary signals. Its main feature remains in visualizing the distribution of the frequency components within the dimension of time. Examples of methods using such approach are: Short Time Fourier Transform (STFT), Wigner-Ville Distribution (WVD) and Wavelet Transform (WT) [85][90][91]. In addition, an enhanced transform is introduced in the context of machinery diagnostic is the Empirical Mode Decomposition (EMD).

Consequently, as the mostly used, and as the study in this thesis is limited to simple cases of bearing signals rotating at a constant speed (thus stationary) the vibration analysis used in this work for bearing monitoring is based on the EA in the frequency domain. In fact, due to structure resonance, the bearing vibrations are carried to higher frequencies, thus according to [88] one of the earliest bearing diagnostic studies proposed searching for faults in the resonance region of high frequencies (multiple of 10 kHz), then, in the same period of time, synchronous averaging was performed on rectified envelope signal to explore local deflections in bearings, to finally obtain the High Frequency Resonance Technique or EA that is developed as a demodulation of the vibration signal to separate it from the resonant carrier so the frequency analysis of bearing is shifted to a lower frequency range and thus fault frequencies are analyzed with good resolution. Hence, the new concept, at that time, led to multiple bearing diagnostic methods introduced by bearing companies. In these methods, the resonance of the accelerometer was considered as a carrier, so the bandpass filtering, used in the EA, was determined according to the structure of the accelerometer implemented in the corresponding device. Consequently, one of the most important issues in the

EA was the selection of the bandpass filtering which is followed by the demodulation phase. Thus, three recommendations were proposed for this selection: the first one is based on searching for peaks at high frequencies assuming that these peaks are created by the bearing faults, the second relies on hammer tap to explore the bearing resonances, while the third is based on choosing the region of biggest dB change between the examined and the original condition spectrums, which requires the acquisition of vibration signals for the bearing in good states as reference records [88]. In conclusion, EA has been considered for long as a powerful technique for diagnosing bearings rolling at constant speed. Typically, its first step consists of a bandpass filtering around a frequency band where the impulsive excitation is amplified, and the second step is based on a demodulation that extracts the signal envelope. The spectrum of the envelope is expected to contain the desired diagnostic information, including the repetition rate of the fault and potential modulations. According to [92] it has been shown that the squared envelope (SE) is preferable to use instead of the envelope which may introduce misleading peaks in the envelope spectrum. Thereafter, due to its low complexity and computational cost, the squared envelope spectrum (SES) becomes the standard technique for bearing diagnostics.

However, the application of EA within the US mode may encounter some difficulties when implemented in real-time remote monitoring for a set of rotating machinery. As mentioned previously, the bandpass filtering or the exploration of faults frequencies in high resonance regions are applied around multiple of tens of kHz, which requires a minimum sampling frequency higher than the double of the frequency of interest according to Shannon-Nyquist condition in US, hence the sampling rate may reach hundreds of kHz with an acquisition of a large amount of data in order to guarantee a satisfying resolution and clear results. Besides, the vibration signature of bearings and gears are known to be sparse in the frequency domain, as shown in chapter 1 and declared in [19], thus the main contribution in this thesis is to explore the effect of RS on such signals in order to evaluate its potential in reducing the sampling frequency and the amount of data.

### 4.3 Gear

In this part, after defining and describing the gear component, a brief review on its possible deflections is presented to conclude with the diagnostic tools used for monitoring such element. This overview is needed to clarify the decisions made in the RS application on the gear vibration signature.

#### 4.3.1 Definition

By definition, the gear is an assembly that performs a transmission configuration in machinery. It is composed of a toothed part such as a wheel or cylinder that meshes with another toothed part to transmit motion by changing the speed value or direction. Gears are a crucial part of many motors and machines, they help in increasing torque output by providing gear reduction and in adjusting the direction of rotation like the shaft to the rear wheels of automotive vehicles. Many types of gears are used in the industry: Spur, Helical, Planetary, Bevel and others. Each specific design has a determined functionality, thus it is chosen according to the needs of the application. The most commonly used are the spur gears especially in series for large gear reductions. The teeth on spur gears are straight and are mounted in parallel on different shafts, an example of a couple of two gears is shown in figure 4.4, where the direction is inversed and the speed is reduced as the ratio  $G_f$  is defined by (4.5). Spur gears are used in washing machines, screwdrivers, motors, pumps, and other devices. They are particularly loud, due to the gear tooth engaging and colliding. Each impact makes loud noises and causes vibration, and the teeth experience a large amount of stress [93].

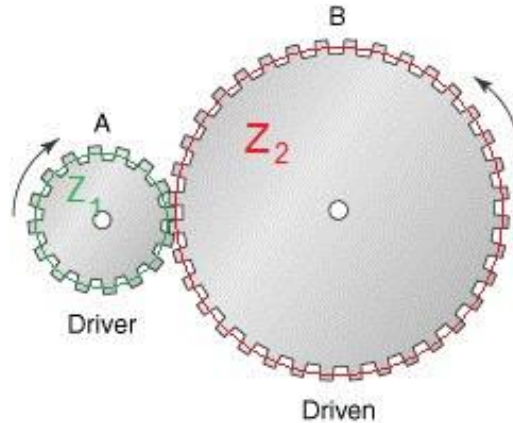


**Figure 4.2 A Pair of Gears with a ratio  $G_f$**

$$G_f = \frac{Z_2}{Z_1} \quad (4.5)$$

All the gears in the same gearbox mesh at the same time with their respective pinions which results in sliding of each tooth on other thereby generating vibrations. Due to the variable stiffness in this meshing process, all these gear vibrations are governed by the gear mesh frequency and its

harmonics [94]. Thus, for a pair of rotating gears in fixed-axis gearboxes, rotation frequencies emerge symmetrically as sidebands around the meshing frequency and its harmonics in the spectrum. In addition, signals are usually acquired from accelerometers attached on a structure housing several meshing gears. Due to structure resonance, similarly to the bearing case, the gear vibrations are convoluted with the structure transfer function. And, in some cases, several type of rotating components are packed with gears, as bearings, shaft and others. Hence, the useful characteristics are masked due to strong noise background which will require denoising strategies [95]. Indeed, the distinctive frequencies of a pair of gear is composed of the meshing frequency surrounded by rotation frequencies of both gears to form sidebands. In case of defection, these frequencies and their harmonics are affected by fault. The identification of defection is related to the occurrence of the characteristic frequency linked to the given fault. Therefore, the primary objective in vibration analysis is to detect the meshing frequency with its sidebands which helps in detecting the fault when occurred. The meshing frequency is defined by the features of the pair of gear and is expressed by (4.3) [96].

$$F_{mesh} = F_1 Z_1 = F_2 Z_2 \quad (4.6)$$

where  $F_1$  and  $F_2$  are the rotation frequencies of gear A and gear B respectively, and  $Z_1$  and  $Z_2$  are the numbers of teeth of gear A and gear B respectively.

#### 4.3.2 Possible Defections

The possible defections that might occur in the gear component include fatigue failure, impact fracture, wear and stress rupture. In fact, fatigue is the most frequent type of defection, where tooth bending and surface contact exhaustion are two of the most common consequences of fatigue failure found in gears. Poor design of the set, improper assembly or misalignment of the gears, overloading, inadvertent stress raisers or subsurface faults appearing in critical areas, and the use of inappropriate materials and heat treatments are all factors that might cause the fatigue failure [97]. Consequently, the fatigue failure is the most interesting mode to be explored, and thus, its corresponding vibration signature must be analyzed. According to [98], if the gear has a local defection as a fatigue crack, then changes will occur in the vibration as the affected teeth mesh with the other gear. These changes can be represented by an amplitude and phase modulation. The magnitude of the high-order sidebands will depend on the form of the modulation and also on the magnitude of the relevant meshing harmonic. Hence, as the main objective of this thesis is to apply the RS on vibration signals within the diagnostic context, performing RS in acquiring the signature

of a normal gear and detecting its meshing frequency with the corresponding sidebands is considered satisfying as a preliminary step in applying RS on the gear vibration signal.

#### 4.3.3 Diagnostic Methods

Many advanced techniques have been employed to detect representative features of the gear conditions. As mentioned in paragraph 4.2.3 these techniques are either based on time, frequency or time-frequency analysis. For instance, in [99] a new time-domain approach based on dynamic time warping and correlated kurtosis is introduced for local fault detection in gears. Besides, since gear motion is often rotational, periodicity is regarded as an important characteristic of its vibration signature. Thus, many techniques are based on or related to periodic analysis, such as spectral analysis, bispectrum, WT, time–frequency distribution, cyclostationary approach and EMD [theo]. According to the same reference, analyzing gear signals is often obscured by the presence of noise, including random noise and uninteresting vibration associated components. However, the main objective of using any technique of diagnosing is the detection of the meshing frequency and its sidebands that correspond to a particular gear component in the studied system. Due to the complexity of applying most advanced techniques in a varying time step conditions within RS, the proposed analysis in this study for gear signals is the Welch and the LS periodograms in the aim of detecting the meshing frequency and the sidebands as a first step.

Finally, on one hand, the bearing while rolling in order to reduce friction and handle stress, is mostly susceptible to race faults which appear in its vibration signature as a peak in the frequency domain. Thus, among multiple techniques the EA is considered the most reliable method to analyze the vibration signal in the spectral domain to identify the bearing condition. On the other hand, the gear is prone to many defections whose the most frequent is fatigue failures. However, these failures impact affects the amplitude and the phase of the spectrum of the gear vibration. Hence, a spectral analysis that could detect the meshing frequency with the corresponding rotation frequencies sidebands is considered satisfying in condition monitoring. In fact the most complicating issue in analyzing vibrations of both components is the structure resonance, uninteresting vibrations arising from other components in addition to random noise. Thus, the application of RS on bearing and gear is performed in different conditions in order to have a clear observation. In the first step of experimentation, the RS is applied on a normal bearing implemented in a very simple test bench that contains the rotating motor and the studied bearing only, in order to obtain a simple spectrum without a need to any filtering. The second step is based on acquiring vibrations from a defected bearing replacing the normal one in the same test bench. Both steps are conducted in the aim of examining the ability of RS in distinguishing between bearing in normal

and faulty states. The third step is in applying RS in acquiring vibrations from a couple of spur gear mounted back to back with three other couples. In this case the spectrum of the vibration signal is much more complicated due to the convolution of the structure transfer function with the vibrations issued from all rotating components. Actually, the purpose of this step is to identify the ability of detecting the meshing frequency of the gear of interest and the corresponding sidebands in the RS context.

#### 4.4 RS Application

The RS application is presented in two phases, the first when applied on the bearing, the second when applied on the gear. In both cases, the results are presented in the same methodology; after viewing the vibrations in time and frequency domain in case of US, the effect of the sampling frequency and the number of samples on resulting spectra are presented in order to evaluate the most adequate values in each RS mode, and finally the best spectrum of each mode is shown to verify its conformity with the US results. Thus, randomly sampled signals (squared in case of bearing) are transformed to the frequency domain by the mean of two methods. The first by applying zero insertion and using the Welch periodogram, the second by using the LS periodogram. So, the main purpose of this part is to evaluate the most adequate parameters and modes of RS with a qualification of the chosen spectral analysis in this context.

##### 4.4.1 Bearing

The experiment is done in LASPI, on a rotating motor shown in Figure 4.3, attached to the bearing 6205 RS manufactured by MTM, with two possible cases: normal and defected inner race. The rotation speed was approximately 37 Hz. Vibration signals are acquired by an accelerometer placed radially to the bearing as in Figure 4.4.



**Figure 4.3 The bench containing the rotating motor with bearing**

The output of the accelerometer is wired to a conditioner circuit connected to the Arduino microcontroller, so the signals can be sampled randomly. the conditioner circuitry is needed as The output of the accelerometer is limited between -1V and +1V with a sensitivity equal to 100mV/g, so it should be amplified and added to an offset to be compatible with the ADC input of the used microcontroller, which should be limited between 0V and 5V.

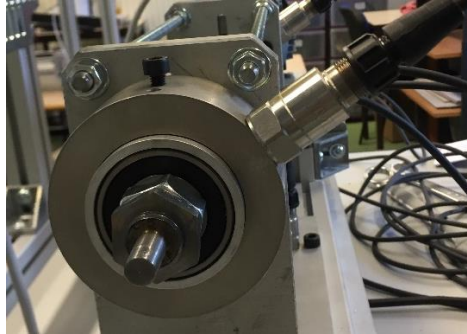


**Figure 4.4 The accelerometer acquiring vibration signals from the bearing**

After the samples and their corresponding instants are collected, the data is uploaded to Matlab in order to estimate the spectrum of the vibration signal. According to paragraph 4.2.1 the spectrum in case of normal or defected bearing contains the characteristic frequencies of rotation and deflection as peaks according to 4.1 and 4.4 with their harmonics, the SES of this signal is able to reveal these frequencies in order to accomplish the task of diagnosing. Thus, the spectral analysis applied in this test is based on the spectrum of the squared envelope deduced from the acquired signal. As already declared, the spectral representation of randomly sampled signal in this study is done by a phase of zero insertion and zero padding, to calculate then the spectrum by the FFT or the Welch periodogram method. In order to enhance this spectrum estimation, the window chosen in Hamming with a number of segments equal to 8 and an overlapping percentage equal to 50%. In addition the LS periodogram of the squared envelope is calculated by the mean of “Plomb” function built in Matlab.

#### A) Normal Bearing Case with US

In first place, using National Instrument DAQ device, an acquisition of the vibration within uniform sampling is done at a frequency of 51.2 kHz, from the same accelerometer used in RS. The acquired signal is processed also in Matlab. In this study, as the test bench is simply based on a rotating motor attached to the rolling bearing, resulting vibrations are neither prone to high level noise nor a large number of uninteresting vibrations, thus all acquired signals, randomly or uniformly sampled, are explored without any pre-processing or filtering.

First, in case of normal bearing, the frequency to detect is the rotation frequency. In uniform sampling, the signal in time domain is shown in Figure 4.5 (a). Due to the use of a high frequency of sampling, the signal within 4 seconds is very dense so, only 1000 points of the signal are plotted in figure 4.5 b, which lay in approximately 0.02 seconds.

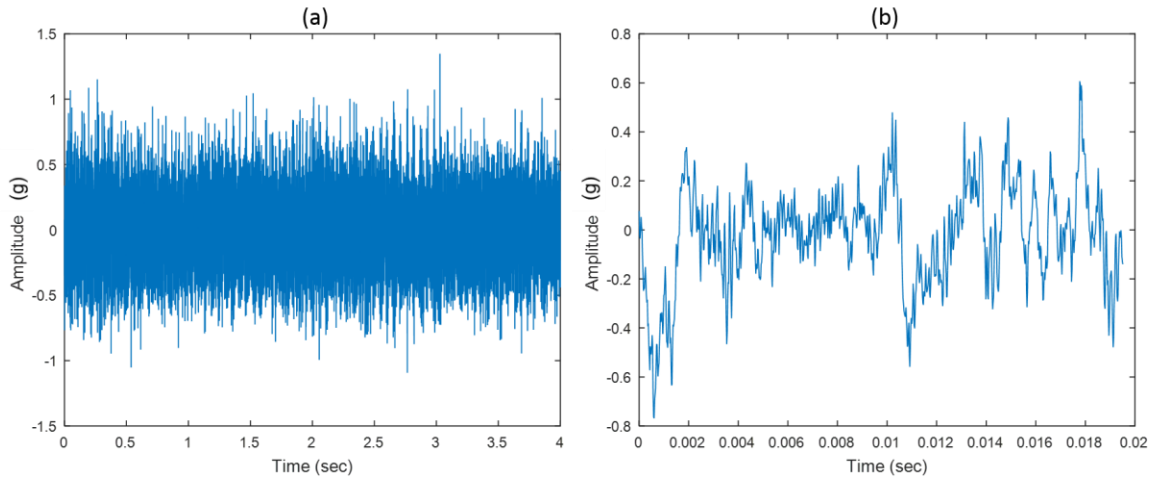


**Figure 4.5 The uniformly sampled signal of the normal bearing in time domain within 4 seconds (a) and 0.02 seconds (b)**

To detect the frequency of rotation, the FFT of the envelope is calculated, and the corresponding Welch periodogram is also presented to reduce the noise level and to compare it to the periodogram of the randomly sampled signal. Both are presented in figure 4.6 for a uniformly sampled signal of 100 000 points. It is obvious how in the FFT and in the periodogram, the rotation frequency is clearly detected with its harmonics.

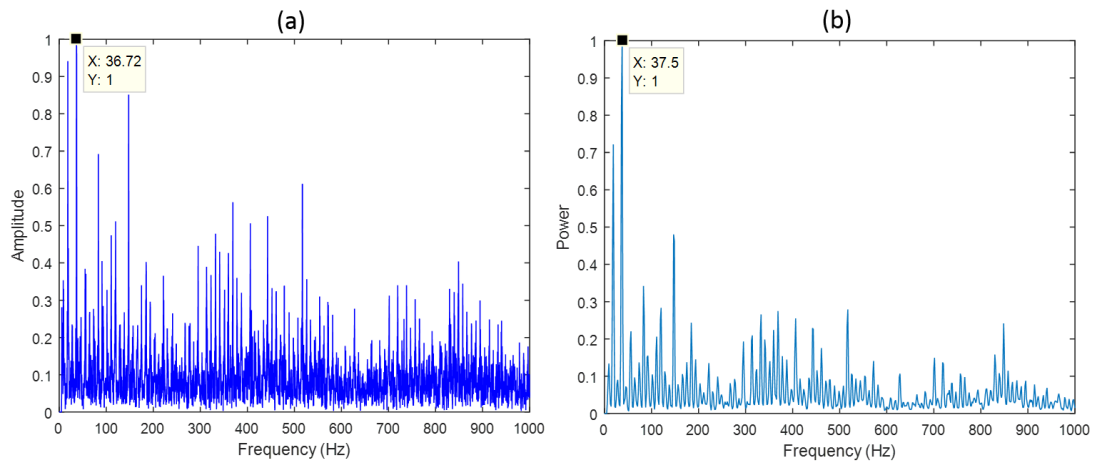


**Figure 4.6 The FFT (a) and the Welch periodogram (b) of the envelope of the uniformly sampled signal of a normal bearing**

## B) Normal Bearing Case with RS

Multiple tests are performed in acquiring the vibration of the normal bearing with RS in order to evaluate the effect of each mode and each parameter. The evaluation is based on comparing the amplitude of the rotation frequency with the amplitude of the noise maximum level. As the RS is applied in the TQRS mode, it is a must to identify the best value of  $\Delta$  in first place. As the JRS with uniform distribution is the most liable mode to have aliasing in the resulting spectrum, a comparison between the highest noise value and the amplitude at 36.9 Hz are compared (according to the SFDR definition) with the variation of  $\Delta$  to view the impact of quantization on RS. In figure 4.7 the amplitudes are shown for the JRS with uniform with a fixed  $T_{Sm}=0.02$  s, the number of samples is 6000 point and R is almost 1. The amplitudes are extracted for the normalized LS periodogram.

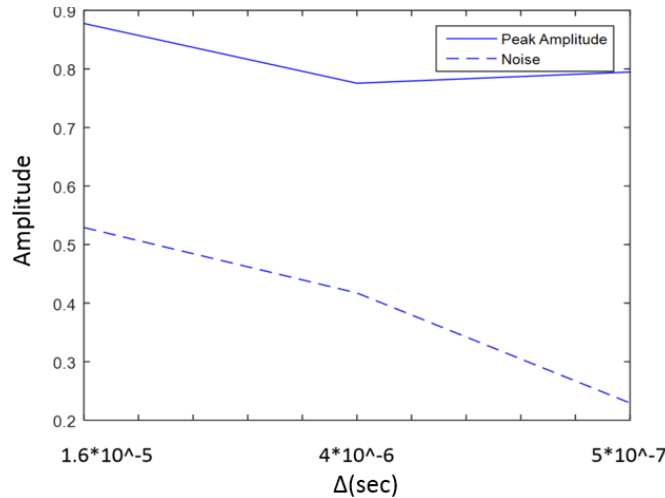


**Figure 4.7 Variation of amplitudes in term of  $\Delta$  (sec)**

It can be inferred from Figure 4.9 that the best value to choose for  $\Delta$  is the minimum; however, the amplitude of the rotation is high enough to be detected in all cases of  $\Delta$ . Thus, in the majority of the tests,  $\Delta$  is taken equal to 4 or 0.5  $\mu$ s.

In order to evaluate the effect of  $T_{Sm}$ , the application of all the possible modes of RS is done within same conditions. The results of the Welch periodogram are presented in Figure 4.8, where the amplitude of the rotation frequency peak is compared to the highest noise amplitude. In this test,  $\Delta$  is fixed to 4  $\mu$ s, the ratio R is approximately equal to 1, and the number of points is 6000. In figure 4.9 the same comparison is presented for the LS periodogram. In order to compare both methods of spectral analysis.

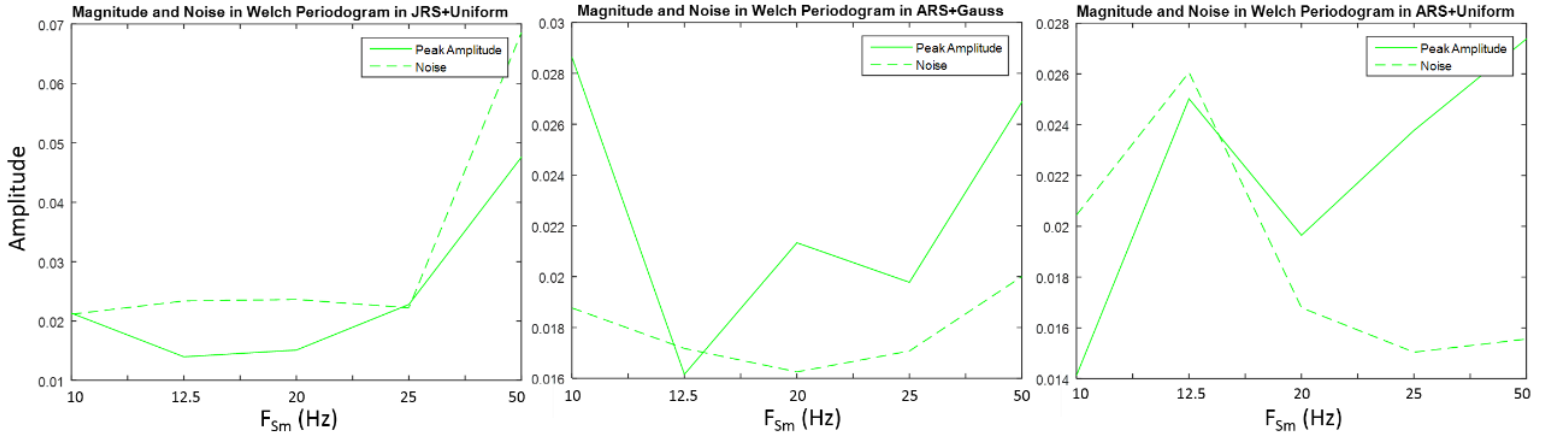


**Figure 4.8** The variation of amplitudes in term of  $F_{Sm}$  (Hz) in Welch periodogram

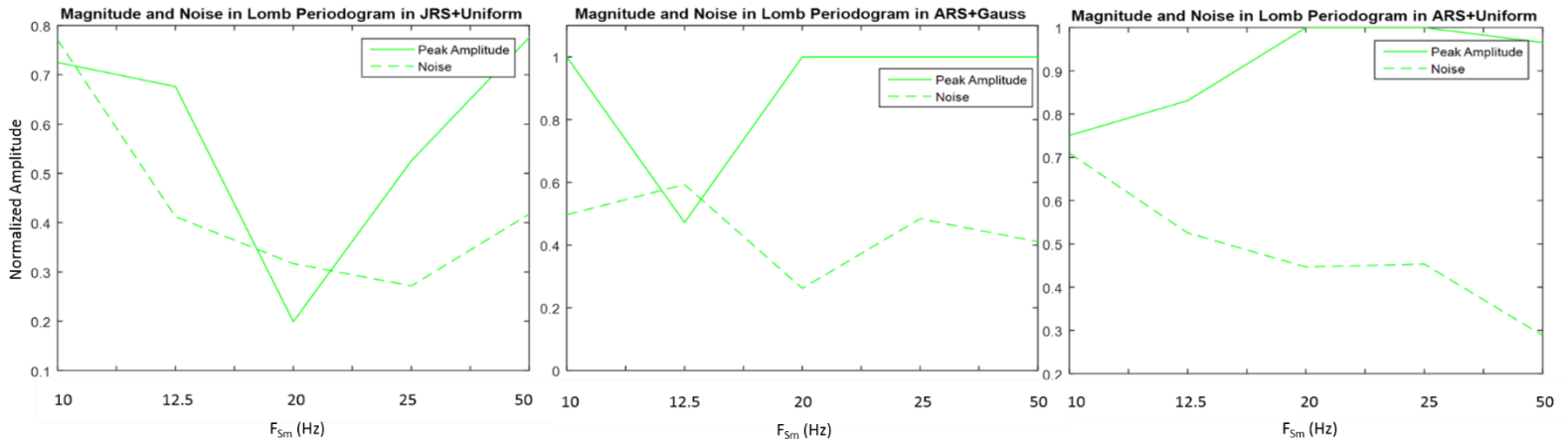


**Figure 4.9** The variation of amplitudes in term of  $F_{Sm}$  (Hz) in LS periodogram

According to both figures, obviously, the ARS with uniform distribution provide the best noise reduction within same conditions. However, for the frequencies equal or higher than 20 Hz, ARS with Gaussian can give fairly acceptable results. Thus, the ARS mode with uniform results is presented in Figures 4.10 and 4.11 in time and frequency domains as it is having fewer limitations than other modes. As the rotation of the bearing is at a low frequency signal, the chosen mean frequency is 25 Hz, the ratio  $R$  equal to 0.8 and the number of acquired samples is 6000.

As the sampling frequency is low, acquired signal within 4 seconds (figure 4.10 (a)) is not representative enough, a longer signal is then presented in figure 4.10 (b) to visualize 1000 samples that take 40 seconds to be acquired. Thus, in comparing US and RS signals in time domain, it is preferred to fix the number of samples instead of the time interval as the sampling frequencies are far different in values. The Welch and the LS periodogram of the envelope are presented in Figure 4.11.

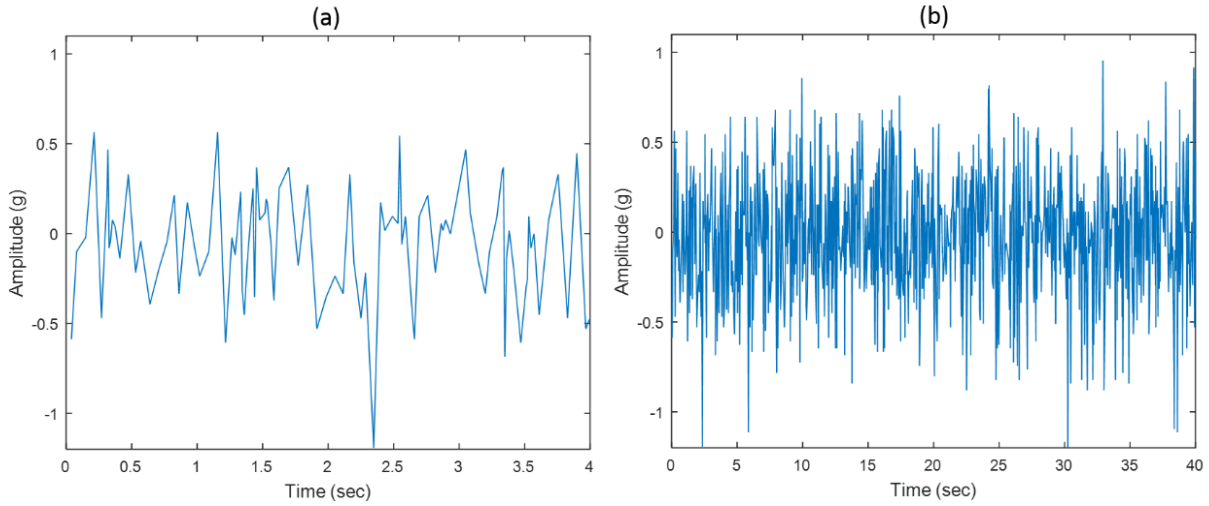


**Figure 4.11** The randomly sampled signal of the normal bearing in time domain within 4 seconds (a) and 40 seconds (b)

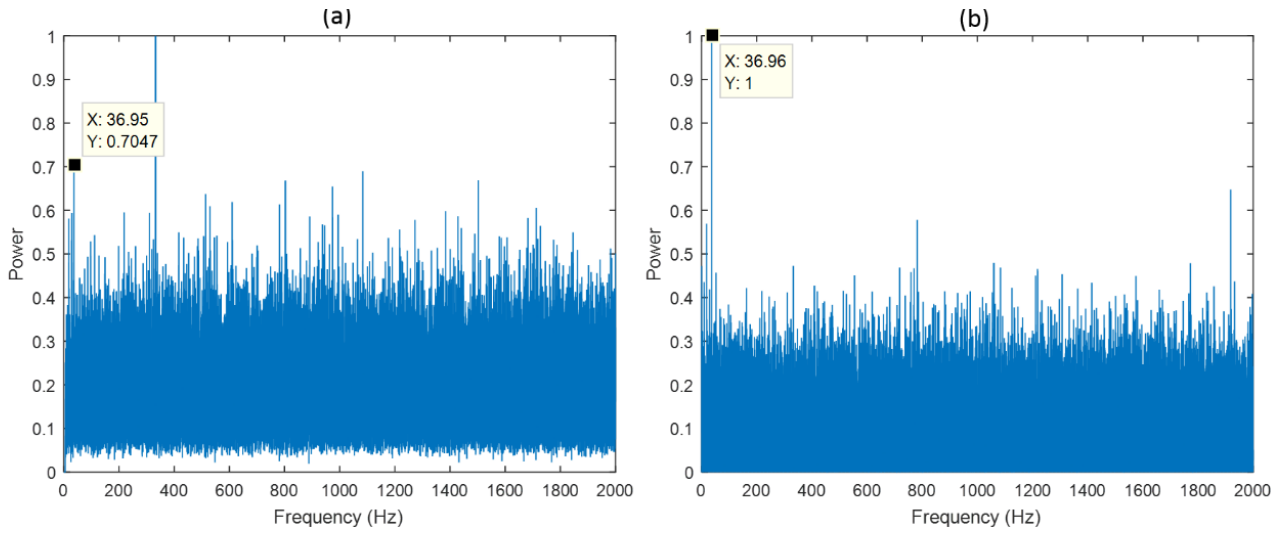


**Figure 4.10** The Welch (a) and the LS (b) periodogram of the envelope of the randomly sampled signal in ARS with uniform of the normal bearing

It can be deduced from Figure 4.11 that with a low sampling frequency and a moderate number of samples, the rotation frequency can be detected by using the ARS with uniform distribution. Although, the LS periodogram is preferred, having better noise reduction, both spectrum compared to welch periodogram of the US signal in figure 4.8 are considered acceptable as they reveal the most important information.

### C) Defected Bearing Case with US

In case of defected bearing, the deflection is situated in the inner race. According to the bearing type and its characteristics, the BFIR characteristic frequency defined by (4.1) is 199.4 Hz. So, the most important peaks to be detected are: 37 Hz and 199.4 Hz. As in the previous case, the uniformly sampled signal is presented with its spectrum to have a reference of the information that should be detected, then the randomly sampled signal will be shown with its spectrum to compare the result and evaluate the effect of RS. 1000 samples of the uniformly sampled signal in time domain are plotted in Figure 4.12, as the frequency of sampling remains in this part equal to 51.2 kHz. The calculated FFT (a) and Welch periodogram (b) of the envelope are shown in Figure 4.13.

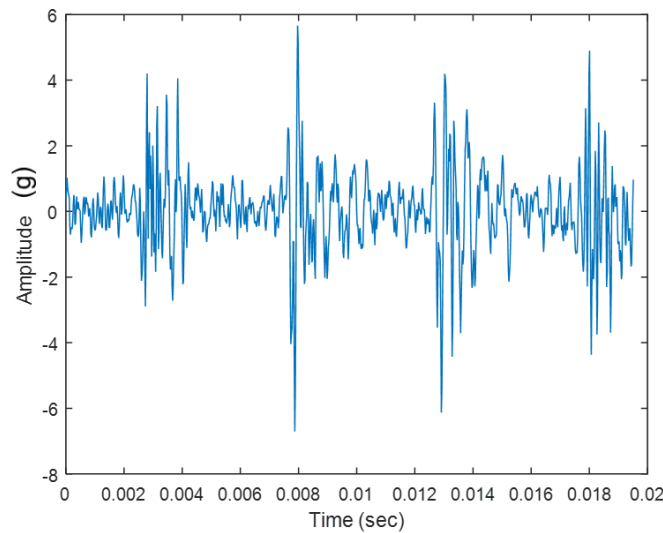


**Figure 4.13 The uniformly sampled signal of defected bearing time domain**

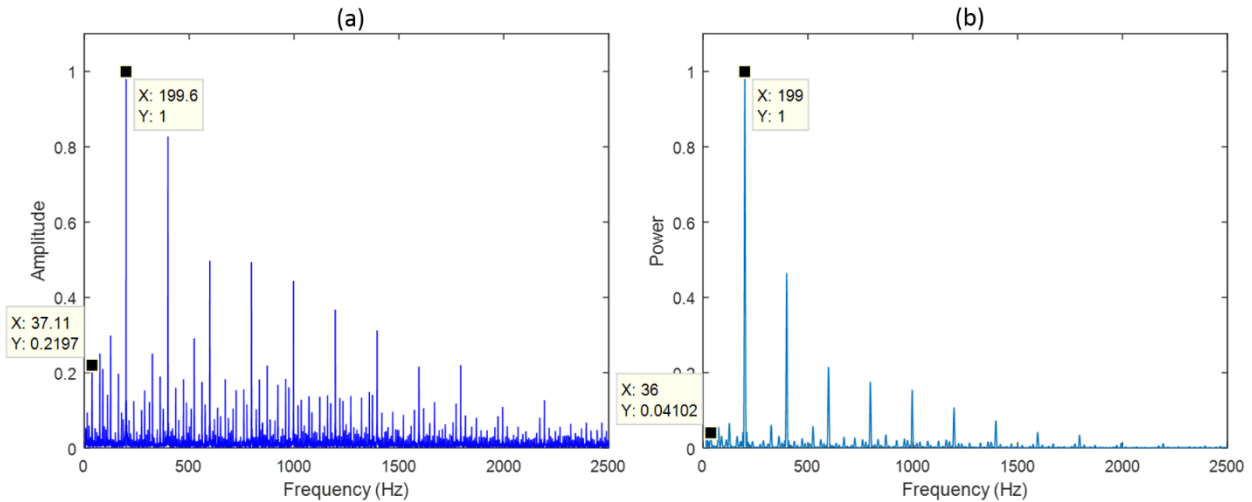


**Figure 4.12 The FFT (a) and the Welch periodogram (b) of the envelop of the uniformly sampled signal of defected bearing**

From Figure 4.13, it can be seen how the rotation frequency and the deflection frequency appear both in the FFT and in the periodogram with their harmonics. The purpose of applying the RS on the vibration signal is to obtain such results with lower frequency and moderate number of samples.

#### D) Defected Bearing Case with RS

Multiple tests were driven to explore the effect of parameters on the resulting spectrum by observing the amplitudes at 36.9 Hz and 199.4 Hz which are the most important frequencies. In first place, for the same value of  $T_{Sm}$  ( $F_{Sm}=100$  Hz), multiple value of  $R$  are tried within the JRS with uniform mode, as this mode anti-aliasing property is very critical,  $N$  is equal 6000 and  $\Delta$  is  $0.5 \mu s$ . In Figure 4.14 the amplitudes extracted from the welch periodogram are shown with the variation of  $R$ . the frequency of this maximal noise is confirmed to be 300Hz, which is the alias of the deflection frequency situated at a distant equal to the sampling frequency.

With the same methodology followed in the normal bearing case, the application of RS in the acquisition of defected bearing signals is performed by testing different values of  $T_{Sm}$  and  $N$  in each mode, and the evaluation is done by plotting the amplitudes of characteristic frequencies (rotation and deflection) with the noise maxima in both periodograms Welch and LS of the signal envelop. Then, best results are examined by presenting their corresponding spectrum to verify their conformity with US spectrums and analyze the used parameters to confirm the recommendations declared in chapter 3.

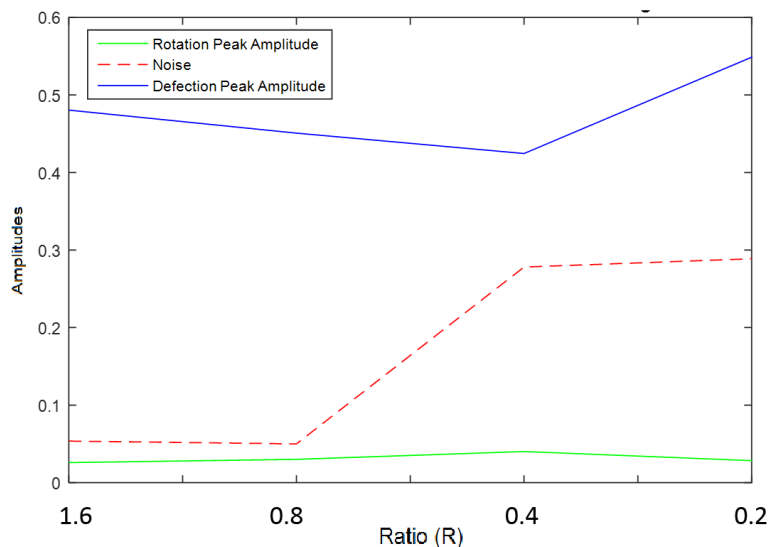


**Figure 4.14 The amplitudes of characteristic frequencies compared to noise amplitude in term of  $R$  in case of JRS+Unif in Welch periodogram**

In the second test, the different modes of RS are applied with the same  $\Delta$  ( $4 \mu\text{s}$ ),  $N$  (6000points), and  $R$  (approximately equal 1) while  $F_{\text{Sm}}$  is varying from 10 to 200 Hz. The results are presented in both normalized periodograms in figures 4.15 to 4.17 ((a) for the Welch periodogram and (b) for the LS). The enhancement of the spectrum is obviously proportional to the frequency of sampling, the best amplitudes of the deflection frequency are provided by the ARS with uniform distribution. However the JRS with same distribution presents a better noise reduction due to the shape of noise added in this mode of sampling and to its low requirement towards the number of points, thus a further test is made in order to view the effect of the number of points on the noise reduction in the next step. By comparing the results of the Welch periodogram with the LS, the consistency in the noise reduction with the increasing sampling frequency can be obviously revealed in the LS more than the Welch, while the amplitude variation is approximately the same.

The third test is performed by varying the number of sampled data in each mode of RS. The results are shown in figures 4.18 to 4.20, (a) for the Welch periodogram and (b) for the LS, where the  $F_{\text{Sm}}=50\text{Hz}$ ,  $\Delta = 0.5 \mu\text{s}$  and  $R \sim 1$ . According to these results, the increased number of samples enhances the spectrum by reducing the noise level to the minimum in all the RS modes. Though, the amplitudes of peaks in the ARS with uniform distribution are higher than other modes. In addition, the distinction of the rotation amplitude, which is lower than the deflection peak, from the noise is easier in the LS periodogram than the Welch. The best spectrums to be presented are the ones corresponding signals acquired with ARS and JRS with uniform distribution with  $F_{\text{Sm}}=200\text{Hz}$ ,  $\Delta = 4 \mu\text{s}$ ,  $R \sim 1$  and  $N=6000$ . The signal in time domain shown in figure 4.21 is for the ARS case, where 1000 samples are acquired within 5 seconds. The Welch and LS periodograms of the envelope are plotted in figures 4.22 and 4.23 ((a) and (b) respectively).

By comparing these periodograms to the resulting spectrum of the same state with US, it can be deduced that within RS, almost same result is obtained as the bearing deflection can be easily detected due to its corresponding peak at its characteristic frequency. It can be inferred from the comparison between figures (a) and (b) (in 4.22 and 4.23) that the high order harmonics are lost in the noise in the LS earlier than in the Welch due to the feature of the latter in reducing noise by averaging and overlapping. The examination of spectrums of both modes ARS and JRS lead to the appreciation of ARS due the amplitude recovery.

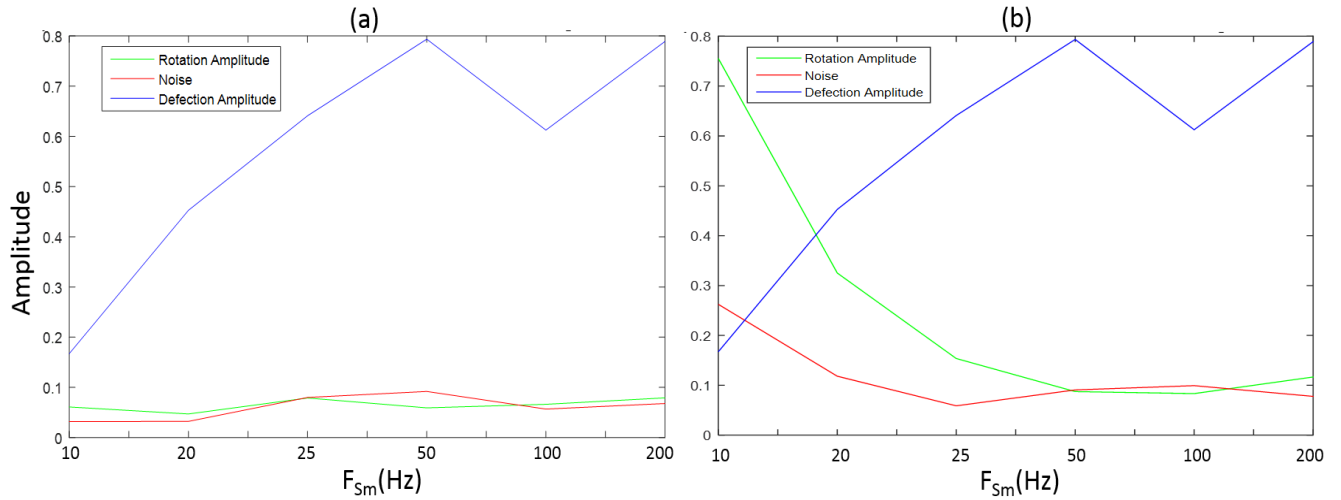


Figure 4.15 The variation of the amplitudes in term of  $F_{Sm}$  ( $1/T_{Sm}$ ) in ARS+Unif

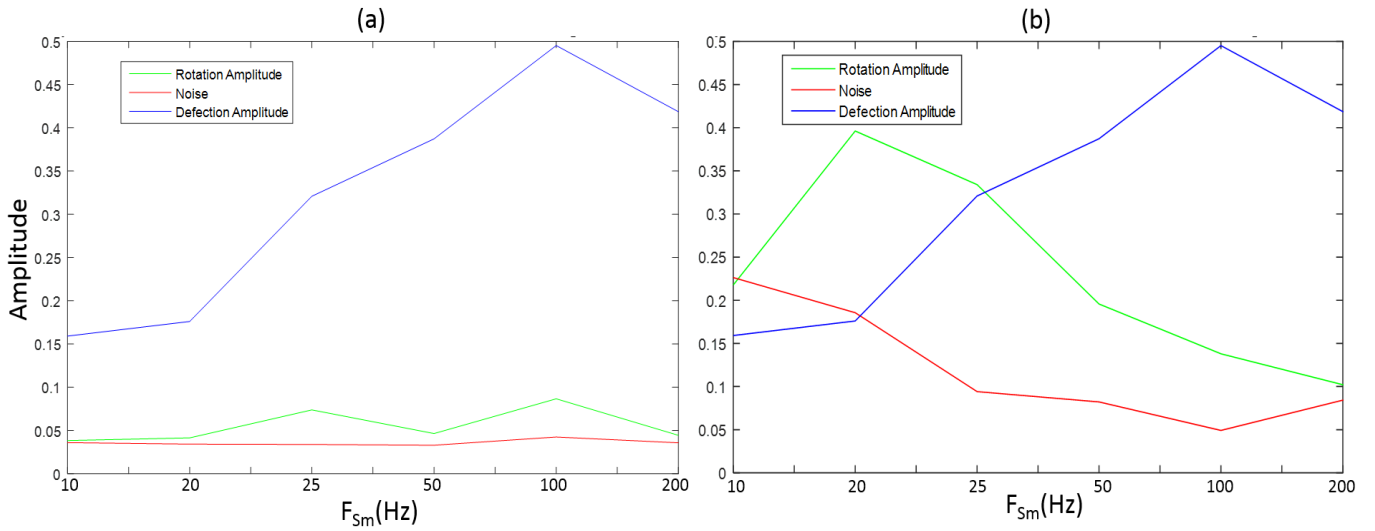


Figure 4.16 The variation of amplitudes in term of  $F_{Sm}$  ( $1/T_{Sm}$ ) in ARS+Gauss

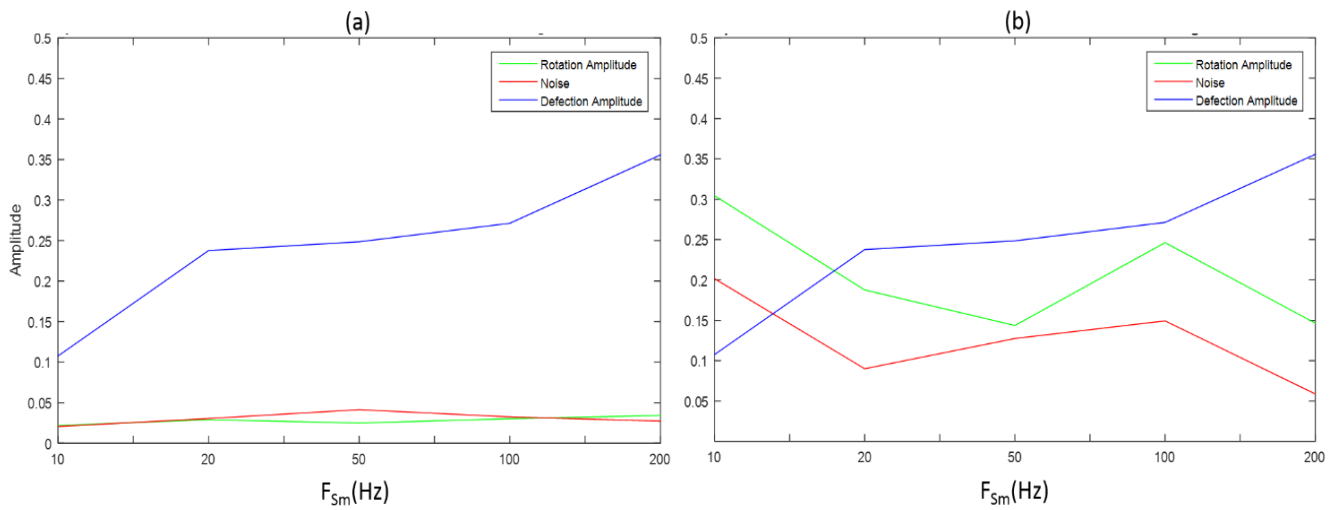
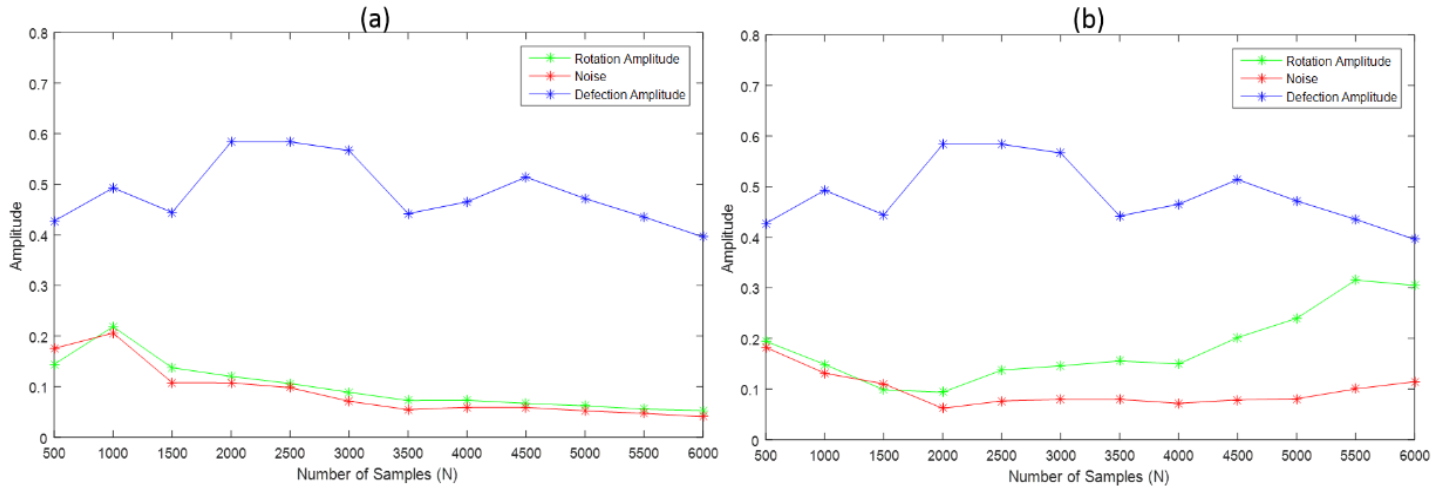
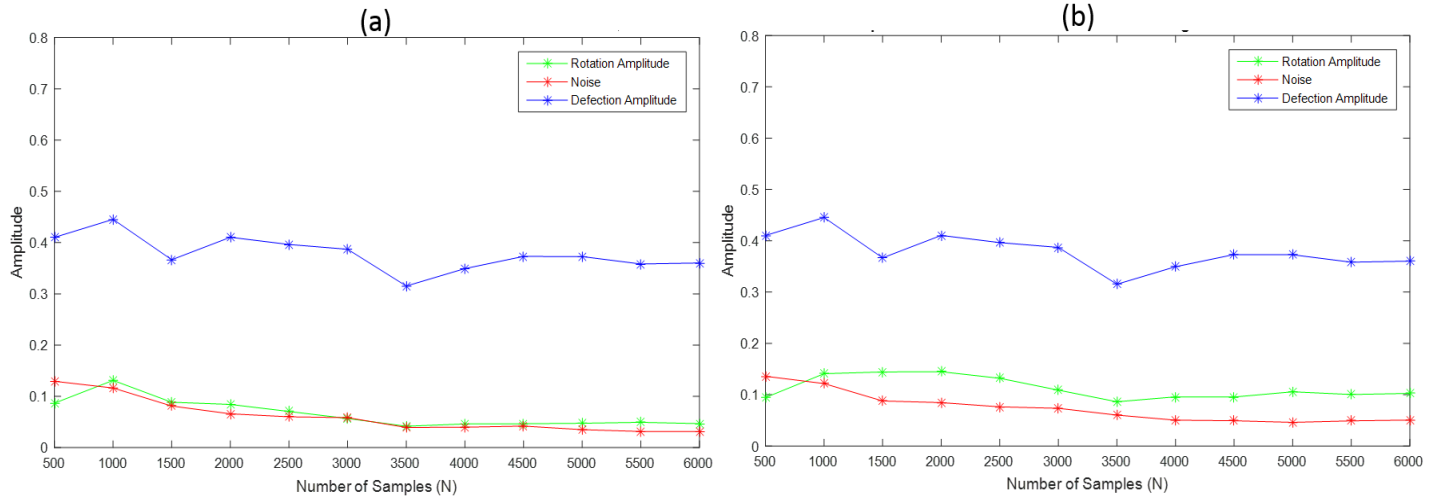


Figure 4.17 The variation of amplitudes in term of  $F_{Sm}$  ( $1/T_{Sm}$ ) in JRS+Unif



**Figure 4.18 The variation of amplitudes in term of N in ARS+Unif**



**Figure 4.19 The variation of amplitudes in term of N in ARS+Gauss**

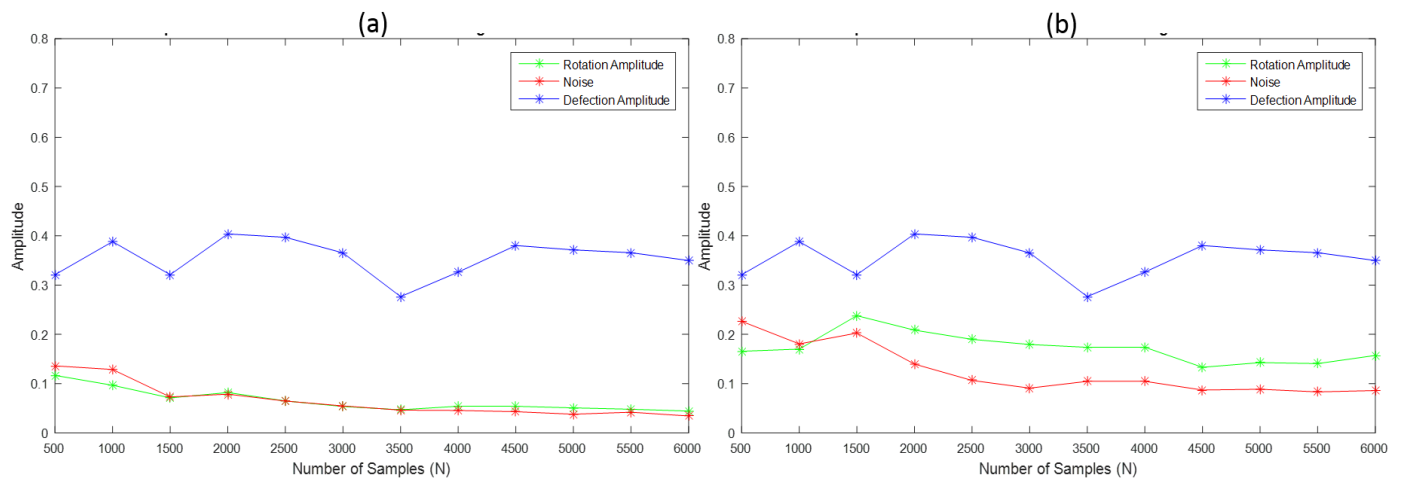


**Figure 4.20 The variation of amplitudes in term of N in JRS+Unif**

Consequently, the best results are obtained in RS are for  $F_{Sm}$  equal to 200Hz and N equal to 6000, which are perfectly respecting the recommendations already declared in chapter 2, as the noise is reduced to the minimum when the sampling frequency is almost equal to the peak frequency to be detected (frequency of deflection 199.4 Hz) and the number of samples is proportional to the number of harmonics detected (in the ARS 6 harmonics are appearing clearly). In conclusion, the RS application in acquiring bearing vibrations conserves the state condition of this component in the resulting spectrum by preserving the corresponding characteristic frequencies which guarantees the fault detection whenever it occurs. This acquisition is highly appreciated for its low frequency rate and reduced amount of data used.

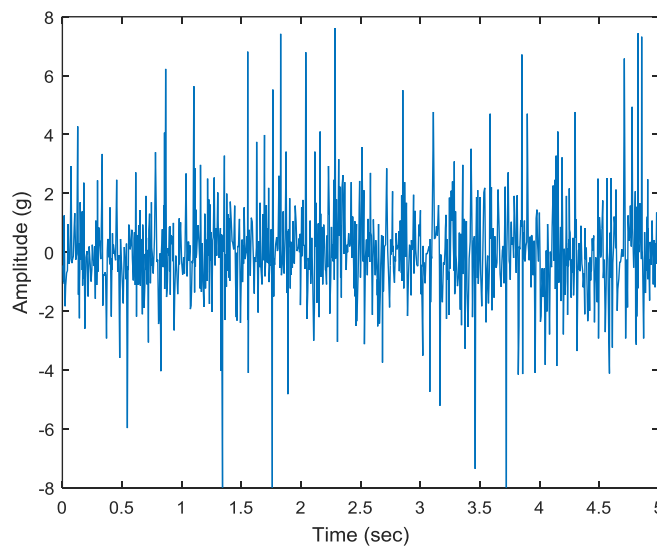


**Figure 4.21** The randomly sampled signal of the defected bearing within ARS+Unif in time domain

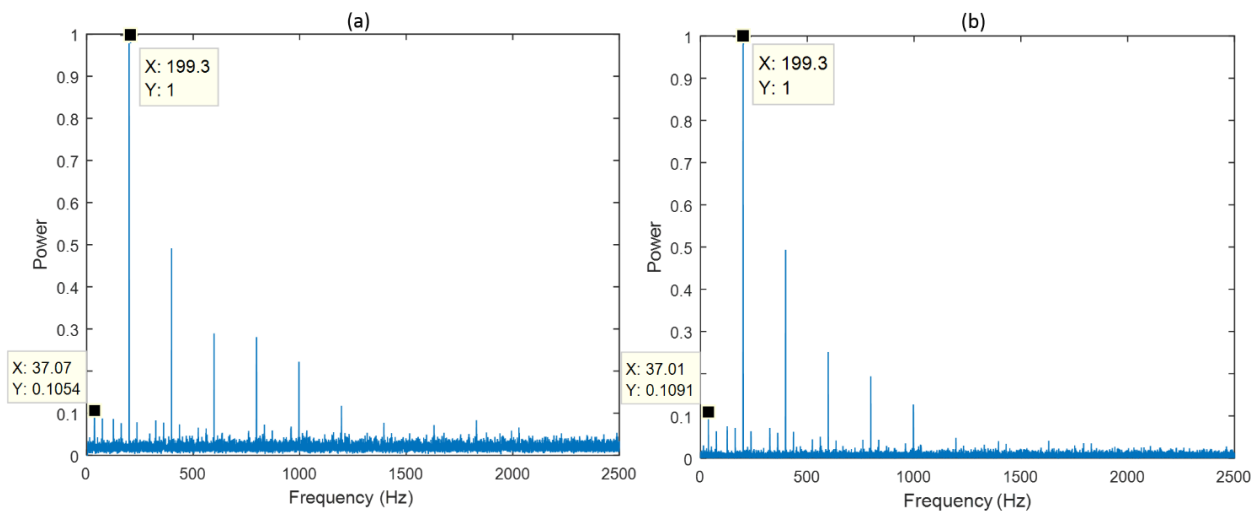


**Figure 4.22** The Welch (a) and the LS (b) periodograms of the randomly sampled signal envelope of the defected bearing in ARS+Unif

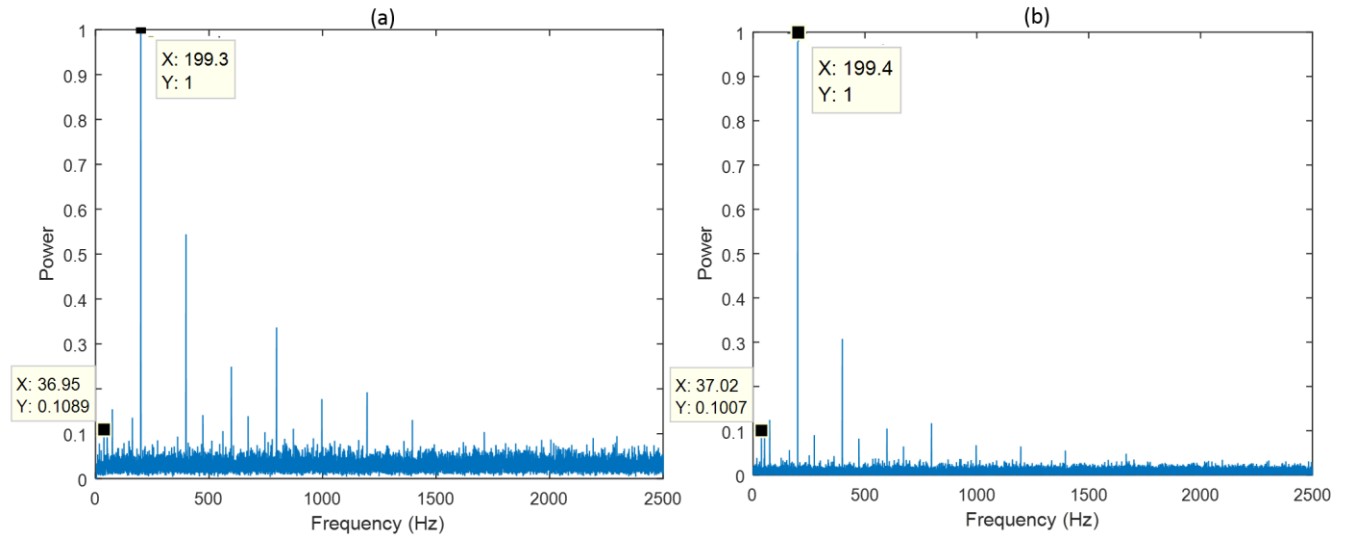


**Figure 4.23 The Welch (a) and the LS (b) periodograms of the randomly sampled signal envelope of the defected bearing in JRS+Unif**

#### 4.4.2 Gear

After the successful results obtained by the application of RS on bearing signals in a simple test bench, further tests were conducted to apply different modes of RS on gear vibrations. At the beginning, the same procedure followed in the first experimentation was repeated on the gear test bench by using the Arduino microcontroller with the same codes and same accelerometers. In figures 4.24 and 4.25 the test bench containing multiple gears and its kinematic scheme are shown, in 4.24 the accelerometer appears placed on the housing structure and positioned directly above the pair of gears under test. In fact the test bench contains 4 couples of spur gears mounted back to back to offer a speed reducer with a factor of reduction equal to 139.74. In order to simplify the task, the pair placed directly under the accelerometer is the only one taken in consideration. According to paragraph 4.3, the characteristic frequencies are deduced from the geometric properties of the gear. The studied pair is composed of two gear with  $Z_1=23$  and  $Z_2=62$ , which makes the ratio  $G_f=2.69$ . Hence, in case of the first rotation speed,  $F_1$  is equal 25Hz, the meshing frequency  $F_{mesh}$  is deduced according to (4.6) and is equal to 575Hz. The second rotation frequency is then  $F_2=575/62=9,27$ Hz. So, the objective within applying the RS is to detect the meshing frequency  $F_{mesh}$  and the rotation frequencies emerged around as sidebands.



Figure 4.24 Gear test bench with an accelerometer directly above the gear under test

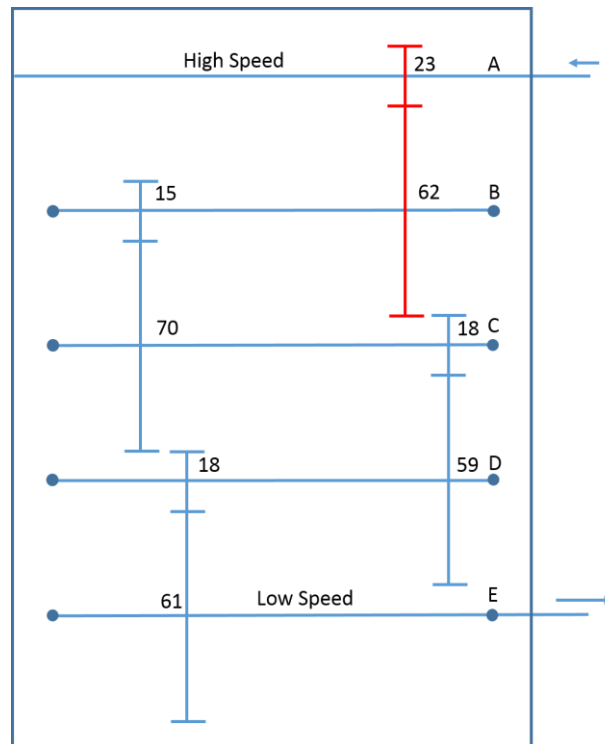
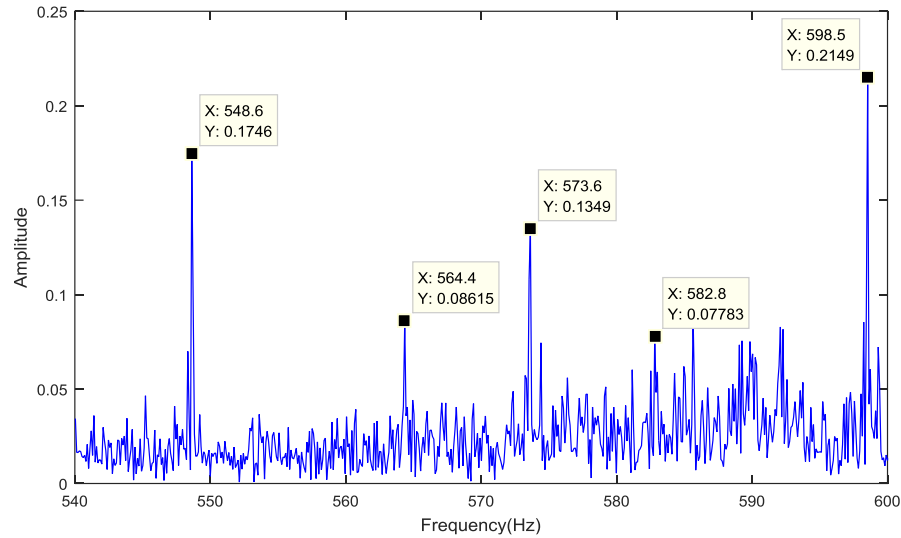


Figure 4.25 Gear test bench kinematic scheme

A) Gear Case with US

In a similar way of the bearing experiment, the first step in the gear test is to acquire the corresponding signal at a constant frequency to explore the spectrum of the vibration to be captured randomly with RS in the next step. By using the DAQ device, the vibration signature

of the gear is acquired at 51.2 kHz with  $N=200000$  points. In the aim of exploring the characteristic frequencies of the tested gear, the FFT of the acquired signal is calculated, yet, the obtained spectrum is hardly interpreted due to its high complexity resulting from the apparition of vibrations coming from other components mounted in the same bench in addition to the noise and to the effect of the structure resonance. Nevertheless, by zooming around the meshing frequency, it appears clearly with the sideband frequencies of the corresponding rotations  $F_1$  and  $F_2$ . This part of spectrum is shown in figure 4.26.



**Figure 4.26** The FFT of the uniformly sampled gear vibration around  $F_{\text{mesh}}$

Thus, in order to reduce the noise within conserving peaks at the characteristic frequencies, Welch periodogram is used for the spectrum estimation. The chosen apodization window is Kaiser due to its selective aspect and its high rejection property [81] that are illustrated in figure 3.15 in chapter 3. The number of segments and the percentage of overlapping are moderately chosen in order to reduce the noise without suppressing the characteristic peaks. A comparison between the variety of Welch periodogram trials is shown in Figures 4.27 to 4.29 in order to illustrate the important part of spectrum that must be detected and verify the decision in choosing Welch parameters. According to figure 4.27, many window types are tested on the gear spectrum, owing to its selective aspect, the Kaiser window conserves the characteristic peaks and prevents them from suppression or smearing as in other spectrum obtained with other windows. In Figure 4.28 and 4.29 the windows having best spectrums (Kaiser and Hamming) in 4.27 are chosen to be tested with different number of segments ( $L$ ) to qualify the best window to choose, the same methodology is also applied for the overlapping percentage. Consequently, the Kaiser window with  $L=16$  and overlapping =50% is approved to be the best combination as it is able to conserve the most critical peak 582 Hz.

However, in all these spectrum estimations the peak around 585Hz remains with high amplitudes which disturb the detection of the characteristic frequencies which is a result to the harsh environment that surrounds gears.

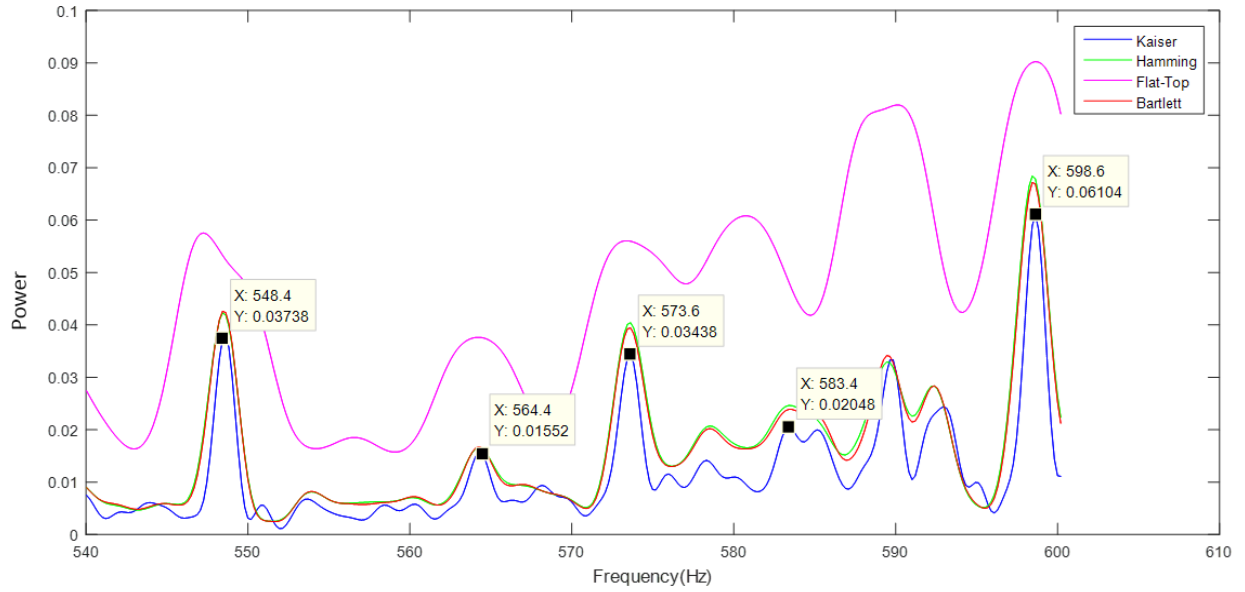


**Figure 4.27 The Welch periodogram of gear vibration with different apodization windows around  $F_{\text{mesh}}$**

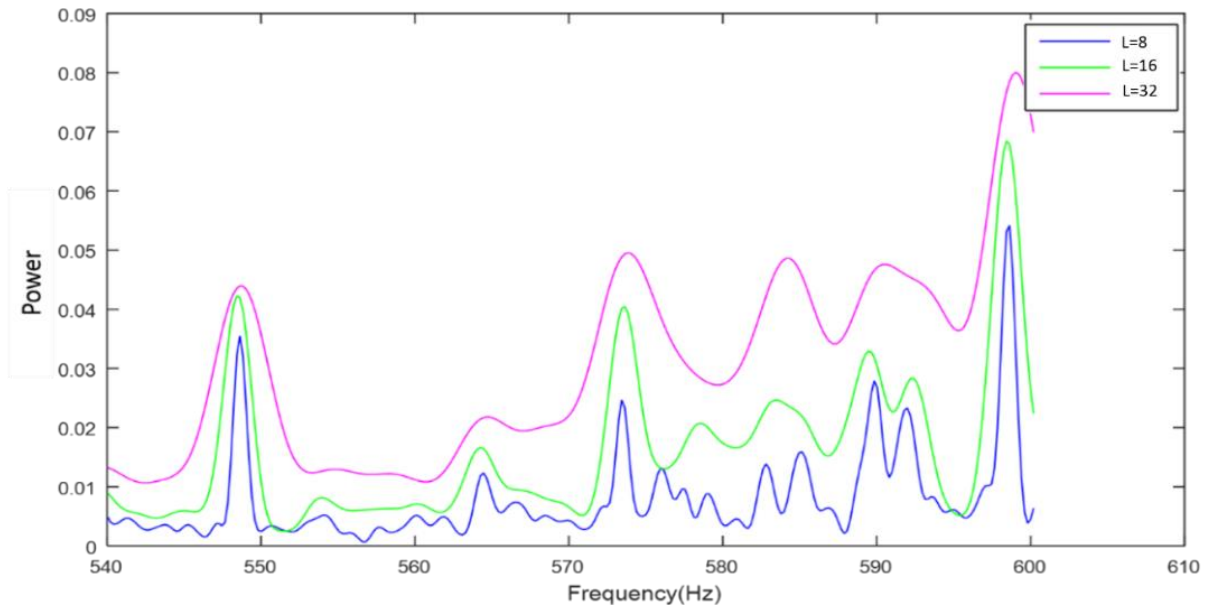


**Figure 4.28 the Welch periodogram of gear vibration with Kaiser window for different  $L$**

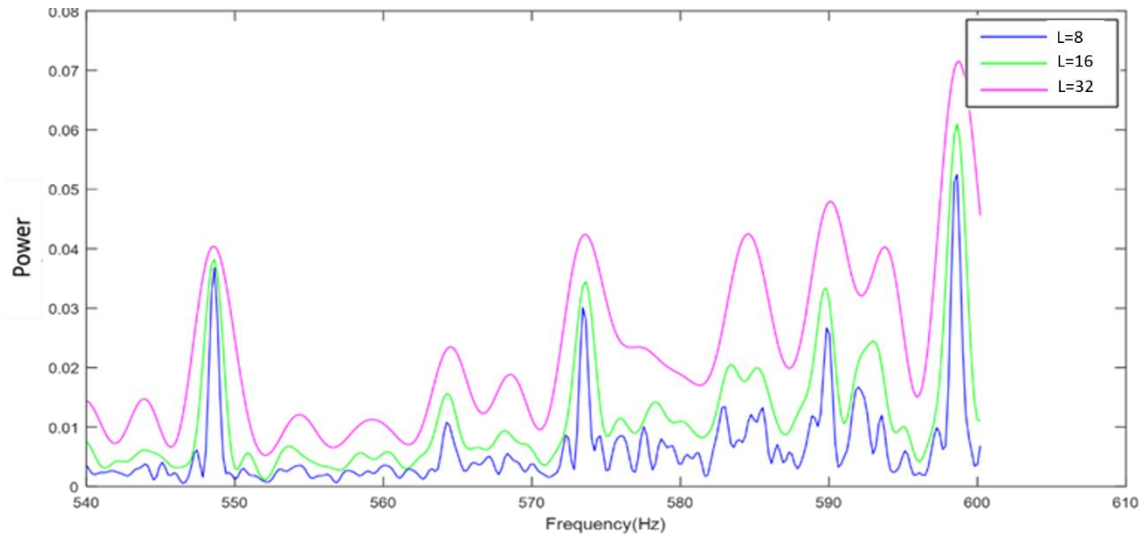


**Figure 4.29 the Welch periodogram of gear vibration with Hamming window for different L**

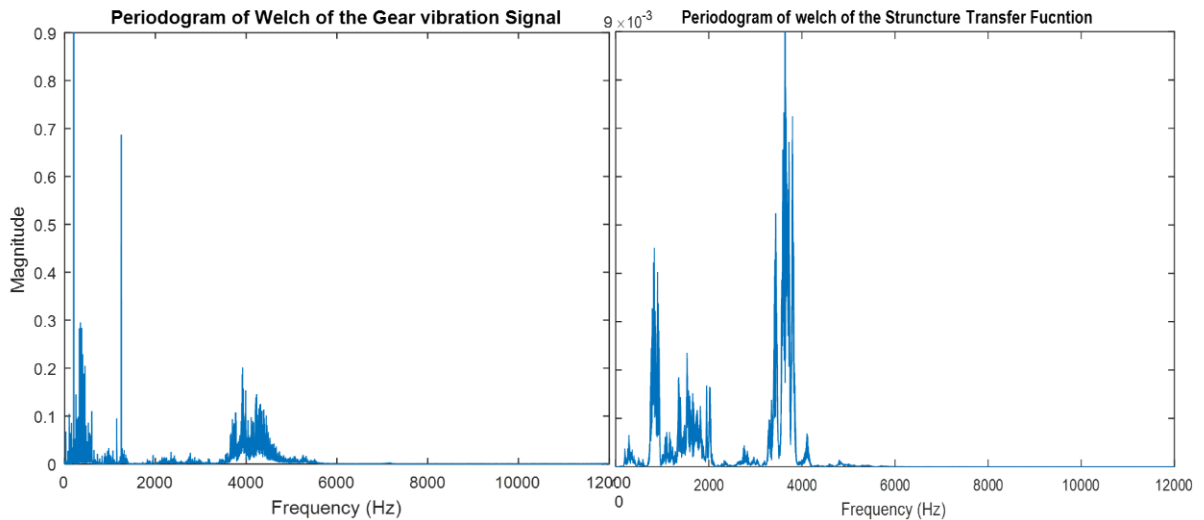


**Figure 4.30 the Welch periodograms of the gear vibration and the structure transfer function**

Furthermore, to have a clear view on the gear vibration with a significant interpretation, the spectrum of this signal and the structure transfer function are estimated by the Welch periodogram with already cited parameters and shown in figure 4.30. As declared in part 4.2 of this chapter, the structure transfer function can be obtained by the vibration acquired from the housing while a hammer tap is applied. In general, the comparison between these two spectra is necessary to observe the effect of resonance, and deduce the bandpass filtering if needed. In case of RS, this step is required to reveal the highest frequency of interest in the spectrum of the signal under test to deduce

the sampling frequency. As the characteristic frequencies are detected by simple zooming, the analysis of vibration signals in following steps is performed without filtering.

#### B) Gear Case with RS

Continuing with the same procedure followed in the bearing experiment, the next step in this test is to apply RS on gears vibration. In fact, the first trial was by the execution of the Arduino code of acquiring signals from accelerometer via the ADC. Unfortunately, all the conducted tests with low frequencies were ended by failure, which is verified by the fact of the existence of too many peaks in the spectrum which will increase the number of impulses convoluting the noise term  $N(f)$  in the PSD of the signal as discussed in the section (2.4.5) in Chapter 2. Thus, the mean sampling frequency must be increased to reach the highest frequency in the spectrum of the structure transfer function to reduce the noise to enhance the results. However, the ADC performance is limited by the time needed by the ADC to accomplish the conversion of one sampling. In the used Arduino microcontroller, the conversion process duration is  $250\mu s$ , which can limit the sampling frequency to 500Hz when R is higher than 1. Consequently, another implementation of RS was used with better features and higher performance. Yet, the description of this implementation is not presented due to confidential reasons. Hence, many tests were done in applying RS within its different modes on the gear vibration. The same methodology used in the bearing case is followed in evaluating the success of RS application, by varying the RS parameters and exploring their effect on the resulting vibration spectrum. In this test, the amplitudes compared to the noise maxima are that corresponding to the meshing frequency and to the sideband frequencies  $F_{mesh}-F_2$  and  $F_{mesh}+F_1$  as they are the lowest. As in the spectrum in US case some noise appeared around 585 Hz, the maximum of noise is not considered as a sufficient criteria to evaluate the resulting spectrum, thus, the mean of the noise is calculated in addition to its deviation in order to observe the variation of noise clearly in each mode of RS. Similarly to the bearing case, the spectrum is estimated by two methods: zero insertion with Welch periodogram and LS periodogram. However, in gear case the estimation is applied on the raw vibration signal.

The first test in this phase of experimentation is based on varying  $F_{Sm}$  from 500 Hz to 5000Hz with N equal to 50000 points,  $\Delta$  equal to 40  $\mu s$  and R equal to 1. In figures 4.31 to 4.33 the results of different RS modes are presented, the Welch periodogram is shown in (a) and the LS is shown in (b).

By comparing the results of the LS with the Welch periodogram, it can be deduced that the LS is more reliable due to the presented consistency in noise reduction with the sampling frequency. The

results of Welch periodogram reveal the weakness of this estimation in RS in case of dense spectra due to the problem of smearing. The LS results show the effect of the sampling frequency in reducing the noise maxima and deviation with an enhancement of the meshing peak amplitude recovery, which lead to higher SFDR in all modes of RS.

The second test is based on varying the number of samples acquired in order to evaluate its effect on RS result,  $F_{Sm}$  is fixed to 5000Hz with  $\Delta$  equal to 40  $\mu$ s and R equal to 1. In figures 4.34 to 4.36 the results of different RS modes are presented, the LS periodogram is used for the spectral estimation as it was proven to be more reliable in case of gear vibration analysis. It can be inferred from these figures that the number of data is important for noise reduction, as the noise maxima and the mean added to the noise deviation are decreasing clearly with the increasing number of samples while the meshing peak amplitude is barely modified with the variation of N. In addition, all modes of RS present satisfying results for  $F_{Sm}$  equal to 5000 Hz from N equal to 20 000points and up. Hence, the LS periodograms resulting from applying all the modes of RS in the gear vibration acquisition are presented in figures 4.37 to 4.39 around the meshing frequency.

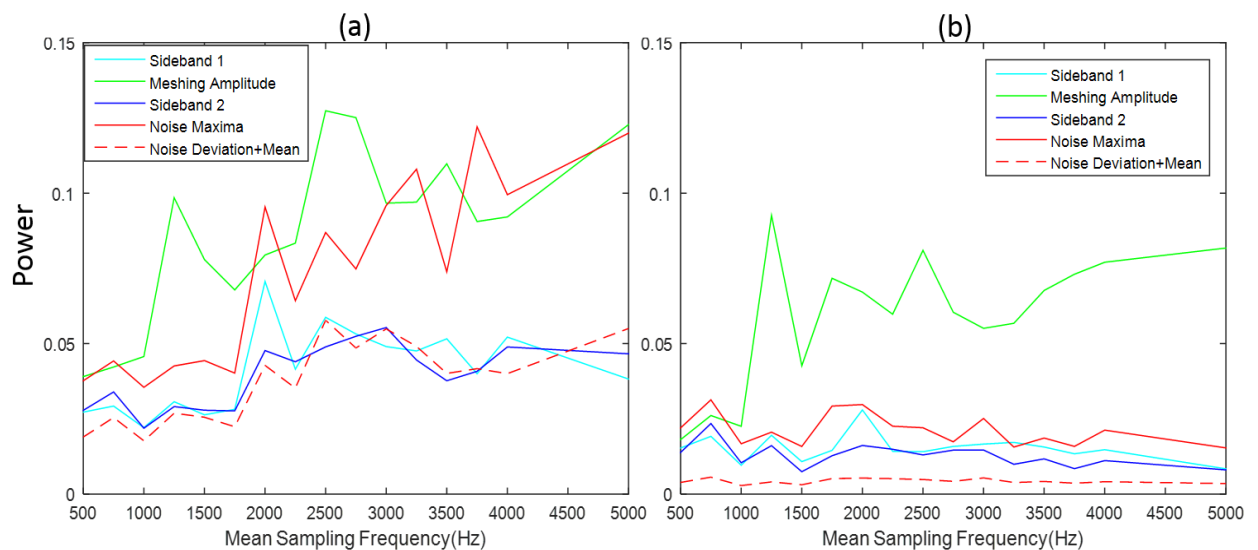


**Figure 4.31 Amplitudes and noise variation with  $F_{Sm}$  in Welch and LS periodograms of the gear vibration in ARS+Unif**

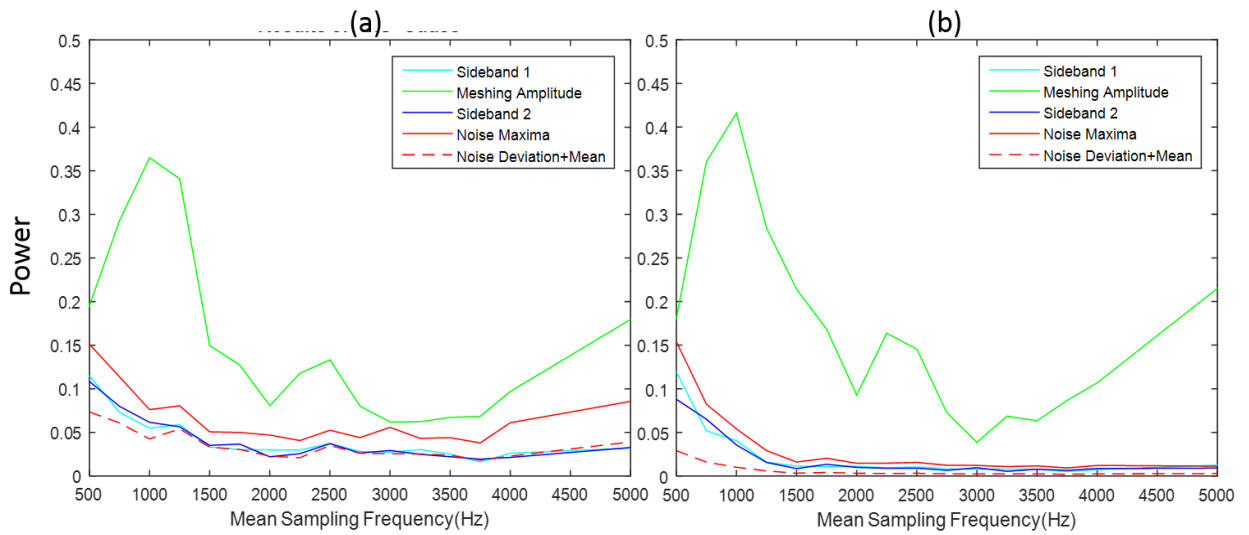


**Figure 4.32 Amplitudes and noise variation with  $F_{Sm}$  in Welch and LS periodograms of the gear vibration in ARS+Gauss**

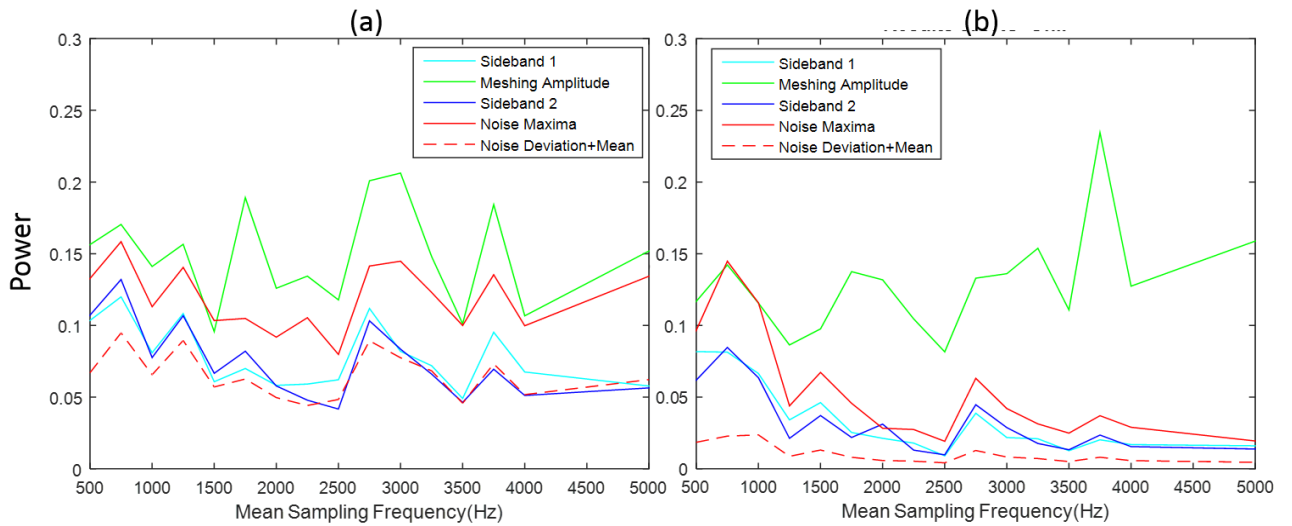


**Figure 4.33 Amplitudes and noise variation with  $F_{Sm}$  in Welch and LS periodograms of the gear vibration in JRS+Unif**

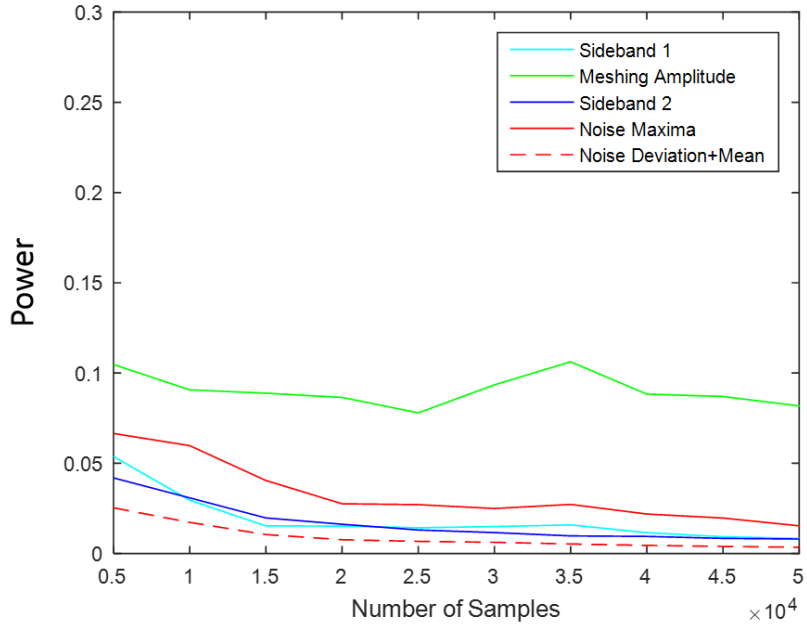


**Figure 4.34 Amplitudes and noise variation with N in LS periodogram of the gear vibration in ARS+Unif**

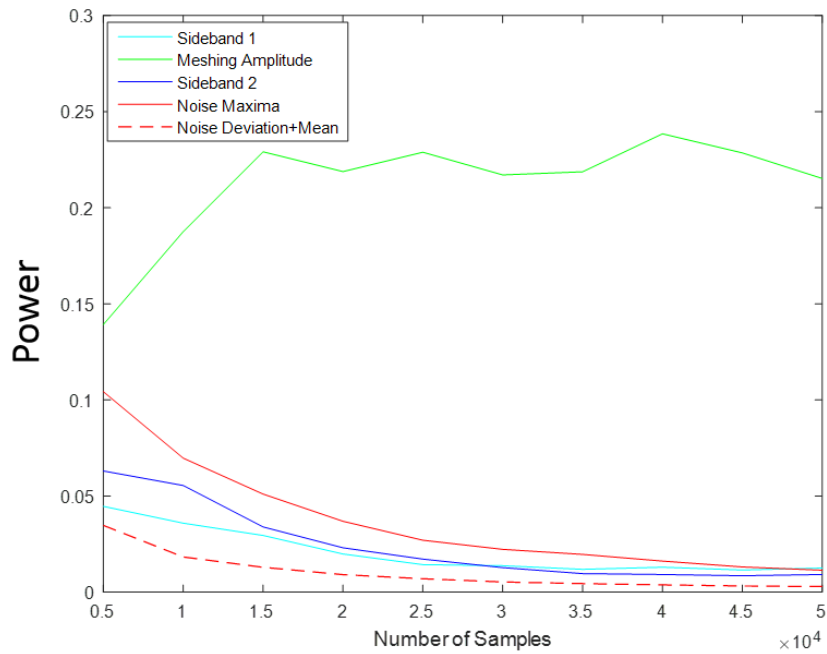


**Figure 4.35 Amplitudes and noise variation with N in LS periodogram of the gear vibration in ARS+Gauss**

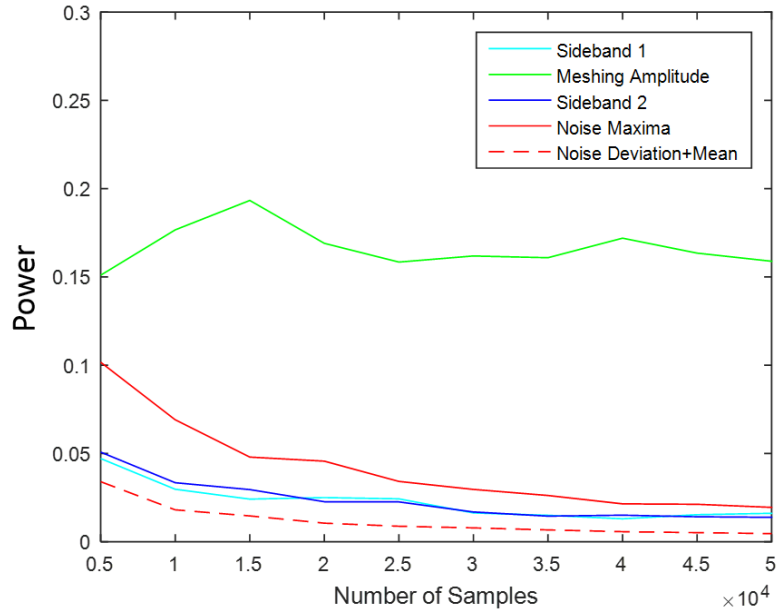


**Figure 4.36 Amplitudes and noise variation with N in LS periodogram of the gear vibration in JRS+Unif**

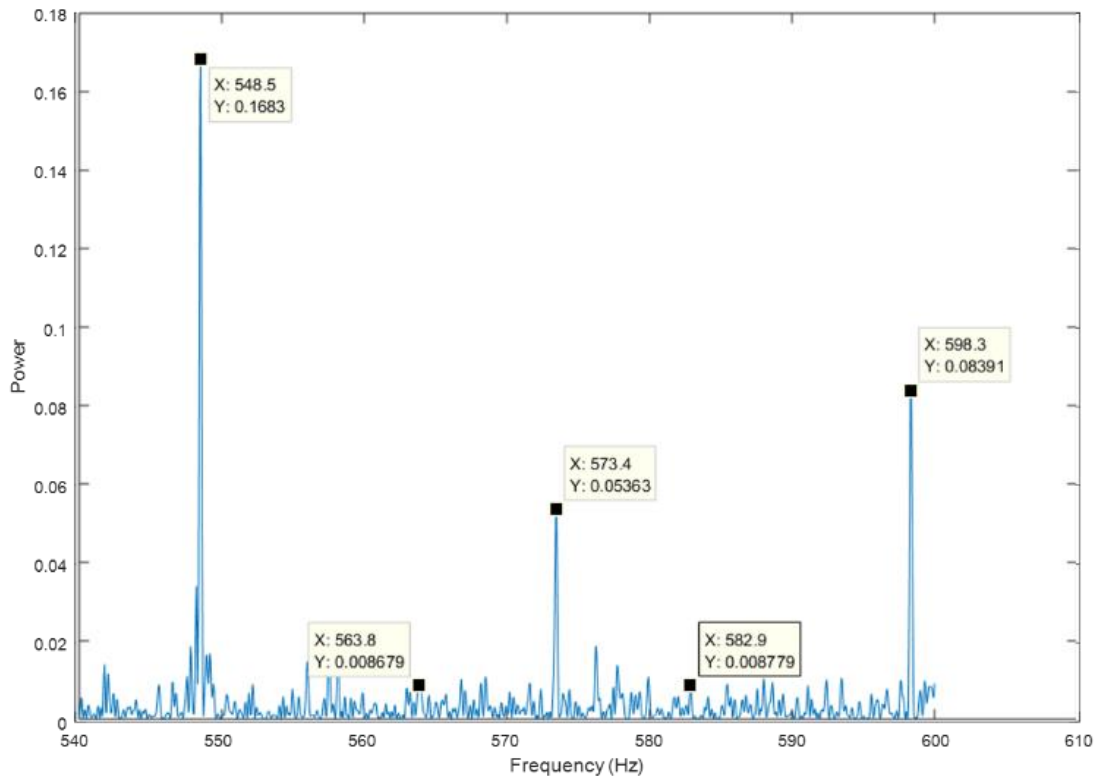


**Figure 4.37 LS periodogram around  $F_{\text{mesh}}$  of the gear vibration in ARS+Unif**

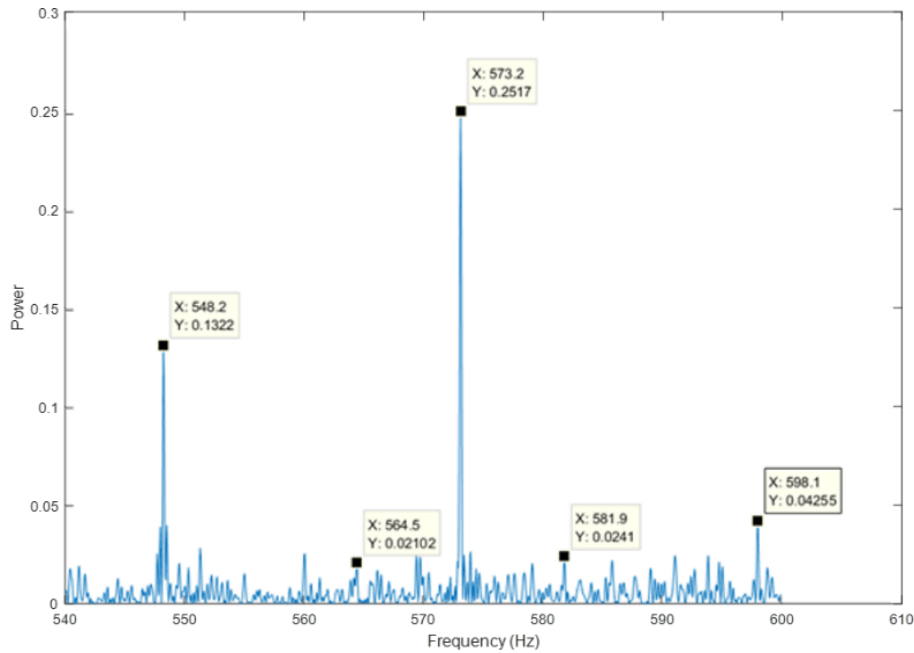


**Figure 4.38 LS periodogram around  $F_{\text{mesh}}$  of the gear vibration in ARS+Gauss**

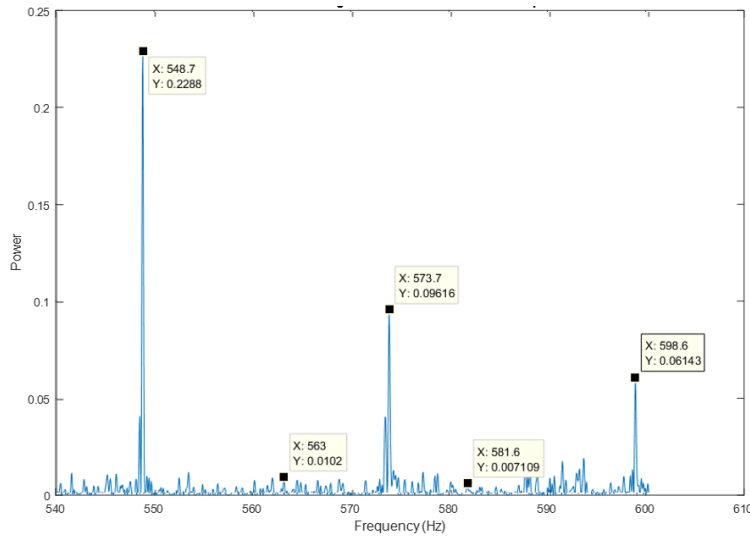


**Figure 4.39 LS periodogram around  $F_{\text{mesh}}$  of the gear vibration in JRS+Unif**

According to figures 4.37 to 4.39, the meshing frequency is obviously detected in all RS modes with both sideband peaks located at  $F_{\text{mesh}}-F_1$  and  $F_{\text{mesh}}+F_1$ . However, peaks at  $F_{\text{mesh}}-F_2$  and  $F_{\text{mesh}}+F_2$  are barely detected. The comparison of these spectra with the gear vibration spectrum in US case, reveals that the problem remains in the amplitude recovery in RS, where the ARS with uniform distribution offers the best recovery among all RS modes. Because of the dense spectrum studied in this case and the additive noise arising from RS application, small amplitudes, like those of sideband peaks of  $F_{\text{mesh}}\pm F_2$ , are surpassed by the noise level which makes them hardly

distinguishable. Thus, noise filtering is a must for a high efficiency of RS. As it is already deduced on the cyclostationarity aspect of the noise added by RS, cyclic filters can play an important role in reducing RS disadvantages in such case of heavy spectra.

Finally, it can be inferred that the RS is applicable on bearing and gear vibrations, with more limitations in the second case caused by intervention of uninteresting vibrations, noise and structure resonance. However, by comparing the resulting spectrum to the US case with taking in consideration the frequency of sampling (5kHz in RS and 51.2 kHz in US) and the amount of acquired data (20 000pts in RS and 200 000 pts in US) it can be easily concluded how much the potential of RS is convincing and advantageous to be used as a solution for the issue of the real-time remote monitoring for industrial machinery.

#### 4.5 Conclusion

The main objective of this chapter was to apply the different modes of RS on vibration signals acquired from rotating machinery components. As considered of the mostly used elements in the industry, rolling bearing and spur gear were the subject of a brief review at the beginning of this chapter, where they were defined, described and presented in their different possible state of deflection. In addition a short overview on the different methods of diagnostic of such components is given to justify the use of spectral analysis techniques in processing vibration signals acquired within RS in the second part of this chapter. The application of RS is conducted in multiple tests as it is the first contribution of RS in condition monitoring of rotating components.

The first test is about acquiring vibrations from a normal bearing set in a simple test bench, the second is based on sampling vibration from a defected bearing implemented in the same bench. The results obtained from both tests are presented in the SES estimated by the Welch and the LS periodograms, where all the characteristic frequencies are clearly detected in both state conditions of the bearing, which approve the use of RS on bearing vibration signal. The LS results are slightly more enhanced than those of the Welch periodogram, though, both are reliable despite using low sampling frequencies and low amount of data. In fact, the sampling frequency in both tests almost didn't overpass the highest frequency of interest in the studied spectra, and all the modes presented satisfying results, but the ARS with uniform distribution is distinguished by its high quality in recovering amplitudes. Consequently, when aiming to acquire the vibrations of a bearing, from its specifications, all the corresponding characteristic frequencies can be easily deduced, thus the highest frequency in the signature vibration is known and should be chosen as the mean sampling frequency of the RS mode. As for the number of samples, it should be selected proportionally to the number of harmonics needed to be shown.

The third test is on applying the RS in acquiring vibration from a couple of spur gears mounted back to back with other couples of gears in a test bench a way more complicated than the first one. The main purpose of this experimentation was to detect the meshing frequency with its corresponding sidebands in the estimated spectrum despite the structure resonance, the high level noise and the uninteresting vibrations. Due to the exploration of the structure transfer function, the highest frequency in the spectrum of vibration is deduced. Many acquisitions were performed using all the RS modes with different values of  $F_{Sm}$  and  $N$ . The results of the Welch periodogram were disappointing because of the smearing problem and thus merging important frequencies with noise peaks. However, the spectral analysis offered by the LS periodogram revealed all the characteristic frequencies of interest especially the meshing frequency with some deficiencies in the amplitude recovery caused by the high noise level arising from the harsh industrial environment and the additive cyclostationary noise coming from the RS process, the fact that encourages for future work on applying cyclic filtering. In this test, the ARS with uniform distribution, again, presents the best results in recovering peaks amplitudes. In all RS modes, best results are for  $F_{Sm}$  equal to the highest frequency in the structure transfer function spectrum and for  $N$  higher than 20 000 points, which are much less than the values chosen in US. As a conclusion, for components implemented in a housing structure, as in US case where it is recommended to identify the structure transfer function by acquiring the vibration while applying a hammer tap, the same is recommended in RS to identify the highest frequency in the spectrum of interest and thus conclude the mean sampling frequency. The important difference between both sampling, is that in US the acquisition must be at a rate equal to the multiple of the highest frequency while in RS the rate will be sufficiently equal or less.

## 5 Conclusion & Perspective

Instead of using high performance devices and looking for ultra-advanced technologies to find solutions for alleviating the duty on the real-time processor in managing operations of excessively high frequency and dealing with large amount of redundant data, the RS is proposed, by an inspiration from the CS concept, to acquire a reduced quantity of data at a low frequency rate. Due to its anti-aliasing property, the RS potential remains in capturing the needed information within few reasonable conditions expressed with simple practical requirements.

The RS and CS are recently used in many different application domains, which facilitates the procedure of searching for theoretical and practical studies. However, some critical gaps were worth to be completed to provide for any user a clear guide to apply RS in new fields. Thus, a detailed review on RS in time domain is presented by defining all its available modes and by studying the major possible probability distributions that may be used, with a clear strategy that may be followed in studying any other distributions. As a consequence, the condition of an advantageous RS are summarized in two concepts: Temporal Condition and Stationarity of the Sampling Process. Where the first imposes limitations on some distributions and prevents them from being used in real applications like the Exponential distribution and the second defines the essential origin of anti-aliasing sampling, that in some cases is verified beyond the temporal condition which makes such mode out of interest as the JRS with Gaussian distribution. According to these conditions, it can be inferred that the consistency in the randomness is needed within a strictly increasing time sequence to guarantee an RS process able to be implemented in real systems with no aliasing in resulting signal spectrum. As the RS is planned to be applied in real applications, a generalized study is proposed to analyze the effect of time quantization in order to reduce it to the minimum. In fact, by quantizing the time, the interval of support of the chosen distribution becomes with less possibilities in generating the sampling sequence, an adequate time step must be selected to keep a good number of possibilities to be chosen which conserves the randomness needed for the anti-aliasing property.

The research and the study of new processes must be usually based on the study of similar classical ones to provide the ultimate guide and make an efficient comparison that leads to clear conclusions. Thus, a summary on the US concepts is presented to remind of the origin of the Shannon-Nyquist frequency which is essential for preventing the spectrum from distortion by keeping the replicas away from the original spectrum, and consequently how long data is required for high resolution

spectra. The spectral analysis study represented by the FT of deterministic signals and the PSD of random signals, are reviewed in US to identify the basic techniques used in transforming the signal from time to frequency domain. And, the most used methods of spectrum estimations are overviewed within a clarified structure to recognize the basics in spectral analysis techniques that are conceived to meet a variant of needs within different application contexts. Consequently, the spectral analysis study of RS is established in the same methodology of US and based on the already conceived theory. In order to find the origin of the noise added by the impact of RS, the link between the FT of the randomly sampled signal and its PSD, where the noise term is explicitly defined, is conceived. When expressed in time domain, the noise term is identified as of cyclostationary aspect according to the used sampling sequence. The PSD analysis is developed in details in order to study the impact of RS within its different modes to conclude with concise formulations that determine the condition of high performance. Some recommendations are provided to enhance the RS behavior and reduce its additive noise to the minimum. The value of the recommended frequency for RS is half the frequency imposed by Shannon-Nyquist, the first is to guarantee a maximum reduced noise while the second is to prevent from major distortion. Plus, the recommendation on the number of points for the same reason of noise reduction, gives an additional expectation of a beneficial aspect of RS. Although the study of RS is based on its PSD, the chosen techniques of spectral estimations are based on the concept of periodogram, as there were no correlogram conceived for RS signals in the literature, and the link between the FT and the PSD provides the evidence of the equivalence between both estimators. All the spectral estimations present in the bibliography are concluded from US methods, which facilitates the decision made in choosing the most convenient for the RS applied on vibration signals. Three periodograms were chosen, each one for a different reason. The Schuster is selected for its basic theoretical concept to be used for the evaluation of RS in simulation. The LS for its reduced complexity, and the Welch periodogram for its noise reduction and prevention from leakage, both are used in the analysis of signals acquired in real applications.

The objective of simulation, in addition to the validation of the theoretical conclusions, is to find a way to pass smoothly from pure theory to real practice. Few simple examples are figured to directly view the impact of RS on the shape of the signal, and to validate the recommendations already stated. Then, a more extended simulation was driven on a signal that modestly represents a spectrum of vibration signals which contains multiple impulses that should be detected to identify the status of the studied component. To avoid redundancy in presenting results, the most meaningful are presented. Consequently, the modes having anti-aliasing properties were definitely identified to be used in practical implementations, while others are viewed to justify the reason of

eliminating them from practical trials. In addition, all the recommendations on  $T_{sm}$ ,  $R$  and  $N$  are verified. Previous implementation of RS were driven in CS architecture, however the concept of randomly choosing samples from the signal is the same. Thus, from the literature of CS some example of practical implementations are presented, to conclude with the most convenient concept. Before, the application on vibration signal many tests were done on simple signals to preview the behavior of RS in real applications and enhance the acquisition to meet with high performance.

For the same reason, a short summary on gears and bearings is figured to predict how to deal with such signals and to avoid probable issues. In the experimentation of acquiring signals form bearing, the objective was mainly to evaluate the RS in the diagnosis context, so the acquisition was made from two bearings: normal and inner race defected. The spectrum in both cases are recovered perfectly in all RS modes, each one within its predetermined conditions, with low frequency and reduced amount of data, which validates the success of RS in diagnostic applications for bearings. In the experimentation on the gear, whose vibration aspect is known for its complexity, the intention was limited to detect the sidebands around the meshing frequency. Further requirements were needed in this case, due to the demand of higher frequencies, however, the meshing frequency and the sidebands are successfully detected in case of frequencies much lower than the Nyquist frequency, but the amplitude recovery imposes some additional enhancement of the spectral analysis in RS especially in filtering the added cyclostationary noise. Although the number of data is not reduced, compared to the amount used in US the result is much satisfying. In tests based on simple components, the results of Ls and Welch were very similar while in complicated cases, the estimated spectrum of LS is preferred on the Welch due to smearing appeared in the latter. The fact that opens the perspective on two possibilities, the first in enhancing the spectra by filtering noise added by RS, the second in searching for possible techniques based on spectral indicators that might be added to the RS application in the machine monitoring domain, in order to go further in advanced automated systems that are able to communicate with remote monitoring devices responsible of collecting data, and then taking decision without human intervention. The RS in such context contributes in dramatically reducing the processing complexity and remediating the big data problem. These propositions are to be ignored if the RS is not strongly immune against noise intervention. Hence, the additive noise caused by the RS impact must be eliminated in first place. Due to its aspect of cyclo-stationarity, cyclic filters may accomplish such task. Thus, further studies may be proposed to be driven in order to find best solutions in eliminating noise in RS to profit from its potential to the extreme limits.

In conclusion, the research on RS and its study in time and frequency domain to conclude with the conditions and limitations on the mode, the distribution and the different parameters within quantitative relations followed by a simulation study and practical experimentation are all accomplished in the aim of proving its potential in resolving the real-time challenge in frequency and data storage in the context of condition monitoring for rotating machinery. Although the amount of data captured by RS is much reduced than the amount acquired usually in US, this reduction can be improved and increased by the application of CS in the same context of machine monitoring due to the promising sparsity of the corresponding vibration spectra. In fact, the contribution of applying RS in the diagnostic domain with the satisfying results encourage future works on profiting from CS in the same field. In addition, beside the guide provided for the application of RS on vibration signals, a methodology that could be easily followed in any other domain with any possible addition or modification is delivered. Finally, adding to its verified profit, the RS is proven to be quiet promising in resolving modern concerns.

## BIBLIOGRAPHY

- [1] M. L. Adams, "Rotating Machinery Vibration From Analysis To Troubleshooting", 2<sup>nd</sup> edition, December 2009.
- [2] J. S. Rao, "History of rotating machinery dynamics", vol. 20. Springer Science & Business Media, 2011.
- [3] Q. Gao, C. Duan, H. Fan, and Q. Meng, "Rotating machine fault diagnosis using empirical mode decomposition," *Mech. Syst. Signal Process.*, vol. 22, no. 5, pp. 1072–1081, 2008.
- [4] S. Ericsson, N. Grip, E. Johansson, L. E. Persson, R. Sjöberg, and J. O. Strömberg, "Towards automatic detection of local bearing defects in rotating machines," *Mech. Syst. Signal Process.*, vol. 19, no. 3, pp. 509–535, 2005.
- [5] B. Liu, S. F. Ling, and R. Gribonval, "Bearing failure detection using matching pursuit," *Ndt E Int.*, vol. 35, no. 4, pp. 255–262, 2002.
- [6] N. G. Nikolaou and I. A. Antoniadis, "Rolling element bearing fault diagnosis using wavelet packets," *Ndt E Int.*, vol. 35, no. 3, pp. 197–205, 2002.
- [7] N. Mitton and E. Natalizio, "Applications of Industrial Wireless Sensor Networks," pp. 3–27.
- [8] J. D. Lee and K. A. See, "Trust in automation: Designing for appropriate reliance," *Hum. Factors*, vol. 46, no. 1, pp. 50–80, 2004.
- [9] P. Koopman, "Embedded system design issues (the rest of the story)," in *Computer Design: VLSI in Computers and Processors, 1996. ICCD'96. Proceedings., 1996 IEEE International Conference on, 1996*, pp. 310–317.
- [10] H. Kopetz et al., "Distributed fault-tolerant real-time systems: The Mars approach," *IEEE Micro*, vol. 9, no. 1, pp. 25–40, 1989.
- [11] Y. Du and G. De Veciana, "Scheduling for cloud-based computing systems to support soft real-time applications," *ACM Trans. Model. Perform. Eval. Comput. Syst.*, vol. 2, no. 3, p. 13, 2017.
- [12] E. Serrano and A. Arsénio, "Cloud Framework for Wireless Sensor Networks", Thesis paper.
- [13] A. Talari and N. Rahnavard, "Cstorage: Distributed data storage in wireless sensor networks

- employing compressive sensing,” in Global Telecommunications Conference (GLOBECOM 2011), 2011 IEEE, 2011, pp. 1–5.
- [14] B. Kong, G. Zhang, W. Zhang, D. Bian, and Z. Xie, “Efficient distributed storage strategy based on compressed sensing for space information network,” *Int. J. Distrib. Sens. Networks*, vol. 12, no. 8, p. 1550147716664253, 2016.
- [15] E. J. Candes and M. B. Wakin, “An Introduction To Compressive Sampling,” *IEEE Signal Process. Mag.*, vol. 25, no. 2, pp. 21–30, 2008.
- [16] C. Paper, “compressive sampling Compressive Sensing and JPEG Compression : A Comparative Approach,” no. September, 2015.
- [17] C. Paper, “Compressive Sampling on Speech Signal using Random Demodulator Compressive Sampling on Speech Signal using Random Demodulator,” no. JANUARY, pp. 0–4, 2015.
- [18] J. Laska et al., “Random sampling for analog-to-information conversion of wideband signals,” in *Design, Applications, Integration and Software, 2006 IEEE Dallas/CAS Workshop on*, 2006, pp. 119–122.
- [19] W. He, Y. Ding, Y. Zi, and I. W. Selesnick, “Sparsity-based algorithm for detecting faults in rotating machines,” *Mech. Syst. Signal Process.*, vol. 72, no. Supplement C, pp. 46–64, 2016.
- [20] P. Babu and P. Stoica, “Spectral analysis of nonuniformly sampled data – a review,” *Digit. Signal Process.*, vol. 20, no. 2, pp. 359–378, 2010.
- [21] K. J. Aström, “Event based control,” *Anal. Des. nonlinear Control Syst.*, vol. 3, pp. 127–147, 2008.
- [22] S. Traore, “Contribution ` a l ’ ´ etude de l ’ ´ echantillonnage non uniforme dans le domaine de la radio intelligente . Samba Traore To cite this version : CentraleSupélec,” 2016.
- [23] E. Kofman and J. H. Braslavsky, “Level Crossing Sampling in Feedback Stabilization under Data-Rate Constraints,” *Proc. 45th IEEE Conf. Decis. Control*, pp. 4423–4428, 2006.
- [24] F. Marvasti, *Nonuniform sampling: theory and practice*. Springer Science & Business Media, 2012.
- [25] J. L. Yen, “On nonuniform sampling of bandlimited signals,” *IRE Trans. Circuit Theory*,

vol. 3, no. 4, pp. 251–257, 1956.

- [26] D. J. Wingham, “The reconstruction of a band-limited function and its Fourier transform from a finite number of samples at arbitrary locations by singular value decomposition,” *IEEE Trans. signal Process.*, vol. 40, no. 3, pp. 559–570, 1992.
- [27] P. J. S. G. Ferreira, “Incomplete sampling series and the recovery of missing samples from oversampled band-limited signals,” *IEEE Trans. signal Process.*, vol. 40, no. 1, pp. 225–227, 1992.
- [28] I. Bilinskis, *Digital alias-free signal processing*. John Wiley & Sons, 2007.
- [29] Y. Yang and S. Nagarajaiah, “Output-only modal identification by compressed sensing: Non-uniform low-rate random sampling,” *Mech. Syst. Signal Process.*, vol. 56, pp. 15–34, 2015.
- [30] J. F. Claerbout and F. Muir, “Robust modeling with erratic data,” *Geophysics*, vol. 38, no. 5, pp. 826–844, 1973.
- [31] H. S. Shapiro and R. A. Silverman, “Alias-free sampling of random noise,” *J. Soc. Ind. Appl. Math.*, vol. 8, no. 2, pp. 225–248, 1960.
- [32] F. J. Beutler and O. A. Z. Leneman, “The spectral analysis of impulse processes,” *Inf. Control*, vol. 12, no. 3, pp. 236–258, 1968.
- [33] J. Beutler, “A stationary point process, like a recurrent or renewal process, may be interpreted,” no. 1, 1966.
- [34] O. A. Z. Leneman, “Random Sampling of Random Processes - Impulse Processes,” *Inf. Control*, vol. 9, no. 4, pp. 347–363, 1966.
- [35] J. J. Wojtiuk, “Randomised Sampling for Radio Design by,” no. March, 2000.
- [36] M. Ben Romdhane, “Échantillonnage non uniforme appliqué à la numérisation des signaux radio multistandard,” *TICOM ParisTech*, 2009.
- [37] C. Luo, “Non-Uniform Sampling: Algorithms and Architectures Non-Uniform Sampling: Algorithms and,” no. December, 2012.
- [38] E. J. Candes, J. K. Romberg, and T. Tao, “Stable signal recovery from incomplete and inaccurate measurements,” *Commun. pure Appl. Math.*, vol. 59, no. 8, pp. 1207–1223, 2006.

- [39] M. Lustig, D. Donoho, and J. M. Pauly, "Sparse MRI: The application of compressed sensing for rapid MR imaging," *Magn. Reson. Med.*, vol. 58, no. 6, pp. 1182–1195, 2007.
- [40] M. Wakin et al., "A Nonuniform Sampler for Wideband Spectrally-Sparse Environments.pdf," pp. 1–14, 2009.
- [41] J. Bobin, J.-L. Starck, and R. Ottensamer, "Compressed sensing in astronomy," *IEEE J. Sel. Top. Signal Process.*, vol. 2, no. 5, pp. 718–726, 2008.
- [42] M. Mohtashemi, H. Smith, D. Walburger, F. Sutton, and J. Diggans, "Sparse sensing DNA microarray-based biosensor: Is it feasible?," in *Sensors Applications Symposium (SAS)*, 2010 IEEE, 2010, pp. 127–130.
- [43] D. L. Donoho, "Compressed sensing," *IEEE Trans. Inf. Theory*, vol. 52, no. 4, pp. 1289–1306, 2006.
- [44] S. Qaisar, R. M. Bilal, W. Iqbal, M. Naureen, and S. Lee, "Compressive Sensing : From Theory to Applications , a Survey," vol. 15, no. 5, pp. 443–456, 2013.
- [45] R. G. Baraniuk, "Compressive Sensing [Lecture Notes]," *IEEE Signal Process. Mag.*, vol. 24, no. July, pp. 118–121, 2007.
- [46] E. J. Candes and T. Tao, "Decoding by linear programming," *IEEE Trans. Inf. theory*, vol. 51, no. 12, pp. 4203–4215, 2005.
- [47] F. P. Schoenberg, "Introduction to point processes," *Wiley Encycl. Oper. Res. Manag. Sci.*, 2010.
- [48] P. H. Wittke, "A Unified Approach to Zero-Crossings and Nonuniform Sampling: Of Single and Multidimensional Signals and Systems (Farokh A. Marvasti)." *Society for Industrial and Applied Mathematics*, 1990.
- [49] K. C. Lo and A. Purvis, "A new approach for estimating spectra from randomly sampled sequences," *Circuits Syst. Signal Process.*, vol. 16, no. 3, pp. 375–386, 1997.
- [50] M. El Badaoui and F. Bonnardot, "Impact of the non-uniform angular sampling on mechanical signals," *Mech. Syst. Signal Process.*, vol. 44, no. 1–2, pp. 199–210, 2014.
- [51] a. Balakrishnan, "On the problem of time jitter in sampling," *IRE Trans. Inf. Theory*, vol. 8, no. 3, pp. 253–257, 1962.
- [52] F. Eng, *Non-Uniform Sampling in Statistical Signal Processing*, no. 1082. 2007.

- [53] Y. Artyukh, I. Bilinskis, M. Greitans, and V. Vedin, "Signal Digitizing and Recording in the DASP-Lab System," *System*, no. July, pp. 1–4, 2014.
- [54] P. U. Prof. Paul Cuff, "Sampling and Quantization," no. i, pp. 1–7, 2016.
- [55] R. I. Marks, *Advanced Topics in Shannon Sampling and Interpolation Theory*. 2012.
- [56] J. O'Neal, *Introduction to Signal Transmission*, vol. 20, no. 5. 1972.
- [57] P. Hall and U. S. River, *Spectral Analysis of Signals*. 2009.
- [58] K. S. Shanmugam, "Digital and analog communication systems," *NASA STI/Recon Tech. Rep. A*, vol. 80, 1979.
- [59] G. L. Bretthorst, "Generalizing the Lomb-Scargle periodogram," in *AIP Conference Proceedings*, 2001, vol. 568, no. 1, pp. 241–245.
- [60] T. S. Rao, M. B. Priestly, and O. Lessi, "Applications of Time Series Analysis in Astronomy and Meteorology." Taylor & Francis Group, 1998.
- [61] M. S. Bartlett, "Periodogram analysis and continuous spectra," *Biometrika*, vol. 37, no. 1/2, pp. 1–16, 1950.
- [62] P. Welch, "The use of fast Fourier transform for the estimation of power spectra: a method based on time averaging over short, modified periodograms," *IEEE Trans. audio Electroacoust.*, vol. 15, no. 2, pp. 70–73, 1967.
- [63] R. B. Blackman and J. W. Tukey, "The measurement of power spectra from the point of view of communications engineering Part I," *Bell Labs Tech. J.*, vol. 37, no. 1, pp. 185–282, 1958.
- [64] R. Schmidt, "Multiple emitter location and signal parameter estimation," *IEEE Trans. Antennas Propag.*, vol. 34, no. 3, pp. 276–280, 1986.
- [65] J. Capon, "High-resolution frequency-wavenumber spectrum analysis," *Proc. IEEE*, vol. 57, no. 8, pp. 1408–1418, 1969.
- [66] R. J. Martin, "Irregularly sampled signals: theories and techniques for analysis," no. January, 1998.
- [67] D. M. Bland, T. I. Laakso, and A. Tarczynski, "Analysis of algorithms for nonuniform-time discrete Fourier transform," *Circuits and Systems*, 1996. *ISCAS '96.*, Connecting the

- World., 1996 IEEE International Symposium on, vol. 2. pp. 453–456, 1996.
- [68] A. Tarczynski, D. Bland, and T. Laakso, “Spectral Estimation of Non-Uniformly Sampled Signals,” *Proc. IEEE Int. Symp. Ind. Electron.* 1996, vol. 1, pp. 196–200, 1996.
- [69] A. Tarczynski and N. Allay, “Spectral analysis of randomly sampled signals: Suppression of aliasing and sampler jitter,” *IEEE Trans. Signal Process.*, vol. 52, no. 12, pp. 3324–3334, 2004.
- [70] D. H. Roberts, J. Lehár, and J. W. Dreher, “Time Series Analysis with Clean-Part One-Derivation of a Spectrum,” *Astron. J.*, vol. 93, p. 968, 1987.
- [71] N. R. Lomb, “Least-squares frequency analysis of unequally spaced data,” *Astrophys. Space Sci.*, vol. 39, no. 2, pp. 447–462, 1976.
- [72] J. D. Scargle, “Studies in astronomical time series analysis. II - Statistical aspects of spectral analysis of unevenly spaced data,” *Astrophys. J.*, vol. 263, p. 835, 1982.
- [73] J. H. Horne and S. L. Baliunas, “A prescription for period analysis of unevenly sampled time series,” *Astrophys. J.*, vol. 302, p. 757, 1986.
- [74] I. Jalón-Rojas, S. Schmidt, and A. Sottolichio, “Analyse de 10 ans de mesures continues de turbidité dans les sections fluviales de l'estuaire de la Gironde,” *Mes. haute résolution dans l'environnement Mar. côtier*, Press. du CNRS, 2015.
- [75] M. Orlob, “Project Paper: LOMB-SCARGLE SPECTRAL ANALYSIS OF NONEQUISPACED DATA.”
- [76] P. Stoica, J. Li, and H. He, “Spectral Analysis of Nonuniformly Sampled Data: A New Approach Versus the Periodogram,” *IEEE Trans. Signal Process.*, vol. 57, no. 3, pp. 843–858, 2009.
- [77] K. S. Agyepong, F. H. Hsu, E. R. Dougherty, and E. Serpedin, “Spectral analysis on time-course expression data: Detecting periodic genes using a real-valued iterative adaptive approach,” *Adv. Bioinformatics*, vol. 2013, 2013.
- [78] B. Leroy, “Fast calculation of the Lomb-Scargle periodogram using nonequispaced fast Fourier transforms,” *Astron. Astrophys.*, vol. 545, p. A50, 2012.
- [79] S. V. Vaseghi, *Interpolation*, vol. 33. 2012.
- [80] S. Kirolos, J. Laska, M. Wakin, M. Duarte, and D. Baron, “Analog-to-Information

Conversion via Random emudulation,” pp. 3–6.

- [81] G. Heinzel, a Rüdiger, R. Schilling, and T. Hannover, “Spectrum and spectral density estimation by the Discrete Fourier transform (DFT), including a comprehensive list of window functions and some new flat-top,” Max Plank Inst., pp. 1–84, 2002.
- [82] M. H. Hayes, *Statistical Digital Signal Processing and Modeling*. Wiley New York, 1996.
- [83] H. Mamaghanian, N. Khaled, D. Atienza, and P. Vandergheynst, “Design and exploration of low-power analog to information conversion based on compressed sensing,” *IEEE J. Emerg. Sel. Top. Circuits Syst.*, vol. 2, no. 3, pp. 493–501, 2012.
- [84] T. Ragheb et al., “Implementation models for analog-to-information conversion via random sampling,” *Midwest Symp. Circuits Syst.*, pp. 325–328, 2007.
- [85] P. Gupta and M. . Pradhan, “Fault detection analysis in rolling element bearing: A review,” *Mater. Today Proc.*, vol. 4, no. 2, pp. 2085–2094, 2017.
- [86] D. Bently, “Predictive maintenance through the monitoring and diagnostics of rolling element bearings,” *Appl. Note*, no. ANO44, pp. 2–8, 1989.
- [87] C. S. Sunnersjö, “Varying compliance vibrations of rolling bearings,” *J. Sound Vib.*, vol. 58, no. 3, pp. 363–373, 1978.
- [88] R. B. Randall and J. Antoni, “Rolling element bearing diagnostics-A tutorial,” *Mech. Syst. Signal Process.*, vol. 25, no. 2, pp. 485–520, 2011.
- [89] N. Tandon and A. Choudhury, “A review of vibration and acoustic measurement methods for the detection of defects in rolling element bearings,” *Tribol. Int.*, vol. 32, no. 8, pp. 469–480, 1999.
- [90] A. K. S. Jardine, D. Lin, and D. Banjevic, “A review on machinery diagnostics and prognostics implementing condition-based maintenance,” *Mech. Syst. Signal Process.*, vol. 20, no. 7, pp. 1483–1510, 2006.
- [91] J. Antoni, “Cyclic spectral analysis of rolling-element bearing signals: Facts and fictions,” *J. Sound Vib.*, vol. 304, no. 3–5, pp. 497–529, 2007.
- [92] D. Abboud, J. Antoni, S. Sieg-Zieba, and M. Eltabach, “Envelope analysis of rotating machine vibrations in variable speed conditions: A comprehensive treatment,” *Mech. Syst. Signal Process.*, vol. 84, pp. 200–226, 2017.

- [93] C. Gonzales, "What's the Difference Between Spur, Helical, Bevel, and Worm Gears?," 2016.
- [94] A. F. del Rincon, F. Viadero, M. Iglesias, A. de-Juan, P. Garcia, and R. Sancibrian, "Effect of cracks and pitting defects on gear meshing," *Proc. Inst. Mech. Eng. Part C J. Mech. Eng. Sci.*, vol. 226, no. 11, pp. 2805–2815, 2012.
- [95] J. Chen, Y. Zi, Z. He, and X. Wang, "Adaptive redundant multiwavelet denoising with improved neighboring coefficients for gearbox fault detection," *Mech. Syst. Signal Process.*, vol. 38, no. 2, pp. 549–568, 2013.
- [96] V. Sharma and A. Parey, "A Review of Gear Fault Diagnosis Using Various Condition Indicators," *Procedia Eng.*, vol. 144, pp. 253–263, 2016.
- [97] V. S. Panwar, S. P. Mogal, and N. D. M. V. P. K. B. T. Coe, "A CASE STUDY ON VARIOUS DEFECTS FOUND IN A GEAR SYSTEM," pp. 425–429, 2015.
- [98] M. Systems, "TECHNICAL DETERMINING THE THE LOCATION FROM IN THE NOTE OF A FATIGUE PHASE OF VIBRATION CRACK IN A GEAR CHANGE THE," vol. 2, pp. 403–409, 1988.
- [99] L. Hong and J. Singh, "A time domain approach to diagnose gearbox fault based on measured vibration signals," *J. Sound Vib.*, vol. 333, no. 7, pp. 2164–2180, 2014.

# Appendix A: Compressed Sensing Review

## A.1 Compressed Sensing Theory

The intent of this section is to overview the basic theory of Compressed Sensing (known also as Compressive Sampling) (CS), present the key mathematical ideas underlying this theory and survey a couple of important results in this field, in order to highlight the fact that randomness can lead to very effective sensing mechanism. In fact, the CS was conceived for two major advantages: compressing data and managing the under-sampling situations. The main contribution in data compression in such sampling technique is in directly acquiring a compact amount of data instead of acquiring and then compressing, a process that requires a large data storage and higher energy consumption. Moreover, CS is considered as a solution for situations where under-sampling is imposed, where the number of sensors is limited, the measurements are expensive or even unreachable in some circumstances. The CS was developed to give an accurate reconstruction of the original signal from the available measurements sampled in a compressive way [15]. Therefore, the CS is used in many different domains where the data compression is needed or the number of measurements is limited. For instance, in Medical Resonance Imaging (MRI), the sensing process is slow and the object may be measured only few times. Thus, many research corporations within hospitals payed close attention to CS in MRI [39][40]. Besides, CS is mainly a research subject in astronomy imaging [41], Microarray sequencing in Biology [42], seismic imaging, and modal identification within Civil engineering [38] and in many other fields. In fact, CS is advantageous for any application using wireless sensor networks, due to decreasing the number of measurements acquired by the sensors and thus decreasing the energy consumed and the amount of transmitted data [29].

## A.2 CS Definition

CS is defined as a technique to acquire and represent compressible signals in a compressive way, at a rate significantly below the Nyquist rate. It employs non-adaptive linear projections that preserve the structure and the properties of the signal; the signal is then reconstructed from these projections or measurements using an optimization algorithm [43].

Foremost, the signal to be sampled or measured is  $x \in \mathbb{R}^n$ , the observation of  $x$  designated by  $y$  is defined by:

$$y = \Phi x \quad (a.1)$$

Where  $y \in \mathbb{R}^m$  and  $\Phi \in \mathbb{R}^{m \times n}$ .  $\Phi$  is defined as the sensing matrix, where  $\{\varphi_k\}_{k=1 \dots m}$  are the sensing waveforms.

The problem of CS is expressed by how to choose  $\Phi$  in order to find an observation  $y$  of size  $m \ll n$  with the ability to reconstruct  $x$  from  $y$ . Although the CS theory can be developed for continuous signals, in the literature the main established studies were conceived for discrete signals and focused on reducing the number of measurements from  $n$  to  $m$  [15], [45].

Hence, the CS is based on two main principles: the Sparsity and Incoherence, where the first is a condition concerning the original signal  $x$  and the second is related to the sensing matrix  $\Phi$ . These two conditions are judged to be indispensable for the reconstruction of  $x$  from its compressed observation  $y$ .

### A.3 Sparsity Definition

This property is equivalent to the compressibility of the signal, and it is verified when there exists a basis  $\Psi$  (known also as a dictionary) where the projection of the signal  $x$  is  $k$ -sparse. This means that the majority of the coefficients of  $x$  in the basis  $\Psi$  are zeros except  $k$  elements. Thus, when applying the CS on a compressible signal  $x$ , it is essential to find the basis  $\Psi$  where  $a_i$ , the coefficients of  $x$  in  $\Psi$ , are of majority of zero, so  $x$  can be expressed by:

$$x = \Psi a = \sum_{i=1}^n a_i \psi_i \quad (a.2)$$

Where  $\{\psi_i\}_{i=1 \dots n}$  are the column vectors of the matrix  $\Psi$  that forms an  $n \times n$  basis matrix that is assumed orthonormal for simplicity. Hence,  $x$  and  $a$  are equivalent representations of the original signal:  $x$  in the time domain and  $a$  in the  $\Psi$  domain. A variant of transformations is used to find a sparse expansion of  $x$ , the selection of this transformation is based on the nature of the signal that is related to the application domain. The Fourier, the Wavelet, the Curvelet and the Discrete Cosine Transform (DCT) are examples of these transformations that are used within CS in [15], [38], [41]. The result of this conversion is the  $n \times 1$  vector  $a$ , that is  $k$ -sparse having  $k$  large coefficients and many small coefficients that are considered as zeros [45]. In case of using the Fourier basis, the vectors  $\{\psi_i\}$  are defined by:

$$\psi_i(t) = \frac{1}{\sqrt{n}} e^{j2\pi it/n} \quad (a.3)$$

Finally, due to the representation of  $x$  in the  $\Psi$  domain, the relation between  $x$  and its observation  $y$  becomes:

$$y = \Phi x = \Phi \Psi a = Aa \tag{a.4}$$

### A.4 Incoherence

As mentioned before, this property defines the aspect of the sensing matrix  $\Phi$ . Going back to the main issue, the purpose of CS is to conceive efficient sampling protocols that acquire the essential content of the sparse signal and condense it into a minor amount of data. These protocols must be non-adaptive and should capture the signal with a small number of fixed waveforms. These waveforms must be incoherent with the sparsifying basis  $\Psi$ . In other words, unlike the signal  $x$ , the sensing waveforms, that define the sensing matrix  $\Phi$ , must have a dense representation in the  $\Psi$  domain.

By definition, the coherence between two orthobasis,  $\Phi$  and  $\Psi$  of  $\mathbb{R}^n$  is expressed by:

$$\mu(\Phi, \Psi) = \sqrt{n} \cdot \max_{1 \leq k, j \leq n} |\langle \varphi_k, \psi_j \rangle| \tag{a.5}$$

Thus, the coherence measures the largest correlation between any two elements of  $\Phi$  and  $\Psi$ , if their elements are correlated their coherence is high and tend to  $\sqrt{n}$ , otherwise, it is low and tend to 1. In CS, the coherence between  $\Phi$  (the sensing matrix) and  $\Psi$  (the representation matrix) must be as low as possible (equal to 1) [15]. However, In [43] one of the pioneers references in CS, it was concluded that the random matrices are largely incoherent with any fixed basis  $\Psi$ . So, random sensing/sampling matrices are used within CS to guarantee incoherence condition. Therefore, the efficiency of RS is proven within the context of CS, where the data is acquired compressively with low rate sampling and can be reconstructed without loss.

### A.5 Restricted Isometry Property

To find a general property that guarantees a robust CS, the Restricted Isometry Property (RIP) is defined for the  $k$ -sparse vector  $a$  with the constant  $\delta_k$  as:

$$(1 - \delta_k) \|a\|_{l_2}^2 \leq \|Aa\|_{l_2}^2 \leq (1 + \delta_k) \|a\|_{l_2}^2 \tag{a.6}$$

The isometry constant  $\delta_k$  is defined as the smallest number that verifies the property (1.6). The matrix  $A$  is verifies the RIP when  $\delta_k$  is not too close to one. Although, this verification is hard to be validated, as considered a non-deterministic polynomial-time problem, it was proven, according to [15][45][46], that the random sensing matrices satisfy the RIP with an overwhelming probability when the number of measurements is:

$$m = O\left(k \log\left(\frac{n}{k}\right)\right) = \text{Cte. } k \quad (\text{a.7})$$

Finally, the main conditions of data reconstruction within CS are summarized by: the Sparsity of  $x$  in a certain basis  $\Psi$ , a random sensing matrix and a number of measurements  $m$  respecting (1.7).

## A.6 Reconstruction in CS

The reconstruction in the CS context is to find the sparse solution ‘ $a$ ’ that verifies the equation (1.4), the sparse solution  $s$  can be then expressed by:

$$s = \min_{a: Aa=y} \|a\|_{l_p} = A^T(AA^T)^{-1}y \quad (\text{a.8})$$

Most of the reconstruction algorithms are based on this concept in finding the exact signal reconstructed, though, they differ in the criteria of minimization. The most interesting to cite are the  $l_2$  and  $l_1$  minimizations defined by their corresponding norm where the norm of a vector  $v$  composed of  $N$  elements:

$$\|v\|_{l_p} = \sqrt[p]{\sum_{i=1}^N |v_i|^p} \quad (\text{a.9})$$

On one hand, the algorithms based on the  $l_2$  minimization, known also as the least square solution, are categorized as the Greedy Iterative Algorithms. In an iterative way, the solution of (1.8) is found by minimizing the least square error between the proposed solution and  $y$ . The most known algorithms are the Matching Pursuit and its derivative the Orthogonal Matching Pursuit, other variants of these methods are also used, they differ only in the stopping condition.

On the other hand, the algorithms based on the  $l_1$  minimization are known by Convex optimization. They find the solution of (1.8) by linear programming. The most used one is the Basis Pursuit. These algorithms are advantageous in their exact reconstruction from small number of measurements, though their computational complexity is high. While, the Greedy Iterative Algorithms are of low implementation cost and high speed recovery in case of sparse signals. For interested readers, more details and other categories of algorithm and their variants are explained in [44]. Consequently, there exists a wide variety of methods in Spectral Analysis for random signals uniformly and irregularly sampled. In this section a brief review on the methods of analyzing the random signals that are uniformly sampled only, the ones conceived for the randomly sampled signals are discussed in later paragraphs. In fact, the windowing technique permits to control the bias/resolution property, and the overlapping reduces the variance by increasing the number of segments to be averaged.

## Appendix B: Calculation of $\sigma/T_{Sm}$ in TQRS

In this appendix the summary of  $\sigma/T_{Sm}$  calculation is presented. The purpose is to find a general formula of this ratio for different values of R. In fact, the start is with the general formula of  $\sigma$  (b.1) in case of a uniform distribution with a quantized interval  $[a_q, b_q]$ .

$$\sigma = \sqrt{\frac{1}{D_q} \sum_{j=a_q}^{b_q} \left( j\Delta - \left( \frac{1}{D_q} \sum_{j=a_q}^{b_q} j\Delta \right) \right)^2} \quad (b.1)$$

To simplify the calculations the limits of summation  $a_q$  and  $b_q$  are replaced by 0 and  $D_q$ , as  $\sigma$  is the same as the deviation of the new interval is remaining equal to  $D_q$ . The formula (b.1) becomes (b.2).

$$\sigma = \sqrt{\frac{1}{D_q} \sum_{j=0}^{D_q} \left( j\Delta - \left( \frac{1}{D_q} \sum_{j=0}^{D_q} j\Delta \right) \right)^2} \quad (b.2)$$

The first step is to calculate the summation of  $j\Delta$  in (b.3).

$$\frac{1}{D_q} \sum_{j=0}^{D_q} j\Delta = \frac{\Delta}{D_q} \sum_{j=0}^{D_q} j = \frac{\Delta(D_q + 1)}{2} \quad (b.3)$$

By replacing the result of (b.3) in (b.2), the expression of  $\sigma$  becomes (b.4).

$$\begin{aligned} \sigma &= \sqrt{\frac{1}{D_q} \sum_{j=0}^{D_q} \left( j\Delta - \frac{\Delta(D_q + 1)}{2} \right)^2} \\ &= \sqrt{\frac{\Delta^2}{D_q} \sum_{j=0}^{D_q} \left\{ j^2 + \frac{(D_q + 1)^2}{4} - j(D_q + 1) \right\}} \quad (b.4) \end{aligned}$$

After calculating the summation of each term in (b.4) the expression of  $\sigma$  becomes (b.5).

$$\sigma = \sqrt{\frac{\Delta^2}{D_q} \times \frac{D_q(D_q^2 - 1)}{12}} = \Delta \sqrt{\frac{(D_q^2 - 1)}{12}} \quad (b.5)$$

Thus, by replacing  $D_q$  by  $R.q_T$ , the ratio  $\sigma/T_{Sm}$  is finally defined by (b.6).

$$\frac{\sigma}{T_{Sm}} = \frac{\Delta}{T_{Sm}} \sqrt{\frac{(R^2 q_T^2 - 1)}{12}} = \frac{1}{q_T} \sqrt{\frac{R^2 q_T^2 - 1}{12}} \quad (b.6)$$

## Appendix C: PSD calculation of Beutler and Leneman

In [32] the autocorrelation function of  $S(t)$  was deduced from the autocorrelation of its primitive  $N_s(t)$ , which is a stationary increment stochastic process defined by (c.1). Since  $\{\alpha_n\}$  is stationary, the moments of  $N_s(t)$  depends only on  $m$  but not on  $k$ .

$$N_s(t) = \sum_{n=k}^{k+m-1} \alpha_n \quad (c.1)$$

Then, the Random Impulse Process  $S(t)$  is simply deduced by:

$$s(t) = \frac{dN_s(t)}{dt} \quad (c.2)$$

Consequently, the variations in  $N_s(t)$  turns into impulses in  $s(t)$ . These impulses are expressed by delta functions whose intensity is determined by the corresponding  $\alpha_n$ . This differentiation is illustrated in Figure A.1.

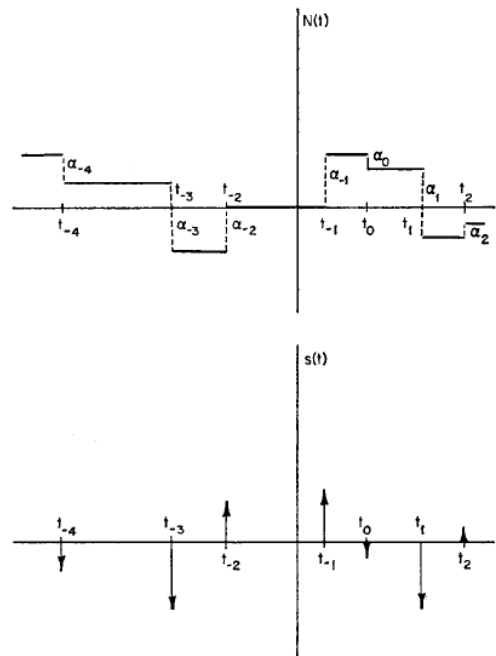


Figure 0.1 Relationship between  $N_s(t)$  and  $s(t)$

In order to determine the expressions of the moments of  $N_s(t)$ , some parameters should be defined.  $\beta$  is the average number of points per unit time interval, and  $\rho(m)$  is the correlation function for the process  $\{\alpha_n\}$ ,  $\rho$  is defined by:

$$\rho(m) = E[\alpha_{u+m}\alpha_u] \quad \forall u \quad (c.3)$$

And  $f_{\sigma_n}$  is the PDF of  $\sigma_n$ : the sum of  $n$  consecutive time intervals, its primitive  $F_{\sigma_n}$  is the repartition function, the characteristic function is the defined by:

$$\varphi_{\sigma_n}(f) = \int_{-\infty}^{\infty} f_{\sigma_n}(t) e^{i2\pi ft} df \quad (c.4)$$

This definition gives a property for negative indices:

$$\varphi_{\sigma(-n)}(f) = \varphi_{\sigma n}(-f) \quad (c.5)$$

The second order moment of  $N_s(t)$  is developed and determined by:

$$E[N_s^2(t)] = \beta\rho(0)t + 2\beta \int_0^t \sum_{n=1}^{\infty} \rho(n)F_{\sigma_n}(u)du \quad (c.6)$$

From (c.6) the autocorrelation of  $N_s(t)$  is deduced by:

$$\begin{aligned} E[N_s(t)N_s(t + \tau)] &= \beta\rho(0) \\ &+ \beta \left\{ \int_0^t \sum_{n=1}^{\infty} \rho(n)F_{\sigma_n}(u)du + \int_0^{t+\tau} \sum_{n=1}^{\infty} \rho(n)F_{\sigma_n}(u)du \right. \\ &\left. - \int_0^{|\tau|} \sum_{n=1}^{\infty} \rho(n)F_{\sigma_n}(u)du \right\} \quad (c.7) \end{aligned}$$

The autocorrelation function of  $s(t)$  is the derivative of the autocorrelation of  $N_s(t)$ , thus the autocorrelation of  $s(t)$  is deduced by (c.8) according to theorem 3 deduced from the SPP condition of [31] and already mentioned in Chapter 1:

$$R_s(\tau) = E[s(t)s(t + \tau)] = \beta\rho(0)\delta(\tau) + \beta \sum_{n=1}^{\infty} \rho(n)f_{\sigma_n}(|\tau|) \quad (c.8)$$

The PSD is then concluded by the derivative of (c.8)

$$\Phi_s(f) = \beta \sum_{n=-\infty}^{\infty} \rho(n)\varphi_{\sigma_n}(f) \quad (c.9)$$

By adopting the convention of  $\phi_0(f)=1$ , and by taking  $\rho(n)=\rho(-n)$  the PSD of  $s(t)$  is finally determined by [32].

$$\Phi_s(f) = \beta\{\rho(0) + \sum_{n=1}^{\infty} \rho(n)[\varphi_{\sigma n}(f) + \varphi_{\sigma n}(-f)]\} \quad (\text{c.10})$$